Tetratopic and hexatopic terpyridine ligands as building blocks in coordination polymers

Inauguraldissertation

zur

Erlangung der Würde eines Doktors der Philosophie

vorgelegt der

Philosophisch-Naturwissenschaftlichen Fakultät

der Universität Basel

von

Giacomo Manfroni

2023

Genehmigt von der Philosophisch-Naturwissenschaftlichen Fakultät

auf Antrag von

Prof. Dr. Edwin C. Constable, Prof. Dr. Christof Sparr and Prof. Dr. Katharina Fromm

Basel, 13.12.2022

Prof. Dr. Marcel Mayor

Dekan der Philosophisch-
Naturwissenschaftlichen Fakultät

In memory of Doriana

Abstract

The work described in this thesis concerns the synthesis of tetratopic bis(3,2':6',3''-tpy) and bis(4,2':6',4''-tpy), hexatopic tris(3,2':6',3''-tpy) and tris(4,2':6',4''-tpy) ligands and their capability to form 1D, 2D and 3D coordination polymers. The ligands were reacted with $[Cu(hfacac)_2]\cdot H_2O$, $[Zn(hfacac)_2]\cdot 2H_2O$ and $Co(NCS)_2$ under single-crystal growth conditions and the resulting crystals were analysed by X-ray diffraction analysis. Good solubility in common organic solvents of the resulting terpyridine building blocks was crucial for the successful crystallisation of the final assemblies. A variety of solubilising substituents have been used throughout this thesis.

Chapter 1 introduces the discipline of coordination polymers. After a few definitions and an overview of classic synthetic approaches to these materials, there follows an important section dealing with the topological description of coordination networks. This is accompanied by an overview of the typically used metal centres and polytopic ligands as building blocks for the assembly of coordination polymers, followed by a focus on the terpyridine compounds. Finally, the chapter concludes with some selected examples of applications to illustrate to the reader the great potential that this class of materials possesses.

Chapter 2 deals with the synthesis and coordination chemistry of V-shaped bis(3,2':6',3''-tpy) and bis(4,2':6',4''-tpy) ligands. In previous works of Newkome and coworkers, analogous V-shaped 2,2':6',2''-isomers have been shown to be valuable precursors for the synthesis of even highly sophisticated molecular constructs. However, the V-shaped bis(3,2':6',3''-tpy) and bis(4,2':6',4''-tpy) ligands used in this thesis, did not prove to be effective for the synthesis of coordination polymers, specifically the growth of single-crystals suitable for X-ray characterisation.

In **Chapter 3**, a combination of tetratopic bis(3,2':6',3''-tpy) ligands and $[M(hfacac)_2]\cdot xH_2O$ (M = Cu, x = 1; M = Zn, x = 2) led to a series of 2D coordination polymers propagating in two dimensions. These networks all share the same underlying (4,4) topology regardless of the nature of the solubilising substituent, crystallisation solvent and configuration of the metal centres.

Chapter 4 describes the reaction of tetratopic bis(3,2':6',3''-tpy) ligands with a 4-connecting metal centre, $Co(NCS)_2$. Layering setups using MeOH and chlorobenzene led to the formation of 3D assemblies with a *cds* topology. In contrast, a solvent switch from chlorobenzene to $CHCl_3$ results in a topological change to a 3D trinodal self-penetrating network. A comparison is then made with the most recent findings obtained by a former Master's candidate in the Constable-Housecroft research group.

An extension beyond the usual 2-4 connecting terpyridine ligands is made in **Chapter 5**. Several hexatopic tris(3,2':6',3''-terpyridine) and tris(4,2':6',4''-terpyridine) compounds were prepared and reacted with $[Cu(hfacac)_2]\cdot H_2O$. The 3,2':6',3''- and 4,2':6',4''-isomers possess different coordination flexibilities yielding an unexpected 1D coordination polymer and a predictable 2D network, respectively. The former is the first single-crystal X-ray characterisation of a tris(terpyridine)-based coordination polymer.

The general results of this thesis, with a brief outlook on the projects, are given in **Chapter 6**.

Publications

Part of this work has been published:

G. Manfroni, A. Prescimone, S. R. Batten, Y. M. Klein, D. J. Gawryluk, E. C. Constable and C. E. Housecroft, *Crystals*, 2019, **9**, 529.
https://doi.org/10.3390/cryst9100529

G. Manfroni, A. Prescimone, E. C. Constable and C. E. Housecroft, *Crystals*, 2021, **11**, 325.
https://doi.org/10.3390/cryst11040325

G. Manfroni, A. Prescimone, E. C. Constable and C. E. Housecroft, *CrystEngComm*, 2022, **24**, 491-503.
https://doi.org/10.1039/D1CE01531A

G. Manfroni, B. Spingler, A. Prescimone, E. C. Constable and C. E. Housecroft, *CrystEngComm*, 2022, **24**, 7073-7082.
https://doi.org/10.1039/D2CE01130A

S. S. Capomolla, G. Manfroni, A. Prescimone, E. C. Constable and C. E. Housecroft, *Helv. Chim. Acta*, 2022, e202200131.
https://doi.org/10.1002/hlca.202200131

Acknowledgements

Nobody plays alone in this world, and this work is the fruit of the contributions of countless people.

First, I would like to thank Prof. Dr. Catherine Housecroft and Prof. Dr. Edwin Constable for hosting me in their 'home' these past 4 years, because that is how I have experienced it. I still do not understand what made you take the third Italian in a row, but I am glad you did. You have the ability to lead a close-knit group, allowing a positive working atmosphere to emerge that is both professional and fun at the same time; it is rarer than you think. I wish to thank Catherine for her constant support, even in the smallest things, and for reminding me that you always need a safe parallel project when you decide to start one with a non-guaranteed success. Also, thank you for improving my written scientific English through the countless corrections both in papers and in this thesis. I am grateful to have Edwin to discuss any problems of organic synthesis, philosophical topics and to give me the freedom to play with our beloved tris(terpyridines). I have always enjoyed our fruitful discussions and your advices on both scientific and culinary matters.

I would like to thank Prof. Dr. Christof Sparr for being my second supervisor. I appreciate the time spent together and the valuable discussions at each annual meeting.

I am grateful to Prof. Dr. Katharina Fromm, who kindly agreed to be my external expert and take the time to read this thesis.

Many thanks go to the crystallographers Dr. Alessandro Prescimone and Prof. Dr. Bernhard Spingler for always dealing with disordered structures. In addition, I thank Alessandro for patiently teaching me how to use X-ray diffractometers and that tedious programme called Full-Prof. I thank the Paul Scherrer Institut for carrying out the synchrotron measurements.

Thanks to Prof. Dr. Stuart Batten for the helpful discussions and for identifying the point symbol of the trinodal self-penetrating network.

I would like to thank Prof. Dr. Catherine Housecroft, Prof. Dr. Edwin Constable, Simona Capomolla and Pietro Porqueddu for proofreading my thesis.

Thanks to the analytic team, namely Sylvie Mittelheisser, Michael Pfeffer and Jonas Zurflüh, for their excellent support regarding elemental analysis and HR-ESI MS.

A thank you goes to Beatrice Erismann and Isa Worni, for their work in the administrative area and answering all my organisational questions.

A huge thank you goes to all current and former members of the Constable/Housecroft research group. Especially Dalila, Guglielmo, Sven, Marco and Deyanira as we are all ending this journey together. Dalila for sharing a home as well as the project, and IQ 40 Lab members Guglielmo, Sven and Marco with whom we have reached the pinnacles of group intelligence and many laughs together. I could not have wished for a more pleasant working atmosphere.

My gratitude also goes to Simona, who decided to do her Master's thesis with me, from which an excellent collaboration resulted. Working with her was a great pleasure, in fact measuring her crystals until late was a pleasure not a duty. Her proofreading was fundamental to this thesis.

I would also like to thank Angela for being a very important part of my life, even though we have recently grown apart. Last but not least, I would like to thank my family and friends for their unconditional support, even from afar.

Abbreviations

2,2':6',2''-tpy	2,2':6',2''-Terpyridine
3,2':6',3''-tpy	3,2':6',3''-Terpyridine
4,2':6',4''-tpy	4,2':6',4''-Terpyridine
B_2Pin_2	Bis(pinacolato)diboron
***n*-BuLi**	*n*-Butyllithium
***n*-BuOH**	*n*-Butanol
4,4'-bipy	4,4'-Bipyridine
CB	Chlorobenzene
CHCA	α-Cyano-4-hydroxycinnamic acid
CP	Coordination polymer
CSD	Cambridge Structural Database
Dca	Dicyanamide
1,2-DCB	1,2-Dichlorobenzene
DHB	2,5-Dihydroxybenzoic acid
DMF	*N*,*N*-Dimethylformamide
DMSO	Dimethyl sulfoxide
dppf	1,1'-Bis(diphenylphosphino)ferrocene
E.A.	Elemental analysis
ESI	Electrospray ionization
EtOH	Ethanol
FT-IR	Fourier-transform infrared spectroscopy
h	Hours
Hacac	Pentane-2,4-dione; acetylacetone
Hhfacac	1,1,1,5,5,5-Hexafluoropentane-2,4-dione; hexafluoroacetylacetone
HR-ESI MS	High-resolution electrospray ionization mass spectrometry
MALDI-TOF	Matrix-assisted laser desorption ionization time-of-flight
MeCN	Acetonitrile
MeOH	Methanol
MOF	Metal-organic framework
M.p.	Melting point
m/z	Mass to charge ratio
NMR	Nuclear magnetic resonance
PLC	Preparative layer chromatography
PXRD	Powder X-ray diffraction
RT	Room temperature
SBU	Secondary building unit
THF	Tetrahydrofuran
tpt	4,6-Tris(4-pyridyl)-1,3,5-triazine
tpy	Terpyridine
UV-Vis	Ultraviolet-visible

Table of contents

1 Introduction

Coordination polymers (CPs)[1] have a long history, stretching back at least to the discovery of Prussian Blue at the beginning of the 18th century.[2] This was the earliest example of a synthetic coordination compound and was also the first modern synthetic pigment. Initially it was widely used in paintings, until it became the predominant colour of the Prussian army's uniform coat. Another early example of an extended coordination compound was a 2-dimensional (2D) structure published by Hofmann in 1897.[3] It was obtained by shaking a solution of freshly-precipitated nickel(II) cyanide in concentrated aqueous ammonia with benzene. Commonly known as Hofmann clathrate and with the general formula $[Ni(CN)_2(NH_3)]\cdot 2C_6H_6$, it was first hypothesised as a molecular compound. However, after the development of X-ray diffraction, it was possible to identify the arrangement of atoms in this compound class. Thus, it was not until 1949 that Powell and Rayner discovered that Hofmann clathrate consists of 2D layers of alternating octahedral and square planar nickel moieties bridged by CN^- ions (Fig. 1.1a).[4, 5] The structure of Prussian Blue was determined 372 years after its discovery, $Fe_4[Fe(CN)_6]_3\cdot xH_2O$, revealing a 3D lattice (Fig. 1.1b).[6] Since then, X-ray crystallography has been fundamental to the development of reticular chemistry, the study of connecting discrete chemical entities via strong bonds to create extended structures,[7] and remains to this day the main method of characterisation.

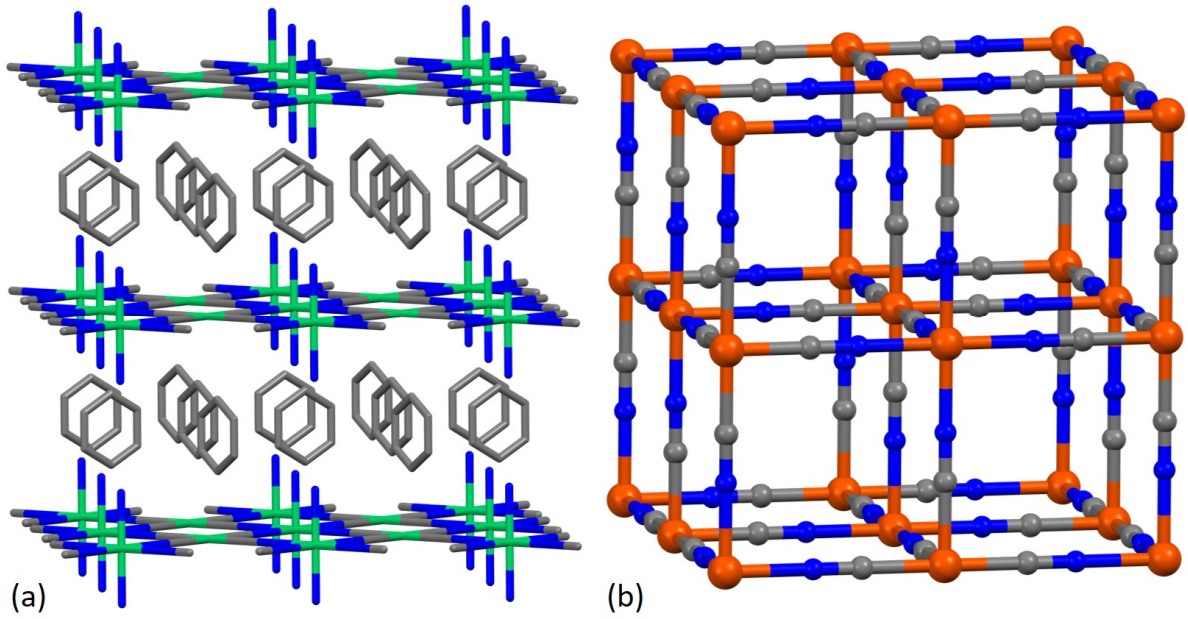

Figure 1.1 The structures of (a) Hofmann clathrate (CSD refcode HEMJIS)[8] and (b) Prussian blue (ICSD refcode 1277).[6]

It may appear surprising that it was only in the late 1980s and early 1990s that interest in these materials exploded.[9, 10] The breakthrough came with the publications of Robson, Hoskins and co-workers, who delineated a network-based methodology for the design of coordination polymers.[11-25] Their viewpoint is based on a fundamental work by Wells, who defined crystal structures in terms of topology, reducing them to a set of interconnected points (nodes).[26-28] By using the "node and spacer" approach, extended structures with attractive qualities such as porosity and catalysis can be consciously planned. These concepts, combined with the possibility of performing routine

single-crystal structural determinations, are the key factors that have permitted the proliferation of studies of these systems.

1.1 What is a coordination polymer?

According to the IUPAC definition, a coordination polymer is “a coordination compound with repeating entities extending in 1, 2, or 3 dimensions”.[29] Metal ions are linked by bridging ligands in an “infinite” array through coordination bonds (Fig. 1.2). This means that multidimensional architectures of metal complexes formed by mere weak interactions, such as hydrogen bonding or π-stacking, are not seen as coordination polymers. The ligand can be of any nature, even a simple inorganic ion, although in most cases organic molecules are considered and used. This thesis will focus only on organic ligands.

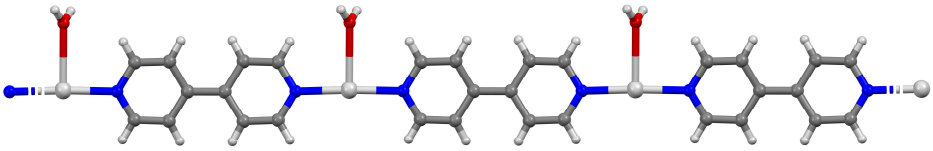

Figure 1.2 An example of a 1D-coordination polymer with 4,4'-bipyridines (4,4'-bipy) bridging silver(I) present in {[Ag_2(4,4'-bipy)$_2$(H_2O)$_2$][4-$H_2NC_6H_4CO_2$][NO_3]}$_n$·$n$$H_2O$ (CSD refcode AQAVOD01).[30] Solvent molecules and counterions have been omitted for clarity.

The term coordination network designates a subclass of coordination polymers, and for the IUPAC it is "a coordination compound extending, through repeating coordination entities, in 1 dimension, but with cross-links between two or more individual chains, loops, or spiro-links, or a coordination compound extending through repeating coordination entities in 2 or 3 dimensions”.[29] For the purpose of this thesis, only 2D and 3D coordination polymers will be called coordination networks (Fig. 1.3). There is a good reason for this. The topological approach is essential to describe 2D and 3D coordination assemblies, and from a topological point of view, a network is a set of interconnected nodes. The use of the term node in a 1D polymer has been called “subjective”,[1] as a chain or a ladder can be described unambiguously in terms of a combination of metal linkers and ligand linkers. Therefore, in order not to mix up the structural and topological definitions of networks, only coordination assemblies with topological nodes will be named coordination networks. A metal-organic framework is “a coordination network with organic ligands containing potential voids”[29]. Since it is not the main topic of this thesis, the acronym MOF will not be used to describe the structures obtained in this doctoral work.

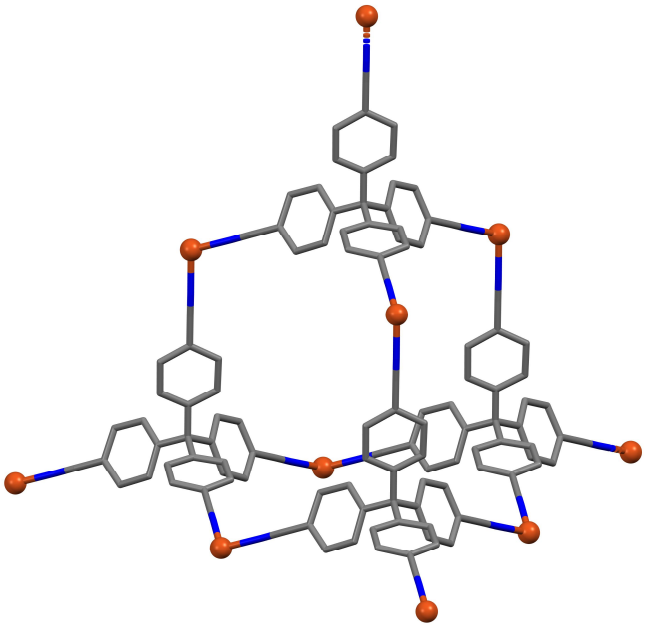

Figure 1.3 An example of a 3D-coordination network with 4,4',4'',4'''-tetracyanotetraphenylmethane and copper(I) present in $\{[Cu(C(C_6H_4CN)_4)][BF_4]\}_n \cdot nC_6H_5NO_2$ (CSD refcode JARMEU).[9] Hydrogen atoms, solvent molecules and counterions have been omitted for clarity.

1.2 Synthesis and characterisation

Coordination polymers are formed by spontaneous self-assembly from metal ions and organic ligands. Not being a stepwise and controlled approach, the prediction of the structure of the emerging coordination polymer remains challenging. There are numerous examples of structures that differ from those expected, since the outcome is influenced by various factors including reaction time, temperature, concentration, and additives (ions and solvents).[31-34] Even knowing the connectivity and the vectorial properties of the chosen metal salt and ligand, these building blocks do not necessarily behave as predicted in the resulting assembly. There have been examples of different structures containing identical components.[35, 36] One obstacle is the contribution of innumerable non-covalent interactions exhibiting little directionality during the assembly process.[34] Furthermore, polymorphs that form in the same reaction mixture have been reported and this emphasises the unpredictability of these processes.[37, 38] Being extended species, coordination polymers are typically insoluble materials. If the material dissolves, perhaps because of a strong coordinating solvent, it forms either short oligomers[39, 40] or has reacted with the solvent to become a new material.[1] The nature of the species in solution is often elusive,[41, 42] and little is known about what happens in solution just before the assembly of the coordination polymer. Thus, any solution properties are not characteristic of solid-state material.

Considering the previously mentioned critical aspects, it follows that single-crystal X-ray crystallography is fundamental to elucidating the solid-state structures, although a few simple coordination polymers have been determined directly by X-ray powder diffraction.[43] The latter remains an important technique for confirming that the structure obtained from a single-crystal is representative of the bulk material. Thus, given that their insolubility makes recrystallisation impracticable, the chemical reaction must lead directly to crystals.[44, 45]

Some species crystallise directly from mixtures of appropriate reagents.[46, 47] In these cases, the methods of slow evaporation, slow cooling or non-solvent diffusion can be used to obtain X-ray quality crystals. Mixing of solutions containing the metal ion and ligand building blocks frequently leads to the immediate precipitation of a coordination polymer. When this happens, methods that allow two separate solutions containing metal salts and ligands to diffuse slowly into each other are usually beneficial in terms of achieving crystal growth.[48-50] This is done by carefully layering one reagent solution on top of the other. A buffer layer of pure solvent is often interposed between the two solutions (Fig. 1.4a) and, in some cases, gels are used as a medium to slow the diffusion and provide support for the crystallisation (Fig. 1.4b). This technique is mainly conducted in NMR tubes, test tubes or vials. However, it is possible to use dedicated H- and U-shaped tubes (Fig. 1.4b and c), which are provided with a frit or separating gel plug in the middle.

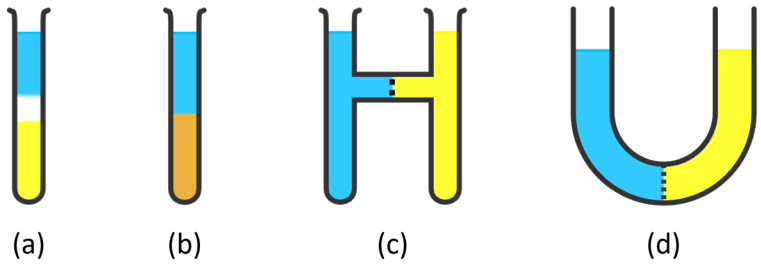

Figure 1.4 Schematic representation of four possible set-ups for slow diffusion of reagent solutions. Layering (a) with a buffer layer of pure solvent, (b) use of a gel as a diffusion medium, use of (c) H- and (d) U-shaped glassware with a fine glass sinter.

Figure 1.5 Front, 23 mL autoclave components with PTFE liner; back, 23 and 125 mL autoclaves. Maximum operational pressure and temperature: 125 Bar and 250 °C.

Solvo- or hydrothermal synthesis is a popular method, especially for preparing MOFs.[51] The relatively high pressures and temperatures enable not only the use of barely soluble or poorly reactive reagents but also can be used to synthesise stable materials or phases that are inaccessible by conventional methods under mild conditions.[52] Reactions are usually carried out in Teflon-lined autoclaves with temperatures above the solvent's boiling point under autogenous pressure (Fig. 1.5). However, solvothermal conditions can lead to unexpected chemical reactions, for example, the formation of new

ligands,[51, 52] and prolonged reaction times may lead to product decomposition.[53, 54] On an industrial scale, MOFs can be prepared by electrochemical synthesis.[55] Anodic dissolution into reaction mixtures that contain both the ligand and electrolyte provides the metal ion. This offers a short reaction time under milder conditions and real-time control of the applied potential. Microwave-assisted, microemulsion, sonochemical or mechanochemical synthesis are also among established preparative methods.[56]

1.3 Topological description – Classification and nomenclature of the networks

Topological descriptions permit the schematisation of intricate crystal structures into a collection of joined branching points (also described as a graph). Introduced by Wells for the study of inorganic compounds,[26, 28] this concept makes it possible to compare chemically different materials, revealing the close underlying relationships.[44] This approach has been known as reticular chemistry.[57, 58]

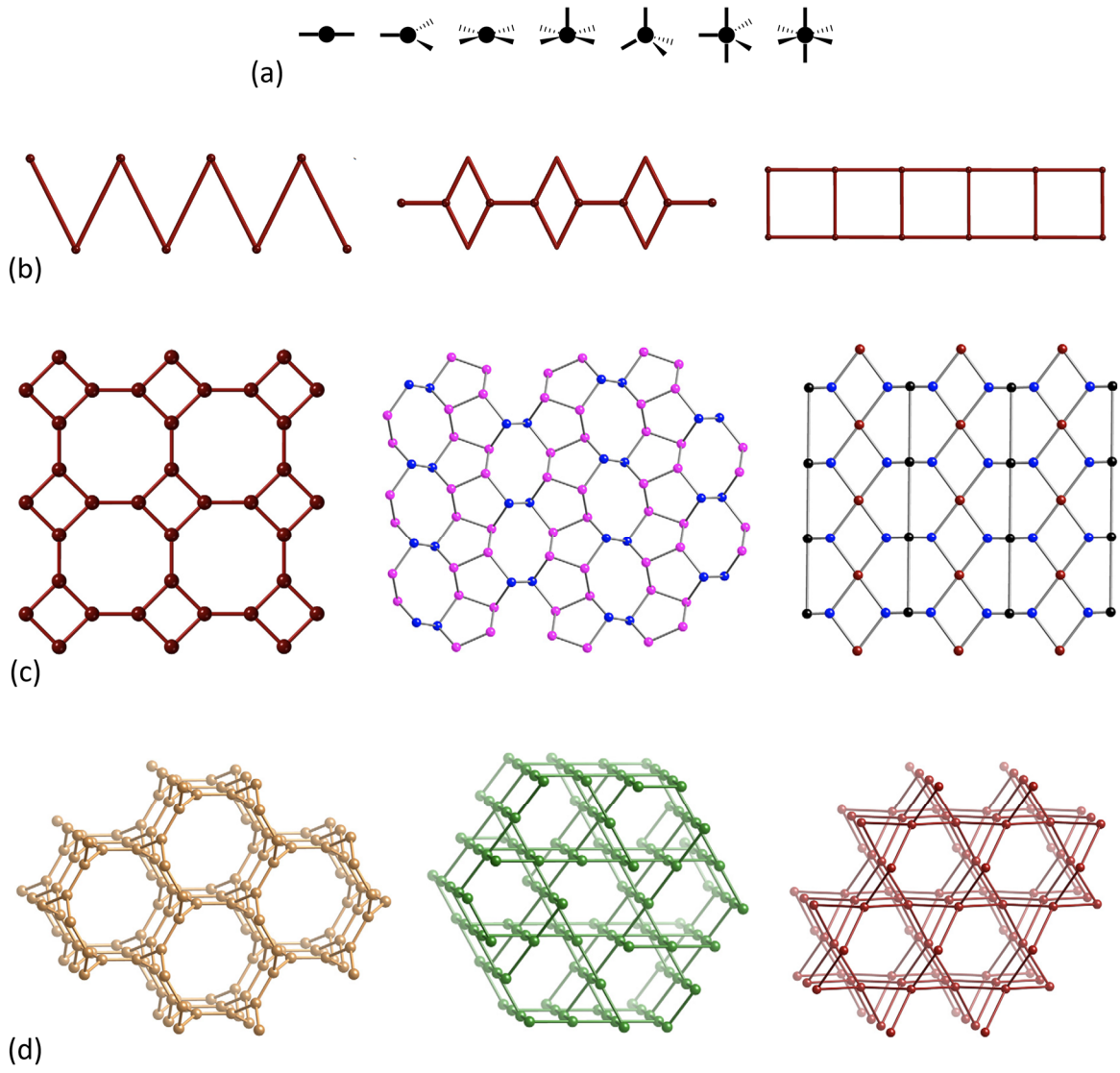

Figure 1.6 (a) Examples of nodes and linker commonly encountered with ligands and metal centres. (b) 1D chains with increasing complexity. (c) 2D networks with one (left), two (middle) and three (right) unique nodes. (d) Different 3D coordination polymers. Left, a 3-connected net; middle, a 4-connected net with square planar nodes; left, network with tetrahedral nodes. Reprinted from S.R. Batten in *Comprehensive Coordination Chemistry III*, eds. E.C. Constable, G. Parkin, L. Que, 3rd edn, Elsevier, 2021, vol. 2, pp. 368-388, with permission from Elsevier.

The coordination network is a periodic pattern of nodes interconnected by linkers, it follows that the number of unique types of nodes is finite. A node must be connected to three or more other nodes via linkers. If a node is only connected to two nodes, then it is not a node but a linker. In other words, a linker connects only two nodes.[1] The chemical nature of the component is not relevant and both ligands and metal centres can behave as nodes (Fig. 1.6a).[44] A selection of 1D-, 2D- and 3D-coordination polymers with different complexities and nodal geometries are depicted in Figure 1.6.

Extended assemblies are formed by either combinations of metal nodes and ligand linkers, metal linkers and ligand nodes, metal nodes and ligand nodes, or metal linkers and ligand linkers.[59] As shown in Scheme 1.1, sometimes different approaches are possible when assigning nodes.[60] The ligand can be seen either as a 4-connecting node or as a pair of 3-connecting nodes. A node with connectivity 4 has the advantage of representing the entire single molecule. Whatever the choice, it is important that the nodes are unambiguously defined and support the better comprehension of the structure.

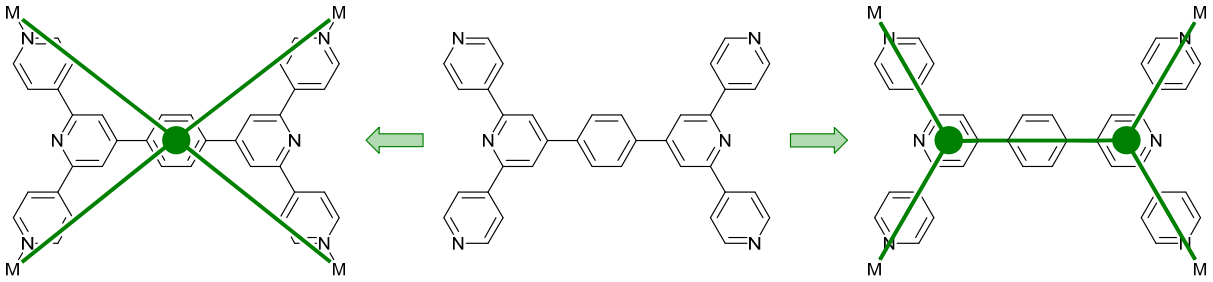

Scheme 1.1 An organic ligand that can be deconstructed either as a single 4-connecting node or as a pair of 3-connecting nodes. Figure redrawn and based on S.R. Batten in *Comprehensive Coordination Chemistry III*, eds. E.C. Constable, G. Parkin, L. Que, 3rd edn, Elsevier, 2021, vol. 2, pp. 368-388.

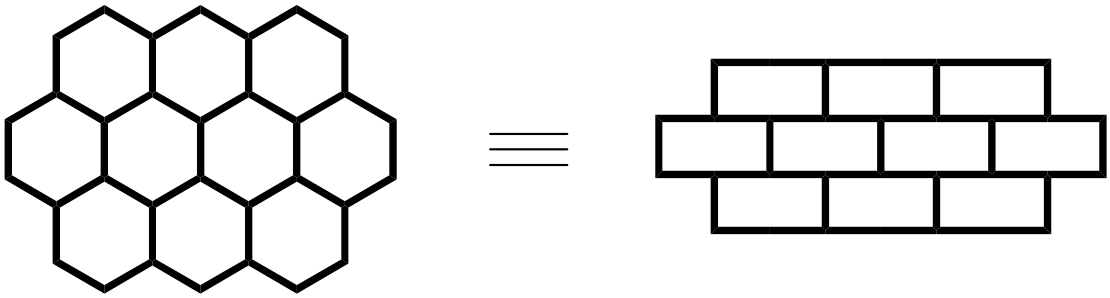

Figure 1.7 Two topologically identical networks with a different nodal geometry. Figure redrawn and based on S.R. Batten in *Comprehensive Coordination Chemistry III*, eds. E.C. Constable, G. Parkin, L. Que, 3rd edn, Elsevier, 2021, vol. 2, pp. 368-388.

Since the network definition is purely topological, it does not depend on the geometric arrangement of the nodes. If two networks can be converted into each other through distortion without breaking bonds they are considered as being topologically identical.[1, 44] As an example, the honeycomb-like network in Fig. 1.7 has trigonal nodes that are equivalent to the T-shaped nodes in the brick-work-like network. The local chemical geometry may happen to be different from both the node geometry and its connectivity. In $Zn(dca)_2$ (dca = dicyanamide), the zinc(II) centres have a tetrahedral coordination sphere but as nodes they form a planar network (Fig. 1.8).[61] Hexatopic ligands and octahedral metal ions can be 3-connecting nodes as shown in Scheme 1.2.

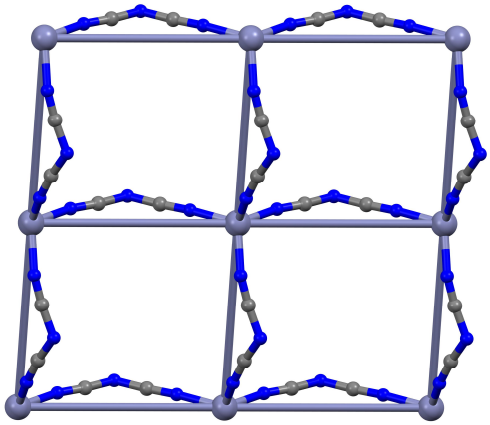

Figure 1.8 Part of the square planar network in $Zn(dca)_2$; the Zn…Zn vectors which define the 2D net are highlighted (CSD refcode HAXFIV).[61]

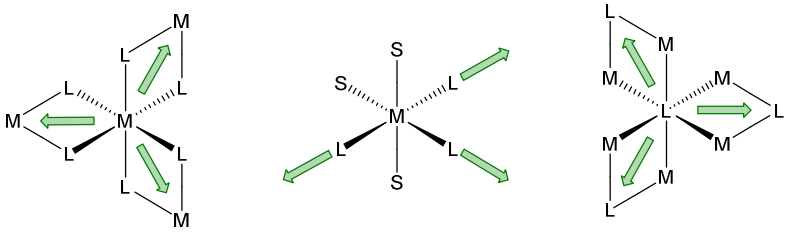

Scheme 1.2 Examples of octahedral metal centres and a hexatopic ligand behaving as 3-connecting nodes. Figure redrawn and based on S.R. Batten in *Comprehensive Coordination Chemistry III*, eds. E.C. Constable, G. Parkin, L. Que, 3rd edn, Elsevier, 2021, vol. 2, pp. 368-388.

After identification, the network can be named with the correct descriptive terminology. This is a prerequisite for recognising any correlation between the topology of the underlying net and material properties. Several notations are commonly used in the literature all based on topological descriptors referring to the mathematical properties of the network. Each unique node has a finite number of smallest circuits of which it is a component. The shortest circuit is the smallest cycle, in terms of the number of nodes, that can be traversed that includes two linkers originating from a particular node. In platonic uniform nets, all nodes have the same connectivity and all the shortest circuits have the same size.[44] Therefore, these simple nets can be described with the (n, p) notation, where (n) denotes the size of the shortest circuit and (p) is the connectivity of the unique node.[26-28] Thus, the planar network in $Zn(dca)_2$ (Fig. 1.8) has the symbol (4,4), with the shortest circuits containing four nodes with connectivity four, all equivalent (Fig. 1.8). Honeycomb- and brick-work-like grids in Fig. 1.7 are examples of (6,3) nets. For more complex structures, where not all the shortest circuits have the same size, the "point symbol" (erroneously known as the Schläfli symbol) is used as descriptor.[1, 44] A given p-connected node, i.e. having p linkers, has p(p-1)/2 unique pairs of linkers from each of which a shortest circuit is associated.[1] Then, the multiplicities and sizes of these cycles can be combined into a "point symbol". Proceeding from the easiest case (Fig. 1.9), the (4,4) net, the 4-connecting node has six unique pairs of linkers generating four 4-membered rings and two 6-membered cycles (including the two pairs of *trans* linkers). The point symbol of this node is hence $(4^4.6^2)$. Note that the connectivity of the node (p) is indirectly given by the sum of the exponents (s) according to the relation $s = p(p-1)/2$.[44]

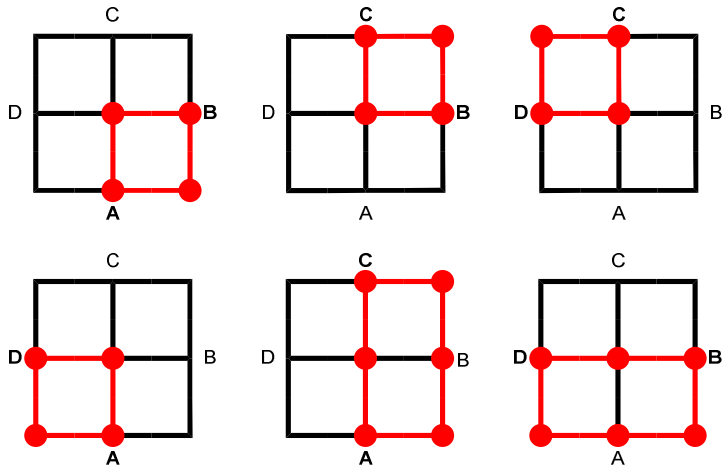

Figure 1.9 Considering the central node, six shortest circuits are counted (red) arising from the unique pairs of linkers A-B, B-C, C-D, D-A, A-C and B-D.

If a network has more than one unique node, the point symbols can be grouped. Each pair of brackets symbolises a node and a subscript is placed to indicate its relative ratio to the others. Figure 1.10 shows a network with two unique nodes (binodal) with a point symbol of $(4.6^2)_4(6^4.10^2)$; from the subscripts, it can be deduced that the 3-connected and 4-connected nodes are in a 4:1 ratio.

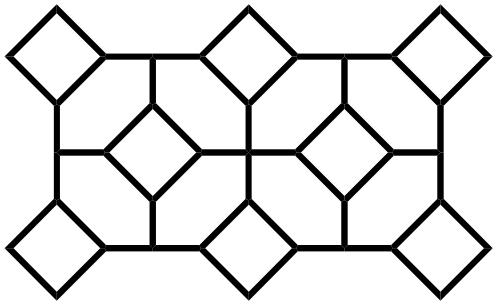

Figure 1.10 Schematic representation of the $(4.6^2)_4(6^4.10^2)$ 2D network.

The advantage of the point symbol system is that it can describe any network regardless of its complexity. However, this is not unique and different networks may share the same point symbol.[44] To overcome this, a further nomenclature derived from topological codes used for zeolites has been developed.[62] This is based on 3-letter codes that are uniquely assigned to a given topology deposited in an open access database.[57, 63] For example, inorganic compounds such as $CdSO_4$, NbO, PtS and diamond have given their names to the corresponding *cds*, *nbo*, *pts* and *dia* networks. It follows that structures with novel topologies, lacking a 3-letter code, must be described with the point symbol or in other ways (e.g. vertex symbols). Two 4-connected 3D networks will appear in this thesis, namely the *cds* and *pts* networks, and will consequently be described here (Fig. 1.11). The *cds* network is achiral and uninodal with a limiting square-planar configuration of nodes (Fig. 1.11a). Half of the neighbouring planar nodes are perpendicular to each other and half of the nodes are coplanar. Five of the six smallest circuits are 6-membered and one includes 8 nodes (point symbol $(6^5.8)$). A portion of the *cds* network with one of the equivalent nodes (emphasised in red) with its related six shortest circuits is illustrated in Fig. 1.11a. The *pts* net is also a 4-connected achiral network, but it is binodal, with an equal number of square-planar and tetrahedral nodes (orange and blue in Fig. 1.11b). The point symbol for the *pts* network is $(4^2.8^4)(4^2.8^4)$ indicating, regardless of the node, two shortest circuits containing four nodes

and four shortest circuits consisting of eight nodes. The tetrahedral and square nodes are arranged in such a way that each node bonds only to nodes of the other type (Fig. 1.11b).

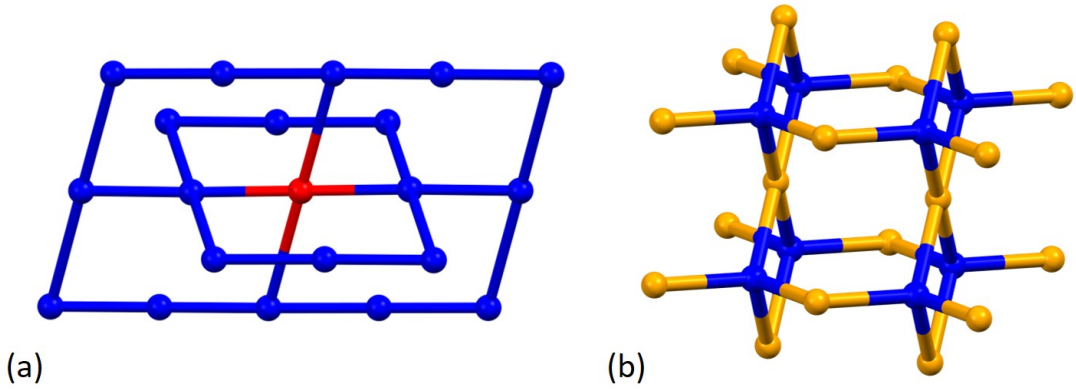

Figure 1.11 (a) One of the equivalent nodes (red) and its six smallest circuits (blue) in the *cds* network. (b) Part of a *pts* network with alternating tetrahedral (blue) and square-planar (orange) nodes.

1.4 Building blocks

Coordination polymers are assembled through the self-recognition and association of polytopic ligands with coordinatively unsaturated metal salts. The geometry of the building blocks, particularly the spatial arrangement of their acceptor and donor subunits, plays an important role and must be chosen according to the planned architecture.[1, 34] As mentioned, serendipity is always around the corner and is the source of unplanned structures.[31-34] This inconvenience is also associated with the structural (organic molecule) or coordinative (metal centre) flexibility of the chosen building blocks. The use of mechanically rigid ligands and metal ions or clusters with well-defined coordination directionalities increases control over the final architecture. The size of the ligand can be critical for the resulting pore size, which in turn is decisive for the corresponding properties of the network.[64]

The coordination chemistry of metal cations, particularly that of the *d*-block metals, is very well developed and understood in terms of ligand affinity, donor types, and coordination geometries. First-row transition metals have been popular due to their kinetic lability, predictable coordination behaviour and broad availability.[1, 65] A reversible coordination bond allows errors during the assembly and crystal growth, to be corrected.[1] This feature contrasts with the covalent bonds of purely organic polymers, the formation of which is mainly irreversible. The presence of coordination bonds in coordination polymers introduces greater versatility in the directionality of bonds compared to organic polymers. Organic chemistry rarely offers orthogonal angles whereas these are easily accessible in metal complexes.[66] Metal cations that favour linear coordination, such as Au(I) and Hg(I), can be linked via a simple organic spacer to provide a one-dimensional chain structure. A two-dimensional structure can be constructed using trigonal-planar (e.g. Cu(I)) or square-planar metal centres (e.g. Pd(II), Pt(II)), while three-dimensional architectures can potentially be achieved by connecting tetrahedral (e.g. Zn(II), Cu(I)) or octahedral metal centres (e.g. Co(II/III), Ni(II), Fe(II/III), Mn(II/III), Zn(II), Cd(II)); pentacoordination is less common.[1, 44, 58] Appropriate capped ligands make it feasible to decrease the number of unsaturated metal coordination sites. Higher connectivities come from lanthanoid metal ions, which are commonly used due to their magnetic and luminescent properties.[67, 68] However, the latter pose a non-trivial challenge caused by their essentially ionic nature: the lability of lanthanoid metal centres, the variety of geometries and coordination numbers are important contributions to the

difficulty in predicting structures. Further factors that boost the construction possibilities of assemblies based upon *d*-block metals are the different size, hardness/softness and ligand-field stabilisation energy of the metal ions.[34, 69] Moreover, aggregates of metal ions can be incorporated into coordination polymers, serving as secondary building blocks (SBUs) for the overall structure.[70] Classic examples are the paddle-wheel motif of copper(II) acetate ($Cu_2(OAc)_4$) and the oxygen-centred Zn_4O cluster present in numerous carboxylate based MOFs.[70, 71]

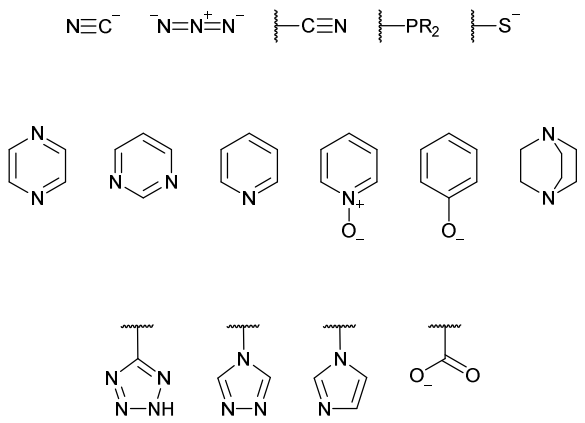

Scheme 1.3 Examples of functional groups used in the assembly of coordination polymers.

The ligand has to bridge metal ions and therefore must possess two or more spatially separated *n*-dentate metal-binding domains. The term *n*-topic indicates the ability of the ligand to coordinate *n*-different metal centres. It is worth remembering that the topicity of a ligand does not necessarily correspond with the number of available coordination sites. For example, 2,2'-bipyridine is a bidentate ligand and, because of the propensity for chelation to a metal centre, it is usually monotopic. A ligand can be either neutral, anionic or cationic, although the latter is rare.[72] It acts as a Lewis base through the donation of free electron pairs and the nature of the bond can range from near-ionic to near-covalent. Examples of functional groups are halides, pseudohalides (cyanides, azides and nitriles donors), heterocycles with O-, N- and S-donors, phosphanes, sulfides, N-oxides and carboxylates (Scheme 1.3). The two predominant ligand classes consist of those containing O- and N-donor atoms,[72] wherein the most successful metal-binding domains are carboxylates (Scheme 1.4), pyridines and related *N*-heterocyclic compounds (Scheme 1.5).[1, 73] Polycarboxylates are anionic ligands with hard oxygen donors. They are abundantly used for the synthesis of MOFs due to their strong bonds and flexible coordination geometry.[1] A carboxylate RCO_2^- can coordinate in either monodentate or bidentate modes. In addition, a single functional group even binds up to five metal centres, which explains its tendency to form metal clusters *in situ*.[70, 73] Benzene polycarboxylates are particularly suitable for the synthesis of porous structures.[74-76] Oligopyridines are neutral Lewis bases that can also act as hydrogen bond acceptors.[73] They frequently occur for the preparation of *d*-metal coordination polymers[72] and have limited literature for extended structures with lanthanides.[77] The pyridine group possesses only one coordination mode. Thus, the vectorial properties of a polypyridine ligand can be tuned relatively easily by choice of different numbers and spatial relationship of the pyridine donors.

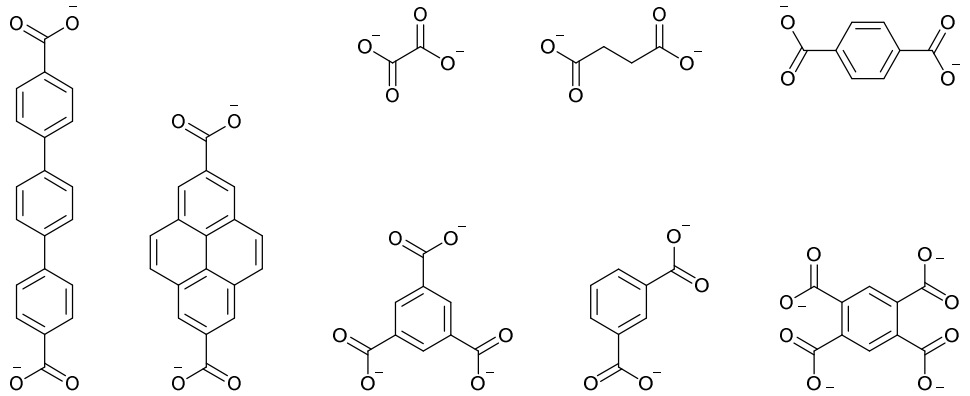

Scheme 1.4 Examples of anionic polycarboxylates used as building blocks in coordination polymers.

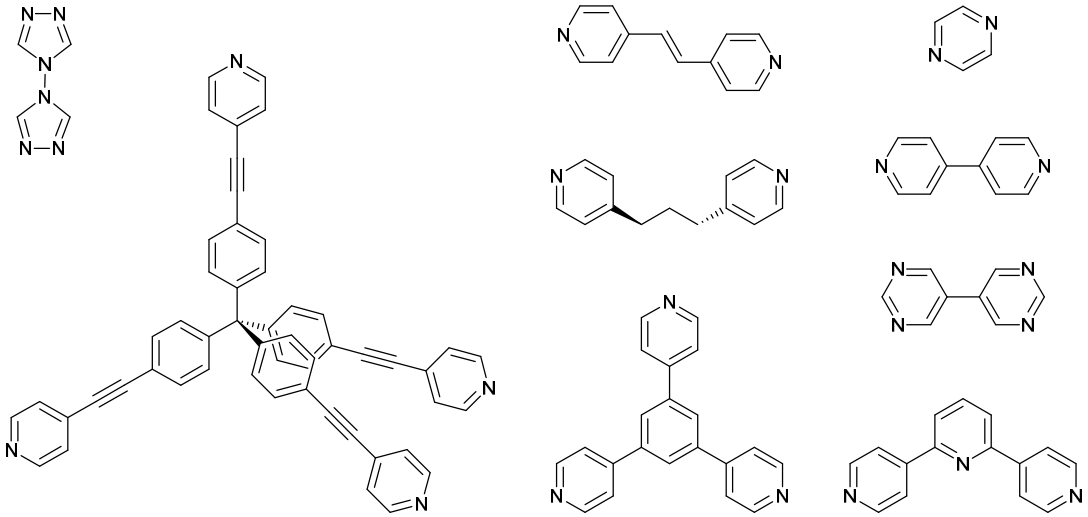

Scheme 1.5 Examples of neutral *N*-heterocyclic ligands used in the assembly of coordination polymers.

The varying affinity of different metal ions towards nitrogen and oxygen donor groups is exploited for the synthesis of heterometallic compounds. An example is the assembly of mixed 3*d*-4*f* coordination polymers by using heterotopic ligands (e.g. pyridine carboxylates).[68, 78] Of course, there is also the possibility of using more than one kind of ligand, perhaps with different flexibilities, connectivity and donor atoms.[79] In general, the use of mixed building blocks provides unique functionality to the coordination polymer that cannot be achieved from the use of a single metal centre or ligand alone.[74]

1.5 Terpyridine ligands

Terpyridine (tpy) ligands are well-established N-donors in coordination chemistry, and have long been successfully exploited for the assembly of discrete and polymeric coordination complexes.[80] The use of these ligands is advantageous due to their ability to participate in π-stacking and directional hydrogen-bonding interactions in addition to binding metal centres. Of the 48 possible isomeric terpyridines, 2,2':6',2''-tpy is the archetypal. It is a monotopic chelating ligand (Scheme 1.6), although the 2:2':6',2''-tpy domain also exhibits multiple metal-binding modes.[81] Thus, if the organic ligand contains a 2:2':6',2''-tpy metal-binding domain, a second-binding domain, such as carboxylate or a heterocycle, is needed to generate an {M(2,2':6',2''-tpy)$_2$} centred 'expanded ligand' (Scheme 1.6).[82]

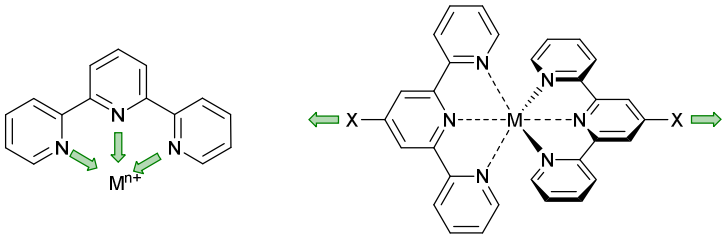

Scheme 1.6 Structure of 2,2':6',2''-tpy as a tridentate κ^3 chelating unit (left), and the {M(2,2':6',2''-tpy)$_2$} motif with X donor groups in the 4'-positions.

A contrasting approach is to employ oligopyridines with divergent sets of donor atoms. Of all the isomers, however, only the symmetrical 4,2':6',4''-terpyridine (4,2':6',4''-tpy) and 3,2':6',3''-terpyridine (3,2':6',3''-tpy) have been widely used in the last decade,[59, 80, 83-86] along with their 4'-functionalized derivatives. The ligands 4,2':6',4''-tpy and 3,2':6',3''-tpy coordinate through the outer pyridine donors, leaving the central pyridyl-N atom unbound (Scheme 1.7). Coordination polymers with uncoordinated Lewis-base sites within solvent-accessible channels have been considered as potential candidates for small-molecule and ion detection applications,[80, 86-89] e.g. through C-H…N pyridine hydrogen bond formation.[80] These tpy isomers possess different vectorial properties of the N-donor set (Scheme 1.7). While 4,2':6',4''-tpy offers a fixed V-shaped metal-binding domain, the less explored isomer 3,2':6',3''-tpy has a greater conformational flexibility which arises from rotation around the inter-ring C-C bonds connecting the pyridine rings, leading to a more variable and less predictable network assembly.[59]

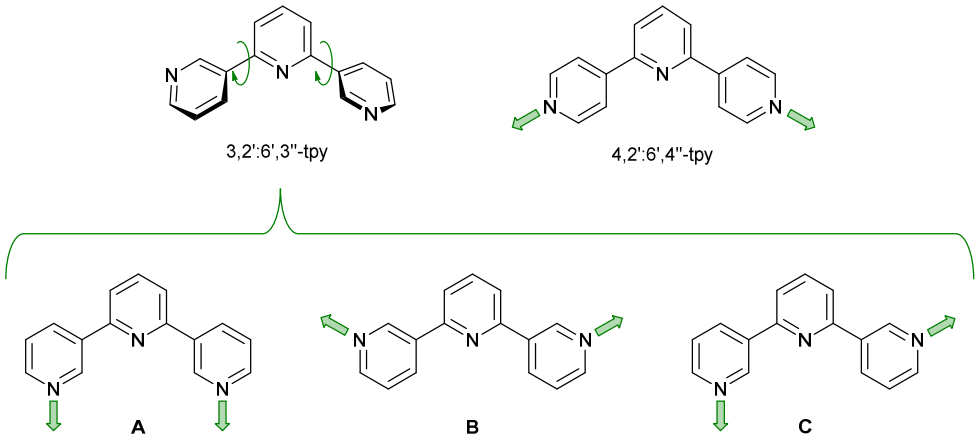

Scheme 1.7 Divergent binding mode of 4,2':6',4''-tpy, and some of the possible binding modes that 3,2':6',3''-tpy can adopt via inter-ring C-C bond rotation. The two tpy isomers coordinate only through the outer N atoms.

Ditopic ligands such as those in Scheme 1.7 have a limited role as 2-connecting linkers and by connecting multiple tpy domains, the ligands can act as directing nodes in the assembly of multidimensional architectures. Two 4,2':6',4''-tpy or 3,2':6',3''-tpy units, connected by a spacer, have the potential to function as a 4-connecting node (Scheme 1.8).[59, 85, 86, 90] This is because the four pyridine metal-binding domains are divergent with respect to one another, making the ligand tetratopic.

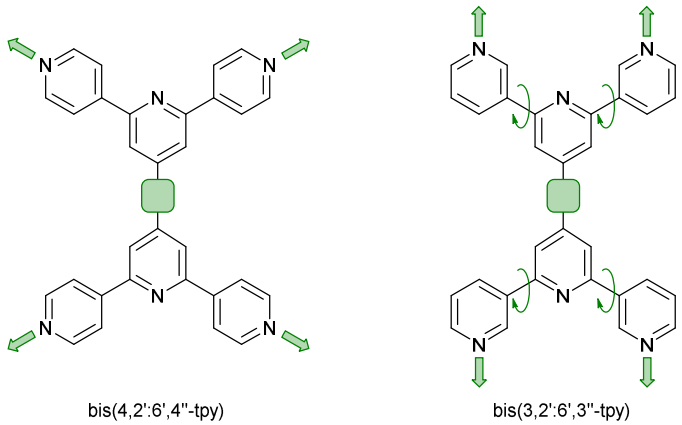

Scheme 1.8 Tetratopic ligands resulting from connecting two 4,2':6',4''-tpy or 3,2':6',3''-tpy domains. The green spacer represents any linker. Only one of three possible planar conformations of 3,2':6',3''-tpy is shown.

Similar to their respective mono(terpyridine) ligands, a transition from a bis(4,2':6',4''-tpy) to bis(3,2':6',3''-tpy) ligand is accompanied by greater vectorial flexibility. However, rotation about the tpy-spacer C–C bonds provides an additional degree of freedom, and indeed the two tpy units together may exhibit planar or pseudo-tetrahedral limiting geometries (Scheme 1.9). The bis(3,2':6',3''-tpy) ligands contained in the coordination networks obtained in this thesis belong to the former limiting conformation.

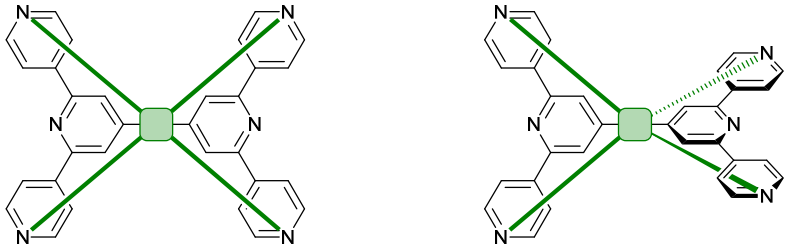

Scheme 1.9 The planar and pseudo-tetrahedral limiting conformations that the tetratopic bis(4,2':6',4''-tpy) ligand can adopt. Bis(3,2':6',3''-tpy) ligands can adopt similar conformations, but complicated by the varying conformations of each 3,2':6',3''-tpy domain (see Scheme 1.7).

The choice of the spacer has a major impact on the assembly of the coordination polymer. Not only does it determine the spatial orientation of tpy domains, but also the substituents, such as *n*-alkyloxy groups, enhance the solubility of the ligand. Nevertheless, the chain length and shape have a profound impact in orienting the assembly.[59, 85, 90] Yoshida and co-workers reported the synthesis and structural determination of the first coordination polymer with a bis(4,2':6',4''-tpy) in 2013,[91] and further examples followed.[85, 90] However, the coordination behaviour of bis(3,2':6',3''-tpy) ligands remains little explored.[50, 91, 92] Of course, a third terpyridine domain can be added to build hexatopic ligands (see Chapter 5). The tris(3,2':6',3''-tpy) and tris(4,2':6',4''-tpy) compounds were chosen to demonstrate the possibility of extending terpyridine ligands beyond the usual 2-4 connections for the synthesis and characterisation of coordination polymers.

The 4'-aryl functionalised terpyridines are readily accessible using the Wang and Hanan's one-pot protocol,[93] which is based on the general method of Kröhnke,[94] although there are some serendipitous instances in which cyclic products are favoured.[95] Aromatic aldehydes can be reacted with 2-, 3- or 4-acetylpyridine in the presence of KOH and aqueous ammonia to give the corresponding isomers

2,2':6',2''-, 3,2':6',3''- and 4,2':6',4''-tpy. The mechanism of the reaction with 3-acetylpyridine in EtOH is illustrated in Scheme 1.10.

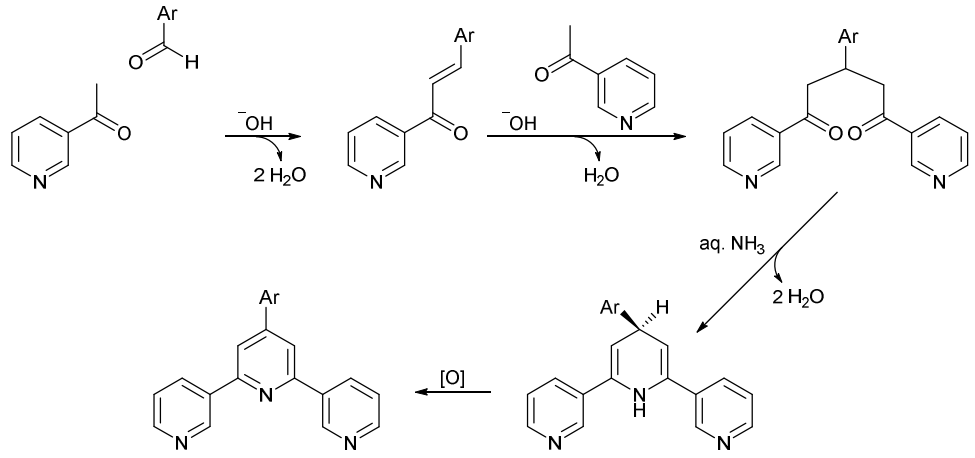

Scheme 1.10 General route to 4'-aryl-3,2':6',3''-terpyridines.

Deprotonation by KOH provides the enolate of 3-acetylpyridine. The nucleophile reacts with the arylaldehyde in an aldolic condensation to give an enone. A Michael addition of a second enolate of 3-acetylpyridine then affords a 1,5-diketone. This is usually a soluble species which may or may not be isolated. Addition of aqueous ammonia leads to a ring closing reaction forming a 1,4-dihydropyridine as inner ring, which undergoes aerial oxidation to the desired 3,2':6',3''- terpyridine.[93, 94] The resultant tpy is usually poorly soluble in the ethanol-water mixture and precipitation occurs. This reaction protocol is valid for a wide variety of aromatic mono- and dialdehydes.[93, 94] In contrast, difficulties have been encountered by this author using aryl trisaldehydes. In some cases, solvent exchange to THF was sufficient for a successful reaction. However, in most instances different synthetic approaches were necessary, such as Suzuki cross-coupling.[96]

1.6 Applications

Coordination polymers exhibit a variety of structural characteristics, such as hole shape and size, high specific surface areas, presence of unsaturated coordination sites, thermal stability and so on. Many researchers have proposed widespread potential applications included catalysis,[97, 98] gas capture,[99, 100] molecular separations,[101-104] proton conduction[105] and sensing.[106, 107] As Janiak stated, "solid-state architecture determines function".[34]

Coordination polymers that maintain a porous structure once the hosted solvent molecules have been removed are perhaps the most studied assemblies. Zeolytic behaviour is a much sought-after feature; the reversible passage of molecules within the structure is important for selective sorption, molecular recognition, gas storage or catalysis. Moreover, the control over the design and synthesis of coordination polymers is much greater than for zeolites.[108] It should come as no surprise that coordination polymers with a high specific surface area three times higher than the maximum results achievable with zeolites have been obtained,[109-112] although the latter have stronger bonds and are therefore more stable.[34] Already in the early 2000s, Yaghi described series of isoreticular MOFs with approximately 56% to 91% free volume (Fig. 1.12).[76] For some members of the series, the ability to store CH_4 or H_2 was tested.[76, 113]

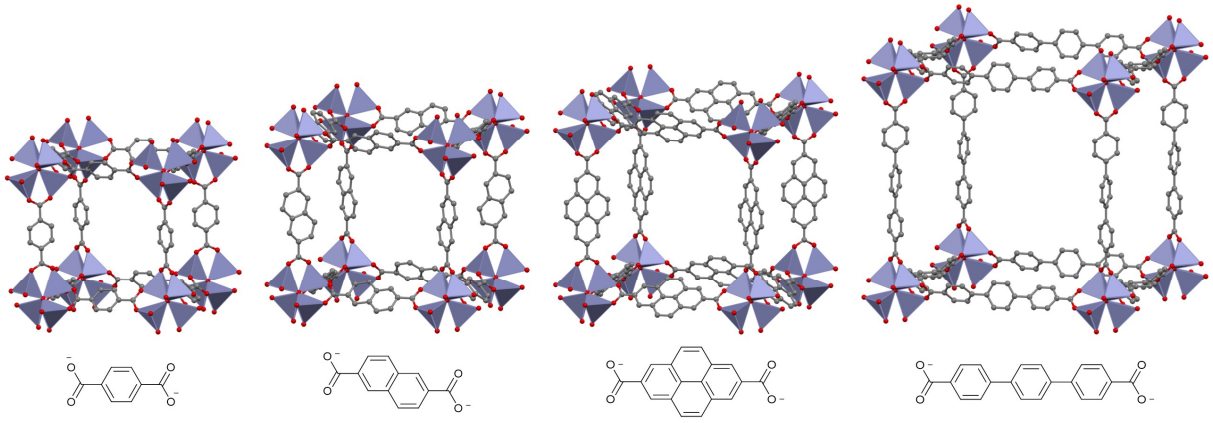

Figure 1.12 Cubic fragments of 4 (CSD refcode EDUSIF, EDUTUS, EDUVOO and EDUWAB) of the 16 isoreticular 3D-MOFs described by Yaghi. The blue tetrahedrons are the coordination spheres of the Zn centres and the chosen dicarboxylate ligand for each polymer is schematised below.[76] The figure was redrawn using data from the CSD.

Coordination polymers designed for selective gas sorption are based either on size exclusion, i.e. the cavities may take up smaller molecules but not larger ones, or on preferential binding energies of one gas molecule over another. CPO-27 (MOF-74), shown in Fig. 1.13, has tuneable gas absorption properties depending on the chosen metal centre.[114, 115] For H_2 and CO_2, the selectivity arises from the combination of polarisability of the unsaturated metal centres and steric effects resulting from the metal-ligand bond lengths. The affinity of the metals centres towards H_2 has been ranked as $Ni^{2+} > Co^{2+} > Mg^{2+} > Zn^{2+}$ and $Mg^{2+} > Ni^{2+} > Co^{2+} > Zn^{2+}$ towards CO_2.[116] Once all the metal sites are occupied, the network loses its selectivity due to its large pores. Functionalisation of CPO-27 and similar networks with amine-based ligands improved the chemisorption of CO_2.[117, 118]

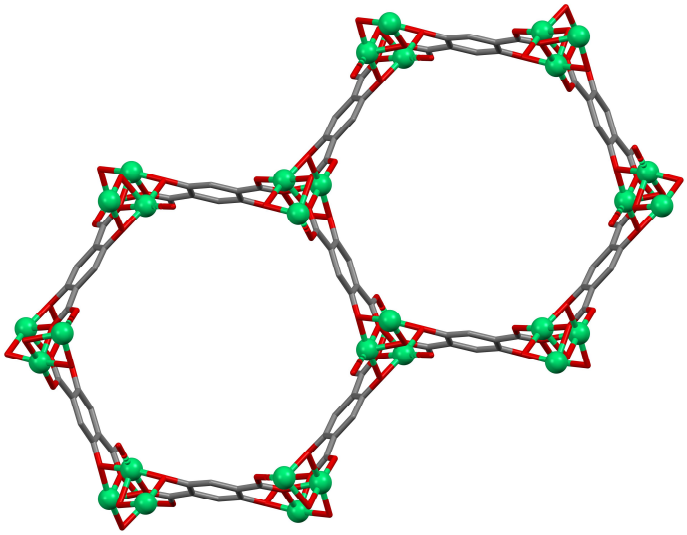

Figure 1.13 Part of the structure of Ni-MOF-74 (CSD refcode LECQEQ) viewed down the c-axis. Ni = green.[114]

A curious application of coordination polymers with permanent porosity is the crystalline sponge method.[119-121] Even today, there are small molecules that are difficult to crystallise and therefore lack structural determination. They are usually characterised by NMR spectroscopy, but in this way, some information is lost, such as absolute configuration for chiral molecules. The procedure consists of the incorporation and orientation of guest molecules inside a single-crystal of a porous structure. Since

the host material is crystalline, the guest molecules will occupy the pores with the same periodicity, thus enabling structural determination by single-crystal X-ray diffraction. Fujita and co-workers first developed this technique. They constructed a 3D assembly by combining $Co(NCS)_2$ and 4,6-tris(4-pyridyl)-1,3,5-triazine (tpt), and a single-crystal of the porous 3D assembly $[Co_3(NCS)_6(tpt)_4]_n \cdot x$*n*(solvent) was immersed in a saturated toluene solution of tetrathiafulvalene. X-ray structural determination showed the presence of four tetrathiafulvalene molecules in each Co_6tpt_4 octahedral chamber motif.[119]

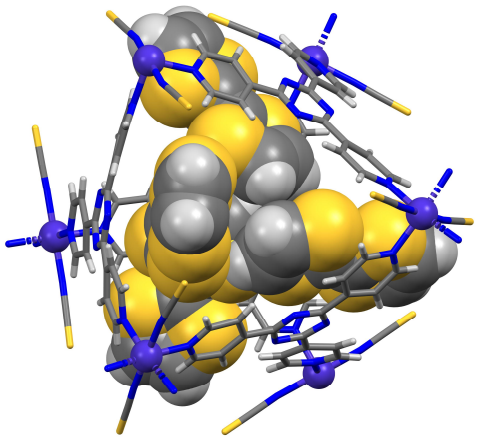

Figure 1.14 Crystal structure of an isolated Co_6tpt_4 octahedral cage with four encapsulated tetrathiafulvalene molecules (CSD refcode PUZLUS). Co = purple.[119]

Insolubility, combined with porosity and the possible presence of exposed reactive sites, provided the impulse for investigating these materials as heterogeneous catalysts. It is impossible not to mention the first example reported by Fujita in 1994 where he describes the catalysed reaction of cyanosilylation by using coordinatively unsaturated cadmium centres in the (4,4)-network.[122] Chiral porous coordination polymers are aimed at enantioselective sorption/separation or asymmetric catalysis. Regarding the latter, extremely high enantioselectivities (95-99%) have already been achieved in several asymmetric catalytic reactions. Despite this, there are still some critical aspects related to catalytic efficiency, thermal, hydrolithic and/or under oxidising conditions stability that do not make them industrially mature at present.[123]

Not all the interesting properties of coordination polymers can be traced back to the search for porous materials. One example is the design of magnetic coordination polymers. For these materials, the priority is to achieve strong coupling between the spin carriers, usually paramagnetic metals and less commonly organic radicals (or both), and therefore the distance between them must be as short as possible. This is achieved by using ligands that favour short oxo-, cyano- or azido-type bridges.[124] Another hot topic is the great potential of coordination polymers in medical imaging, electro-optical devices and chemical or biological detection applications. These assemblies can have the most diverse luminescent behaviour, as emission can be based on metal ions, organic ligands, and adsorbates that can interact with them.[125] The examples mentioned here are just a small drop in the ocean of the study of the applications of coordination polymers.

2 Angular bis(terpyridine) ligands: Ether and sulfide spacers

2.1 Motivation

The functional properties of a coordination assembly are often determined by how its constituents, in particular the metal-binding domains, are spatially arranged. A control over this arrangement is a formidable challenge. As mentioned in the introduction, the resulting architecture is influenced by the ligands and metal ions as well as the synthesis conditions. The coordination chemistry of the most studied tpy isomer bis(2,2':6',2''-tpy) is so well developed that, through the choice of the proper metal centres and with the right ligand design, the assembly process can be controlled to produce highly sophisticated discrete assemblies.[126-136] Angular bis(2,2':6',2''-tpy) ligands have been widely and successfully employed for the formation of metallopolygons, i.e. metallomacrocycles with well-defined vertices.[127, 131-142] Within this ligand class, the strategy to achieve the desired geometric shape is to tune the directional properties of the ligand by defining a fixed internal angle through which the metal-binding domains are linked. This method was called the ligand "corners" strategy as opposed to the directional bonding approach, in which free coordination sites of a metal centre dictate the internal angle of the metallomacrocycle.[143] Representative examples are provided by Newkome and co-workers, where rigid V-shaped bis(terpyridine) linkers yield various geometrical shapes depending on the angle and nature of the spacer (Scheme 2.1 and 2.2).[138, 139]

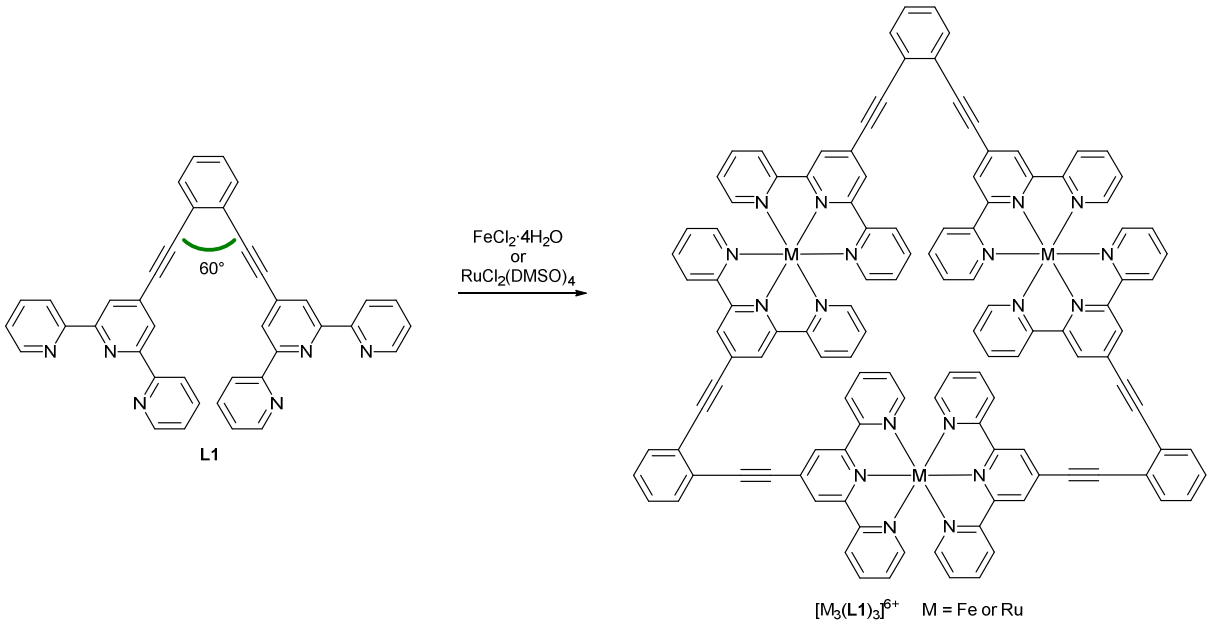

Scheme 2.1 Ligand **L1** has a predefined internal angle of 60° and directs the assembly of a metallotriangle.

Metallotriangles are easily obtained using building blocks with predefined internal angles of 60°. As shown in the Scheme 2.1, symmetrical **L1** reacts with $FeCl_2 \cdot 4H_2O$ or $RuCl_2(DMSO)_4$ to give $[Fe_3(\mathbf{L1})_3]^{6+}$ and $[Ru_3(\mathbf{L1})_3]^{6+}$, respectively.[139] Moving to 1,3-substituted arene cores, the internal angle becomes 120°, ideal for assembling metallohexacycles. One example is shown with ligand **L2** in Scheme 2.2.[138] Although **L2** is a rigid ligand with a well-defined angularity, the nature of the substituents on the central arene ring has a profound impact on the final geometry. Related ligands to **L2** with different substituents form mixtures of different sized metallocycles.[131, 140, 141]

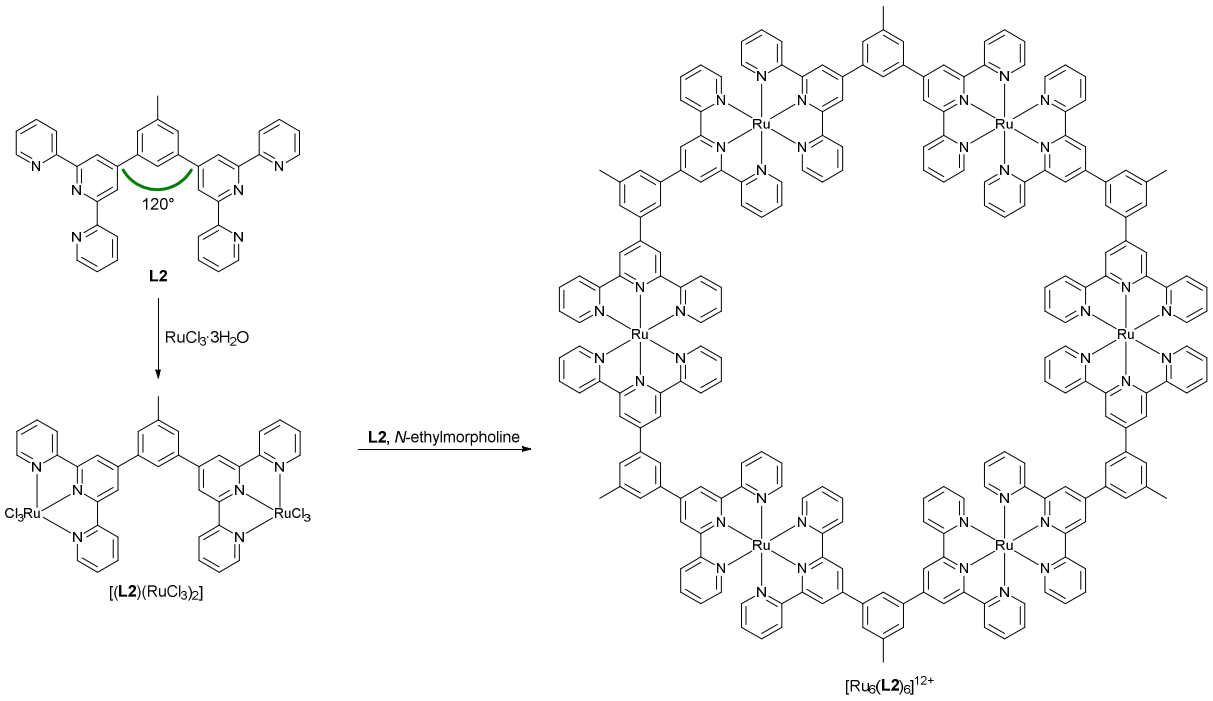

Scheme 2.2 Ligand **L2** has a predefined internal angle of 120° and directs the assembly of a metallohexacycle.

Chen and co-workers showed that triangular arrays are accessible even by using asymmetrical bis(2,2':6',2''-tpy) ligands **L3**, **L4** e **L5** (Scheme 2.3).[142] However, these asymmetrical ligands have two different tpy metal-binding domains (head/tail, Scheme 2.3) implying regioselectivity complications. With Zn^{2+} ions, it was observed that only **L4** gives a regioselective reaction with head/tail combinations in $[Zn_3(\mathbf{L4})_3]^{6+}$ (Fig. 2.1).

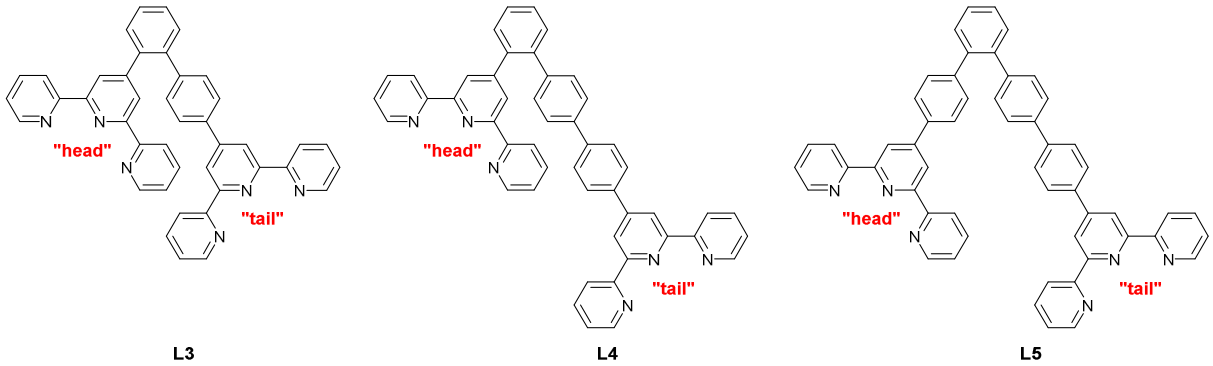

Scheme 2.3 Selected asymmetric ligands for the assembly of metallotriangles.

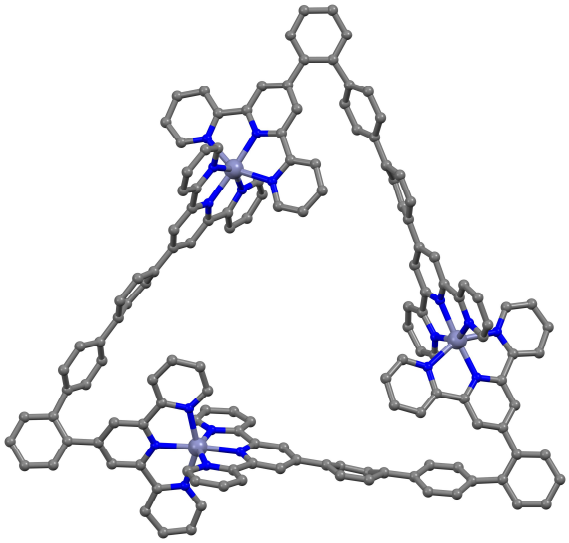

Figure 2.1 The crystallographically determined structure of the $[Zn_3(\mathbf{L4})_3]^{6+}$ cation (CSD refcode VUCQUH). For clarity, H atoms are omitted.[142]

The structures just described are only archetypal examples of what can be achieved by using carefully designed V-shaped bis(2,2':6',2''-tpy) ligands. However, studies with the bis(4,2':6',4''-tpy) and bis(3,2':6',3''-tpy) isomers are absent and, to gain an insight into the coordination behaviour of these tetratopic ligands, a systematic approach is required. In this project, two 4,2':6',4''-tpy or 3,2':6',3''-tpy units were connected through a diphenyl chalcogenide linkage (ligands **1**-**4**, Scheme 2.4). Ethers and sulfides are angular groups. As diaryl prototypes, for 4,4'-sulfanediyldiphenol the C_{aryl}–S–C_{aryl} angle is 104.2°, which is smaller than the 118.8° for C_{aryl}–O–C_{aryl} in 4,4'-oxydiphenol (Scheme 2.5).[144] The aim of this work was to prepare a suite of four V-shaped ligands, and then to react them with selected metal salts. Ultimately, the aim was to examine the differences in the crystal structures of the targeted coordination polymers as a function of the angle at the O- or S-linker in the nonlinear arrangement of the metal-binding domains.

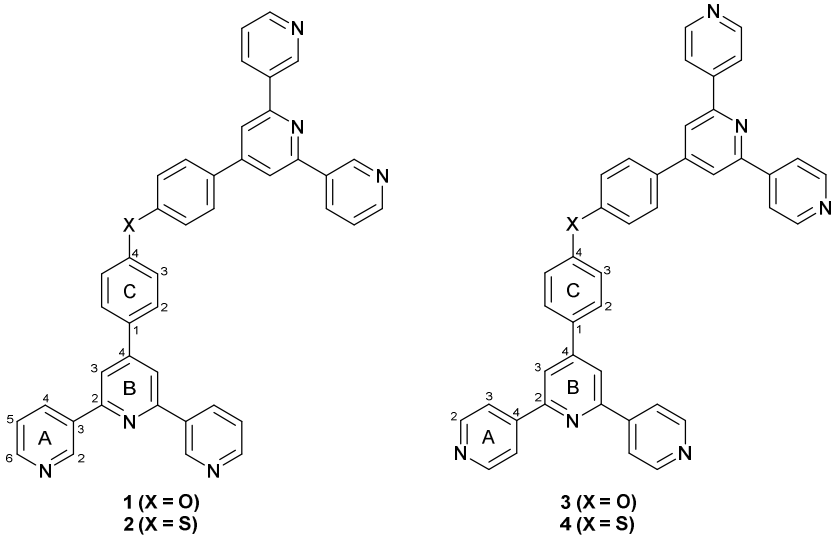

Scheme 2.4 Structures of the tetratopic bis(tpy) ligands **1**-**4** with the numbering scheme used for the NMR spectroscopic assignments in the experimental section.

Scheme 2.5 C_{aryl}–X–C_{aryl} (X = O and S) bond angles for 4,4'-oxydiphenol (left) and 4,4'-sulfanediyldiphenol (right).[144]

2.2 Ligand synthesis

The precursor 4,4'-oxydibenzaldehyde was prepared according to the literature[145] whereas 4,4'-sulfanediyldibenzaldehyde was obtained using the Bouveault aldehyde protocol.[146] While other routes to 4,4'-sulfanediyldibenzaldehyde have been described, such as coupling of 4-halobenzaldehydes and potassium thiocyanate,[147-149] the route chosen here via bis(4-bromophenyl)sulfide has proved to be very efficient in our hands (Scheme 2.6, top). The reaction of bis(4-bromophenyl)sulfide with *n*-BuLi and DMF in dry THF at –78 °C, followed by treatment with 3 M HCl, gave the desired 4,4'-sulfanediyldibenzaldehyde in high yield (92%). Starting from the O- or S-centred dialdehyde intermediates, the one-pot strategy described by Hanan and Wang[93] finally led to the desired bis(3,2':6',3''-tpy) and bis(4,2':6',4''-tpy) ligands **1**-**4** and the yields ranged between 22-50% (Scheme 2.6, bottom). No effort was made to further optimize the reaction conditions to enhance the achieved yields.

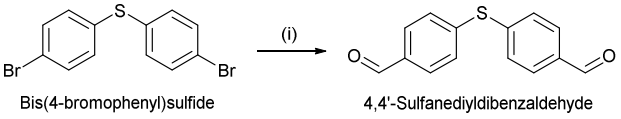

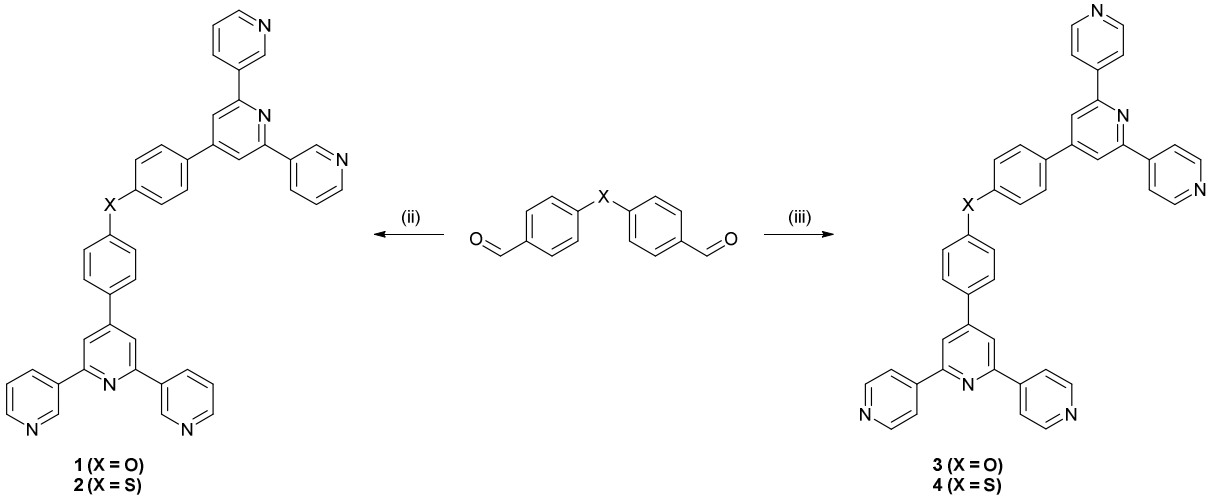

Scheme 2.6 Synthetic route to **1**-**4**. Reagents conditions (see experimental part for full details): (i) *n*-BuLi, THF, -78 °C, 2 h; dry DMF, 30 min and then warmed to RT; (ii) 3-acetylpyridine, KOH, aqueous NH_3, EtOH, RT, 5 days for **1** and 3 days for **2**; (iii) 4-acetylpyridine, KOH, aqueous NH_3, EtOH, RT, 5 days for **3** and 1 day for **4**.

The already known 4,4'-sulfanediyldibenzaldehyde was characterised by ^{1}H NMR spectroscopy and MALDI-TOF mass spectrometry, and the data matched those previously reported.[147] Ligands **1**-**4** were fully characterised by ^{1}H and ^{13}C{^{1}H} NMR spectroscopy, melting point determination, FT-IR spectroscopies, UV-Vis, MALDI-TOF mass spectrometry and HR-ESI mass spectrometry (see Appendix for full details). NMR spectra were all recorded in $CDCl_3$ except for **4**, for which DMF-d_7 was used due to its poor solubility. Therefore, the differing influence of ether and sulfide groups can be identified by

comparing the NMR spectra of **1** and **2** (Fig. 2.2). The positive mesomeric effect of the sulfur atom is weaker compared to the one of the oxygen atom. Indeed, in the NMR spectrum of ligand **1** (Fig. 2.2a), there is a substantial upfield-shift of H^{C3} (ether and sulfide groups are *ortho-para* directors). On the other hand, the spectroscopic signatures of the 3,2':6',3''-tpy units in **1** and **2** are little affected by the change of the central linker and show comparable chemical shifts.

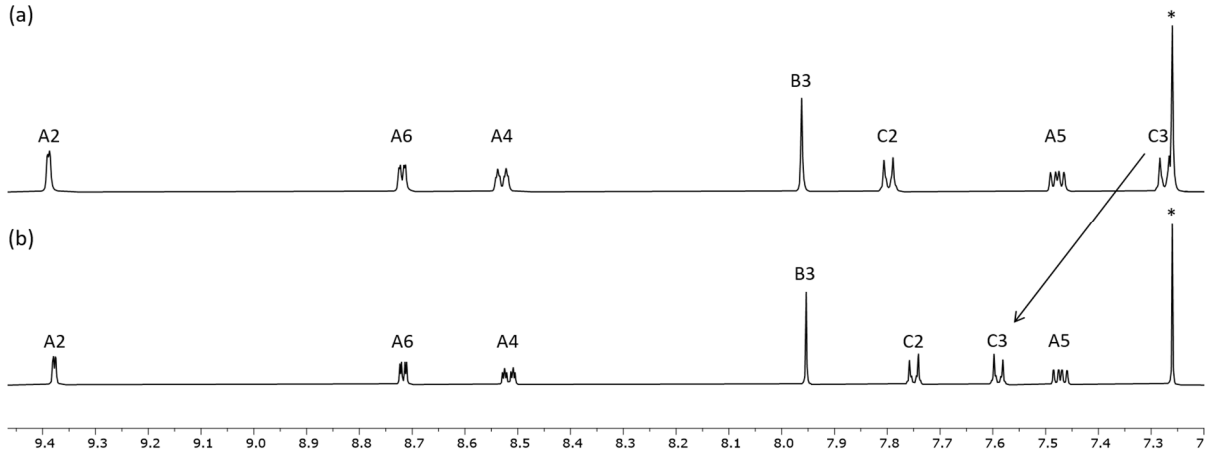

Figure 2.2 ^{1}H NMR (500 MHz, $CDCl_3$, 298 K) spectra (aromatic region) of (a) **1** and (b) **2**. Chemical shifts in δ / ppm. * = $CHCl_3$. Atom labels are shown in Scheme 2.4.

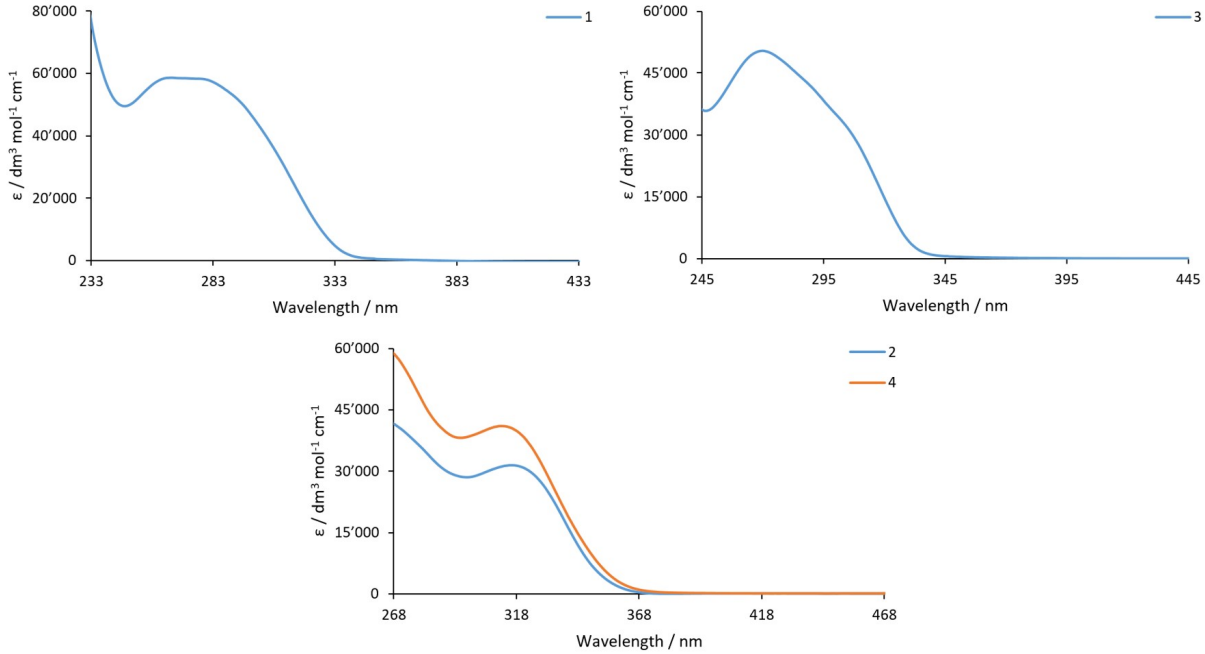

Figure 2.3 Solution absorption spectra of **1** in CH_2Cl_2 (2.6×10^{-5} mol dm^{-3}), **3** in $CHCl_3$ (2.2×10^{-5} mol dm^{-3}), **2** and **4** in DMF (2.1×10^{-5} mol dm^{-3}). Solvent cut-offs are 233 nm for CH_2Cl_2, 245 nm for $CHCl_3$ and 268 nm for DMF.

The absorption spectra of ligands **1**-**4** were recorded in different solvents due to the varying solubilities of the compounds (Fig. 2.3). All four ligands demonstrate similar behaviour with absorption bands arising from spin-allowed π*←π and π*←*n* transitions. In the MALDI-TOF-MS of each compound, the $[M+H]^+$ ion corresponded to the base peak (m/z = 633.05, 649.62, 633.24 and 649.56, respectively).

Attempts were made to prepare the selenium analogues of **1**-**4**. Since the literature synthesis of bis(4-bromophenyl)sulfide[150] starting with diphenylsulfide was successful, the same approach was used to synthesize the bis(4-bromophenyl)selenide. The commercial diphenylselenide was reacted with bromine in the presence of H_2O_2 in the two-phase system CH_2Cl_2/H_2O (Scheme 2.7a). The outcome of the synthesis proved to be inconclusive since neither product peaks nor mass could be assigned in the analytical methods. At the time of this project (2019), the literature offered two feasible solutions (Scheme 2.7b and c).[151, 152] Applying identical reaction conditions to those reported led to no conversion of the starting material for the route depicted in Scheme 2.7b. The reaction in Scheme 2.7c afforded a yield of 1% after purification by column chromatography. Due to this low yield in the first of three steps for the synthesis of the bis(tpy) ligand, an attempt was made to perform this coupling reaction directly with the corresponding aldehyde (Scheme 2.7d). Once again, the reaction was unsuccessful. Despite determined efforts to prepare the seleno-analogues of **1**-**4**, there was no successful outcome, and it was decided to abandon further attempts.

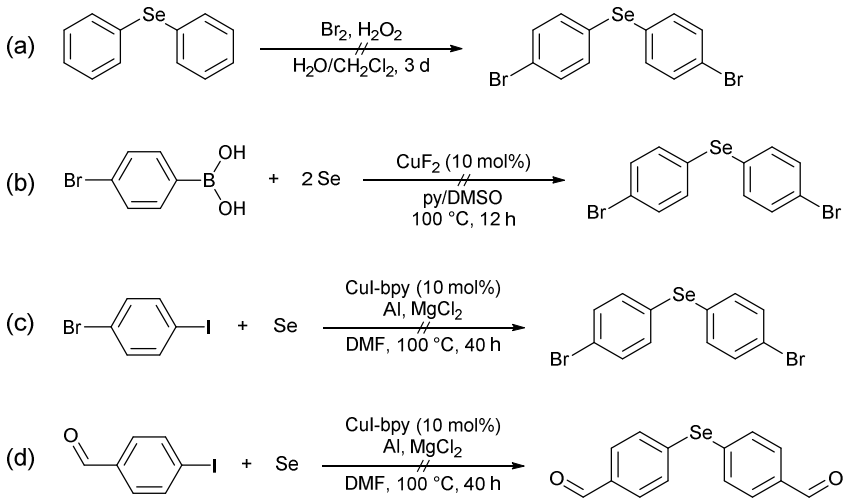

Scheme 2.7 Synthetic attempts to afford the selenium intermediates.

2.3 Crystal growth experiments

The ligands **1**-**4** were allowed to react with several metal salts under crystal growth conditions (Scheme 2.8). Crystal growth experiments were carried out by layering either at room temperature (ca. 22 °C) or at 5 °C. For each ligand and metal combination, different crystallisation solvents combinations were investigated (Scheme 2.8). A solution (6–7 mL) of the metal salt was layered over a solution (5 mL) of the ligand in a crystallisation tube (i.d. = 13.6 mm, vol. = 24 mL) sealed with a septum. The ligand concentration was typically around 2 mM and the metal salt was in a stoichiometric ratio.

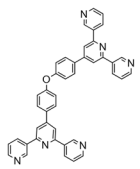

1

$Cd(OAc)_2$: $CHCl_3$/**MeOH**
$Co(NO_3)_2$: $CHCl_3$/**MeOH**
$Co(SCN)_2$: $CHCl_3$/**MeOH**, $CHCl_3$/**EtOH**
$Cu(hfacac)_2$: $CHCl_3$/**CCl_4**, $CHCl_3$/**Toluene**, $CHCl_3$/**1,2-DCB**
$Cu(OAc)_2$: $CHCl_3$/**MeOH**, $CHCl_3$/**EtOH**
$Fe(acac)_2$: $CHCl_3$/**Toluene**, $CHCl_3$/**1,2-DCB**
$ZnBr_2$: $CHCl_3$/**MeOH**
$ZnCl_2$: $CHCl_3$/**MeOH**, 1,2-DCB/**MeOH**

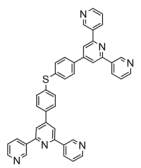

2

$Cd(NO_3)_2$: $CHCl_3$/**MeOH**
$Co(NO_3)_2$: $CHCl_3$/**MeOH**
$Co(SCN)_2$: $CHCl_3$/**MeOH**, DMF/**MeOH**
$Cu(hfacac)_2$: $CHCl_3$/**Toluene**, $CHCl_3$/**CB**, $CHCl_3$/**1,2-DCB**
$Cu(OAc)_2$: $CHCl_3$/**MeOH**, DMF/**MeOH**
$Fe(acac)_2$: $CHCl_3$/**Toluene**, $CHCl_3$/**CB**, $CHCl_3$/**1,2-DCB**

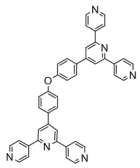

3

$Cd(NO_3)_2$: $CHCl_3$/**MeOH**
$Co(NO_3)_2$: $CHCl_3$/**MeOH**, Anisol/**MeOH**, Anisol/**EtOH**
$Co(SCN)_2$: $CHCl_3$/**MeOH**, DMF/**MeOH**, Dioxane/**MeOH**, Dioxane/**EtOH**, Anisol/**MeOH**, Anisol/**EtOH**
$Cu(hfacac)_2$: $CHCl_3$/**CCl_4**, $CHCl_3$/**Toluene**, $CHCl_3$/**1,2-DCB**, $CHCl_3$/**CB**, $CHCl_3$/**Dioxane**
$Cu(OAc)_2$: $CHCl_3$/**MeOH**, DMF/**MeOH**
$Fe(acac)_2$: $CHCl_3$/**Toluene**, $CHCl_3$/**1,2-DCB**

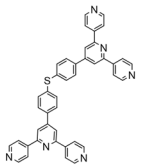

4

$Cd(NO_3)_2$: $CHCl_3$/**MeOH**
$Co(NO_3)_2$: $CHCl_3$/**MeOH**, Anisol/**MeOH**, Anisol/**EtOH**
$Co(SCN)_2$: $CHCl_3$/**MeOH**, DMF/**MeOH**
$Cu(hfacac)_2$: $CHCl_3$/**Toluene**, $CHCl_3$/**CB**, $CHCl_3$/**1,2-DCB**
$Cu(OAc)_2$: $CHCl_3$/**MeOH**, DMF/**MeOH**
$Fe(acac)_2$: $CHCl_3$/**Toluene**, $CHCl_3$/**CB**, $CHCl_3$/**1,2-DCB**

Scheme 2.8 Overview of the metal salts and crystallisation solvents used for each ligand **1**-**4**. Legend: ligand solvent/**metal salt solvent (bold)**. CB = chlorobenzene; 1,2-DCB = 1,2-dichlorobenzene.

Successful crystal growth was observed mainly with an aromatic solution of $[Cu(hfacac)_2]\cdot H_2O$ with a $CHCl_3$ solution of ligand **4**. The crystals were sensitive to solvent loss and, despite all care in handling them, their X-ray diffraction was too weak for full data set collection.

2.4 Conclusions

The bis(tpy) ligands **1**-**4** were prepared using the one-pot strategy describe by Wang and Hanan.[93] For each pair of bis(4,2':6',4''-tpy) or bis(3,2':6',3''-tpy) ligands, the bent $O(4\text{-}C_6H_4)_2$ and $S(4\text{-}C_6H_4)_2$ spacers were introduced. Ligands **1**-**4** were fully characterised. Their coordination behaviour was explored with numerous metal salts but no measurable single-crystals for X-ray diffraction experiments were obtained. The main issue was the limited diffraction at low angles, if at all, of the single-crystals. This could be rationalised by crystal sensitivity to solvent loss, probably due to the presence of large solvent-accessible voids in the crystal lattice. Furthermore, additives, such as C_{60} fullerene or anthracene, did not aid crystallisation. The introduction of alkyloxy or phenylalkoxy chains attached to the central spacer is one of the solutions to address this problem, as also adding the beneficial effect of improving the solubility of the ligand. This strategy is described in the next chapter.

3 Linear bis(3,2':6',3''-terpyridines): (4,4)-Nets with [M(hfacac)$_2$] (M = Cu, Zn)

3.1 Motivation

Although many examples of 1D-, 2D- and 3D-assemblies have been prepared from ligands containing one or more 4,2':6',4''-tpy units, the coordination behaviour of 3,2':6',3''-tpy ligands remains less exploited.[59, 80, 83-85, 91, 153-168] As part of her Masters' studies, Simona Capomolla, under the supervision of this author, investigated three copper(II) 1D-coordination polymers [Cu_2(hfacac)$_4$(**L6**)$_2$]$_n$·n(1,2-$Cl_2C_6H_4$), [Cu_2(hfacac)$_4$(**L6**)$_2$]$_n$·$n$$C_6H_5Cl$, and [Cu(hfacac)$_2$(**L7**)]$_n$·$n$$C_6H_5Cl$, containing ditopic 3,2':6',3''-tpy ligands with coordinatively innocent 4'-substituents. In [Cu_2(hfacac)$_4$(**L6**)$_2$]$_n$·n(1,2-$Cl_2C_6H_4$) and [Cu_2(hfacac)$_4$(**L6**)$_2$]$_n$·$n$$C_6H_5Cl$, the 3,2':6',3''-tpy domains exhibit conformation **C**, while with [Cu(hfacac)$_2$(**L7**)]$_n$·$n$$C_6H_5Cl$ conformation **B** is adopted (Scheme 3.2).[169] Structures of ligands **L6** and **L7** are shown in Scheme 3.1.

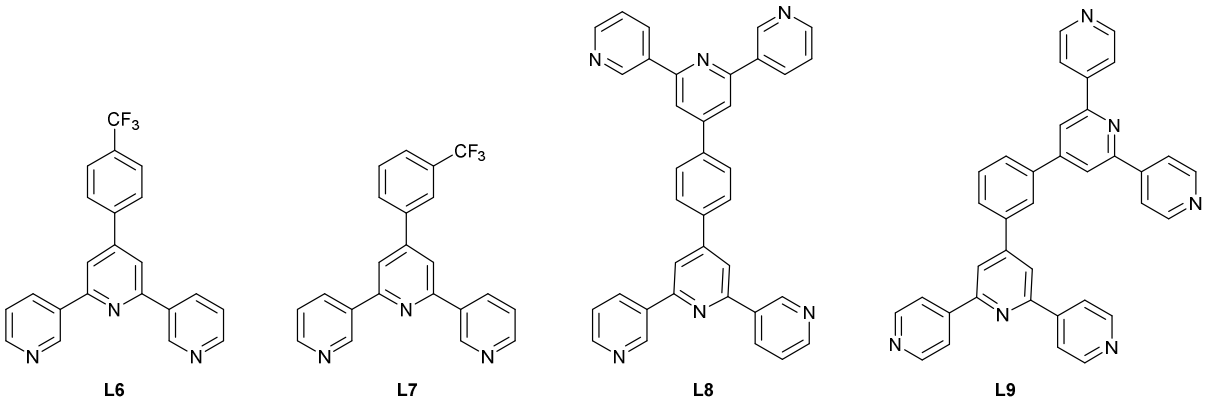

Scheme 3.1 Structures of the ditopic ligands **L6** and **L7**,[169] and the tetratopic ligands **L8** and **L9**.[91]

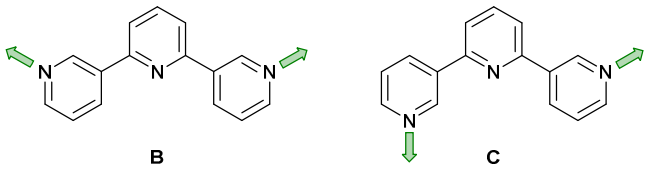

Scheme 3.2 Two limiting conformation **B** and **C** that planar 3,2':6',3''-tpy units can adopt. For all possible conformations see Scheme 1.7 in the introduction.

One strategy for increasing the dimensionality of an assembly is to select metal centres which favour higher coordination numbers combined with ditopic 3,2':6',3''-tpy or 4,2':6',4''-tpy linkers. The assembly of the resulting coordination network is thereby directed by the topological preferences of the metal node.[59, 170] An alternative methodology to encourage the formation of 2D- and 3D-assemblies is by connecting multiple tpy domains to appropriate scaffolds. As mentioned in the introduction, two 3,2':6',3''-tpy or 4,2':6',4''-tpy units can be linked in a "back-to-back" fashion by any organic spacer, generating a potentially tetratopic ligand.[85, 90] It was decided to extend the investigation of [M(hfacac)$_2$] coordination chemistry to tetratopic bis(terpyridine) ligands, and Simona Capomolla also demonstrated the assembly of a series of (4,4) nets based on 1,4-bis(*n*-alkyloxy)-2,5-

bis(3,2':6',3''terpyridin-4'-yl)benzene ligands.[36] A search of the Cambridge Structural Database (CSD v. 2021.3.0, April 2022) revealed only three other structures involving a bis(4,2':6',4''-tpy) or bis(3,2':6',3''-tpy) with a metal 1,3-diketonate. Yoshida *et al.* showed that ligand **L8** (Scheme 3.1) combined with $[Co(acacCN)_2]$ (HacacCN = 2-acetyl-3-oxobutanenitrile) gave the 2D-dimensional (4,4) net $[Co_2(acacCN)_4(\mathbf{L8})]_n$. The replacement of $[Co(acacCN)_2]$ by $[Co(dbm)_2]$ (Hdbm = 1,3-diphenylpropane-1,3-dione) led to a 1D-chain $[Co(dbm)_2(\mathbf{L8})]_n$, in which **L8** is bidentate through one pyridine N-donor from each tpy domain. The low connectivity is perhaps sterically induced by the presence of larger phenyl rings in $[Co(dbm)_2]$. In contrast, in $[Co_2(acacCN)_4(\mathbf{L9})]_n$, a change in the ligand from **L8** to **L9** (Scheme 3.1) with $[Co(dbm)_2]$ does not change the topology of the coordination network, but the networks exhibit 3-fold interpenetration in the solid state structure.[91] In this work, the synthesis of two bis(3,2':6',3''-tpy) ligands **5** and **6** (Scheme 3.3) with 1,4-phenylene spacers containing 2-phenylethoxy and 3-phenylpropoxy substituents attached to the phenylene moiety is reported. The Constable and Housecroft research group had already demonstrated that introducing alkyloxy groups into the central spacer in this family of ligands enhances the solubility of the ligand in organic solvents which is beneficial for crystal growth. In addition, the nature of the alkyloxy group can influence the assembly and if terminal phenyl groups are present, they may participate in π-π stacking interactions within the solid state.[59, 85, 90]

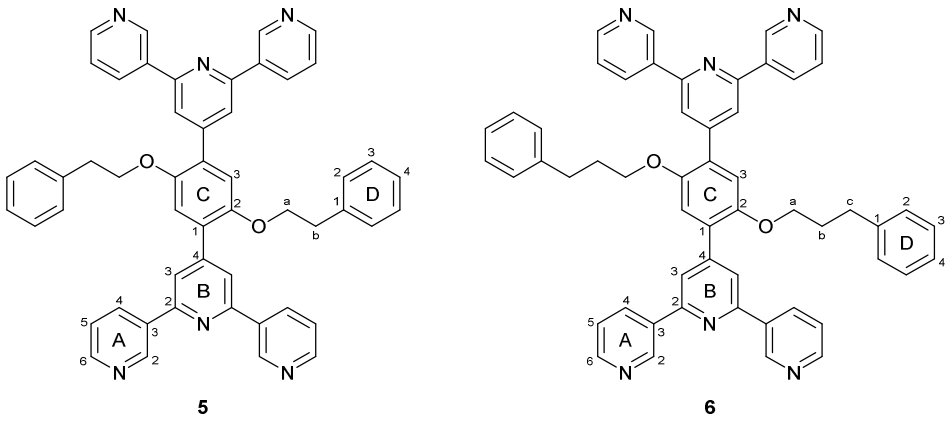

Scheme 3.3 Structures of the tetratopic bis(3,2':6',3''-terpyridine) ligands **5** and **6** with the numbering scheme used for the NMR spectroscopic assignments in the experimental section.

Herein, the reaction of **5** and **6** (potentially tetratopic ligands) with $[M(hfacac)_2]$ (M = Cu, Zn), a two connecting building block, to generate a series of 2-dimensional (4,4)-networks is described. The electron-withdrawing effect of the CF_3 substituents improves the affinity of the complex towards coordination with the pyridine donors of the tetratopic ligands as well as improving its solubility in organic solvents.

3.2 Ligand synthesis

Ligands **5** and **6** were prepared in three steps starting from the commercially available 2,5-dibromobenzene-1,4-diol (Scheme 3.4). The substitution of 2,5-dibromobenzene-1,4-diol with (2-bromoethyl)benzene or (3-bromopropyl)benzene was performed under basic conditions and the intermediates were obtained in good yields (**5a**, 72% and **6a**, 87%). This method had already been used for the synthesis of related 1,4-dibromo-2,5-bis(alkyloxy)benzene derivatives[171] and proved to be more convenient than the general procedure reported by Neil and co-workers.[172]

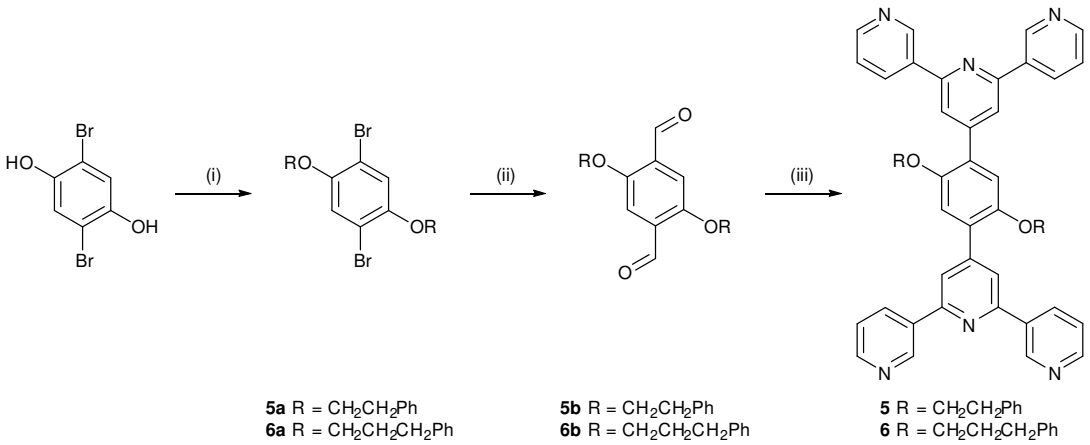

Scheme 3.4 Synthetic route to **5**-**6**. Reagents conditions (see experimental part for full details): (i) (2-bromoethyl)benzene for **5a** or (3-bromopropyl)benzene for **6a**, anhydrous K_2CO_3, DMF, 100 °C, 22 h; (ii) *n*-BuLi, Et_2O, 0 °C; dry DMF, warmed to RT, 22 h; (iii) 3-acetylpyridine, KOH, aqueous NH_3, EtOH, RT, 6 days for **5** and 5 days for **6**.

Bouveault aldehyde syntheses[146] starting from the reaction of **5a** or **6a** with *n*-BuLi and DMF in dry Et_2O at 0 °C, gave **5b** (59%) and **6b** (37%), respectively. Despite the use of excess of *n*-BuLi and DMF, monoaldehyde by-products persisted and purification by column chromatography was required. Finally, Hanan and Wang's one-pot strategy,[93] provided the desired terpyridines **5** (35%) and **6** (36%) after filtration and washing with water, EtOH and Et_2O, and no further purification was needed. The ^1H and $^{13}C\{^1H\}$ NMR spectra of intermediates **5a**-**6a**, **5b**-**6b** and **5**-**6** were assigned using NOESY, COSY, HMQC and HMBC techniques. The spectroscopic signatures are consistent with the structures displayed in Scheme 3.4. Although being structurally similar, differences in the NMR signatures of ligand **5** and **6** can be spotted. In the aromatic region H^{B3}, H^{A4} and H^{A2} of ligand **6** are down-field shifted while H^{A6}, H^{D2}, H^{D3} and HD4 are up-field shifted. The additional CH_2 unit in **6** seems to be responsible for redistribution of the bond polarizations (Fig. 3.1 and Fig. 3.2). The protons H^a and H^c in **6** are more shielded than protons H^a and H^b in **5**.

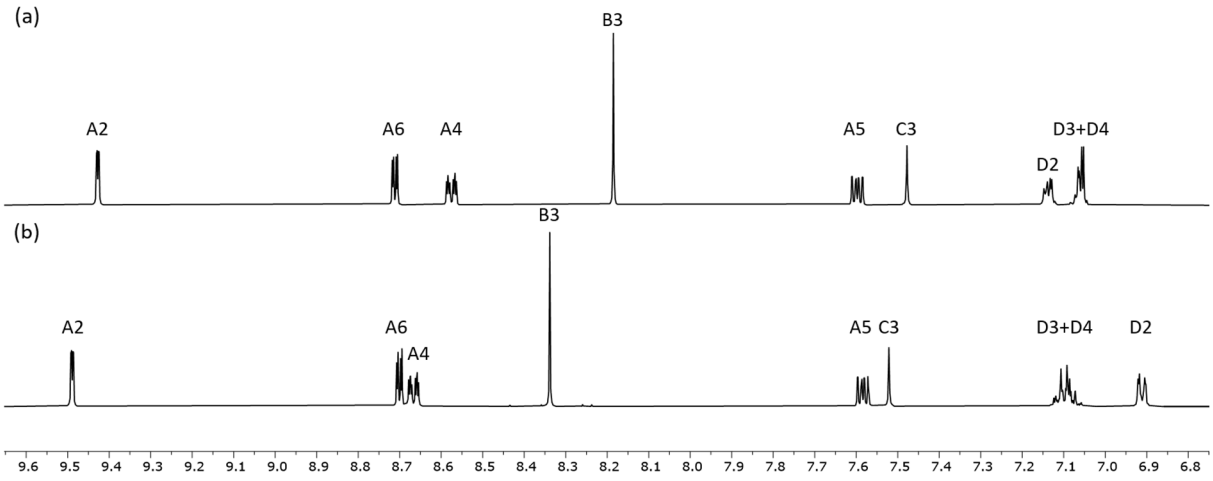

Figure 3.1 ^1H NMR (500 MHz, DMSO-d_6, 298 K) spectra (aromatic region) of (a) **5** and (b) **6**. Chemical shifts in δ / ppm. Atom labels are shown in Scheme 3.3.

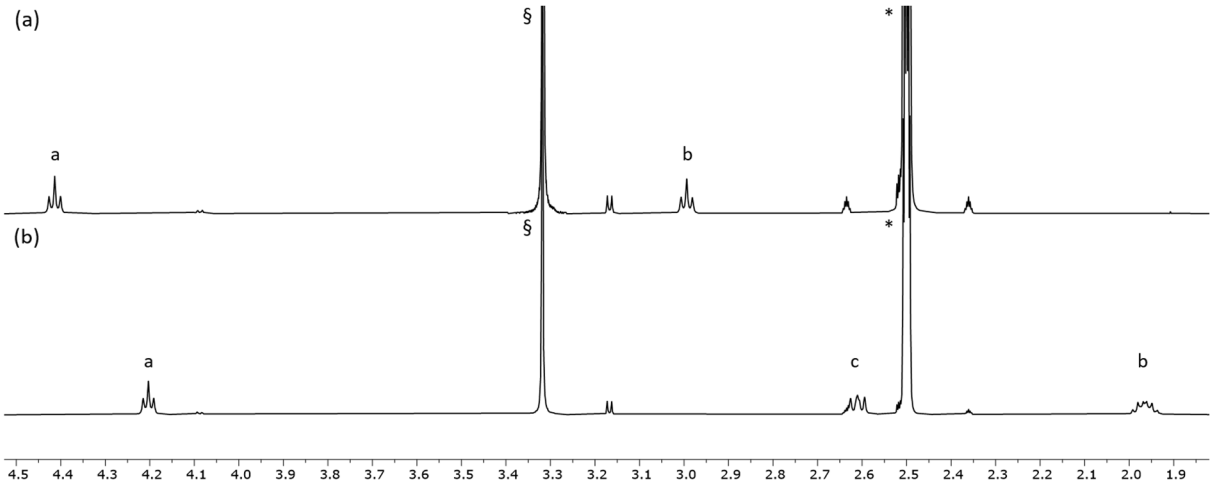

Figure 3.2 ^{1}H NMR (500 MHz, DMSO-d_6, 298 K) spectra (aliphatic region) of (a) **5** and (b) **6**. Chemical shifts in δ / ppm. * = DMSO-d_5, § = HOD. Atom labels are shown in Scheme 3.3.

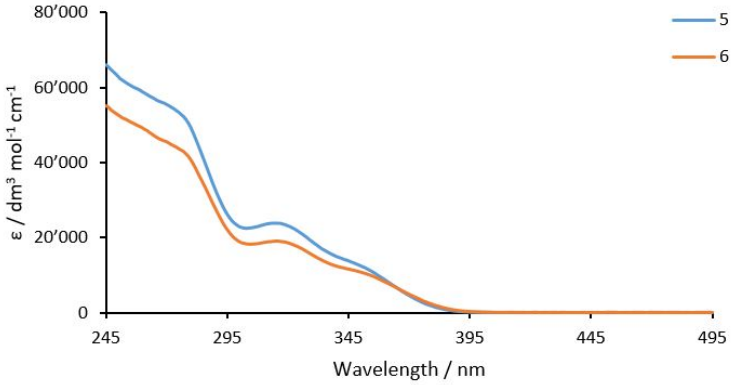

Figure 3.3 Solution absorption spectra of **5** and **6** in $CHCl_3$ (2.0×10^{-5} mol dm^{-3}).

The solution absorption spectra of compounds **5** and **6** exhibit similar absorption bands arising from spin-allowed π*←π and π*←*n* transitions. The length of the phenylalkoxy tail and the presence of a terminal phenyl ring on its end does not significantly influence the absorption spectra. The absorption pattern is comparable to the related bis(3,2′:6′,3″-tpy) ligands with *n*-alkyloxy substituents (see next chapter). In the MALDI-TOF-MS of each compound, the highest-mass peak corresponded to the $[M+H]^+$ ion (m/z = 781.24 and 809.31, respectively). For **5**, this was the base peak. Melting point determination, FT-IR spectroscopies and either HR-ESI mass spectrometry and/or elemental analysis complemented the characterisation (see experimental section for full details).

3.3 Crystal structures of 1,4-dibromo-2,5-bis(phenylalkoxy)benzene derivatives

Single-crystals of **5a** (polymorph I, see later for polymorph II) and **6a** were grown as hot MeOH/$CHCl_3$ solutions of the compounds were allowed to cool to room temperature. Both **5a** and **6a** crystallise in the triclinic space group *P*–1. In **5a**, the asymmetric unit consists of four independent half-molecules, while the phenylene centroids each lie on an inversion centre. The bond lengths and angles of the four molecules are comparable, and therefore Table 3.1 specifies the parameters only of the molecule with the Br1 atom (Fig. 3.4a). The asymmetric unit of **6a** is formed by one and a half crystallographically

independent molecules (Fig. 3.4b). The phenylalkoxy substituents are in extended conformations in both **5a** and **6a**.

Table 3.1 Selected bond parameters in compounds **5a** (polymorph I, for the molecule having Br1) and **6a** (both independent molecules A (containing Br1 and Br2) and B (with Br3)).

Bond parameter	5a	6a molecule A	6a molecule B
C–Br /Å	1.891(2)[a]	1.889(3), 1.891(3)	1.892(3)
C_{arene}–O /Å	1.361(3)[a]	1.358(4), 1.363(4)	1.365(4)
C_{alkyl}–O /Å	1.422(3)[a]	1.434(4), 1.418(5)	1.433(4)
C_{arene}–O–C_{alkyl} /°	118.51(19)[a]	117.7(3), 118.4(3)	116.5(2)
Angle between planes of phenyl and central arene rings/°	82.6[b]	29.3, 38.1	73.3

[a]Range of values for all four independent molecules: C–Br = 1.890(2) to 1.894(2) Å; C_{arene}–O = 1.351(3) to 1.386(3) Å, C_{alkyl}–O = 1.406(3) to 1.447(3) Å; C_{arene}–O–C_{alkyl} = 118.3(2) to 118.57(19)°. [b]The corresponding angles in molecules containing Br2, Br3 and Br4 are 81.6, 82.3, and 81.1°, respectively.

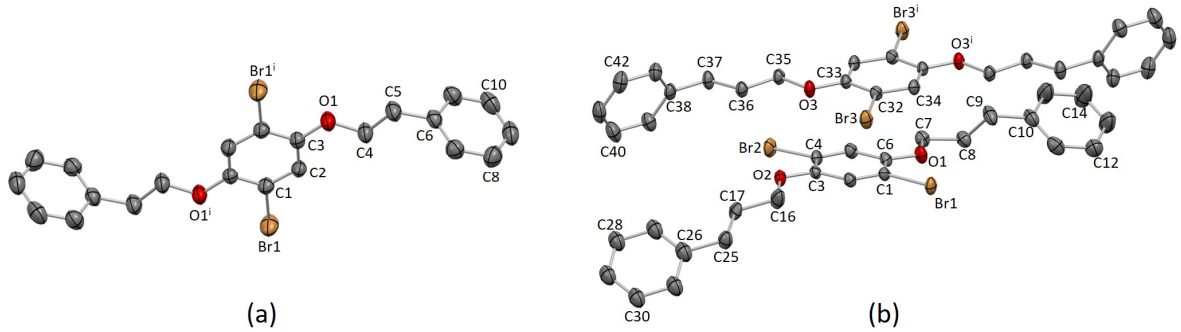

Figure 3.4 Molecular structures of (a) one of the crystallographically independent molecules of polymorph I of **5a** (symmetry code i = –*x*, –*y*, –*z*), and (b) the two independent molecules of **6a** (symmetry code i = –*x*, 1–*y*, 1–*z*). In **6a**, the 3-phenylpropoxy chain with C26 is disordered and only one position is shown. H atoms are omitted for clarity, and thermal ellipsoids are drawn at 40% probability level.

Each molecule of **5a** (polymorph I) and **6a** can be regarded as a stick-like unit spanning between the two *para*-carbon atoms of the terminal phenyl rings. In **5a**, the distance between the *para*-C atoms of the phenyl rings is ≈ 17.5 Å. With the incorporation of an additional CH_2 in **6a** the distance increases to ≈ 20.0 Å and this has a significant influence on the crystal structure. In polymorph I of **5a**, an almost orthogonal arrangement of their phenylene rings is present between the pairs of molecules containing Br1/Br3 and Br2/Br4 (Fig. 3.5a). Each Br atom is pointed towards the central arene ring of an adjacent molecule, producing stacks of molecules (Fig. 3.5a). These can be described as semi-localised C–Br...π(arene) interactions (Scheme 3.5) in which each Br atom engages with two C atoms (Fig. 3.5a). Short contacts are Br1...C25^{i} = 3.475(2) Å and Br1...C23^{ii} = 3.529(2) Å (symmetry codes i = 1–*x*, –*y*, –*z*; ii = 1+*x*, –1+*y*, *z*), with C1–Br1…C25^{i} and C1–Br1…C23^{ii} angles of 161.25(8) and 176.15(8)°. Likewise, Br4 makes two short contacts Br4...C12^{ii} = 3.529(2) Å and Br4...C14^{iii} = 3.468(2) Å (symmetry code iii = 1–*x*, 1–*y*, 1–*z*), with C34–Br4…C12^{ii} and C34–Br4…C14^{iii} angles of 176.22(8) and 160.54(8)°. Atoms Br2 and Br3 are engaged in similar interactions with arene rings containing C34^{iv} and C36^{v}, and C1^{iv} and C3^{vi}, respectively (symmetry codes: iv = *x*, 1+*y*, *z*; v = 1–*x*, 2–*y*, 1–*z*; vi = 1–*x*, 1–*y*, –*z*), at distances of 3.543(2), 3.449 (2), 3.541(2), and 3.516(2) Å and with C–Br…C angles of 176.14(8), 160.72(8), 176.14(8) and 161.28(8)°, respectively. These packing interactions lead to the lattice illustrated in Fig. 3.5b.

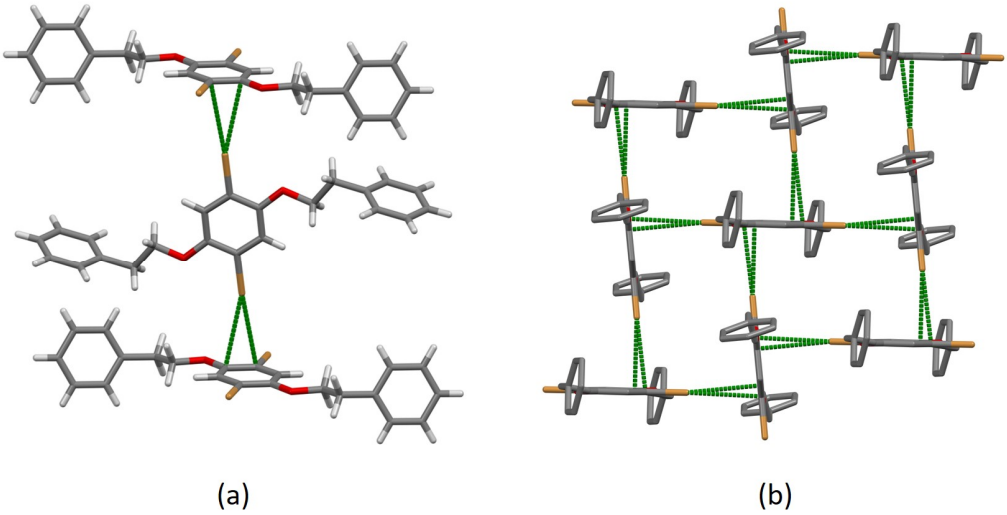

Figure 3.5 Packing of molecules of compound **5a** (polymorph I) (a) Semi-localized interactions between each Br and two arene C atoms of adjacent molecules. (b) Orthogonal sets of Br...arene interactions; H atoms are omitted for clarity.

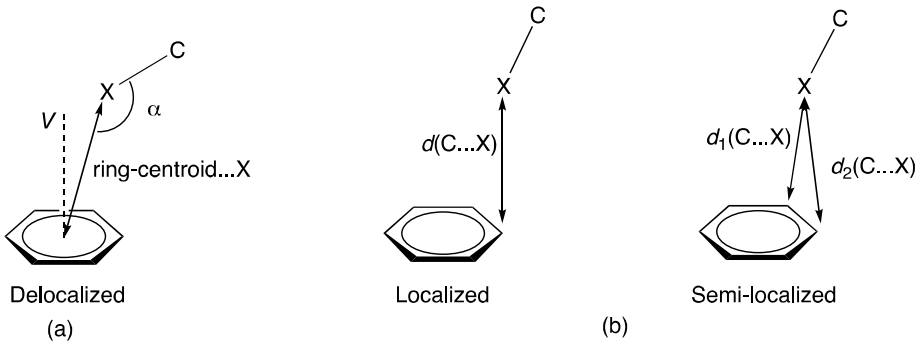

Scheme 3.5 (a) Tiekink's[173] criteria for identifying a C–X...π(arene) interaction: 160° ≤ α ≤ 180°, and the ring-centroid...X distance is 3.88 Å. (b) Classification of localized and semi-localized C–X...π(arene) interactions; for the semi-localized interaction, d_1(C–X) is close in value to d_2(C–X).[174, 175] Scheme reproduced from the open access reference.[176]

6a exhibits a richer diversity of interactions, where arene–arene π-stacking, C–H...Br hydrogen bonds and short Br...Br contacts dominate in the packing. Face-to-face π-stacking interactions are present between the two independent molecules of **6a**. The central phenylene rings are offset from each other (Fig. 3.6a), generating the columnar packing illustrated in Fig. 3.6b. The ring plane-to-centroid and inter-centroid separations are 3.58 and 3.76 Å, respectively. In the solid-state structure of **6a**, Br...Br and C–H...Br contacts emerge from the Br1 and Br2 atoms belonging to the independent molecule, which is present as a whole in the asymmetric unit. However, for the independent half-molecule, Br3 is not involved in analogous interactions and the molecule acts as a hydrogen bond donor via the C34–H34 group shown in Fig. 3.7 (C34–H34...Br2^{ii} distance of 2.87 Å and angle of 159°). It is worth mentioning that according to Steiner's definition,[177] the C–H group is treated as a hydrogen bond donor. The distance Br1^{ii}...Br1^{iii} of 3.4584(6) Å is less than the sum of the van der Waals radii, i.e. 3.70 Å,[178] and is unexceptional.[179] The C–Br–Br angles for the C–Br...Br–C interaction is 150.6(1)°, which belongs to the type I orientation defined in Scheme 3.6.

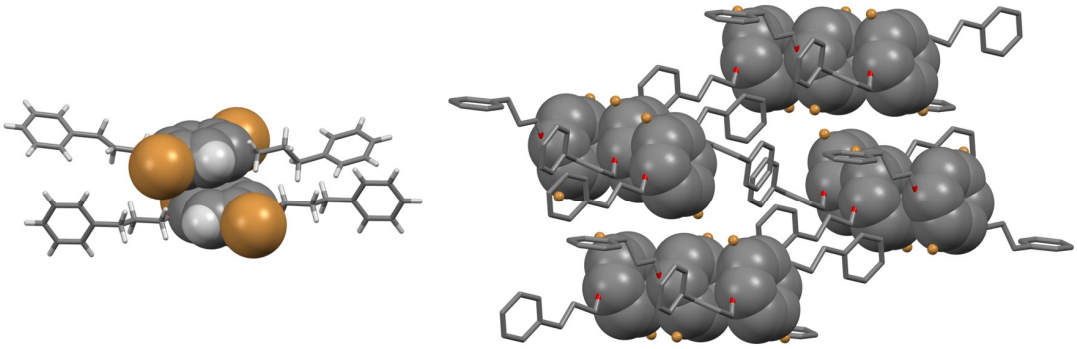

Figure 3.6 (a) π-Stacking between the two crystallographically independent molecules of **6a** with the C and H atoms of the stacked rings shown in space-filling representation. (b) Extension of the same π-stacking contacts through the lattice (H atoms are omitted for clarity and Br atoms are displayed in ball and stick representation).

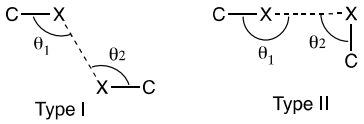

Scheme 3.6 Classification of halogen...halogen interactions. In type I, θ1 = θ2, and in type II, θ1 ≈ 180° and θ2 ≈ 90°. Figure reproduced from the open access reference.[176]

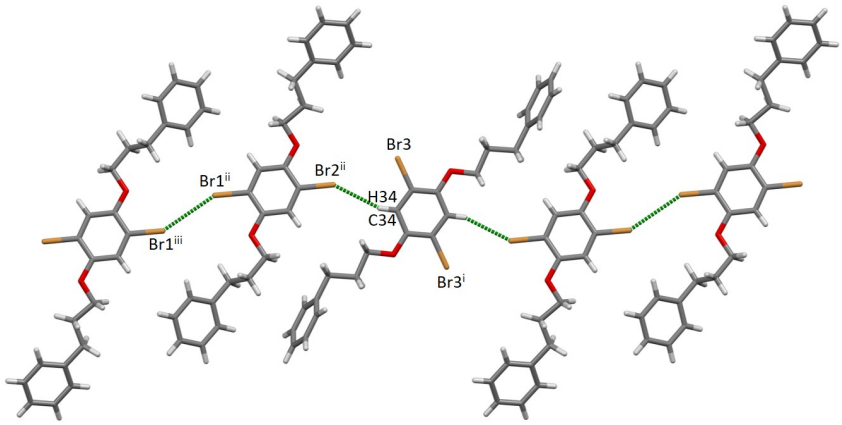

Figure 3.7 Br...Br short contacts and C–H...Br hydrogen bonds between alternating crystallographically independent molecules of **6a** lead to ribbons (symmetry codes i = –*x*, 1–*y*, 1–*z*; ii = –1+*x*, *y*, *z*; iii = –1–*x*, –*y*, 1–*z*).

The bulk materials of **5a** (polymorph I) and **6a** were analysed by powder X-ray diffraction in order to investigate whether the single-crystals were representative of the bulk sample. For **6a**, an excellent match between the experimental PXRD pattern for the bulk material and the pattern predicted from the single-crystal structure was found (Figure 3.8a). Every peak in the experimental plot had a corresponding peak in the calculated plot and no additional peaks were spotted.

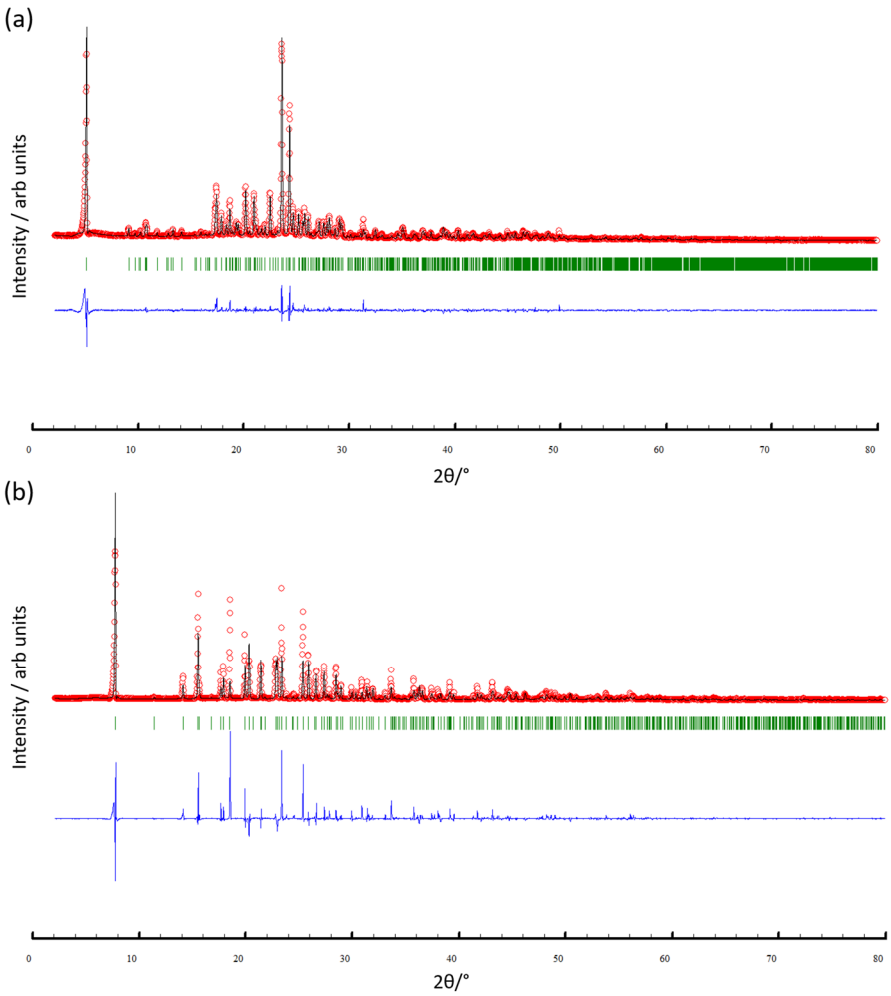

Figure 3.8 X-Ray diffraction (CuKα1 radiation) patterns (red circles) of the bulk crystalline material of (a) **6a** and (b) **5a** polymorph II (orthorhombic), fitting to the predicted pattern from single-crystal structure. The black lines are the best fit from Rietveld refinements, and green lines display the Bragg peak positions. The blue plot gives the difference between calculated and experimental points.

However, for **5a** (polymorph I) a mismatch between the predicted pattern from the single-crystal structure and the experimental PXRD was observed, indicating that the selected single-crystal was not representative of the bulk sample. In specific the experimental pattern has an additional peak at 2θ = 18.53° (see Fig. 3.9a). For this reason, the material used for PXRD was recrystallised from a hot solution of MeOH and $CHCl_3$ cooled down to ambient temperature (ca. 22°C). This produced X-ray quality crystals and cell checks of four single-crystals were performed. Table 3.2 summarises the consistency of the cell parameters for the four selected crystals, which themselves differ from those of the single-crystal selected from the first batch of crystals (labelled polymorph I in Table 3.2). The low temperature structural determination of one of the four single-crystals confirms the existence of a second polymorph (II) of **5a** crystallising in the orthorhombic space group *Pbca* (for cell parameters see last line of Table 3.2). This time, the PXRD of the second recrystallised bulk sample fits with the calculated pattern from the single-crystal structure data of polymorph II (Fig. 3.8b). The predicted PXRD patterns of both polymorphs I (triclinic) and II (orthorhombic) are shown in Fig. 3.9b. Now, from the experimental pattern of the first bulk of **5a** (grey line, Fig. 3.9a), it is evident that both polymorphs are present. For example, the low-angle peaks 2θ = 18.53° and 2θ = 13.38° were identified as being characteristic for the polymorph II (orthorhombic) and polymorph I (triclinic), respectively.

Table 3.2 Cell parameters for polymorphs I and II of **5a**, and for four crystals selected from the recryst. of the bulk sample.

Crystal	*a* /Å	*b* /Å	*c* /Å	*α*/°	*β*/°	*γ*/°
Polymorph I (*P*–1)[a]	8.2806(13)	10.6327(16)	22.885(4)	91.027(14)	91.663(14)	89.806(13)
Recryst. bulk, crystal 1[b]	8.23[c]	10.55	22.84	89.88	89.81	89.93
Recryst. bulk, crystal 2[a]	8.22[c]	10.52	22.78	89.97	89.92	89.99
Recryst. bulk, crystal 3[a]	8.22[c]	10.52	22.76	89.99	89.98	90.00
Recryst. bulk, crystal 4[a]	8.21[c]	10.52	22.77	90.07	90.07	90.05
Polymorph II (*Pbca*)[a]	10.5176(7)	8.2178(5)	22.7853(14)	90	90	90

[a]Measured at 200 K; [b]measured at 150 K; [c]the axis order has been chosen for direct comparison with those of polymorph I.

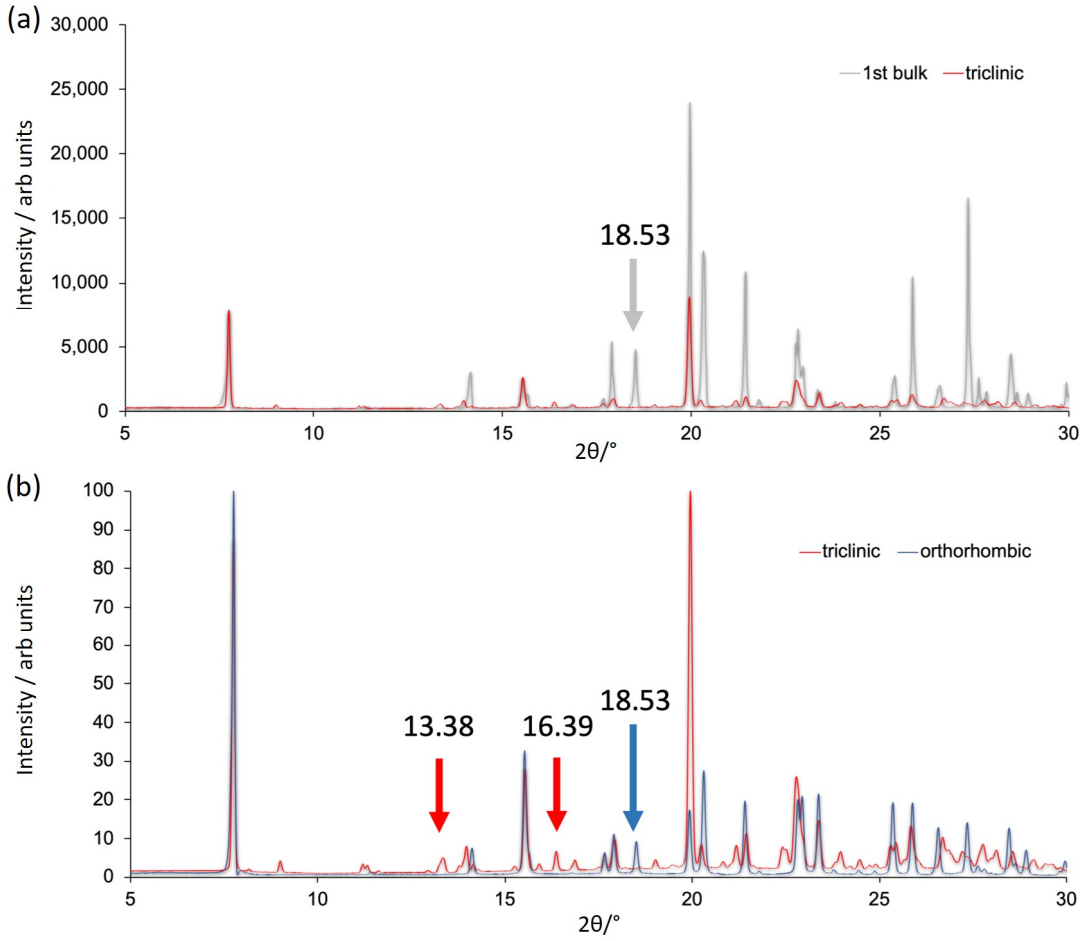

Figure 3.9 (a) Comparison of the PXRD patterns (expansion of the range between 2θ = 5–30°) for the bulk sample from the first crystallisation (grey) and the pattern predicted from the single-crystal data for the triclinic polymorph of **5a** (red); the peak at 2θ = 18.53° arises from the second (orthorhombic) polymorph. (b) Comparison of the PXRD patterns (expansion of the range between 2θ = 5–30°, and normalized to maximum intensity = 100) predicted from the single-crystal data of the triclinic polymorph I of **5a** (red) and of the orthorhombic polymorph II (blue); peaks at 2θ = 13.38° and 16.39° are representative of low angle data characteristic of polymorph I. Picture reproduced from the open access reference.[176]

The asymmetric unit of polymorph II of **5a** consists of a half-molecule while the other half is generated by inversion (Figure 3.10a). The angles and bond lengths are comparable to the ones observed in polymorph I (Table 3.1). An overlay of the four independent molecules of polymorph I and the molecule in polymorph II, with symmetry generated molecules, is shown in Figure 3.10b. This highlights the correspondences of the relative positions of the molecules in the crystal lattice and the packing interactions of the two polymorphs.

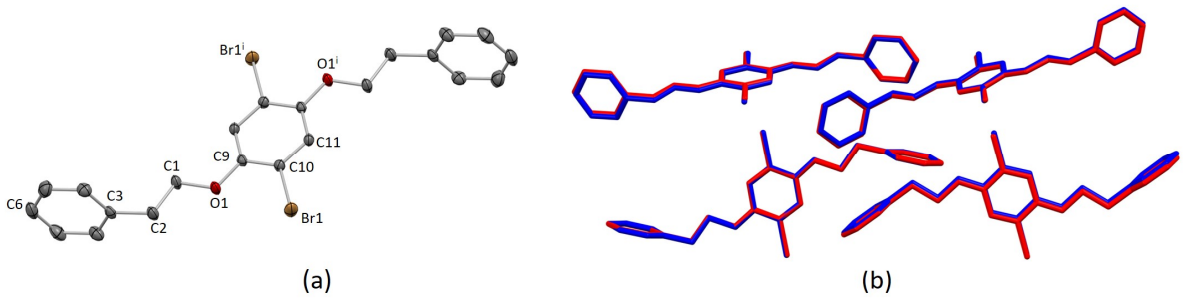

Figure 3.10 (a) Molecular structure of **5a**, polymorph II (orthorhombic) with ellipsoids at 40% probability level. Symmetry code i: 1–*x*, 1–*y*, 1–*z*. Selected bond parameters: C10–Br1 = 1.889(2), C9–O1 = 1.363(3), C1–O1 = 1.429(3) Å; C1–O1–C9 = 117.92(17)°. (b) Overlay of the four independent molecules of polymorph I of **5a** (in red), and the molecule of polymorph II of **5a** (blue) with additional symmetry-generated molecules. H atoms are omitted for clarity.

3.4 Crystal structures of 2,5-bis(phenylalkoxy)terephthalaldehyde derivatives

Single-crystals of **5b** grew from the chromatographic fractions after purification (EtOAc in cyclohexane, 2-5% gradient). X-ray quality crystals of **6b** were obtained as a hot EtOAc solution of **6b** was allowed to cool to –20 °C. **5b** crystallises in the monoclinic space group $P2_1/n$ and **6b** in the orthorhombic *Pbca* space group. In both **5b** and **6b**, the asymmetric unit contains one crystallographic independent half-molecule and the second half is generated by inversion with the inversion centre located in the arene core centroid. The conformations of **5b** and **6b** are slightly different (Fig. 3.11a and b). The extension of the phenylalkoxy substituent by the addition of an extra CH_2 has a considerable impact on the crystal packing. Intermolecular interactions in crystal lattices in **5b** arise from a combination of C–H...O hydrogen bonds, short C–H...π(arene) contacts, and arene–arene π-stacking. The C–H...O bonds arise from the oxygen atom of the aldehydes and the hydrogen atoms H5A and H5B attached to C5, with C…O distance of 3.12 Å (C–H...O range of 2.65–2.95 Å) and C–H...O angles range of 90.4–126.3°. Only one crystallographically independent π-stacking interaction occurs (Fig. 3.11c). The terminal phenyl ring containing C10 stacks with the neighbouring ring containing $C10^{ii}$ across an inversion centre (symmetry code ii = 1−*x*, 1−*y*, −*z*). The rings are offset with respect to each other and the centroid⋯centroid separation is 4.12 Å. The interactions are then supplemented by short C–H...π(arene) contacts.

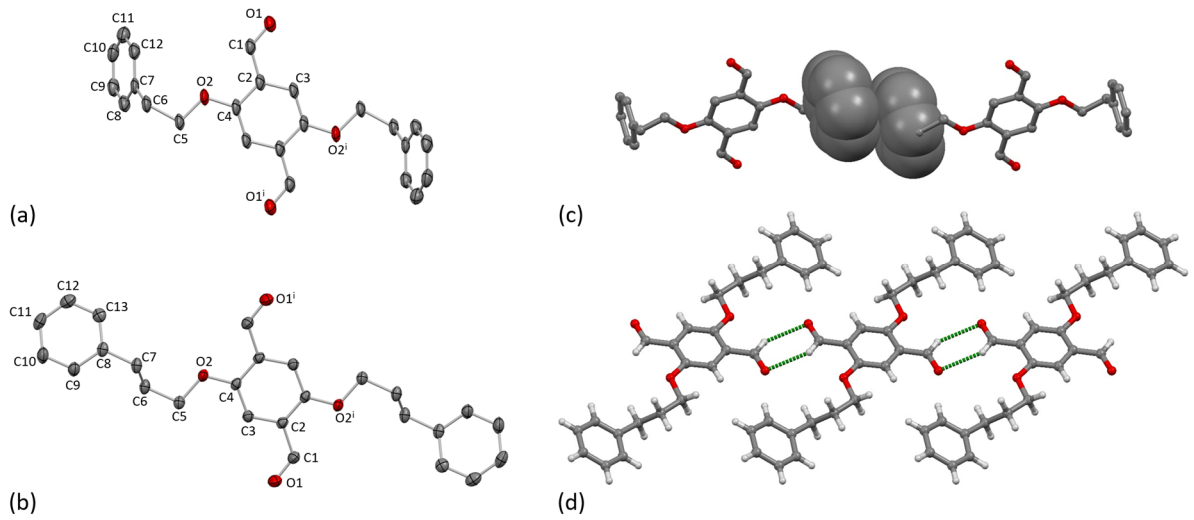

Figure 3.11 The molecular structures of (a) **5b** and (b) **6b**. H atoms are omitted for clarity, and thermal ellipsoids are drawn at 40% probability level. Symmetry code: i = 1−*x*, −*y*, 1−*z*. (c) Face-to-face π-stacking between two molecules of **5b**. H atoms are omitted for clarity. (d) C–H...O hydrogen bonding between molecules of **6b** leads to ribbons.

In contrast, the packing in **6b** is dominated by C–H...O hydrogen bonds. Two CHO groups interact via a pair of C–H...O hydrogen bonds, generating a six-membered ring through a centrosymmetric arrangement; hydrogen bond metrics are C1^{ii}...O1 = 3.27 Å (C1^{ii}–H1^{ii}...O1 = 2.52 Å), C1^{ii}–H1^{ii}...O1 = 135.9° (symmetry code ii = −*x*, −*y*, 1−*z*). The interconnection of the CHO groups arranges the molecules into 1D ribbons as shown in Fig. 3.11d. The individual ribbons are parallel with respect to each other and the stacking is slightly staggered following an ABAB pattern (Fig. 3.12). Weak short C–H...π(arene) interactions link the different stacks.

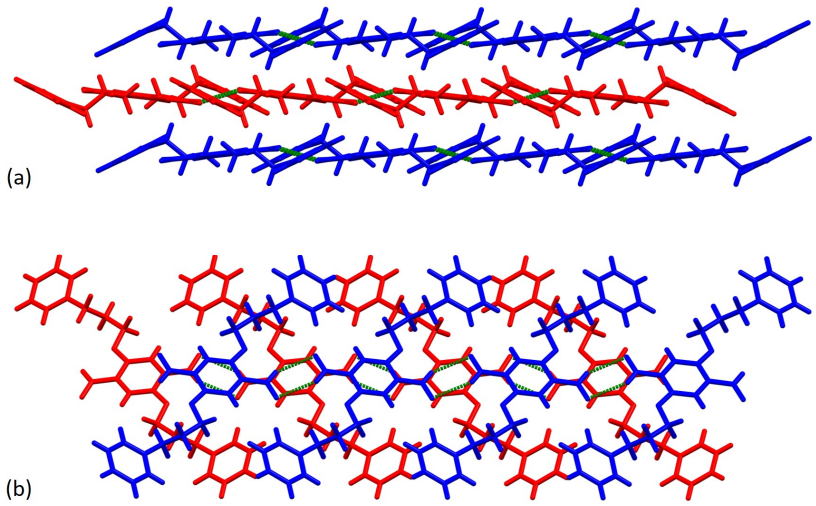

Figure 3.12 (a) Looking along the side of the ribbons in **6b** to illustrate that the packing is following an ABAB pattern. (b) Ribbons are shown down on the stack. The intermolecular O...H–C hydrogen bonds are illustrated in green and the individual ribbons are alternately coloured in red and blue.

The self-association of aromatic aldehydes dimers via C–H…O interactions is rare. A search of the Cambridge Structural Database (CSD v. 2021.3.0, April 2022) for structures containing aromatic aldehydes revealed that only 157 out of 4039 crystal structures form dimers of the type found in **6b**. Statistical analysis, using normalised H, reports mean distances of 2.57(10) and 2.58(9) Å for the pair

of C–H…O interactions involved in dimer formation, with C–H…O angles of 130(14) and 129(14)°, respectively. In our case, a C–H…O distance of 2.42 Å and an angle of 133.6° (with normalised H) are consistent with the mean literature values.

3.5 Crystal growth experiments

Solutions of $[M(hfacac)_2]\cdot xH_2O$ (M = Cu, x = 1; M = Zn, x = 2) in either toluene, chlorobenzene or 1,2-dichlorobenzene were layered over a chloroform solution of **5** or **6** at room temperature. The reactions were carried out using molar metal/ligand ratios of 2:1 (see experimental for full details). For each ligand, X-ray quality crystals were obtained with different solvent combinations, leading to sets of crystals that provided five crystal structures listed in Table 3.3.

Table 3.3 Crystal structures and the solvent for $[Cu(hfacac)_2]\cdot H_2O$ and $[Zn(hfacac)_2]\cdot 2H_2O$, and space groups. The solvent for ligands **5** and **6** was $CHCl_3$.

Coordination polymer	Solvent for $[M(hfacac)_2]\cdot xH_2O$	Space group
$[Cu_2(hfacac)_4(\mathbf{5})]_n\cdot 3.6n(1,2\text{-}Cl_2C_6H_4)\cdot 2nCHCl_3$	1,2-Dichlorobenzene	$P2_1/n$
$[Zn_2(hfacac)_4(\mathbf{5})]_n\cdot nMeC_6H_5\cdot 1.8nCHCl_3$	Toluene	$P2_1/n$
$[Cu_2(hfacac)_4(\mathbf{6})]_n\cdot nMeC_6H_5\cdot 2nH_2O$	Toluene	$P\bar{1}$
$[Cu_2(hfacac)_4(\mathbf{6})]_n\cdot 2.8nC_6H_5Cl$	Chlorobenzene	$P\bar{1}$
$[Cu_2(hfacac)_4(\mathbf{6})]_n\cdot 2n(1,2\text{-}Cl_2C_6H_4)\cdot 0.4nCHCl_3\cdot 0.5nH_2O$	1,2-Dichlorobenzene	$P\bar{1}$

Structural analysis confirmed the assembly of a 2D-coordination polymer in each case, comprising solvated coordination networks with the general formula $[M_2(hfacac)_4(\mathbf{L})]_n$ (M = Cu, Zn). From the reaction between **6** and $[Cu(hfacac)_2]\cdot H_2O$, single-crystals grew from three solvent combinations yielding $[Cu_2(hfacac)_4(\mathbf{6})]_n\cdot nMeC_6H_5\cdot 2nH_2O$ (from toluene/$CHCl_3$), $[Cu_2(hfacac)_4(\mathbf{6})]_n\cdot 2.8nC_6H_5Cl$ (from chlorobenzene/$CHCl_3$) and $[Cu_2(hfacac)_4(\mathbf{6})]_n\cdot 2n(1,2\text{-}Cl_2C_6H_4)\cdot 0.4nCHCl_3\cdot 0.5nH_2O$ (from 1,2-dichlorobenzene/$CHCl_3$). The first two are isostructural networks which crystallise in the triclinic space group $P\bar{1}$ and possess comparable cell dimensions (a = 8.9300(2), b = 15.7218(3), c = 16.4219(3) Å, α = 100.0302(15), β = 93.7146(16), γ = 96.8981(18)° for $[Cu_2(hfacac)_4(\mathbf{6})]_n\cdot nMeC_6H_5\cdot 2nH_2O$, and a = 8.9544(2), b = 15.7417(4), c = 16.3905(4) Å, α = 100.053(2), β = 94.071(2), γ = 97.071(2)° for $[Cu_2(hfacac)_4(\mathbf{6})]_n\cdot 2.8nC_6H_5Cl$). Therefore, only the structure of $[Cu_2(hfacac)_4(\mathbf{6})]_n\cdot 2.8nC_6H_5Cl$ is discussed in detail. In $[Cu_2(hfacac)_4(\mathbf{6})]_n\cdot 2n(1,2\text{-}Cl_2C_6H_4)\cdot 0.4nCHCl_3\cdot 0.5nH_2O$, a change in conformation of the 3,2':6',3''-tpy domains justifies a separate description of this structure. All five assemblies are (4,4)-nets, but two structurally distinct designs can be identified and are discussed separately: (4,4)-nets with a *trans*-arrangement of the $\{Cu(hfacac)_2(N_1)(N_2)\}$ units and a (4,4)-net with *cis*-arrangement of the $\{Zn(hfacac)_2(N_1)(N_2)\}$ units (Scheme 3.7)

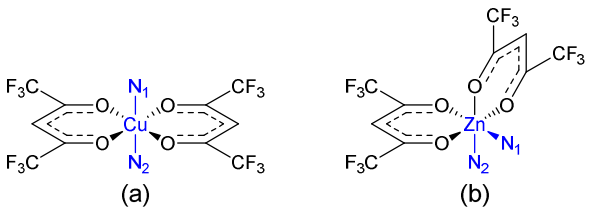

Scheme 3.7 Schematic representations of (a) *trans*-$\{Cu(hfacac)_2(N_1)(N_2)\}$ and (b) *cis*-$\{Zn(hfacac)_2(N_1)(N_2)\}$ fragments. N_1 and N_2 originate from two different bis(tpy) ligands.

3.6 (4,4)-Networks containing [Cu(hfacac)$_2$] linkers

$[Cu_2(hfacac)_4(\mathbf{5})]_n{\cdot}3.6n(1,2\text{-}Cl_2C_6H_4){\cdot}2n CHCl_3$ crystallises in the monoclinic space group $P2_1/n$, while $[Cu_2(hfacac)_4(\mathbf{6})]_n{\cdot}2.8nC_6H_5Cl$ and $[Cu_2(hfacac)_4(\mathbf{6})]_n{\cdot}2n(1,2\text{-}Cl_2C_6H_4){\cdot}0.4nCHCl_3{\cdot}0.5nH_2O$ crystallise in the triclinic space group $P\text{–}1$. In $[Cu_2(hfacac)_4(\mathbf{5})]_n{\cdot}3.6n(1,2\text{-}Cl_2C_6H_4){\cdot}2nCHCl_3$ the asymmetric unit contains one independent copper atom and one independent half-ligand. In contrast, the asymmetric units of $[Cu_2(hfacac)_4(\mathbf{6})]_n{\cdot}2.8nC_6H_5Cl$ and $[Cu_2(hfacac)_4(\mathbf{6})]_n{\cdot}2n(1,2\text{-}Cl_2C_6H_4){\cdot}0.4nCHCl_3{\cdot}0.5nH_2O$ contain two independent half copper atoms and one independent half-ligand. The copper centres lie on crystallographic inversion centres. For $[Cu_2(hfacac)_4(\mathbf{6})]_n{\cdot}2n(1,2\text{-}Cl_2C_6H_4){\cdot}0.4nCHCl_3{\cdot}0.5nH_2O$, Cu2 is disordered over an inversion centre; for the discussion of the polymer, only the mean position is considered. The representations of their repeating units are displayed in Fig. 3.13.

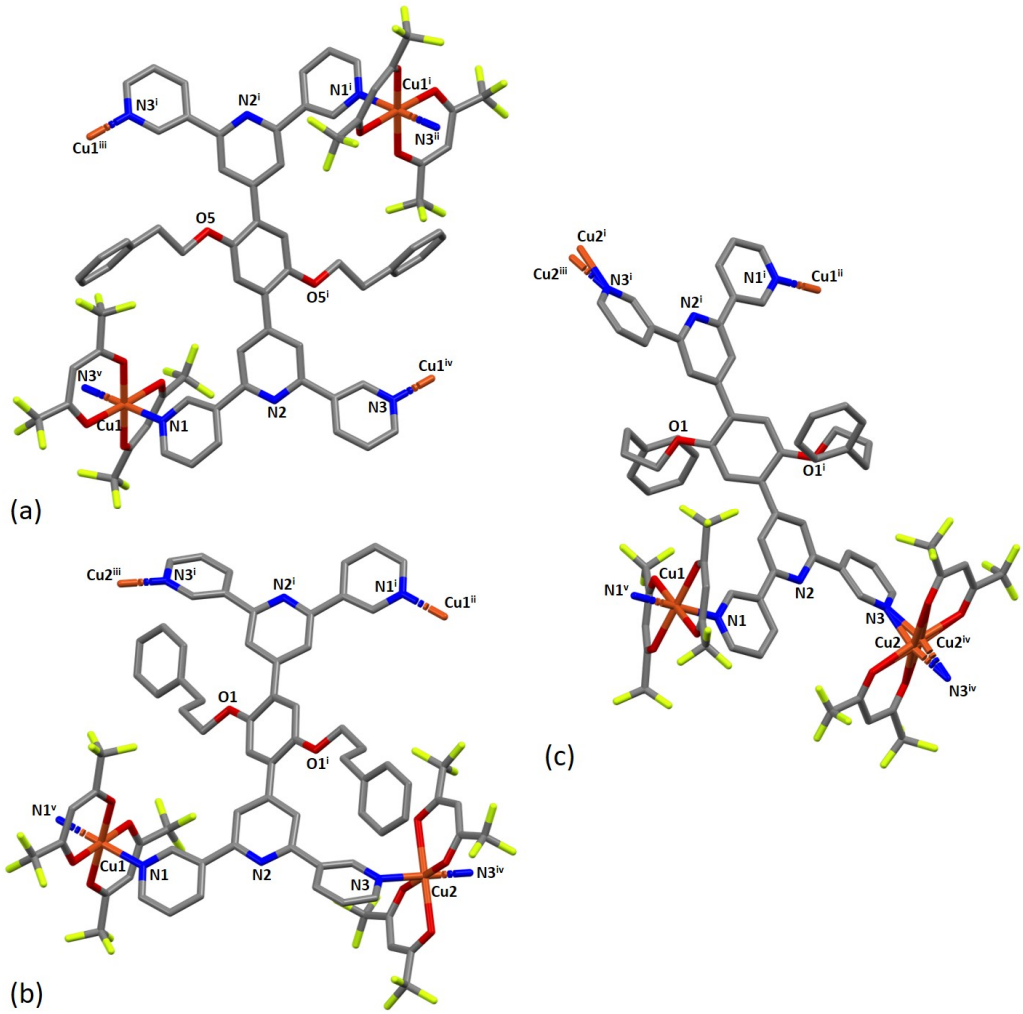

Figure 3.13 The structure of the repeating unit in (a) $[Cu_2(hfacac)_4(\mathbf{5})]_n{\cdot}3.6n(1,2\text{-}Cl_2C_6H_4){\cdot}2nCHCl_3$ (symmetry codes: i = 1–*x*, 1–*y*, 1–*z*; ii = $^1/_2$+*x*, 1.5–*y*, $-^1/_2$+*z*; iii= $^1/_2$+*x*, $^1/_2$–*y*, $-^1/_2$+*z*; iv = $^1/_2$–*x*, $^1/_2$+*y*, 1.5–*z*; v = $^1/_2$–*x*, $-^1/_2$+*y*, 1.5–*z*), (b) $[Cu_2(hfacac)_4(\mathbf{6})]_n{\cdot}2.8nC_6H_5Cl$ (symmetry codes: i = 1–*x*, 1–*y*, 2–*z*; ii = *x*, *y*, 1+*z*; iii= 1+*x*, 1+*y*, *z*; iv = –*x*, –*y*, 2–*z*; v = 1–*x*, 1–*y*, 1–*z*) and (c) $[Cu_2(hfacac)_4(\mathbf{6})]_n{\cdot}2n(1,2\text{-}Cl_2C_6H_4){\cdot}0.4nCHCl_3{\cdot}0.5nH_2O$ (symmetry codes: i = –*x*, –*y*, 1–*z*; ii = –1+*x*, –1+*y*, *z*; iii= *x*, –1+*y*, –1+*z*; iv = –*x*, 1–*y*, 2–*z*; v = 1–*x*, 1–*y*, 1–*z*) with symmetry generated atoms. H atoms and solvent molecules are omitted, and only the major occupancy is shown (see experimental section).

In all three compounds, each Cu(II) centre is octahedrally coordinated with a *trans*-arrangement of coordinated [hfacac]$^-$ ligands. Bond lengths and angles in the Cu(II) coordination sphere are typical, with Cu–N distances in the range 1.981(5)-2.048(9) Å and Cu–O in the range 1.979(4)-2.330(5) Å. In both coordinated ligand **5** and **6**, the two tpy domains are crystallographically related, with the phenylene spacer centroid lying on an inversion centre. Each bis(tpy) ligand binds through the outer nitrogen donors to four Cu(II) centers, therefore acting as the 4-connecting node and directing the assembly of a (4,4)-net. The tpy units are non-planar and the torsion angles between the ring planes range between 4.5° and 33.6° (Table 3.4). Torsion angles of 34.5°, 39.1° and 51.1° between the planes of the central pyridine ring and the central arene spacer are typical for minimising inter-ring H···H repulsions.

Table 3.4 Angles between the planes of pairs of connected rings in coordinated ligands.

Compound	py-py /°	py_{N2}-phenyl /°[a]
$[Cu_2(hfacac)_4(\mathbf{5})]_n \cdot 3.6n(1,2\text{-}Cl_2C_6H_4) \cdot 2nCHCl_3$	27.5, 33.6	39.1
$[Cu_2(hfacac)_4(\mathbf{6})]_n \cdot 2.8nC_6H_5Cl$	4.5, 32.9	34.5
$[Cu_2(hfacac)_4(\mathbf{6})]_n \cdot 2n(1,2\text{-}Cl_2C_6H_4) \cdot 0.4nCHCl_3 \cdot 0.5nH_2O$	5.9, 28.4	51.1

[a] N2, for labelling schemes see Fig. 3.13.

In $[Cu_2(hfacac)_4(\mathbf{5})]_n \cdot 3.6n(1,2\text{-}Cl_2C_6H_4) \cdot 2nCHCl_3$ and $[Cu_2(hfacac)_4(\mathbf{6})]_n \cdot 2.8nC_6H_5Cl$ both ligand **5** and **6** adopt conformation **B** (Scheme 3.2). Interestingly, with ligand **6**, a solvent change from chlorobenzene (or toluene) to 1,2-dichlorobenzene leads to a conformational change of the tpy groups within the 2D-polymer (Fig. 3.14b and 3.14c, top). In fact, in $[Cu_2(hfacac)_4(\mathbf{6})]_n \cdot 2n(1,2\text{-}Cl_2C_6H_4) \cdot 0.4nCHCl_3 \cdot 0.5nH_2O$, ligand **6** displays conformation **C** (Scheme 3.2), although this does not lead to a significant change in the network (Fig. 3.14b and 3.14c, middle). In all three structures, the combination of ligand **5** or **6** with $[Cu(hfacac)_2] \cdot H_2O$ leads to a 2D-net directed by the tetratopic ligands. The centroids of the phenylene spacers are the nodes of the network, whereas the copper centres act as linkers (Fig. 3.14, middle). The network in $[Cu_2(hfacac)_4(\mathbf{5})]_n \cdot 3.6n(1,2\text{-}Cl_2C_6H_4) \cdot 2nCHCl_3$ contains a rhombic shortest circuit with internal angles of 87.0 and 93.0° and a node...node distance of 16.94 Å. The copper atoms are close to the plane of the (4,4)-net generating a small deformation in the structure (Fig. 3.14a, middle and bottom). In contrast, in $[Cu_2(hfacac)_4(\mathbf{6})]_n \cdot 2.8nC_6H_5Cl$ and $[Cu_2(hfacac)_4(\mathbf{6})]_n \cdot 2n(1,2\text{-}Cl_2C_6H_4) \cdot 0.4nCHCl_3 \cdot 0.5nH_2O$, the shortest circuits are parallelograms (Fig. 3.14b and 3.14c, middle) with the copper centres lying in the plane (Fig. 3.14b and 3.14c, bottom). The conformational change of ligand **6** does not appear to play a crucial role in the assembly. Indeed, from $[Cu_2(hfacac)_4(\mathbf{6})]_n \cdot 2.8nC_6H_5Cl$ to $[Cu_2(hfacac)_4(\mathbf{6})]_n \cdot 2n(1,2\text{-}Cl_2C_6H_4) \cdot 0.4nCHCl_3 \cdot 0.5nH_2O$, only minor changes occur in the distances and angles between the nodes (Table 3.5).

Table 3.5. Distances and angles between the nodes in the (4,4)-nets.

Compound	Node–Node distance/Å	Internal angles of rhombus in (4,4) net/°
$[Cu_2(hfacac)_4(\mathbf{5})]_n \cdot 3.6n(1,2\text{-}Cl_2C_6H_4) \cdot 2nCHCl_3$	16.94	87.0, 93.0
$[Cu_2(hfacac)_4(\mathbf{6})]_n \cdot 2.8nC_6H_5Cl$	16.42, 17.12	78.8, 101.2
$[Cu_2(hfacac)_4(\mathbf{6})]_n \cdot 2n(1,2\text{-}Cl_2C_6H_4) \cdot 0.4nCHCl_3 \cdot 0.5nH_2O$	16.17, 20.68	73.0, 107.0

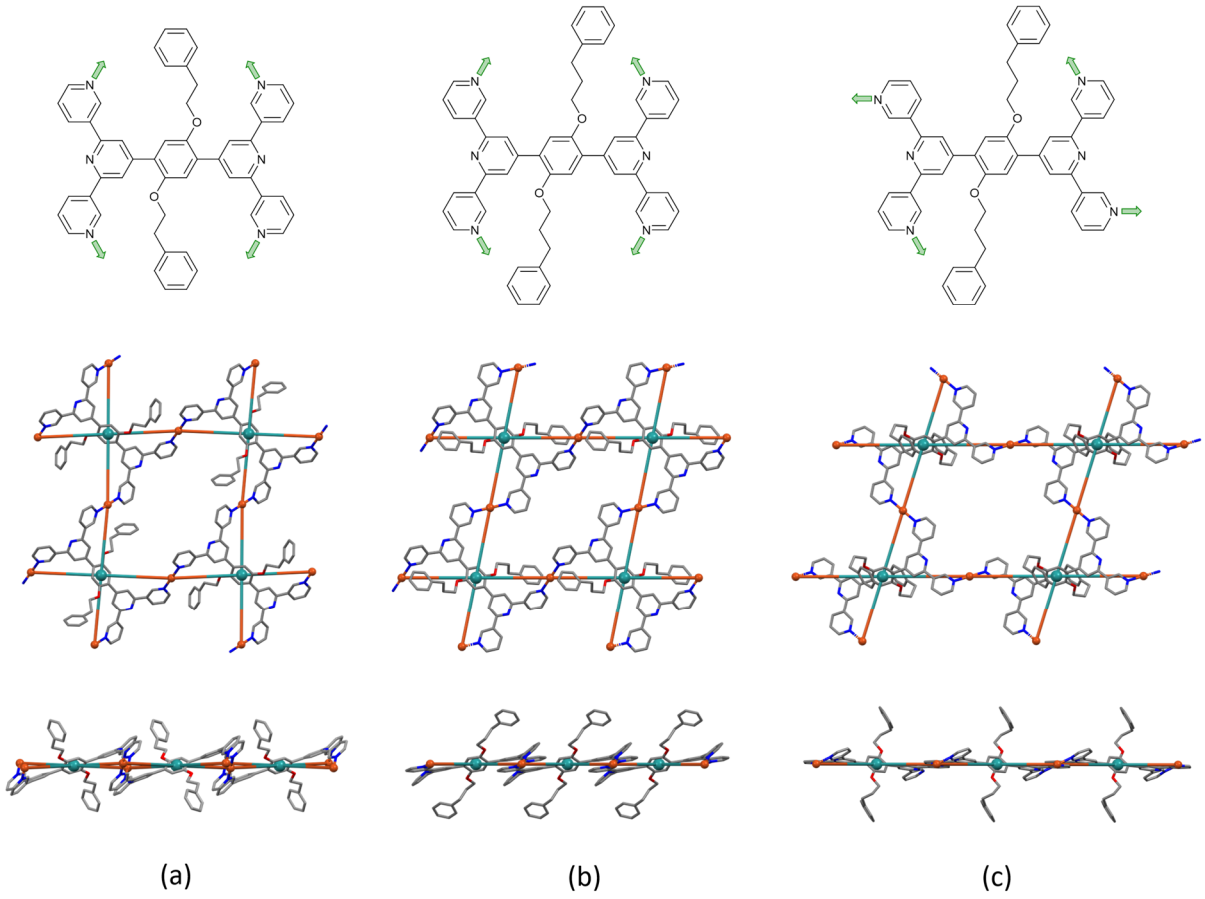

Figure 3.14 Comparison of the ligand conformations and the (4,4) nets in (a) $[Cu_2(hfacac)_4(\mathbf{5})]_n \cdot 3.6n(1,2\text{-}Cl_2C_6H_4) \cdot 2nCHCl_3$, (b) $[Cu_2(hfacac)_4(\mathbf{6})]_n \cdot 2.8nC_6H_5Cl$, and (c) $[Cu_2(hfacac)_4(\mathbf{6})]_n \cdot 2n(1,2\text{-}Cl_2C_6H_4) \cdot 0.4nCHCl_3 \cdot 0.5nH_2O$. Top, conformation of the coordinated ligand; middle, looking down on the sheets; bottom, (4,4) nets observed through the mean plane determined by the nodes of the ligand centroids (green). For clarity, H atoms, coordinated $[hfacac]^-$ ligands and solvent are omitted, and only major occupancies are shown.

All the structures considered in this section have phenylalkoxy groups pointing above and below the plane (Fig. 3.14, bottom). $[Cu_2(hfacac)_4(\mathbf{5})]_n \cdot 3.6n(1,2\text{-}Cl_2C_6H_4) \cdot 2nCHCl_3$ and $[Cu_2(hfacac)_4(\mathbf{6})]_n \cdot 2n(1,2\text{-}Cl_2C_6H_4) \cdot 0.4nCHCl_3 \cdot 0.5nH_2O$ were crystallised in the same solvent mixture (from 1,2-dichlorobenzene/$CHCl_3$) and with the same reagent concentrations. The only difference is in the length of the phenylalkoxy substituent, ligand **5** possesses 2-phenylethoxy groups whereas ligand **6** possesses 3-phenylpropoxy substituents. Despite the difference of only one CH_2 group, the network is significantly affected upon going from $[Cu_2(hfacac)_4(\mathbf{5})]_n \cdot 3.6n(1,2\text{-}Cl_2C_6H_4) \cdot 2nCHCl_3$ to $[Cu_2(hfacac)_4(\mathbf{6})]_n \cdot 2n(1,2\text{-}Cl_2C_6H_4) \cdot 0.4nCHCl_3 \cdot 0.5nH_2O$ (Fig. 3.14a and 3.14c). It is important to note that, in $[Cu_2(hfacac)_4(\mathbf{5})]_n \cdot 3.6n(1,2\text{-}Cl_2C_6H_4) \cdot 2nCHCl_3$, the peripheral phenyl ring is not involved in any significant interactions, whereas in $[Cu_2(hfacac)_4(\mathbf{6})]_n \cdot 2n(1,2\text{-}Cl_2C_6H_4) \cdot 0.4nCHCl_3 \cdot 0.5nH_2O$, short C–H...π(arene) interactions link the pendant phenyl ring with the 1,2-dichlorobenzene molecule and the phenylene spacer of the ligand in the adjacent sheet (Fig. 3.15a). The 3-phenylpropoxy substituent also engages in weak interactions in the crystal structure of $[Cu_2(hfacac)_4(\mathbf{6})]_n \cdot 2.8nC_6H_5Cl$, where the terminal phenyl ring stacks with the central arene spacer of the ligand **6** contained in a neighbouring (4,4)-net (Fig. 3.15b). In each lattice, the individual layers pack with the cavities running down the crystallographic *a*-axis (Fig. 3.16a). The solvent molecules are accommodated within these open channels (Fig. 3.16b).

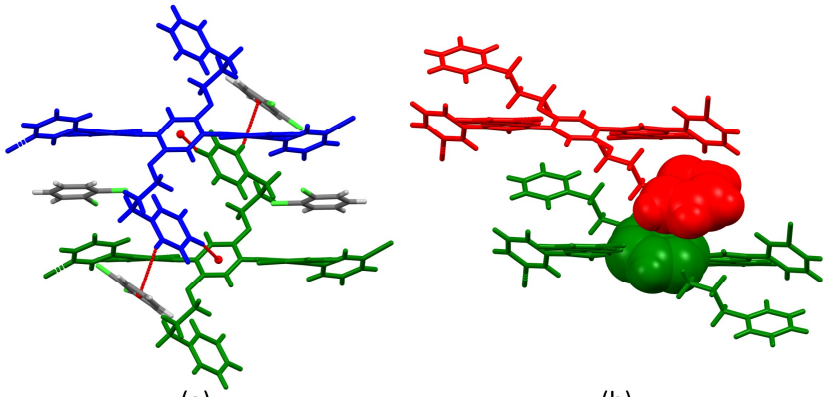

Figure 3.15 (a) Short C–H...π(arene) interactions are present in $[Cu_2(hfacac)_4(\mathbf{6})]_n \cdot 2n(1,2\text{-}Cl_2C_6H_4) \cdot 0.4n CHCl_3 \cdot 0.5n H_2O$. The contacts arise from the interaction of the peripheral phenyl ring with the 1,2-dichlorobenzene molecule (C–H...centroid separation: 3.16 Å) and the phenylene spacer of the ligand in the adjacent sheet (C–H...centroid separation: 3.00 Å). The two neighbouring 2D-nets are coloured in blue and in green. (b) Face-to-face π-stacking interactions are present between the sheets (red and green) in $[Cu_2(hfacac)_4(\mathbf{6})]_n \cdot 2.8n C_6H_5Cl$. The terminal phenyl ring stacks with the central arene spacer of the ligand **6** contained in a neighbouring (4,4)-net. The rings are offset with respect to each other and the centroid...centroid separation is 3.93 Å. For clarity, $[hfacac]^-$ ligands and solvent molecules are omitted, and only the major occupancies of the disordered sites are shown.

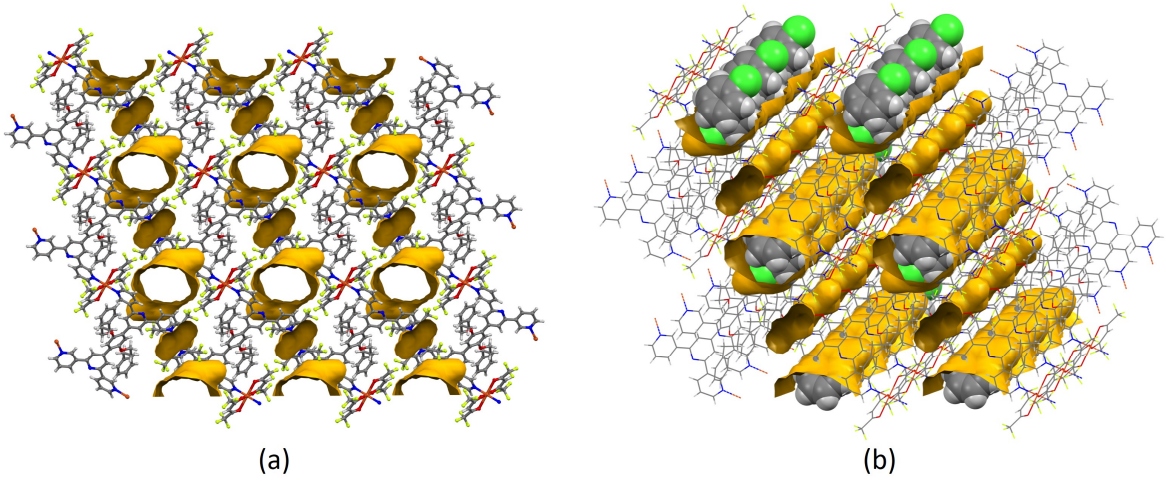

Figure 3.16 (a) Illustration of the void space in the crystal lattices of $[Cu_2(hfacac)_4(\mathbf{6})]_n \cdot 2.8n C_6H_5Cl$ (ca. 21% void) with channels following the *a*-axis. (b) Representation of the same structure with solvent molecules. The void was calculated from the structure without solvent molecules. Subsequently, the same structure with solvent molecules was superimposed on the one without, revealing the chlorobenzene in the channels. Contact surface map with probe radius = 1.2 Å. Calculations made with Mercury (v. 2021.3.0).[180]

3.7 (4,4)-Network containing [Zn(hfacac)$_2$] linkers

Single-crystals of $[Zn_2(hfacac)_4(\mathbf{5})]_n \cdot n MeC_6H_5 \cdot 1.8n CHCl_3$ were grown by layering a toluene solution of $[Zn(hfacac)_2] \cdot 2H_2O$ over a $CHCl_3$ solution of **5**. $[Zn_2(hfacac)_4(\mathbf{5})]_n \cdot n MeC_6H_5 \cdot 1.8n CHCl_3$ crystallises in the monoclinic space group $P2_1/n$. The asymmetric unit contains one independent Zn(II) centre and one independent half-ligand; the second half is generated by inversion. A representation of the repeating unit with symmetry generated atoms is shown in Fig. 3.17.

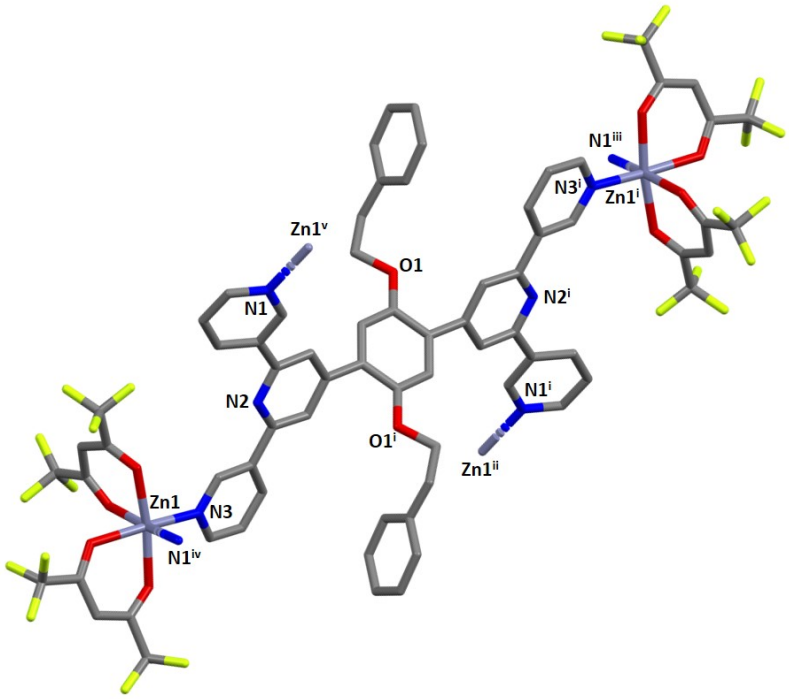

Figure 3.17 The structure of the repeat unit in $[Zn_2(hfacac)_4(\mathbf{5})]_n \cdot n MeC_6H_5 \cdot 1.8 n CHCl_3$ with symmetry generated atoms. Symmetry codes: i = 1–*x*, 1–*y*, 1–*z*; ii = $^1/_2$+*x*, 1.5–*y*, $^1/_2$+*z*; iii= $^1/_2$+*x*, $^1/_2$–*y*, $^1/_2$+*z*; iv = $^1/_2$–*x*, $^1/_2$+*y*, $^1/_2$–*z*; v = $^1/_2$–*x*, –$^1/_2$+*y*, $^1/_2$–*z*. H atoms and solvent molecules are omitted. The phenylene spacer together with its 3-phenylethoxy substituent is disordered in a 1:1 ratio and only one of the equal occupancy disordered sites is shown.

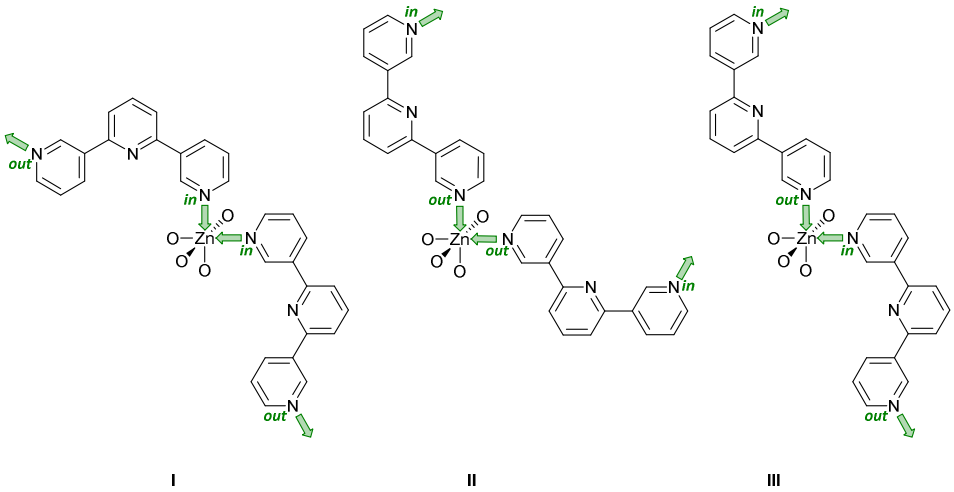

Scheme 3.8 With pairs of 3,2':6',3''-tpy ligands in conformation **C** (Scheme 3.2), there are three possible coordination topologies (I)–(III) at a Zn atom that does not lie on an inversion center. The labels *in* and *out* indicate the orientation of the lone pair of each coordinating N atom relative to the central N atom of the 3,2':6',3''-tpy unit. Only limiting planar conformations are shown and coordinated oxygen atoms arise from $[hfacac]^-$ ligands.

The Zn atom is octahedrally sited and coordinated to four oxygen atoms of two chelating $[hfacac]^-$ ligands (Zn–O in the range 2.083(2)-2.136(2) Å), and to two pyridine donor atoms of two different ligands **5** (Zn–N = 2.100(1), 2.120(3) Å), which are in a *cis*-arrangement. The coordination sphere is distorted with an N–Zn–N bond angle of 97.70(10)° and similar values have been reported previously for *cis*-$\{Zn(hfacac)_2(N_1)(N_2)\}$ complexes with substituted pyridine donors.[181-183] The tpy domain adopts conformation **C** (Scheme 3.2) and the angles between the planes of the rings containing N1/N2 and N2/N3 are 25.2 and 3.9°, respectively. The phenylene spacer is rotated 50.7° relative to the pyridine

ring containing N2. Note that when the metal is not on an inversion centre and the two 3,2':6',3"-tpy units are in conformation **C** (Scheme 3.2), three spatial arrangements of tpy domains are possible (Scheme 3.8). In $[Zn_2(hfacac)_4(\mathbf{5})]_n \cdot n MeC_6H_5 \cdot 1.8 n CHCl_3$, pairs of ligand **5** are arranged in the orientation III as shown in Scheme 3.8.

As with the complexes described in the previous section, ligand **5** behaves as a 4-connecting node, coordinating four different Zn(II) ions and directing the assembly of a planar (4,4)-net (Fig. 3.18a). The distance between adjacent ligand nodes (centroids of the phenylene spacers) is 15.11 Å and the internal angles of the rhombic shortest circuit are 59.4 and 120.6°. Compared to the copper(II) structures reported in this work, the topology of the zinc(II) network is identical. However, structural differences can be seen by examination of how the metal linkers and the phenylalkoxy tails are arranged. The zinc(II) centres are disposed alternately above and beneath the plane generated by the ligand nodes, while the 2-phenylethoxy chains are located in the plane (Fig. 3.18b). Each cavity of the network accommodates two 2-phenylethoxy tails, both originating from the same individual 2D-coordination polymer, and the pendant phenyl rings interact via a face-to-face π-interaction across an inversion centre (Fig. 3.19a).

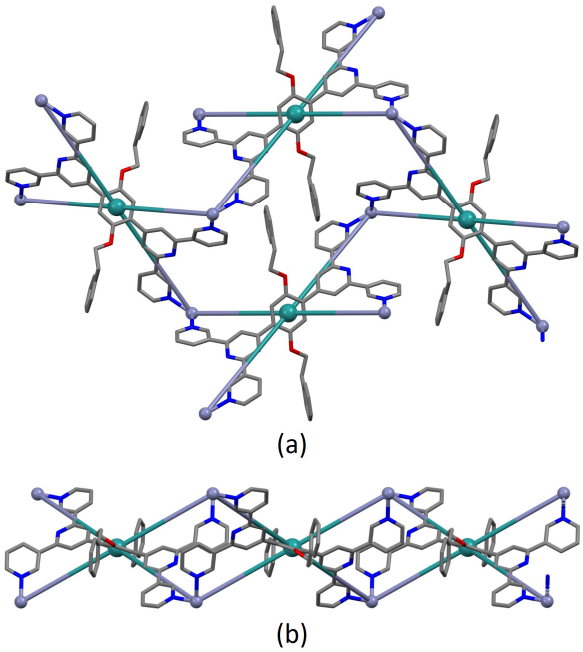

Figure 3.18 Shortest circuit with four nodes (ligand centroids, green) of the (4,4) net in $[Zn_2(hfacac)_4(\mathbf{5})]_n \cdot n MeC_6H_5 \cdot 1.8 n CHCl_3$; (a) looking down on the sheet, (b) (4,4) net observed through the mean plane determined by the nodes. For clarity, H atoms, coordinated $[hfacac]^-$ ligands and solvent are omitted, and only major occupancies are shown.

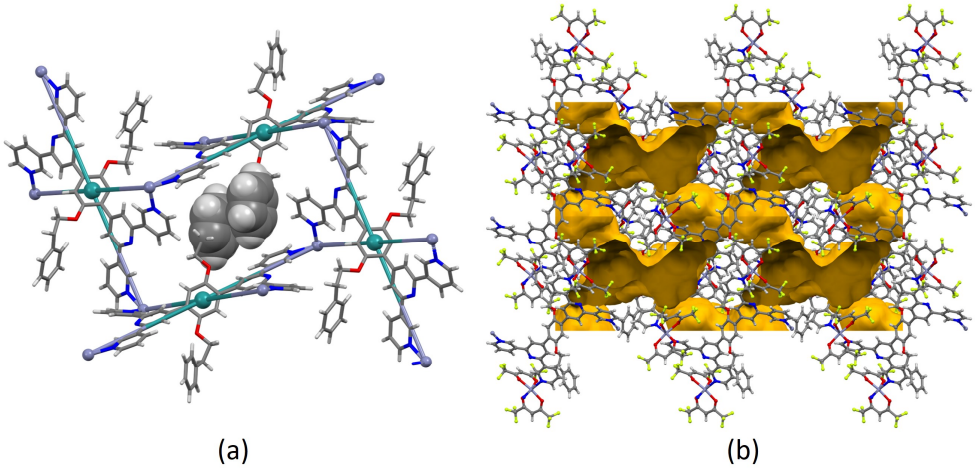

Figure 3.19 (a) Face-to-face π-stacking interactions are present between pairs of terminal phenyl rings accommodated in the cavities of the (4,4)-net in $[Zn_2(hfacac)_4(\mathbf{5})]_n{\cdot}n MeC_6H_5{\cdot}1.8nCHCl_3$. The rings are offset with respect to each other and the centroid...centroid separation is 4.09 Å. The ligand centroids are coloured in green and define the network. For clarity, $[hfacac]^-$ ligands and solvent molecules are omitted, and only one of the equal occupancy disordered sites is shown (b) Illustration of the void space in the crystal lattices of $[Zn_2(hfacac)_4(\mathbf{5})]_n{\cdot}n MeC_6H_5{\cdot}1.8nCHCl_3$ (ca. 33% void) following the *a*-axis. Contact surface map with probe radius = 1.2 Å. Calculations made with Mercury (v. 2021.3.0).[180]

Note that a change from a *trans* to a *cis* arrangement of the N-donors on going from the Cu(II) to Zn(II) structures modifies the architecture of the assembly without changing the underlying (4,4)-network. On the other hand, Masters candidate Simona Capomolla recently reported a planar (4,4)-net with *trans*-$\{Cu(hfacac)_2(N_1)(N_2)\}$ domains lying above and below the plane displaying a similar arrangement of metal linkers.[36] In $[Zn_2(hfacac)_4(\mathbf{5})]_n{\cdot}n MeC_6H_5{\cdot}1.8nCHCl_3$, viewed down the crystallographic *b*-axis, the individual layers are parallel to each other (Fig. 3.20). The packing of the sheets shows a zigzag arrangement with the CF_3 groups protruding out of the plane. Interactions between the layers are dominated by short C–H...F–C contacts between 2-phenylethoxy substituents in one sheet and the CF_3 groups from the neighbouring one. However, since the CF_3 groups are disordered, a detailed discussion is not meaningful. Removal of the solvent molecules from the structure reveals cavities (Fig. 3.19b) rather than open channels in which they are located.

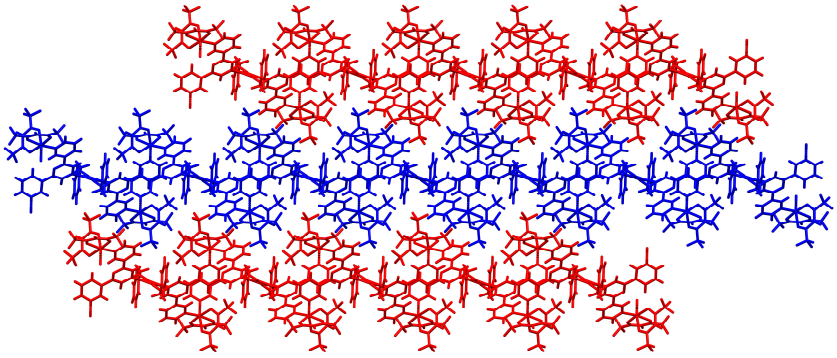

Figure 3.20 Three layers alternately coloured in red and blue in $[Zn_2(hfacac)_4(\mathbf{5})]_n{\cdot}n MeC_6H_5{\cdot}1.8nCHCl_3$ viewed from the crystallographic *b*-axis. For clarity, solvent molecules are omitted, and only one of the equal occupancy sites is shown.

3.8 Bulk sample analysis

Once single-crystals had been selected for single-crystal X-ray structure diffraction, the bulk materials were analysed by powder X-ray diffraction (PXRD). All the crystalline materials were sensitive to loss of solvent upon exposure to air and were thus measured wet and without washing them. For $[Cu_2(hfacac)_4(\mathbf{6})]_n{\cdot}n MeC_6H_5{\cdot}2nH_2O$, all peaks in the experimental PXRD pattern (red traces in Fig. 3.21a) correspond to the predicted pattern from the single-crystal structure (black traces in Fig. 3.21a). Preferred orientations of the crystallites explain the differences in the relative intensities of the peaks (blue traces in Fig. 3.21a). In the same manner, for $[Zn_2(hfacac)_4(\mathbf{5})]_n{\cdot}n MeC_6H_5{\cdot}1.8nCHCl_3$, a good match was found between the experimental PXRD pattern for the bulk material and the pattern predicted from the single-crystal structure (Fig. 3.21b). On the other hand, the fitting between the calculated and experimental patterns of the remaining compounds did not show a good match and are shown in Fig. 3.22. Unlike the single-crystal X-ray determinations, which were carried out at low temperatures, the PXRD patterns were recorded at room temperature. Phase transition and solvent loss can affect the PXRD significantly and in view of the observed facile solvent loss, the crystallographic properties of the bulk material were not further investigated.

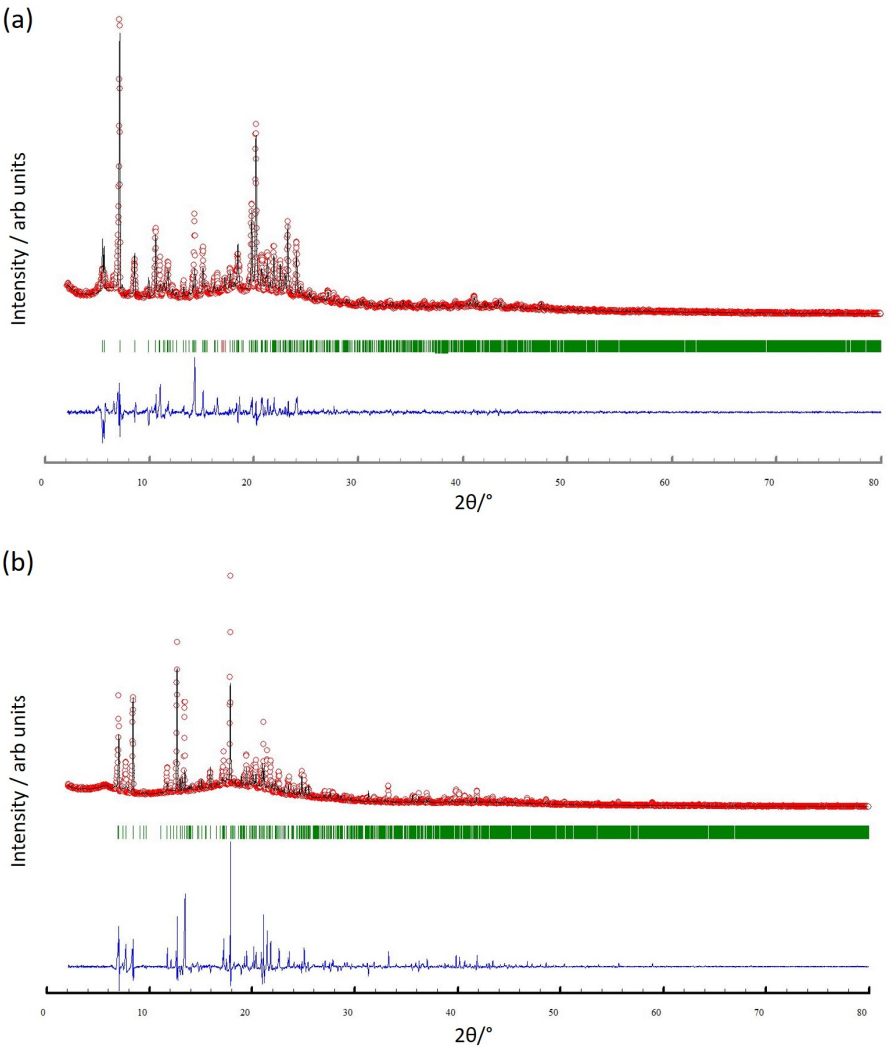

Figure 3.21 X-ray diffraction (CuKα1 radiation) pattern (red circles) of the bulk crystalline material of (a) $[Cu_2(hfacac)_4(\mathbf{6})]_n{\cdot}n MeC_6H_5{\cdot}2nH_2O$ and (b) $[Zn_2(hfacac)_4(\mathbf{5})]_n{\cdot}n MeC_6H_5{\cdot}1.8nCHCl_3$, fitting the predicted pattern from the single-crystal structure. The black lines are the best fit from Rietveld refinements, and green lines display the Bragg peak positions. The blue plot gives the difference between calculated and experimental points.

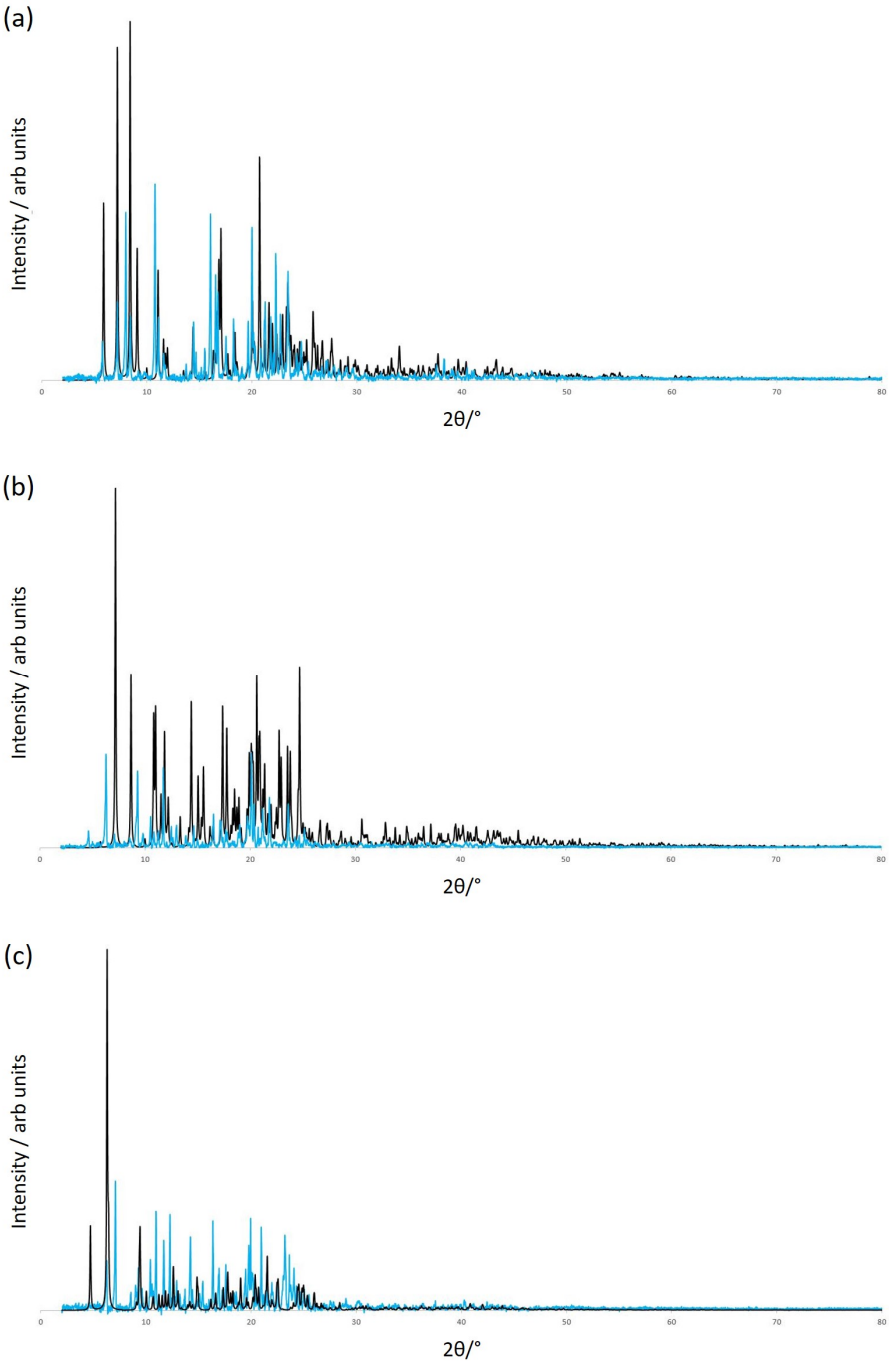

Figure 3.22 Overlay of the experimental (blue) PXRD (298 K) for the bulk material and that predicted (black) from the single-crystal structure of (a) $[Cu_2(hfacac)_4(\mathbf{5})]_n \cdot 3.6n(1,2\text{-}Cl_2C_6H_4) \cdot 2n CHCl_3$ (130 K), (b) $[Cu_2(hfacac)_4(\mathbf{6})]_n \cdot 2.8n C_6H_5Cl$ (160 K), (c) $[Cu_2(hfacac)_4(\mathbf{6})]_n \cdot 2n(1,2\text{-}Cl_2C_6H_4) \cdot 0.4n CHCl_3 \cdot 0.5n H_2O$ (160 K).

In the solid state IR spectra of the dried copper(II) coordination polymers, the absorption of the 1,3-diketonate and the fingerprint regions are almost identical. Given the similarity of the structures, this is not surprising. The IR spectrum of $[Cu_2(hfacac)_4(\mathbf{6})]_n \cdot 2n(1,2\text{-}Cl_2C_6H_4) \cdot 0.4n CHCl_3 \cdot 0.5n H_2O$ is shown in Fig. 3.23 as representative of all others (link to all data: https://zenodo.org/record/7227912).

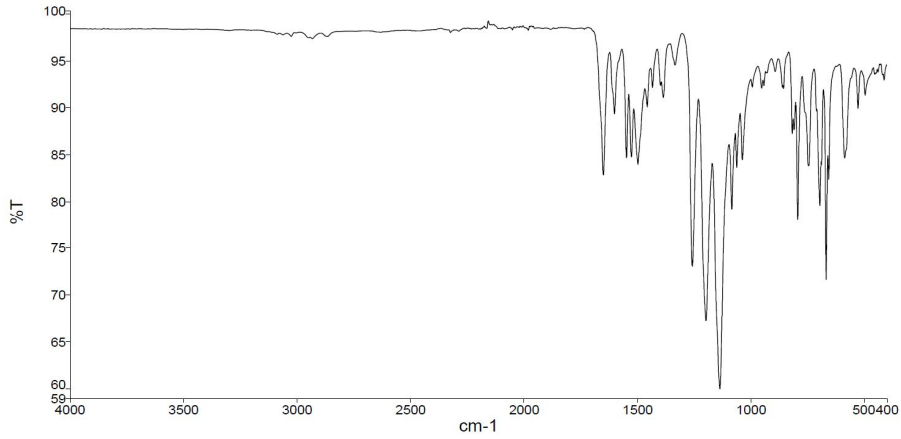

Figure 3.23 The solid state FI-IR spectrum of $[Cu_2(hfacac)_4(\mathbf{6})]_n \cdot 2n(1,2\text{-}Cl_2C_6H_4) \cdot 0.4nCHCl_3 \cdot 0.5nH_2O$.

3.9 Conclusions

Two bis(3,2':6',3'-tpy) **5** and **6** ligands were synthesised and characterised, featuring 2-phenylethoxy and 3-phenylpropoxy substituents attached to the 1,4-phenylene spacer, respectively. Ligands **5** and **6** were then allowed to react with $[M(hfacac)_2] \cdot xH_2O$ (M = Cu, x = 1; M = Zn, x = 2) under ambient condition of crystal growth in a combination of $CHCl_3$ and an aromatic solvent. The single-crystal determination revealed the formation of the 2D-coordination networks $[Cu_2(hfacac)_4(\mathbf{5})]_n \cdot 3.6n(1,2\text{-}Cl_2C_6H_4) \cdot 2nCHCl_3$, $[Zn_2(hfacac)_4(\mathbf{5})]_n \cdot nMeC_6H_5 \cdot 1.8nCHCl_3$, $[Cu_2(hfacac)_4(\mathbf{6})]_n \cdot nMeC_6H_5 \cdot 2nH_2O$, $[Cu_2(hfacac)_4(\mathbf{6})]_n \cdot 2.8nC_6H_5Cl$ and $[Cu_2(hfacac)_4(\mathbf{6})]_n \cdot 2n(1,2\text{-}Cl_2C_6H_4) \cdot 0.4nCHCl_3 \cdot 0.5nH_2O$. $[Cu_2(hfacac)_4(\mathbf{6})]_n \cdot nMeC_6H_5 \cdot 2nH_2O$ and $[Cu_2(hfacac)_4(\mathbf{6})]_n \cdot 2.8nC_6H_5Cl$ are isostructural. In all assemblies, the bis(3,2':6',3''-tpy) ligands coordinate four $[M(hfacac)_2]$ (M = Cu, Zn) units directing the formation of planar (4,4)-nets, with the centroids of the phenylene spacers of **5** or **6** acting as nodes and the metal ions working as linkers.

In the copper(II) coordination polymers the metal ions display a *trans*-arrangement of the N-donor atoms. Differences, such as phenylalkoxy chain length or conformational changes in the 3,2':6',3''-tpy groups, do not change significantly the motif and distinct features remain identical within the series. The Cu(II) centres are located near or in the plane (determined by the nodes) and the phenylalkoxy chains are directed outwards from the individual sheets. By contrast, in $[Zn_2(hfacac)_4(\mathbf{5})]_n \cdot nMeC_6H_5 \cdot 1.8nCHCl_3$, the Zn(II) centres have a *cis*-arrangement of the N atoms and are arranged alternately above and below the network. Pairs of 2-phenylethoxy tails are lodged in each cavity of the (4,4)-net interacting with each other via face-to-face π-interaction.

This work showed that the assembly of planar (4,4)-nets by combining ligands **5** or **6** with $[M(hfacac)_2] \cdot xH_2O$ (M = Cu, x = 1; M = Zn, x = 2) is independent upon the choice of the crystallisation solvents. A switch from Cu(II) to Zn(II) influences the orientation of the metal linkers but does not change the topology of the network.

4 Linear bis(3,2':6',3''-terpyridines): 3D-Nets with $Co(NCS)_2$ 4-connecting nodes

4.1 Motivation

In the preceding chapter, the combination of tetratopic bis(3,2':6',3''-tpy) ligands with metal salts having connectivity two (i.e. a linker) gave (4,4)-networks where the ligands define the nodes. With the ligand-node/metal-linker strategy, the (4,4)-network is a structural motif that has recently been shown to persist.[36] However, the Constable-Housecroft and Yuge research groups have reported examples where the bis(3,2':6',3''-tpy) building block behave as linkers yielding 1D-polymers.[36, 91] Even with bis(4,2':6',4''-tpy) ligands, their reaction with metal linkers often leads to 2D-nets[91, 171, 184, 185] and only one case of a 3D-network has been reported.[171] An easier way to step into the realm of 3D architectures is by using both ligands and metal centres as nodes. Therefore, the connectivity of the metal building block must be three or higher. At the beginning of this project (approx. April 2019), only six 3D-coordination nets comprising bis(3,2':6',3''-tpy) and bis(4,2':6',4''-tpy) ligands were deposited in the Cambridge Structural Database. Except for the case mentioned above of the 3D-framework obtained with a metal linker,[171] specifically $ZnBr_2$, all others were achieved with $Co(NCS)_2$, a four-connecting node.[92, 186-188] However, the coordination behaviour of bis(3,2':6',3''-tpy) ligands remains the least explored with two 3D-nets described.[92, 186, 187] While $[Co(NCS)_2(\mathbf{L10})]_n \cdot 4n CHCl_3$ forms a three-dimensional *pts* net,[92, 187] $[Co(NCS)_2(\mathbf{L11})]_n \cdot 1.6n H_2O \cdot 1.2n(1,2\text{-}Cl_2C_6H_4)$ crystallises in a three-dimensional *cds* net (Fig. 4.1b and c).[186] The structures of **L10** and **L11** are depicted in Fig. 4.1a. These two examples indicate the diversity of 4-connected nets[189] and make predicting the outcome of these combinations far from simple. Changes such as chain length and steric properties of the substituent, as well as synthesis conditions, are expected to play a dominant role in the assembly process.

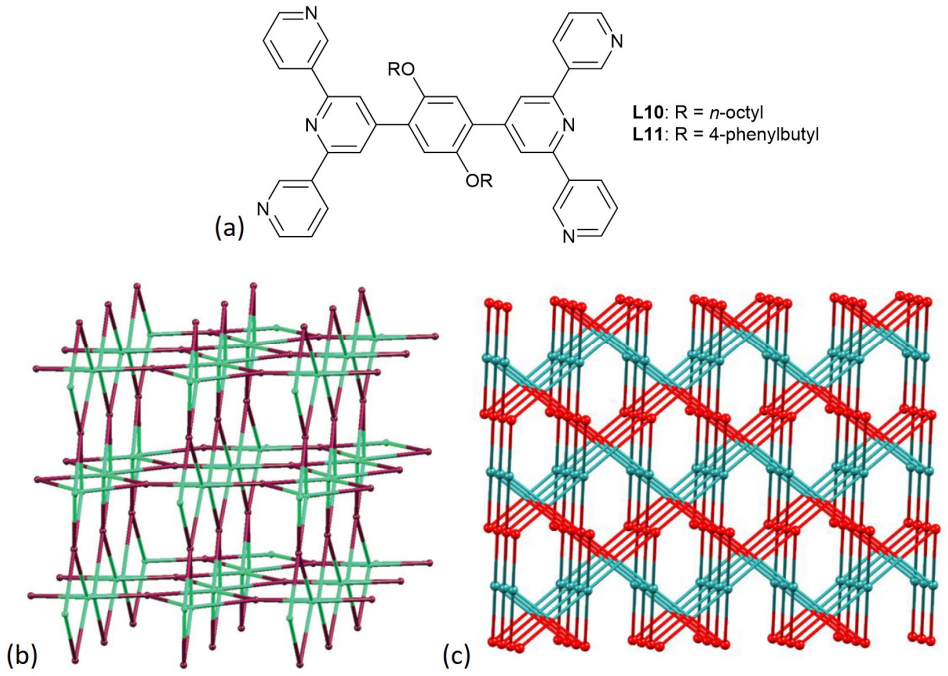

Figure 4.1 (a) Structures of the tetratopic ligands **L10** and **L11** with substituted arene spacers. (b) Part of the *pts* net in $[Co(NCS)_2(\mathbf{L10})]_n \cdot 4n CHCl_3$ and (c) part of the *cds* network in $[Co(NCS)_2(\mathbf{L11})]_n \cdot 1.6n H_2O \cdot 1.2n(1,2\text{-}Cl_2C_6H_4)$. Figures reproduced from open access references.[92, 186, 187]

Here the synthesis and characterisation of two bis(3,2':6',3''-tpy) ligands **7** and **8** are reported (Scheme 4.1). The reactions between $Co(NCS)_2$ and ligands **5**, **7** and **8** under condition of crystal grow lead to 3D-frameworks with trinodal self-penetrating or *cds* topology. Furthermore, with the addition of the latest developments from Simona Capomolla,[190, 191] the role of the solvent in the assembly process of this type of 3D-networks will be discussed.

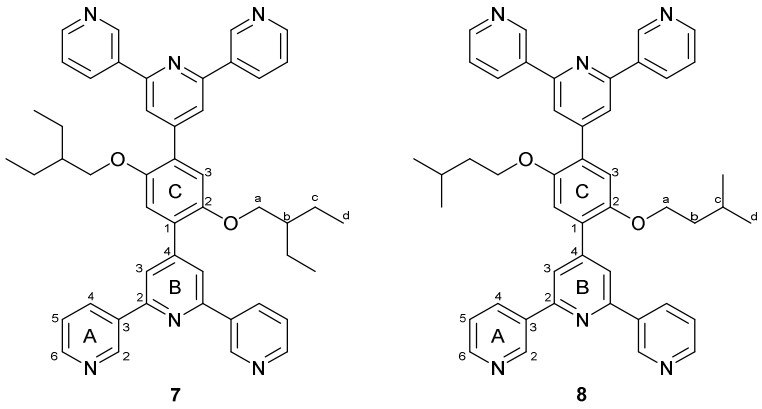

Scheme 4.1 Structures of the tetratopic bis(3,2':6',3''-terpyridine) ligands **7** and **8** with the numbering scheme used for the NMR spectroscopic assignments in the experimental section.

4.2 Ligand synthesis

The strategy for the preparation of compounds **7** and **8** is analogous to that used to synthesise the related tetratopic ligands **5** and **6** and is described in detail in Chapter 3. The route is summarised in Scheme 4.2 (see the experimental part for full details).

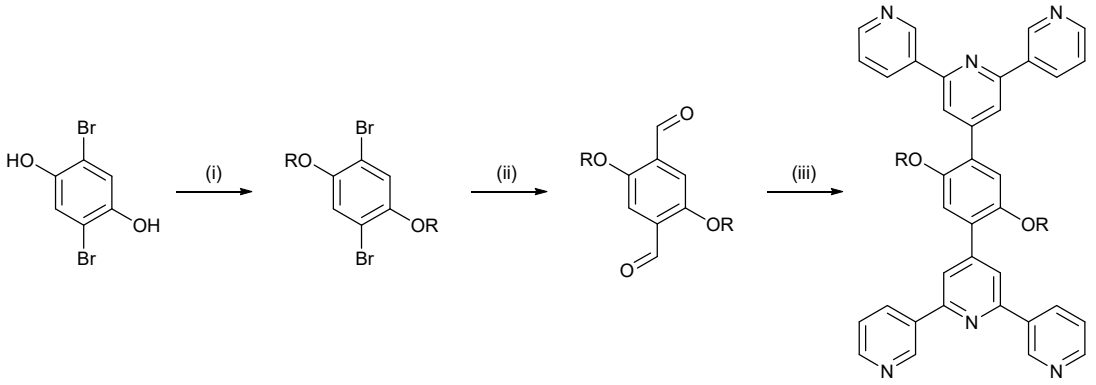

Scheme 4.2 Synthetic route to **7**-**8**. Reagents conditions (see the experimental part for full details): (i) RBr, anhydrous K_2CO_3, dry DMF, 100 °C, 18 h; (ii) *n*-BuLi, Et_2O, 0 °C; dry DMF, warmed to RT, 17 h; (iii) 3-acetylpyridine, KOH, EtOH, aqueous NH_3, RT, 3 days for **7** and 1 day for **8**.

The ^1H and $^{13}C\{^1H\}$ NMR spectra of intermediates **7a**-**7b** and ligands **7**-**8** were recorded in $CDCl_3$ and the signals of **7**-**8** were assigned using NOESY, COSY, HMQC and HMBC techniques. The previously reported **8a**-**8b** were characterised by ^1H and $^{13}C\{^1H\}$ NMR spectroscopy and the data were in accord with the published ones.[192, 193] The spectroscopic signatures of the 3,2':6',3''-tpy domains are not

affected by the change in the alkoxy substituent, and the aliphatic regions of the spectra are consistent with the 2-ethylbutoxy and 3-methylbutoxy groups in **7** and **8**, respectively (Fig. 4.2).

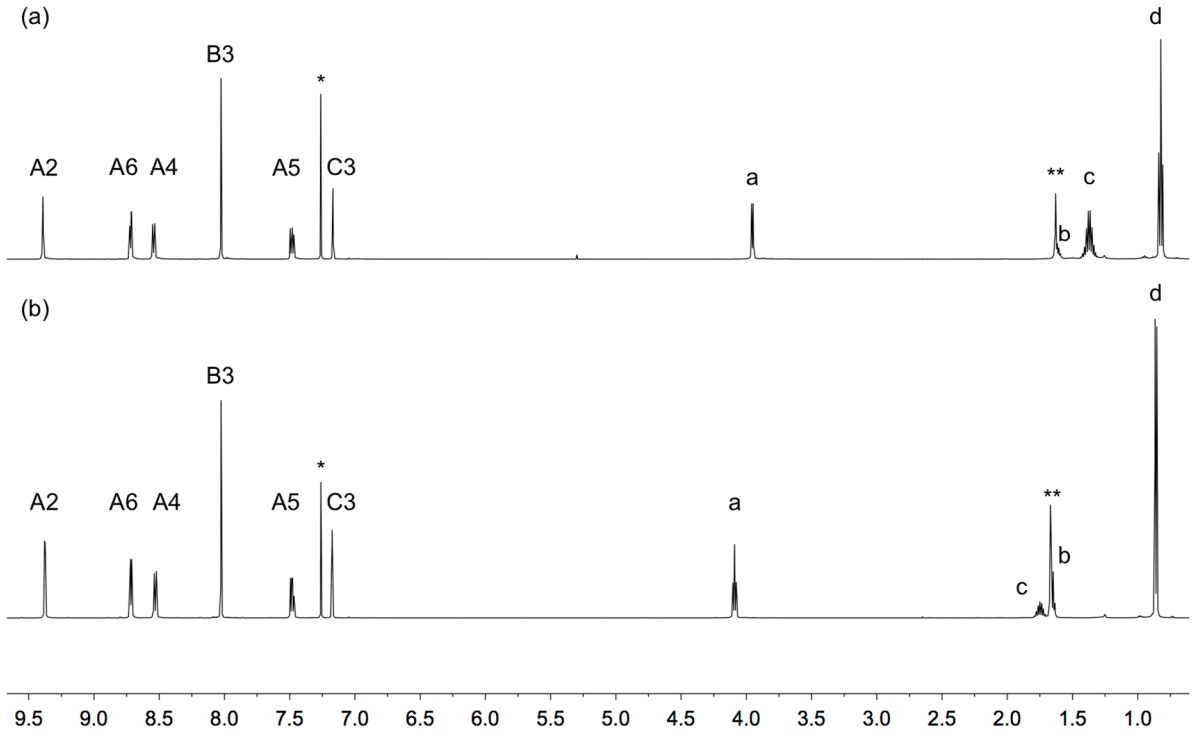

Figure 4.2 ^{1}H NMR (500 MHz, $CDCl_3$, 298 K) of (a) **7** and (b) **8**. Chemical shifts in δ / ppm. * = $CHCl_3$, ** = HOD. Atom labels are shown in Scheme 4.1.

The solution absorption spectra of compounds **7** and **8** are displayed in Fig. 4.3 and are comparable to that observed for **L10**.[187] Absorptions arise from spin-allowed π*←π and π*←*n* transitions. An $[M+H]^+$ peak was found in the MALDI-TOF-MS for both ligand **7** and **8** (see appendix). Melting point determination, FT-IR spectroscopy, and either HR-ESI mass spectrometry or elemental analysis complemented the characterisation (see appendix for full details).

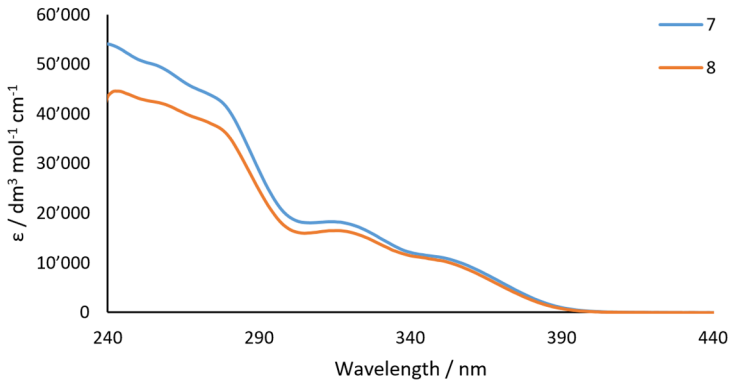

Figure 4.3 Solution absorption spectra of **7** and **8** in $CHCl_3$ (1.2×10^{-5} mol dm^{-3} for **7**, 1.0×10^{-5} mol dm^{-3} for **8**).

4.3 Crystal growth experiments

X-ray quality crystals grew by layering at room temperature a MeOH solution of $Co(NCS)_2$ over either a $CHCl_3$ or chlorobenzene solution of ligands **5**, **7** and **8**. The reactions were carried out using molar metal/ligand ratios of 1:1 (see experimental for full details). Table 4.1 summarises the solvent combinations from which single-crystals were obtained. Many of the crystals were very sensitive to loss of solvent and this can be rationalised in terms of the porosity of the structures described below.

Table 4.1 Crystal structures and the solvent for the ligands **5**, **7** and **8**, topology of the nets, and space groups. The solvent for $Co(NCS)_2$ was MeOH.

Coordination polymer	Solvent for the ligand	Topology	Space group
$[Co(NCS)_2(\mathbf{5})]_n \cdot 2.5n C_6H_5Cl$	Chlorobenzene	*cds*	$P2_1/n$
Solvated $[Co(NCS)_2(\mathbf{5})]_n$ in MeOH/$CHCl_3$[a]	Chloroform	$(6^2.8^4)(6^4.8^2)(6^5.8)_2$	*C2/c*
$[Co(NCS)_2(\mathbf{7})]_n \cdot n$MeOH$\cdot 3n CHCl_3$	Chloroform	$(6^2.8^4)(6^4.8^2)(6^5.8)_2$	*C2/c*
$[Co(NCS)_2(\mathbf{8})]_n \cdot 0.8n$MeOH$\cdot 1.8n CHCl_3$	Chloroform	$(6^2.8^4)(6^4.8^2)(6^5.8)_2$	*C2/c*

[a] Preliminary structure.

The crystal structures revealed the formation of 3D-nets with the general formula $[Co(NCS)_2(\mathbf{L})]_n$. Reactions between ligands **5**, **7** and **8** with $Co(NCS)_2$ in MeOH/$CHCl_3$ formed structurally similar 3D-assemblies $[Co(NCS)_2(\mathbf{7})]_n \cdot n$MeOH$\cdot 3n CHCl_3$, $[Co(NCS)_2(\mathbf{8})]_n \cdot 0.8n$MeOH$\cdot 1.8n CHCl_3$ and solvated $[Co(NCS)_2(\mathbf{5})]_n$. The change from the 2-ethylbutoxy to 3-methylbutoxy and 2-phenylethoxy substituents on the central phenylene spacer in the ligand has little impact on the structural assembly. The three compounds crystallise in the *C*2/*c* space group with similar cell dimensions (a = 37.514(3), b = 17.4813(11), c = 26.6265(17) Å, β = 133.660(3)° for $[Co(NCS)_2(\mathbf{7})]_n \cdot n$MeOH$\cdot 3n CHCl_3$, a = 37.7611(9), b = 17.3396(3), c = 27.5031(6) Å, β = 135.1980(10)° for $[Co(NCS)_2(\mathbf{8})]_n \cdot 0.8n$MeOH$\cdot 1.8n CHCl_3$, and a = 37.926(4) Å, b = 17.6709(19) Å, c = 26.726(5) Å, β = 134.111(4)° for the solvated $[Co(NCS)_2(\mathbf{5})]_n$). Furthermore, the structure of the solvated $[Co(NCS)_2(\mathbf{5})]_n$ suffered severe disorder and only preliminary data are available. In $[Co(NCS)_2(\mathbf{8})]_n \cdot 0.8n$MeOH$\cdot 1.8n CHCl_3$, the 3-methylbutoxy chains are disordered and were modelled using restraints. Therefore, only $[Co(NCS)_2(\mathbf{7})]_n \cdot n$MeOH$\cdot 3n CHCl_3$ will be discussed in detail as being representative of the three trinodal $(6^2.8^4)(6^4.8^2)(6^5.8)_2$ networks.

4.4 Trinodal self-penetrating networks

In $[Co(NCS)_2(\mathbf{7})]_n \cdot n$MeOH$\cdot 3n CHCl_3$, the asymmetric unit contains two independent cobalt atoms, Co1 and Co2, and two independent half-ligands **7**, both second halves being generated across inversion centres. Figure 4.4 shows the repeat unit of the coordination network with symmetry-generated atoms. The two cobalt centres have an octahedral coordination sphere with a *trans*-arrangement of the NCS^- ligands. Co1 and Co2 each binds to four N-donors of four different bis(terpyridine) ligands, thereby acting as a 4-connecting node. Bond lengths for the coordination spheres of Co1 and Co2 are in the range 2.065(6)-2.229(6) Å and N–Co–N bond angles vary between 87.0(2)° to 93.1(3)°.

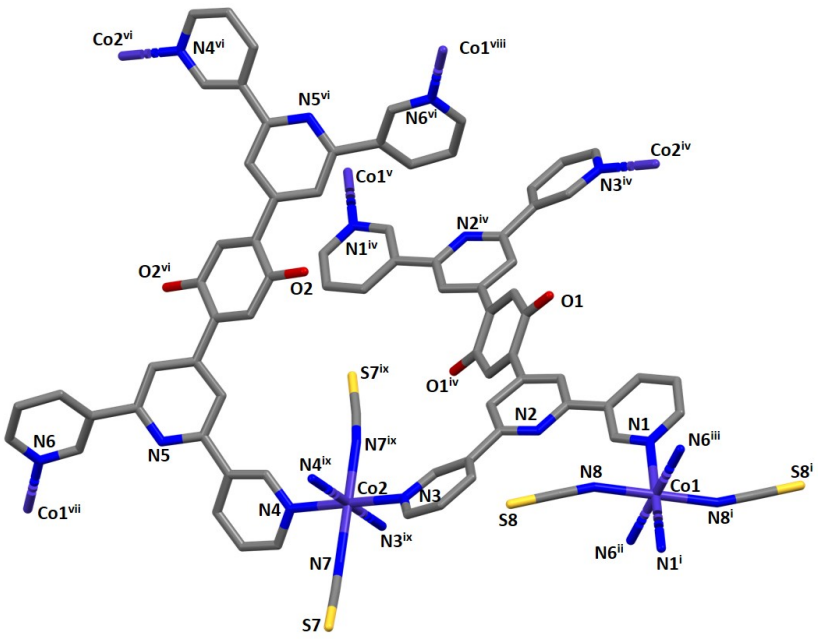

Figure 4.4 The repeat unit in the coordination network of $[Co(NCS)_2(\mathbf{7})]_n \cdot n$MeOH·3$n$CHCl$_3$ with symmetry-generated atoms. For clarity, H atoms and solvent molecules are omitted, and only the O atoms of the alkoxy groups are shown. Symmetry codes: i = $^1/_2$–x, $^1/_2$–y, –z; ii = 1–x, –1+y, $^1/_2$–z; iii = –$^1/_2$+x, $^3/_2$–y, –$^1/_2$+z; iv = 1–x, 1–y, 1–z; v = $^1/_2$+x, $^1/_2$+y, 1+z; vi = 1–x, 2–y, 1–z; vii = 1–x, 1+y, $^1/_2$–z; viii = $^1/_2$–x, $^1/_2$+y, $^1/_2$–z; ix = 1–x, y, $^1/_2$–z.

The 3,2':6',3''-tpy domains in **7** adopt the limiting conformation **C** (Scheme 4.3). Angles between the least squares planes through pairs of pyridine rings containing N1/N2, N2/N3, N4/N5 and N5/N6 are 10.6, 18.6, 29.8 and 36.1°, respectively. The twists of the planes of the central pyridine ring and the central arene spacer are 39.1 and 38.8°. These angles minimise unfavourable H···H inter-ring repulsions and are typical for bonded aromatic rings.

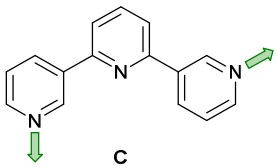

Scheme 4.3 The limiting conformation **C** is adopted by all bis(3,2':6',3''-terpyridines) ligands in $[Co(NCS)_2(\mathbf{5})]_n \cdot 2.5n C_6H_5Cl$, $[Co(NCS)_2(\mathbf{7})]_n \cdot n$MeOH·3$n$CHCl$_3$, $[Co(NCS)_2(\mathbf{8})]_n \cdot 0.8n$MeOH·1.8$n$CHCl$_3$ and solvated $[Co(NCS)_2(\mathbf{5})]_n$. For all possible conformations, see Scheme 1.7 in the introduction.

The 3D-network contains four chemically distinct nodes, all 4-connecting and planar. As the two ligand nodes are topologically equivalent (this was verified using the Systre[194] programme), the net is trinodal. The two Co1 and Co2 centres and the centroid of the phenylene rings of ligands **7** (Fig 4.5a) are the three topologically distinct nodes. The full vertex symbol is $(6^2.8^4)(6^4.8^2)(6^5.8)_2$, with the individual symbols referring to Co1, Co2 and the ligands, respectively (Fig. 4.5a). The combination of ligand and Co2 nodes produces parallel sheets on the *bc*-plane (Fig. 4.5b). Then the distinct sheets are connected *via* Co1 nodes generating the 3D-framework. This is an individual net in which there are smallest circuits that are penetrated by rods of the same net; thus, the net is self-penetrating. The catenane-like arrangement of shortest circuits is highlighted in Fig. 4.5c (red and magenta). Back in 2019, $[Co(NCS)_2(\mathbf{7})]_n \cdot n$MeOH·3$n$CHCl$_3$ and $[Co(NCS)_2(\mathbf{8})]_n \cdot 0.8n$MeOH·1.8$n$CHCl$_3$ were the first examples of

self-penetrating $(6^2.8^4)(6^4.8^2)(6^5.8)_2$ nets with this topology not appearing on the Reticular Chemistry Structure Resource (RCSR) database of 3D nets.[57]

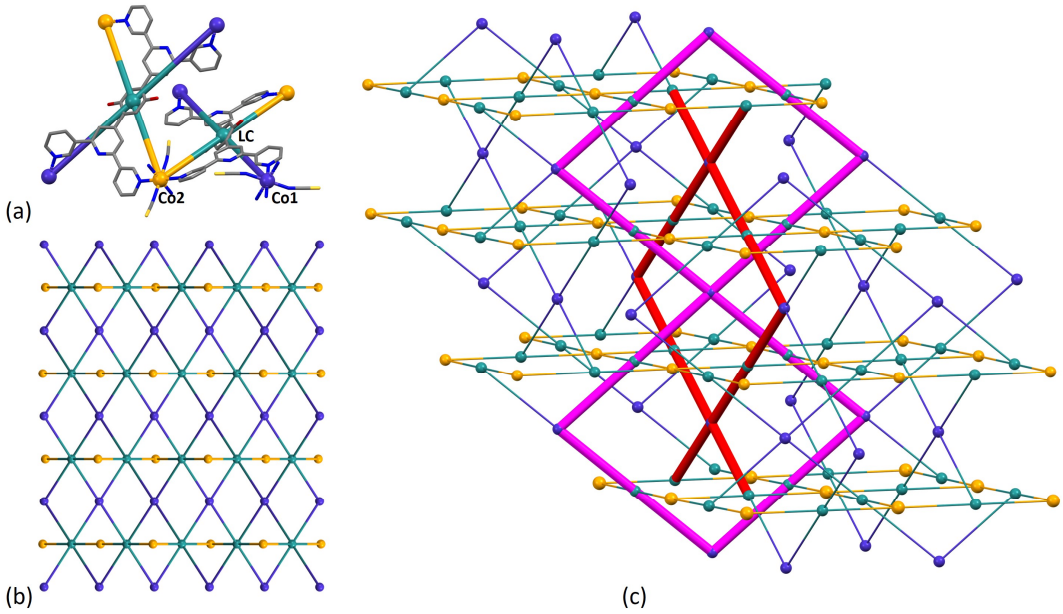

Figure 4.5 (a) The repeat unit of $[Co(NCS)_2(\mathbf{7})]_n{\cdot}n$MeOH$\cdot$3$n$CHCl$_3$. LC: ligand centroid. For clarity, H atoms and solvent molecules are omitted, and only the O atoms of the alkoxy groups are shown. (b) Part of the $(6^2.8^4)(6^4.8^2)(6^5.8)_2$ network viewed down the crystallographic *c*-axis. (c) Highlighting the interlocking of the shortest circuits (red and magenta) of the network. Colour code for the nodes: Co1 blue, Co2 orange, ligand centroids green.

In $[Co(NCS)_2(\mathbf{7})]_n{\cdot}n$MeOH$\cdot$3$n$CHCl$_3$, $[Co(NCS)_2(\mathbf{8})]_n{\cdot}0.8n$MeOH$\cdot$1.8$n$CHCl$_3$ and solvated $[Co(NCS)_2(\mathbf{5})]_n$, the 2-ethylbutoxy, 3-methylbutoxy and 2-phenylethoxy substituents are accommodated within the cavities meaning that the voids in the $(6^2.8^4)(6^4.8^2)(6^5.8)_2$ net satisfy their steric requirements. In contrast, if a more sterically demanding group is introduced, i.e. *n*-octyloxy chain, a change to a $(4^2.8^4){\cdot}(4^2.8^4)$ *pts* network is found from the same crystallisation solvents.[92, 187] $[Co(NCS)_2(\mathbf{L10})]_n{\cdot}4n$CHCl$_3$, the *n*-octyloxy chains are in non-extended conformations and C–H…π contacts between the terminal CH_2CH_3 units and pyridine rings are present.

4.5 Assembly of *cds* networks

In the compound $[Co(NCS)_2(\mathbf{5})]_n{\cdot}2.5nC_6H_5$Cl, the asymmetric unit contains half of the bis(3,2':6',3''-tpy) ligand **5** as well as half a cobalt atom including one NCS^- ligand. The repeat unit is displayed in Fig. 4.6. Both the centroid of the phenylene spacer of **5** and the Co(II) atom are positioned on an inversion centre leading to the four N-donors being coplanar. The Co1 atom is octahedrally coordinated with a *trans*-arrangement of NCS^- ligands (Co–N_{NCS} of 2.060(3) Å). The Co(II) centre binds to four pyridine donor atoms of four different ligands **5** (Co–N_{py} = 2.168(3), 2.241(3) Å), and likewise ligand **5** coordinates with four Co(II) centres. The terpyridine unit adopts conformation **C** (Scheme 4.3) and the angles between planes of pyridine rings containing N1/N2 and N2/N3 are 15.1 and 25.9°, respectively. The phenylene spacer is twisted at 51.6° relative to the pyridine ring containing N2.

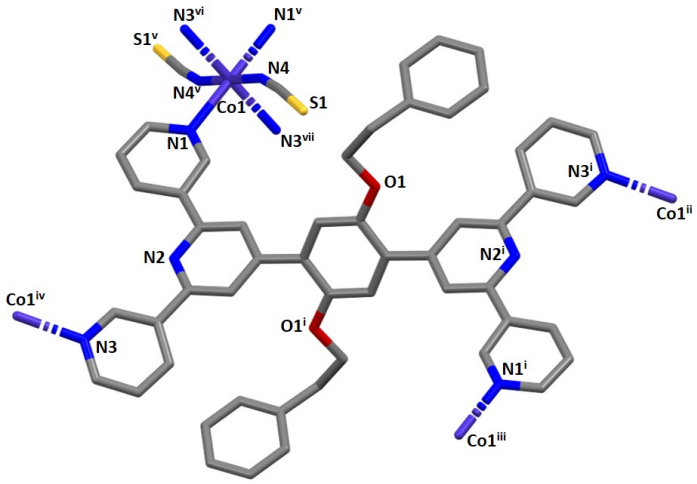

Figure 4.6 The repeat unit in the coordination network of $[Co(NCS)_2(\mathbf{5})]_n \cdot 2.5nC_6H_5Cl$ with symmetry-generated atoms. For clarity, H atoms and solvent molecules are omitted. Symmetry codes: i = 1–*x*, 1–*y*, 1–*z*; ii = $^3/_2$–*x*, $-^1/_2$+*y*, $^3/_2$–*z*; iii = *x*, *y*, –1+*z*; iv = $^1/_2$–*x*, $^1/_2$+*y*, $^3/_2$–*z*; v = 1–*x*, 1–*y*, 2–*z*; vi = $^1/_2$–*x*, $-^1/_2$+*y*, $^3/_2$–*z*; vii = $^1/_2$+*x*, $^3/_2$–*y*, $^1/_2$+*z*.

In $[Co(NCS)_2(\mathbf{5})]_n \cdot 2.5nC_6H_5Cl$, both the metal centre and ligand **5** act as planar 4-connecting nodes, which, in this case, results in the assembly of a 3D net with a *cds* topology (Fig. 4.7). It is important to remark that several 4-connected networks constructed from planar nodes are possible, where the most common are *sql*, *kag*, *nbo*, *lvt* and the mentioned *cds*.[189] The first two are 2D networks, of which *sql* is the familiar square lattice. The other three are 3D-assemblies that differ in size and multiplicity of each shortest circuit (see introduction). The *cds* here obtained is a (6^5.8) uninodal net in which half of the adjacent nodes are coplanar and half are perpendicular to each another. Ligand centroids and cobalt centres are topologically equivalent. This structure is related to that in $[Co(NCS)_2(\mathbf{L11})]_n \cdot 1.6nH_2O \cdot 1.2nC_6H_4Cl_2$, which was briefly mentioned in Fig. 4.1c, and grew from a similar solvent combination (1,2-dichlorobenzene/$CHCl_3$).[186]

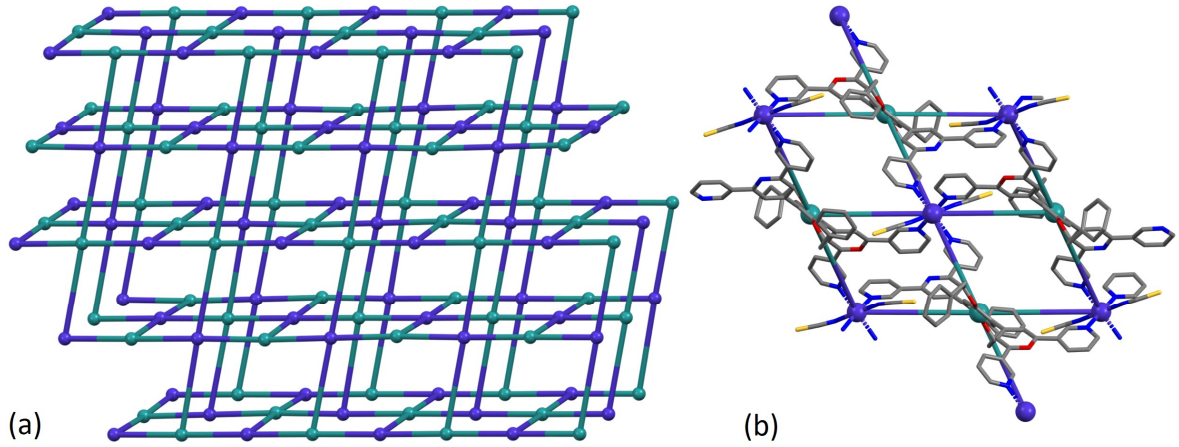

Figure 4.7 (a) Part of the *cds* net in $[Co(NCS)_2(\mathbf{5})]_n \cdot 2.5nC_6H_5Cl$ showing only the 4-connecting nodes. (b) Detail of the same network along the crystallographic *b*-axis. The hydrogen atoms and solvent molecules are omitted for clarity. Colour code for the nodes: Co1 blue, ligand centroids green.

Both the 2-phenylethoxy substituent and chlorobenzene molecules exhibit substantial disorder. Thus, a detailed discussion of the solvent interactions is not meaningful and precise quantification of the void space in the unsolvated structure cannot be given. Nevertheless, a face-to-face π-stacking interaction can be seen between the central pyridine ring containing N2 and a chlorobenzene molecule.

4.6 The effect of solvent on topology

Fig. 4.8 summarises all the outcomes from the combination of bis(3,2':6',3''-tpy) ligands and $Co(NCS)_2$ present in the literature obtained by two former members of the Constable-Housecroft research group and this author.[50, 92, 186, 187, 190, 191] The trinodal self-penetrating net is persistent when a MeOH/$CHCl_3$ solvent combination is used for the crystal growth (Fig. 4.8). The only deviation from this pattern is the binodal $(4^2.8^4)\cdot(4^2.8^4)$ *pts* network obtained with **L10**,[92, 187] and this suggests that the more sterically demanding *n*-octyloxy chain cannot be accommodated in the cavities of the trinodal net. However, for this statement to be unambiguous, further attempts should be made to reproduce the *pts* network. The binodal *pts* net consists of equal numbers of two nodes with different limiting geometries, the square and the tetrahedron. This characteristic differentiates it from the uninodal *cds* and trinodal $(6^2.8^4)(6^4.8^2)(6^5.8)_2$ networks, which have only the planar configuration of nodes. Instead, a regularity of the *cds* network is found for **5**, **L11**-**L18** and even **L10** when $CHCl_3$ is replaced by chlorobenzene or 1,2-dichlorobenzene. A rationalisation of this trend might be that $CHCl_3$ and MeOH molecules are small enough to occupy the cavities accessible to solvent in the trinodal net, while chlorobenzene or 1,2-dichlorobenzene cannot. Whether or not the aryl halide templates the assembly remains unclear. In conclusion, in the reactions between bis(3,2':6',3''-tpy) ligands and $Co(NCS)_2$, the substituents displayed in Fig. 4.8 seem to play a minor role with respect to the chosen solvent in directing the assembly.

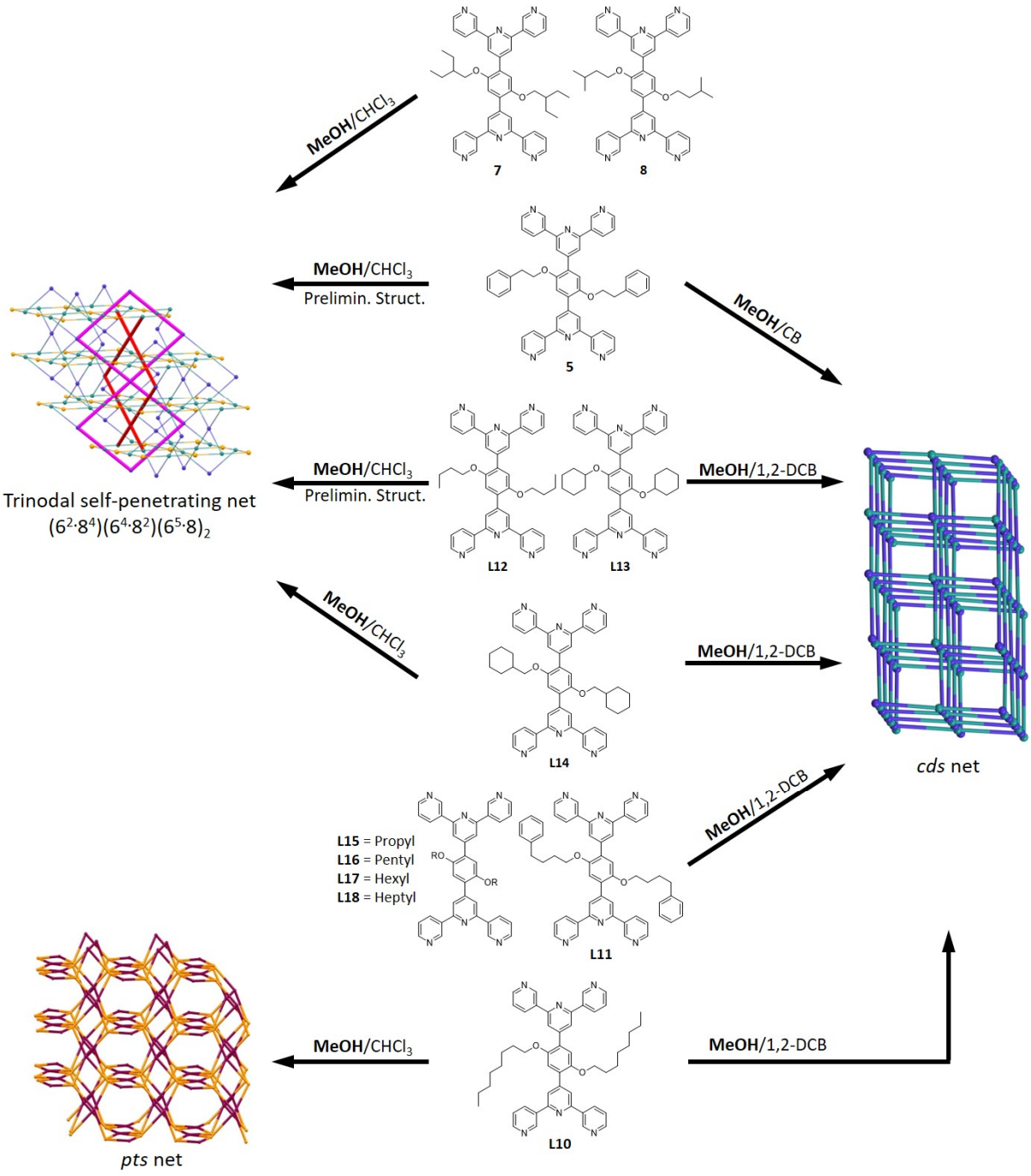

Figure 4.8 Overview of all the coordination networks comprehending bis(3,2':6',3''-tpy) ligands and $Co(NCS)_2$.[50, 186, 187, 190, 191] The single-crystals were grown by layering a MeOH solution of $Co(NCS)_2$ over either a $CHCl_3$, 1,2-dichlorobenzene (1,2-DCB) or chlorobenzene (CB) solution of the corresponding bis(terpyridine) ligands **5**, **7-8** and **L10-L18**. Representation of the *pts* topology reproduced from the open access reference.[90]

4.7 Bulk sample analysis

Powder X-ray diffraction patterns were recorded for $[Co(NCS)_2(\mathbf{5})]_n \cdot 2.5n C_6H_5Cl$, $[Co(NCS)_2(\mathbf{7})]_n \cdot n MeOH \cdot 3n CHCl_3$ and $[Co(NCS)_2(\mathbf{8})]_n \cdot 0.8n MeOH \cdot 1.8n CHCl_3$. Although the spectra of $[Co(NCS)_2(\mathbf{7})]_n \cdot n MeOH \cdot 3n CHCl_3$ and $[Co(NCS)_2(\mathbf{8})]_n \cdot 0.8n MeOH \cdot 1.8n CHCl_3$ were of poor quality, the profile matching refinement confirmed that the single-crystal structures are representative of the bulk sample (Fig. 4.9). For $[Co(NCS)_2(\mathbf{5})]_n \cdot 2.5n C_6H_5Cl$, an excellent fit was found between the predicted pattern from the single-crystal structure and the experimental powder pattern (Fig. 4.10).

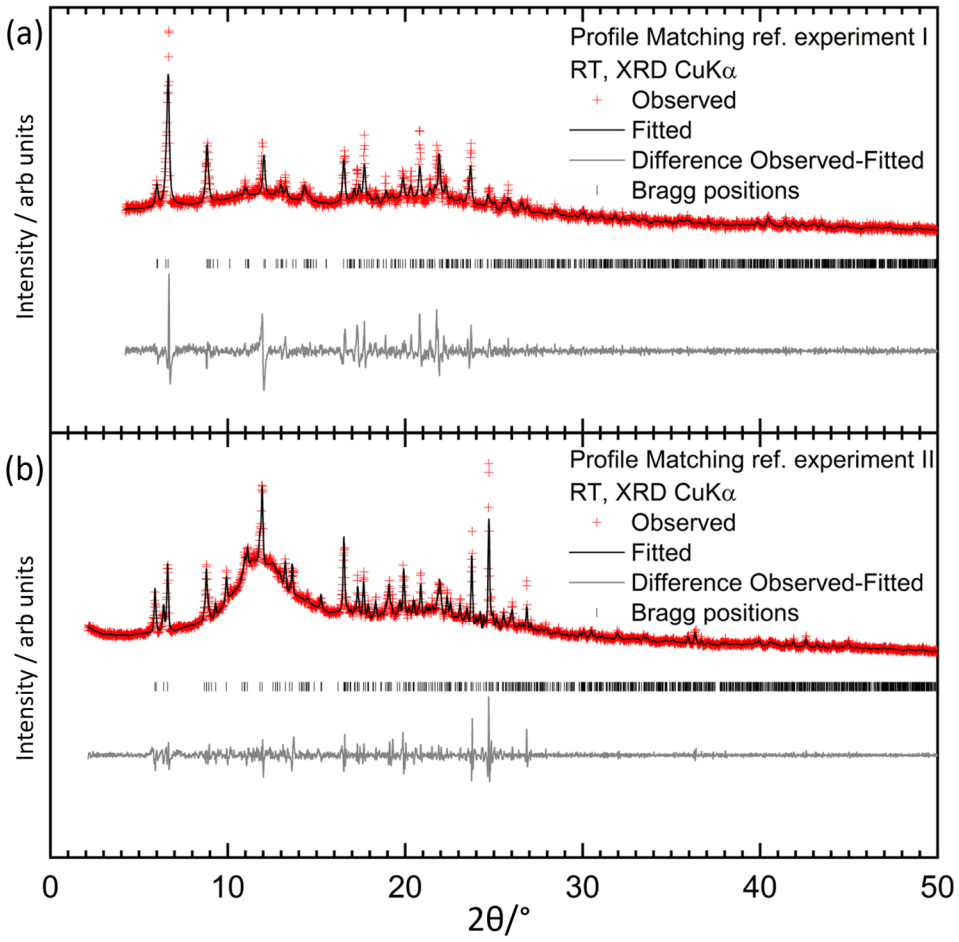

Figure 4.9 X-ray diffraction (CuKα1 radiation) pattern (red crosses) of the bulk crystalline material of (a) $[Co(NCS)_2(\mathbf{7})]_n \cdot n MeOH \cdot 3n CHCl_3$ and (b) $[Co(NCS)_2(\mathbf{8})]_n \cdot 0.8n MeOH \cdot 1.8n CHCl_3$, fitting the predicted pattern from the single-crystal structures. The black lines are the best fit from Rietveld refinements, and lower vertical marks denote the Bragg peak positions. The grey plot gives the difference between calculated and experimental points. Figure reproduced from the open access reference.[50]

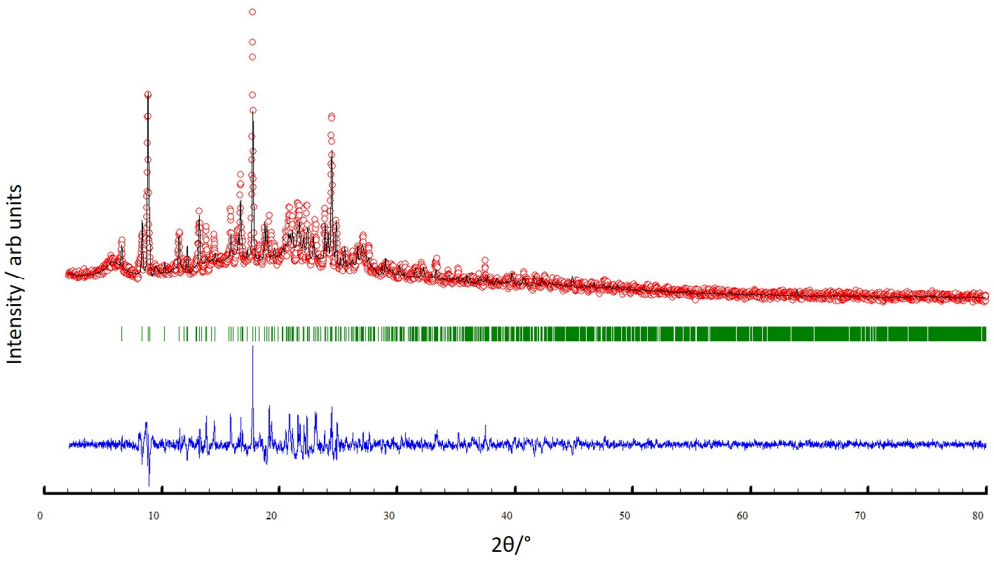

Figure 4.10 X-ray diffraction (CuKα1 radiation) pattern (red circles) of the bulk crystalline material of $[Co(NCS)_2(\mathbf{5})]_n \cdot 2.5n C_6H_5Cl$, fitting the predicted pattern from the single-crystal structure. The black lines are the best fit from Rietveld refinements, and the green lines display the Bragg peak positions. The blue plot gives the difference between calculated and experimental points.

4.8 Conclusions

The bis(3,2':6',3''-tpy) ligands **7** and **8** with 2-ethylbutoxy and 3-methylbutoxy substituents were synthesised and fully characterised. The reactions of $Co(NCS)_2$ with **5**, **7** and **8** yielded the 3D-networks $[Co(NCS)_2(\mathbf{5})]_n \cdot 2.5n C_6H_5Cl$, $[Co(NCS)_2(\mathbf{7})]_n \cdot n MeOH \cdot 3n CHCl_3$ and $[Co(NCS)_2(\mathbf{8})]_n \cdot 0.8n MeOH \cdot 1.8n CHCl_3$, respectively. $[Co(NCS)_2(\mathbf{7})]_n \cdot n MeOH \cdot 3n CHCl_3$ and $[Co(NCS)_2(\mathbf{8})]_n \cdot 0.8n MeOH \cdot 1.8n CHCl_3$ were grown in the same $MeOH/CHCl_3$ mixture and are structurally very similar sharing the identical $(6^2.8^4)(6^4.8^2)(6^5.8)_2$ self-penetrating topology. This is not surprising since 2-ethylbutoxy and 3-methylbutoxy have similar steric demands, and indeed with an *n*-octyloxy chain, a *pts* net was reported instead.[92, 187] In contrast, a *cds* topology was found for $[Co(NCS)_2(\mathbf{5})]_n \cdot 2.5n C_6H_5Cl$, crystallised from a mixture of MeOH and chlorobenzene. Preliminary structural data for single-crystals grown by layering a MeOH solution of $Co(NCS)_2$ over a $CHCl_3$ solution of **5** confirmed the assembly of a trinodal self-penetrating net. The selective assembly of either a *cds* or trinodal self-penetrating 3-dimensional network depending on the chosen solvent in reactions of $Co(NCS)_2$ with **5** is consistent with the latest results obtained by Simona Capomolla, a former Masters candidate in the Constable-Housecroft research group, using 1,4-bis(cyclohexylalkoxy)-2,5-bis(3,2':6',3''-terpyridin-4'-yl)benzene ligands.[191]

5 Star tris(3,2':6',3''-terpyridine) and tris(4,2':6',4''-terpyridine) compounds: A challenging class of hexatopic ligands

5.1 Motivation

In this chapter, the investigation of tetratopic bis(3,2':6',3''-tpy) is extended to hexatopic tris(3,2':6',3''-tpy) and tris(4,2':6',4''-tpy) ligands. Before this project, neither tris(4,2':6',4''-tpy) nor tris(3,2':6',3''-tpy) ligands have been reported, despite the fact that they are attractive building blocks for coordination assemblies (Scheme 5.1a and b). However, this design principle has been exploited with 2,2':6',2''-tpy metal-binding domains and, from the first tris(2,2':6',2''-tpy) in 1992,[195] a wide spectrum of poly(2,2':6',2''-tpy) ligands has been used for metallosupramolecular constructs.[137, 196] This is reflected in a range of complex geometries, such as discrete 2D-[132] and 3D-fractals,[129] metallodendrimers[197] and metallocages[198, 199 126] (e.g. polyhedra).[200] Some 20 years ago, the term metallostar to describe such polynuclear assemblies was introduced[201-205] and the concept of using tritopic tris(2,2':6',2''-tpy) ligands (Scheme 5.1c) for the growth of 2D or 3D coordination polymers was developed by Constable and others,[206, 207] and the potential in materials chemistry subsequently demonstrated.[208-217] The groups of Nishihara,[215, 216] Wong[213] and Chakraborty[210, 214] showed a series of coordination nanosheets using different tris(terpyridine) ligands in which durable electrochromism was observed with Fe^{2+} or Co^{2+} complexes. Moreover, according to Nishihara's group, anion exchange capacities and solvatoluminochromic behaviour were found with $Zn(BF_4)_2$ and $ZnSO_4$, respectively.[217] With 1,3,5-tris[4-(2,2':6',2''-terpyridin-4'-yl)phenyl]benzene, Higuchi and co-workers described the syntheses of Fe^{2+}, Co^{2+} and Ni^{2+}-based coordination polymers showing humidity-responsive ionic conduction.[212] It should be noted, however, that none of these coordination assemblies containing tris(terpyridine) ligands has been unequivocally characterised by single-crystal X-ray diffraction. Before the start of this doctoral project (2021), a search of the Cambridge Structural Database[218] (CSD v. 2021.1.0)[219], using ConQuest (v. 2021.1.0)[219], revealed no coordination polymers or networks assembled with tris(2,2':6',2''-terpyridine), tris(3,2':6',3''-terpyridine) or tris(4,2':6',4''-terpyridine) ligands. Instances where the terpyridine unit is one of the less common 45 isomers are ignored. Many of these isomers are difficult to synthesise, with only a few effective synthetic approaches, and probably because of this they are little studied.[220]

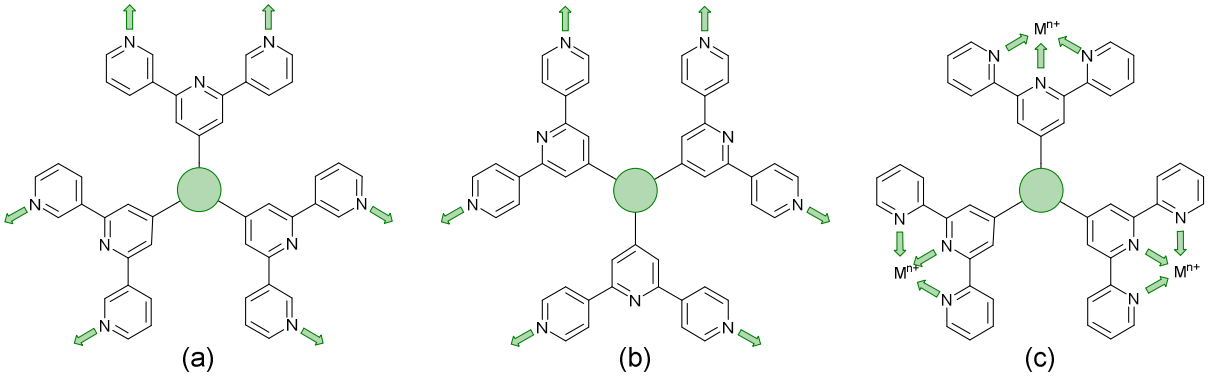

Scheme 5.1: Hexatopic ligands resulting from connecting three (a) 3,2':6',3''-tpy or (b) 4,2':6',4''-tpy domains. Only one of three possible planar conformations of each 3,2':6',3''-tpy unit is shown. (c) Tris(2,2':6',2''-tpy) as a tritopic ligand. Each tpy domain is monotopic, with the three tpy nitrogen atoms binding only one metal ion. The green spacer represents any linker.

Hence, there is significant scope for investigations of building blocks incorporating three or more 4,2':6',4''-tpy or 3,2':6',3''-tpy domains. Herein, the syntheses of a series of star-shaped ligands is presented (Scheme 5.2, next section). The self-assembly and the first single-crystal X-ray characterisation of a tris(terpyridine)-based coordination polymer to generate an unusual 1D architecture is also described. In addition, preliminary structural data for single-crystals from reactions of $[Cu(hfacac)_2]\cdot H_2O$ and a tris(4,2':6',4''-tpy) ligand also evidenced a consistent assembly of a (6,3) net from different solvent combinations.

5.2 Ligand synthesis

Compounds **9** and **10** were prepared using Wang and Hanan's one-pot protocol[93] (Scheme 5.2). After purification, **9** and **10** were obtained with yields of 22 and 13%, respectively. The synthetic route to compounds **11** and **12** was similar to the one used to synthesise the related 1,3,5-tris[4-(2,2':6',2''-terpyrid-4'-yl)phenyl]benzene.[221] A Suzuki cross-coupling reaction between 1,3,5-tribromobenzene and 4'-(4-(4,4,5,5-tetramethyl-1,3,2-dioxaborolan-2-yl)phenyl)-4,2':6',4''-terpyridine (**11a**) or 4'-(4-(4,4,5,5-tetramethyl-1,3,2-dioxaborolan-2-yl)phenyl)-3,2':6',3''-terpyridine (**12a**) (Scheme 5.2) was conducted in refluxing THF, with $[Pd(PPh_3)_4]$ as catalyst and aqueous Na_2CO_3 as base, affording **11** (37%) and **12** (80%). The compounds were analytically pure and no recrystallisation or chromatography was required. However, compounds **11** and **12** were poorly soluble in most common organic solvents, which presumably arises from extensive intermolecular stacking interactions. Since ligand solubility is critical for crystallisation methods in the assembly of coordination polymers, the attention moved from ligands **11** and **12** to analogous compounds with solubilising substituents. Rather than using hindering groups such as long alkyl chains, methyl groups were introduced (ligand **13**, Scheme 5.2). The steric hindrance between adjacent methyl and phenyl groups forces the ligand into a non-planar conformation in the solid state as well as in solution, leading to less efficient π-stacking as is seen in 1,3,5-trimethyl-2,4,6-triphenyl-substituted arenes.[222-226] An approach using the Suzuki coupling of 1,3,5-tribromo-2,4,6-trimethylbenzene and **12a** was not successful when utilising THF and $[Pd(PPh_3)_4]$, but an improved route to **13** was found using $[Pd(dppf)Cl_2]$ and Na_2CO_3 in refluxing toluene-water. However, some homo-coupling and dehalogenation by-products were identified by MALDI-TOF spectrometry. After chromatographic purification eluting with $CHCl_3$, compound **13** was isolated analytically pure in a yield of 33%. Under the same synthetic conditions, the preparation of the analogous 4,2':6',4'' isomer of **13**, i.e. 1,3,5-trimethyl-2,4,6-tris[4-(4,2':6',4''-terpyridin-4'-yl)phenyl]benzene, was planned. The resulting ligand proved to be very difficult to separate from the homo-coupling and dehalogenation by-products and also possessed lower solubilities than **13** in common organic solvents. The strategy of increasing solubility by decreasing the efficiency of π-stacking interactions by breaking the planarity of the molecule was no longer sufficient. The extension of the π-system of the molecule also had to be reduced. Therefore, the arene core in 1,3,5-trimethyl-2,4,6-tris[4-(4,2':6',4''-terpyridin-4'-yl)phenyl]benzene was replaced by an N atom. Ligand **14** (Scheme 5.2) was synthesised from the commercial tris(4-formylphenyl)amine according to the one-pot methods of Hanan[93] as reported by Zhang[227] but using THF in place of EtOH. This compound, obtained in 25% yield, showed superior solubilities not only to those of **11** but also to all the tris(terpyridine) ligands presented here.

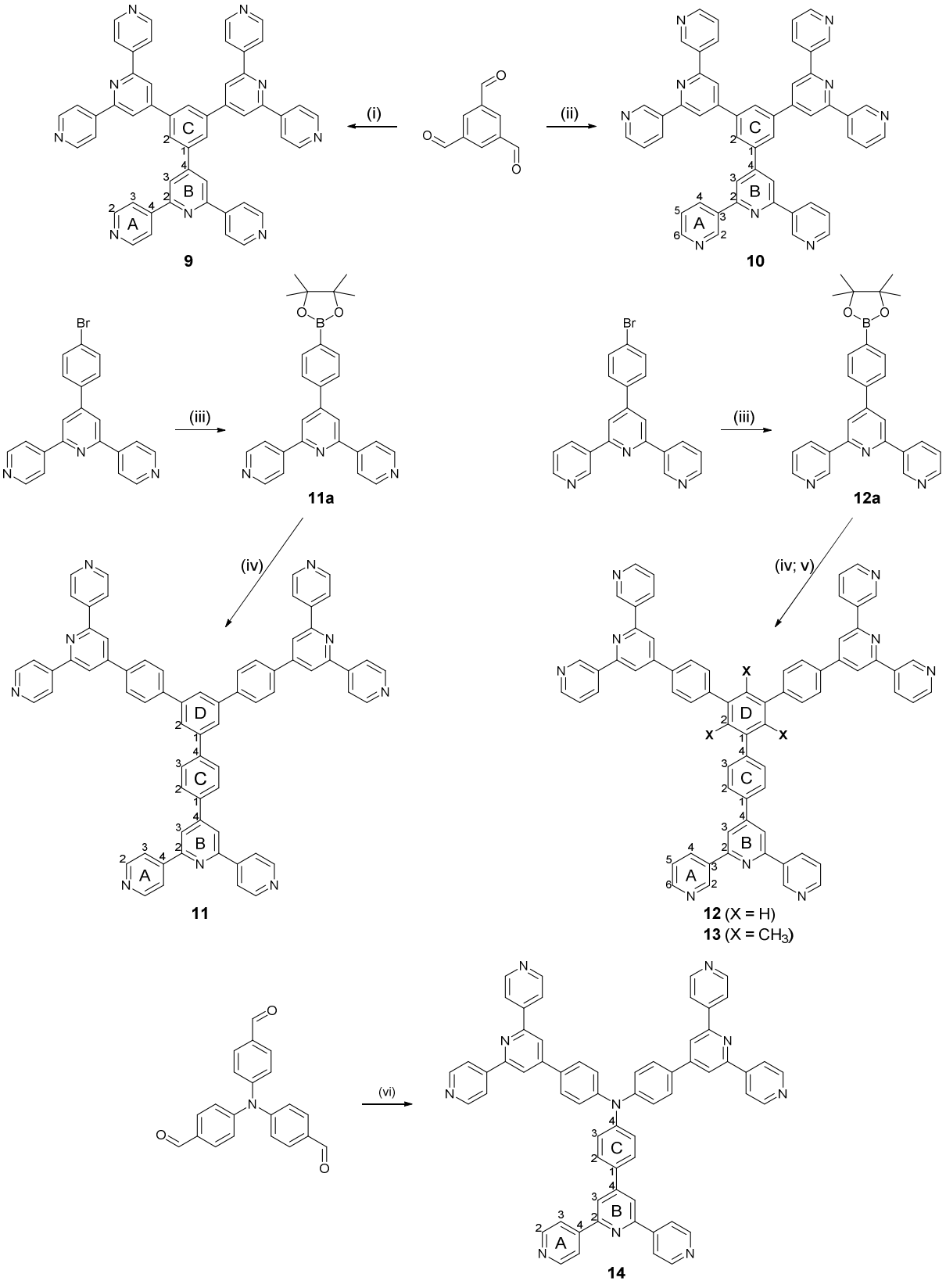

Scheme 5.2 Synthetic route to ligands **9**-**14** and the numbering scheme used for NMR spectroscopic assignments; reagents and conditions: (i) 4-acetylpyridine, KOH, aqueous NH_3, EtOH, RT, 3 days; (ii) 3-acetylpyridine, KOH, aqueous NH_3, EtOH, RT, 3 days; (iii) bis(pinacolato)diboron, $[Pd(dppf)Cl_2]$, AcOK, DMF, 120 °C, 5 h 30 min; (iv) For **11** and **12**, 1,3,5-tribromobenzene, $[Pd(PPh_3)_4]$, aqueous Na_2CO_3, THF, reflux, 12 h; (v) For **13**, 1,3,5-tribromo-2,4,6-trimethylbenzene, $[Pd(dppf)Cl_2]$, Na_2CO_3, toluene/H_2O (1:1), reflux, 1 h; (vi) 4-acetylpyridine, KOH, aqueous NH_3, THF, RT, 15 days.

Ligands **9**–**14** and boronic esters **11a** and **12a** were fully characterised by ^{1}H and $^{13}C\{^{1}H\}$ NMR spectroscopies, UV-Vis and FT-IR spectroscopies, MALDI-TOF spectrometry, and HR-ESI spectrometry or elemental analysis (see appendix for full details). The data were consistent with the structures shown in Scheme 5.2. Due to the varying solubilities of the ligands, the NMR spectra were recorded in different solvents, but a comparison between **12** and **13** and one between **9** and **14** is possible. Fig. 5.1 displays a comparison of the ^{1}H NMR spectra of the aromatic regions for the tris(3,2':6',3''-tpy) ligands **12** and **13**, showing that the methyl groups present in **13** do not have a significant impact on the spectroscopic signatures of the terpyridine units. In contrast, due to its proximity to the $–CH_3$ group, the proton H^{C3} is significantly shifted upfield (Fig. 5.1b).

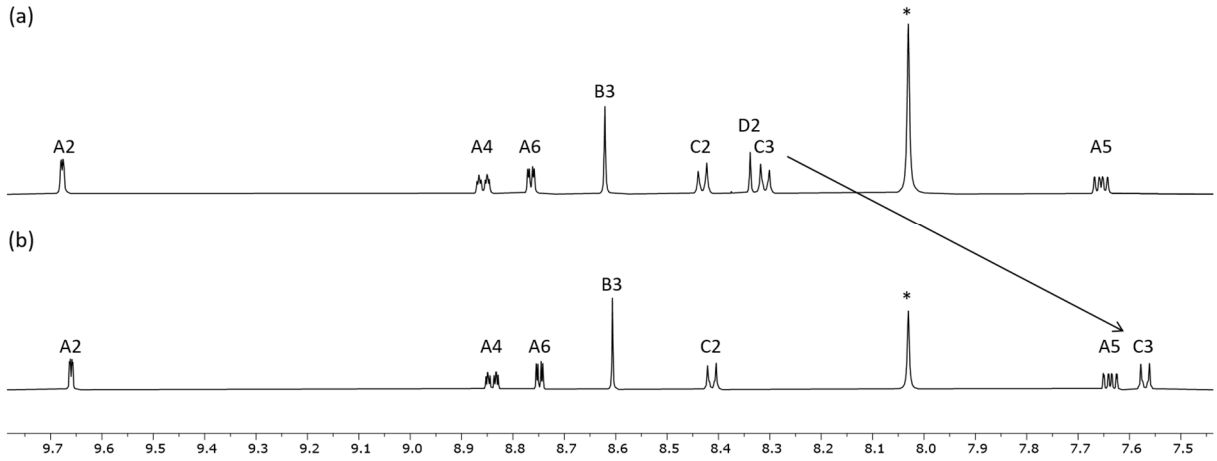

Figure 5.1 ^{1}H NMR (500 MHz, DMF-d_7, 298 K) spectra (aromatic region) of (a) **12** and (b) **13**. Chemical shifts in δ / ppm. * = DMF-d_6. Atom labels are shown in Scheme 5.2.

The spectroscopic signatures of the 4,2':6',4''-tpy domains in **9** and **14** are affected by the change in the organic linker (Fig. 5.2). In **9**, there is only one aryl spacer between the three electron-accepting terpyridine units. On the other hand, in **14**, the triarylamine confers a positive mesomeric effect on terpyridines attached to the *para*-positions. This effect is most evident in H^{B3}, which is the most upfield-shifted signal compared to the others of the terpyridine unit (H^{A2} and H^{A3}).

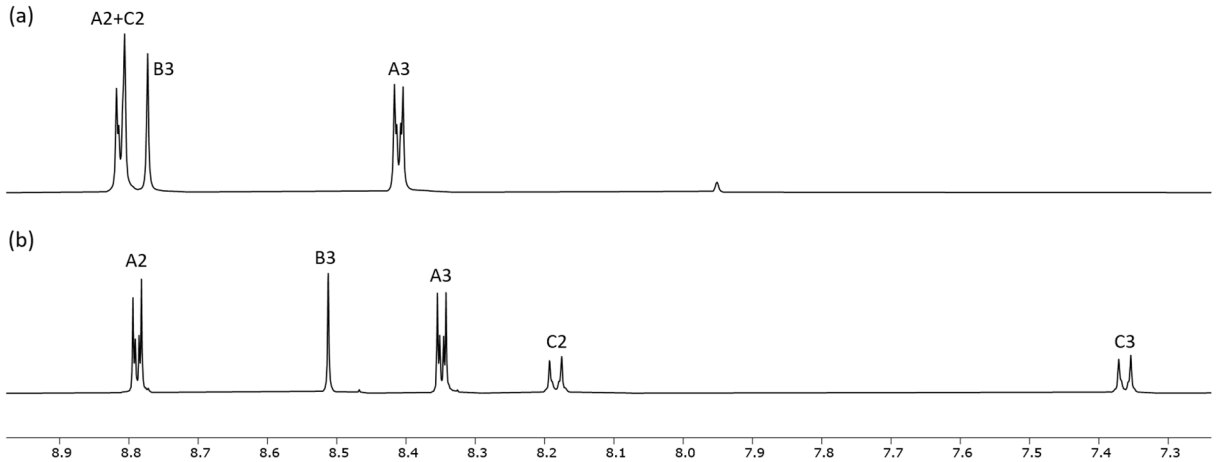

Figure 5.2 ^{1}H NMR (500 MHz, DMSO-d_6, 298 K) spectra (aromatic region) of (a) **9** and (b) **14**. Chemical shifts in δ / ppm. Atom labels are shown in Scheme 5.2.

Note that ligands **11–13** with the phenylene spacers are poorly soluble in many organic solvents, and, for **11**, the absorption spectrum had to be recorded in benzonitrile, this being the only suitable solvent with a high-energy cut-off. Thus, the absorption spectra of **9**-**14** were measured in different solvents and are illustrated in Fig. 5.3. The structural isomers **9** and **10** have absorption bands with similar extinction coefficients in the same spectral region, which extends up to ca. 345 nm (Fig. 5.3, top left). The two bands for both **9** and **11** arise from spin-allowed π*←π transitions. Also, in the case of ligands **11** and **12**, the corresponding spectra are quite similar, despite being measured in different solvents. The absorption spectrum of tris(terpyridine) **13** shows a shoulder at about 320 nm, presumably accompanying the introduction of CH_3 groups. The triarylamine core in **14** extends the absorption spectrum to the edge of the visible region with a band centred at about 380 nm, which may be assigned to an intra-ligand charge transfer (ILCT) band. An $[M+H]^+$ peak was found in the MALDI-TOF-MS for all the ligands **9**-**14** (see appendix).

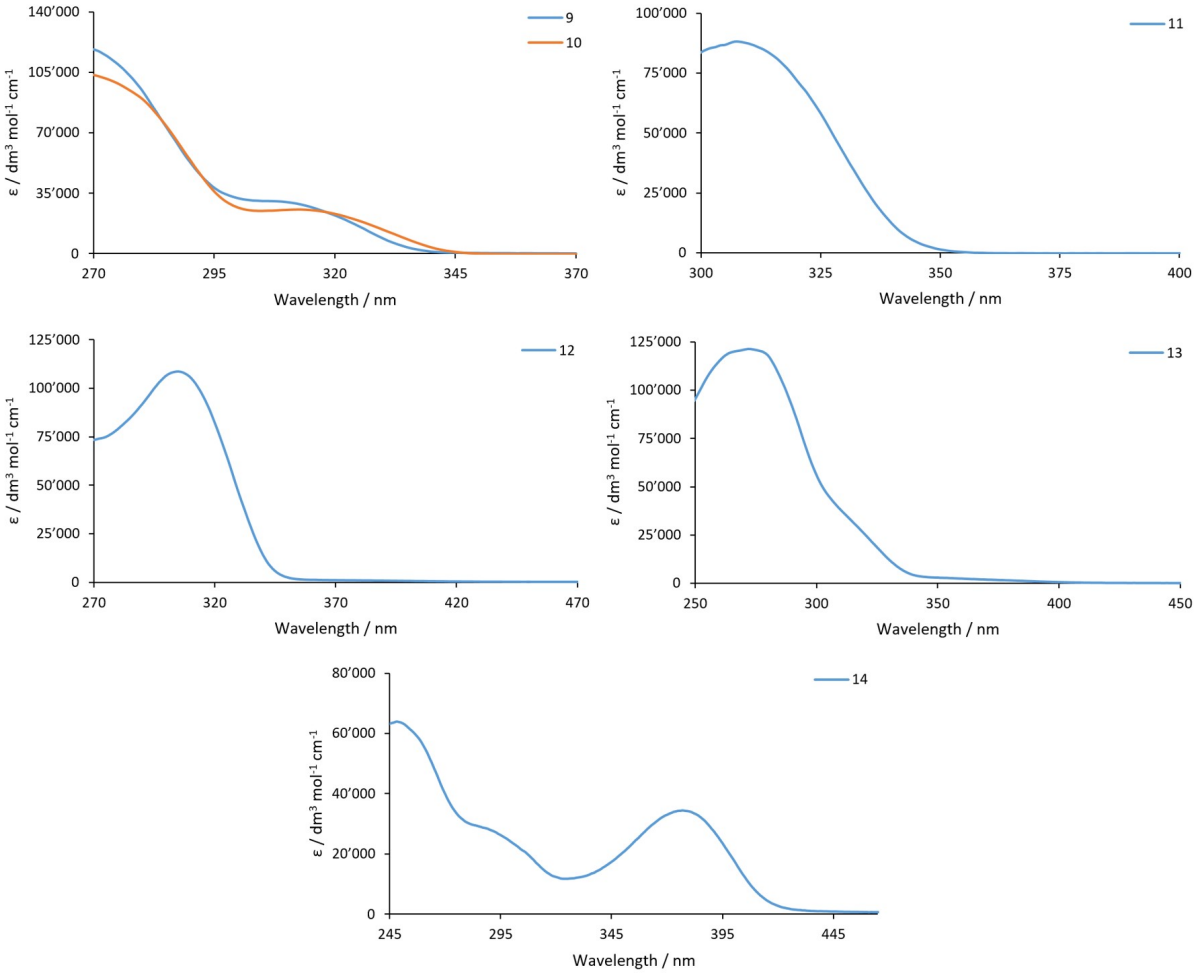

Figure 5.3 Solution absorption spectra of **9** and **10** in DMF (1.0×10^{-5} mol dm^{-3}), **11** in benzonitrile (8.6×10^{-6} mol dm^{-3}), **12** in DMF (8.0×10^{-6} mol dm^{-3}), **13** and **14** in $CHCl_3$ (8.0×10^{-6} mol dm^{-3}). Solvent cut-offs are 245 for $CHCl_3$, 270 nm for DMF, and 300 nm for benzonitrile.

5.3 Crystal structure of 1,3,5-tris(4,2':6',4''-terpyridin-4'-yl)benzene

Single-crystals of **9**·1.75DMF grew as a hot DMF solution of **9** was allowed to cool down to 5 °C. Tris(terpyridine) **9** crystallises in the orthorhombic space group *Pbca,* and its structure (Fig. 5.4a) reveals a propeller-shaped geometry. The asymmetric unit contains one independent molecule and the three terpyridine substituents are crystallographically independent. The angles between the plane of the central arene ring and the planes of the pyridine rings containing N2, N5 and N8 (Fig. 5.4a) are 35.4, 32.8 and 38.0°, respectively. The conformations of the 4,2':6',4'-tpy units also differ. For the terpyridine unit having N1-3, the twist angle between the planes of the rings containing N1/N2 and N2/N3 are 9.4 and 10.5°, respectively. In the tpy containing N7-N9, the angles between the adjacent pyridine rings N7/N8 and N8/N9 are 15.1 and 22.5°, respectively. In contrast, in the tpy possessing N4-N6, the rings are almost coplanar (angles between N4/N5 and N5/N6 are 6.5 and 1.0°).

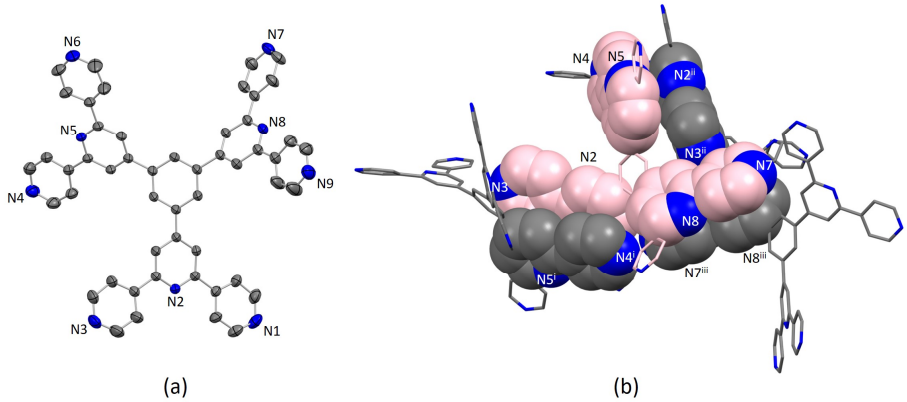

Figure 5.4 (a) Single-crystal X-ray structure of **9**; H atoms and DMF molecules are omitted for clarity. Thermal ellipsoids are drawn at a 40% probability level. (b) Face-to-face π-stacking between molecules of **9**. The carbon atoms of the crystallographically independent molecule are coloured pink. Figure (b) reproduced from the open access reference.[96]

Packing of the molecules is dominated by face-to-face π-stacking, which is consistent with the low solubility of **9**. For the crystallographic independent molecule, two different intermolecular π-stacking interactions can be classified (Fig. 5.4b). First, tpy unit N1N2N3 engages in an interaction with the tpy domain $N4^{i}N5^{i}N6^{i}$ (symmetry code i = 1−*x*, $-{}^{1}/_{2}+y$, ${}^{1}/_{2}-z$). A symmetry-related interaction occurs between the tpy containing N4, N5 and N6 and that with $N1^{ii}$, $N2^{ii}$ and $N3^{ii}$ (symmetry code ii = 1−*x*, ${}^{1}/_{2}+y$, ${}^{1}/_{2}-z$). The centroid…centroid separations for pairs of rings containing $N2/N4^{i}$ and $N3/N5^{i}$ are 3.98 and 4.43 Å, and the corresponding angles between the ring planes are 18.2 and 21.6°. The third tpy ring containing N7–N9 stacks with $N7^{iii}N8^{iii}N9^{iii}$ across an inversion centre (symmetry code iii = 1−*x*, 1−*y*, 1−*z*). The centroid separations between $N7/N8^{iii}$ is 4.21 Å with an angle of 15.1°. All of these centroid...centroid separations are longer than is typical for efficient π-stacking interactions.[228] In addition, the packing of the molecules involves C–H...N hydrogen bonds, with H...N distances in the range 2.47-2.73 Å (C...N range 3.41-3.58 Å, and C–H...N angle range 142.3-175.8°). Overall, the packing interactions lead to an intricate 3D-dimensional lattice.

5.4 Crystal growth experiments

A screening of numerous metal salts and solvent combinations was carried out with ligands **9**-**14**. The formation of X-ray quality crystals was successful for **13** and **14** in combination with $[Cu(hfacac)_2]\cdot H_2O$. For structures containing ligand **14**, only preliminary structures are available. Nevertheless, supported by the reproducibility of these structures, the basic features of the resulting (6,3) nets can be fully described. Solvent aside, the crystal structures all share the general formula $[Cu_3(hfacac)_6(\mathbf{L})]_n$ and are listed in Table 5.1.

Table 5.1 Crystal structures and the solvents for the ligands **13** and **14**, topology of the assemblies and space groups. The solvent for the ligand during the crystallisation process was $CHCl_3$.

Coordination polymer	Solvent for $[Cu(hfacac)_2]\cdot H_2O$	Topology	Space group
$[Cu_3(hfacac)_6(\mathbf{13})]_n\cdot 2.8n MeC_6H_5\cdot 0.4n CHCl_3$	Toluene	1D-chain	$P2_1/n$
Solv. $[Cu_3(hfacac)_6(\mathbf{13})]_n$ in $1,2\text{-}Cl_2C_6H_4/CHCl_3$[a]	1,2-Dichlorobenzene	1D-chain	$P2_1/n$
Solv. $[Cu_3(hfacac)_6(\mathbf{14})]_n$ in $EtOH/CHCl_3$[a]	Ethanol	(6,3)	$P\bar{1}$
Solv. $[Cu_3(hfacac)_6(\mathbf{14})]_n$ in *n*-$BuOH/CHCl_3$[a]	*n*-Butanol	(6,3)	$P\bar{1}$
Solv. $[Cu_3(hfacac)_6(\mathbf{14})]_n$ in $(C_2H_4O)_2/CHCl_3$[a]	1,4-Dioxane	(6,3)	$P\bar{1}$

[a] Preliminary structure. Solv. = Solvated

Single-crystals of $[Cu_3(hfacac)_6(\mathbf{13})]_n\cdot 2.8n MeC_6H_5\cdot 0.4n CHCl_3$ were grown under ambient conditions (see experimental section). Structural analysis revealed the formation of $[Cu_3(hfacac)_6(\mathbf{13})]_n\cdot 2.8n MeC_6H_5\cdot 0.4n CHCl_3$, which crystallises in the monoclinic space group $P2_1/n$. Numerous crystallisation set-ups were attempted with different concentrations of toluene solutions of $[Cu(hfacac)_2]\cdot H_2O$ and chloroform solutions of **13**. The crystals obtained from these attempts had analogous cell parameters to $[Cu_3(hfacac)_6(\mathbf{13})]_n\cdot 2.8n MeC_6H_5\cdot 0.4n CHCl_3$ (see experimental). Single-crystals were also grown by layering a 1,2-dichlorobenzene solution of $[Cu(hfacac)_2]\cdot H_2O$ over a $CHCl_3$ solution of **13** containing anthracene. The latter was added as a potential guest for the assembly. A preliminary structural analysis revealed the assembly of solvated $[Cu_3(hfacac)_6(\mathbf{13})]_n$, which crystallises in the same monoclinic space group ($P2_1/n$) as $[Cu_3(hfacac)_6(\mathbf{13})]_n\cdot 2.8n MeC_6H_5\cdot 0.4n CHCl_3$ with similar cell dimensions (a = 20.693(4) Å, b = 21.145(4) Å, c = 34.404(7) Å, β = 104.72(3)°). The structure suffered severe disorder, but preliminary data confirmed the assembly of a 1D-coordination polymer that was essentially isostructural with that in $[Cu_3(hfacac)_6(\mathbf{13})]_n\cdot 2.8n MeC_6H_5\cdot 0.4n CHCl_3$. The three solvated assemblies of $[Cu_3(hfacac)_6(\mathbf{14})]_n$ crystallised in the triclinic space group $P\bar{1}$. The compounds exhibit similar, extended structures and are therefore discussed together.

5.5 An unexpected 1D-coordination polymer

The structure of the repeat unit in $[Cu_3(hfacac)_6(\mathbf{13})]_n\cdot 2.8n MeC_6H_5\cdot 0.4n CHCl_3$ is shown in Fig. 5.5 with symmetry-generated atoms, and it contains three independent Cu(II) atoms and one independent ligand **13**. Each of the atoms Cu1, Cu2 and Cu3 is octahedrally coordinated with *cis*-arrangements of coordinated $[hfacac]^-$ ligands. Each Cu atom binds to two pyridine donor atoms of two different ligands **5**. The bond lengths and angles for the coordination spheres of Cu1, Cu2 and Cu3 are given in Table 5.2. A search of the Cambridge Structural Database[218] (CSD, v. 2021.3.0 using Conquest v. 2021.3.0, April 2022)[180, 219] for structures containing in $\{Cu(hfacac)_2(N_1)(N_2)\}$ units reveals that in most structures the N–Cu–N angles are close to 180° (Fig. 5.6), i.e. a *trans*-arrangement of N atoms. Most of the *cis*-configurations associated with the N–Cu–N angles of 75-100° in Fig. 5.6 are a consequence of chelating

N^N ligands. Hence, the *cis*-arrangement found in $[Cu_3(hfacac)_6(\mathbf{13})]_n \cdot 2.8n MeC_6H_5 \cdot 0.4n CHCl_3$ is considered to be unusual.

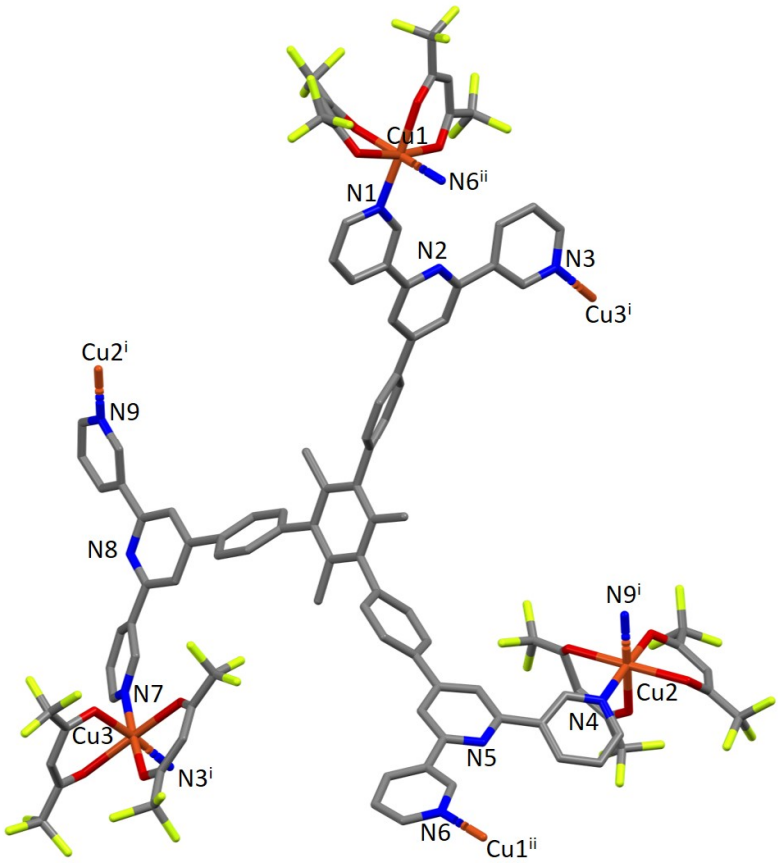

Figure 5.5 The repeat unit in $[Cu_3(hfacac)_6(\mathbf{13})]_n \cdot 2.8n MeC_6H_5 \cdot 0.4n CHCl_3$ with symmetry-generated atoms. For clarity, H atoms and solvent are omitted, and only major occupancies are shown. Symmetry codes: i = 1−*x*, 1−*y*, 1−*z*; ii = 1−*x*, −*y*, 1−*z*.

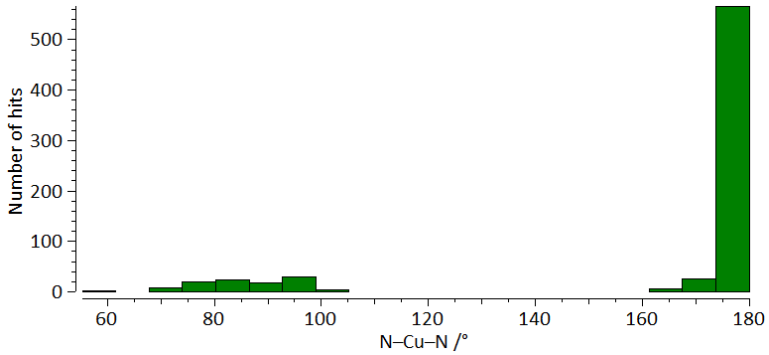

Figure 5.6 Distribution of the N–Cu–N coordination angle in $\{Cu(hfacac)_2(N_1)(N_2)\}$ units from a search of the Cambridge Structural Database (v. 2021.3.0) using ConQuest (v. 2021.3.0).[180, 219]

Table 5.2 Selected bond lengths and angles in the copper(II) coordination spheres.

Metal atom	Cu–N /Å	N–Cu–N /°	Cu–O /Å	N–Cu–O /°
Cu1	2.013(5) 1.995(6)	91.1(2)	2.320(4) 1.993(6) 1.996(4) 2.238(4)	92.6(2), 90.6(2), 177.7(2), 94.69(19), 90.91(18), 175.1(2), 90.6(2), 93.6(2)
Cu2	2.032(5) 2.023(6)	96.6(2)	1.981(5) 2.222(6) 2.001(5) 2.290(5)	86.0(2), 92.2(2), 174.0(2), 94.2(2), 176.7(2), 94.4(2), 89.3(2), 90.4(2)
Cu3	2.075(9) 2.005(7)	93.5(3)	1.983(9) 2.206(7) 2.231(5) 2.017(8)	89.4(4), 95.6(3), 91.1(3), 175.4, 175.1(3), 89.7(3), 94.7(2), 88.2(3)

In coordinated ligand **13** (Fig. 5.5), the three terpyridine domains are crystallographically independent, and coordination occurs only through the two outer nitrogen atoms. The terpyridine units containing N1, N2 and N3 and N4, N5 and N6 display a coordination directionality close to conformation **C** (Scheme 5.3), with N1 and N6 pointing out and N4 and N5 oriented towards the centre core of **13**. In contrast, the terpyridine with N7, N8 and N9 adopts conformation **B** (Scheme 5.3). Angles between the least-squares planes through pairs of adjacent pyridine rings are in the range 7.6-30.7° (Table 5.3). The larger torsion angles of 60.0, 84,2 and 56.7° between the planes of the arene core and the three arene spacers (Table 5.3) minimise unfavourable CH_3…H repulsions. Similar twists occur between the arene spacers and the central pyridine of the terpyridine substituents, although to a lesser extent (35.6, 30.5 and 53.4°), reducing the H...H inter-ring repulsions.

Table 5.3 Angles between the planes of pairs of connected rings in coordinated ligand **13**.

Tpy unit	py-py /°	py_{N2}-arene spacer /°	arene spacer-arene core /°
N1N2N3	7.6, 22.6	35.6	60.0
N4N5N6	17.0, 19.1	30.5	84.2
N7N8N9	30.7, 24,9	53.4	56.7

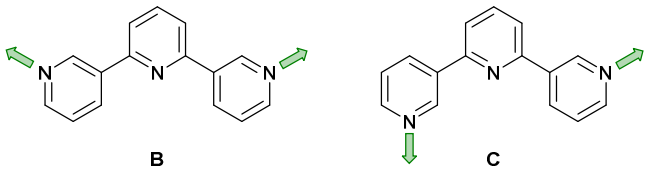

Scheme 5.3 The limiting conformation **B** and **C** is adopted by the terpyridine units in $[Cu_3(hfacac)_6(\mathbf{13})]_n \cdot 2.8n MeC_6H_5 \cdot 0.4n CHCl_3$. For all possible conformations see Scheme 1.7 in the introduction.

Ligand **13** presents a 6-connecting building block (Fig. 5.5) and, combined with the *cis*-arrangement of the pyridine donors in the Cu(II) coordination sphere, this leads, rather unexpectedly, to a 1D-coordination polymer. There are two building blocks which alternate along the chain. The first is the centrosymmetric metallomacrocyclic unit in Fig. 5.7a in which Cu1 and $Cu1^{ii}$ bridge pairs of 3,2':6',3''-tpy domains bound through atoms N1 and $N6^{ii}$, and N6 and $N1^{ii}$ (symmetry code ii = 1−*x*, −*y*, 1−*z*).

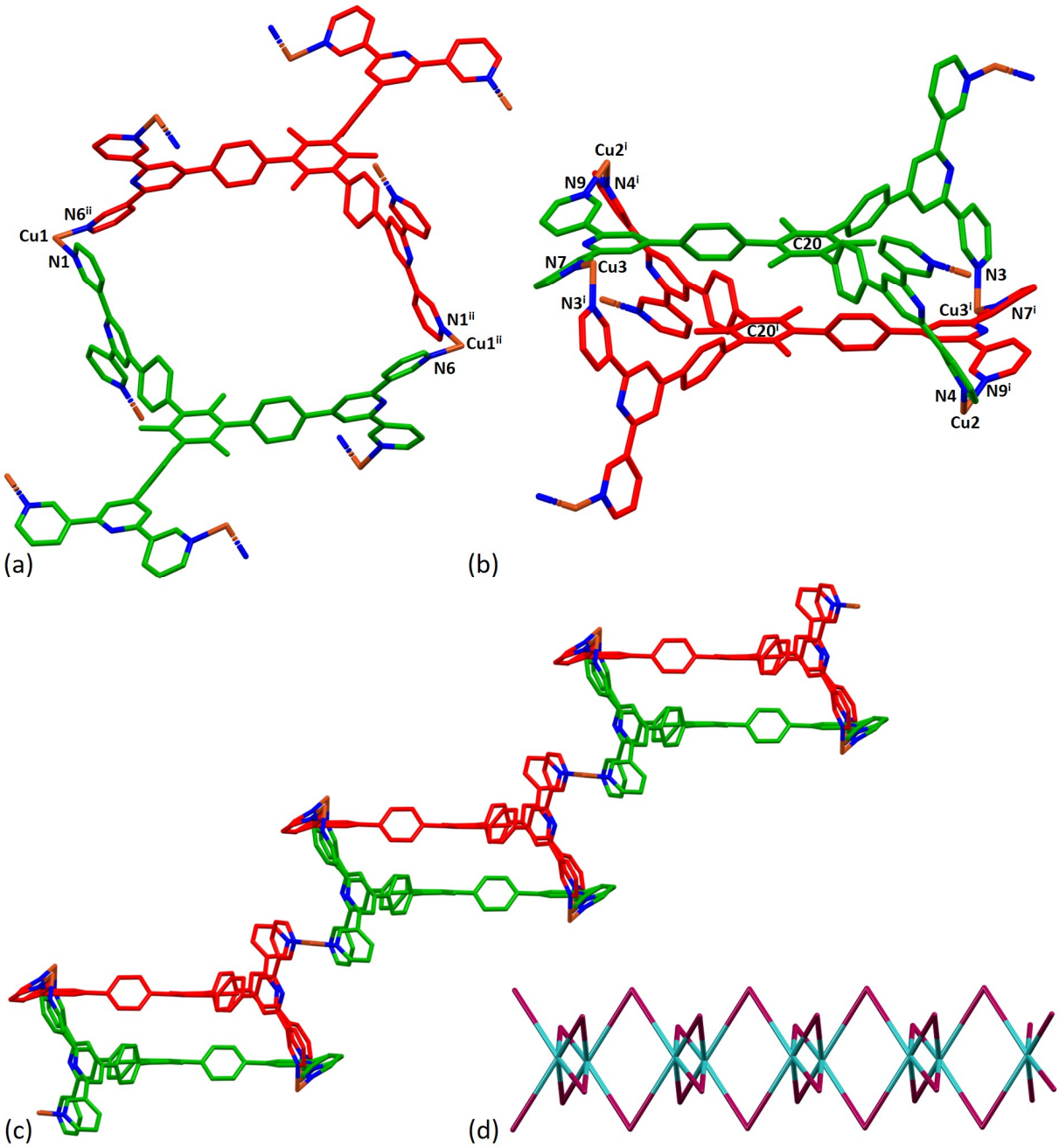

Figure 5.7 (a) Metallomacrocyclic unit consisting of **13** (green), Cu1 and the symmetrical equivalents **13**^{ii} (red) and Cu1^{ii}. (b) The second motif in the 1D-polymer with symmetry generated copper centres and ligand **13**^{i} (red). (c) Part of the 1D-coordination polymer. Tris(terpyridine) building blocks are alternating coloured in green and red. For clarity, H atoms, coordinated $[hfacac]^-$ ligands and solvent are omitted, and only major occupancies are shown. Symmetry codes: i = 1−*x*, 1−*y*, 1−*z*; ii = 1−*x*, −*y*, 1−*z*. (d) Loops forming the 1D-chain. Magenta: Cu; turquoise: ligand centroids. Figure (d) reproduced from the open access reference.[96]

The second motif in the 1D-polymer consists of head-to-tail pairs of two ligands **13** (Fig. 5.7b). The two tris(terpyridine) ligands are coordinated with Cu2, Cu2^{i}, Cu3 and Cu3^{i} across an inversion centre (symmetry code i = 1−*x*, 1−*y*, 1−*z*). All inwardly oriented nitrogen atoms of **13**, which come from all three terpyridine domains, are involved in the building block. The terpyridine unit containing N7, N8 and N9 is connected to the terpyridine unit with N1^{i}, N2^{i} and N3^{i} and that with N4^{i}, N5^{i} and N6^{i} with atoms Cu3 and Cu2^{i} acting as linkers (Fig. 5.7b, symmetry code i = 1−*x*, 1−*y*, 1−*z*). Interestingly, there are no π-stacking interactions within the motif, even though the arene cores are coplanar.

Centroid...centroid separations for pairs of rings containing C20/C20^{i} is 5.00 Å (Fig. 5.7b), and it is clear that the steric hindrance caused by the methyl substituents prevents π-interactions. The combination of the two structural motifs in the 1D-polymer (Fig. 5.7c) leads to a series of connected loops with ligand **13** connecting pairs of Cu atoms (Fig. 5.7c and d). Atoms Cu1 and Cu1^{ii} lie within a single loop in Fig. 5.7d, while Cu2, Cu3, Cu2^{i} and Cu3^{i} lie within the double loops in Fig. 5.7d.

The coordination polymer chains follow the crystallographic *b*-axis and packing interactions between the chains are dominated by short C–H…F–C and C–F…F–C contacts. However, the disordering of some CF_3 groups means that detailed discussion is not meaningful. The nesting of the 1D chains shown in Fig. 5.8a illustrates a zigzag arrangement with the chains slightly offset (Fig. 5.8b). Channels in the structure are occupied by highly disordered toluene and $CHCl_3$ molecules.

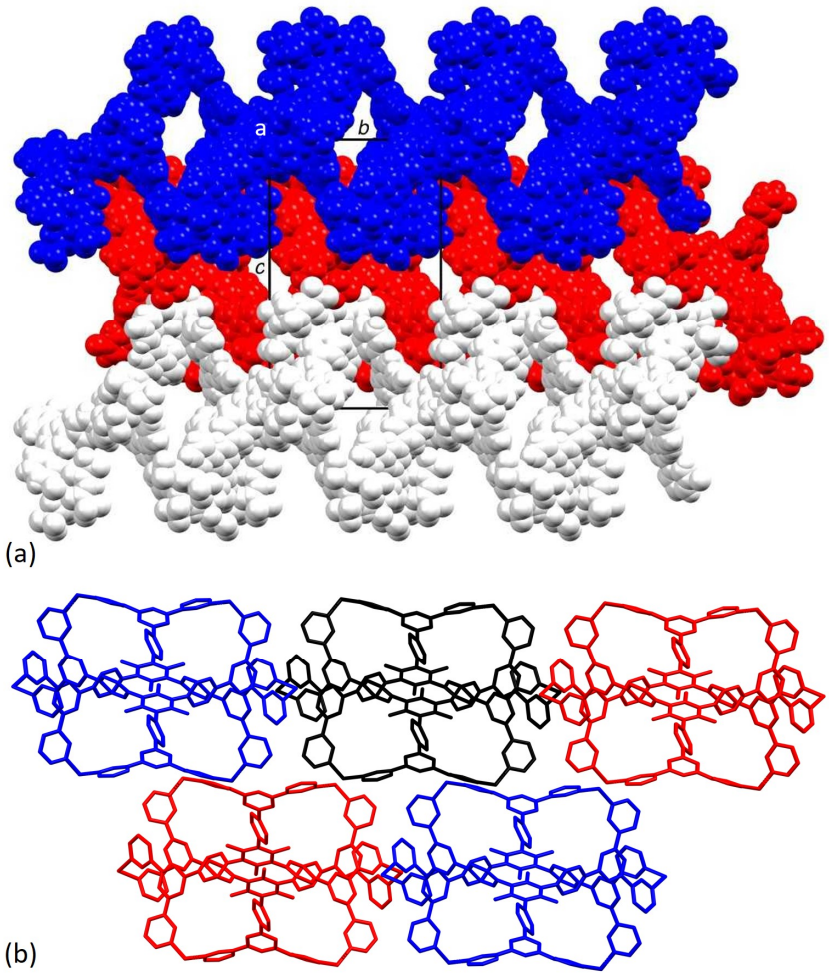

Figure 5.8 (a) Packing of three 1D ribbons which follow the *b*-axis, shown in blue, red and white, and viewed down the crystallographic *a*-axis. For clarity, solvent is omitted and only major occupancies are shown. (b) Packing and cross-section of five 1D ladders (alternatively coloured), viewed down the crystallographic *b*-axis along which the 1D-polymers propagate. For clarity, H atoms, $[hfacac]^-$ ligands and solvent molecules are omitted, and only major occupancies are shown. Figures reproduced from the open access reference.[96]

5.6 Comments on 1D-coordination polymers containing terpyridine metal-binding domains

The structure of the 1D-chain in $[Cu_3(hfacac)_6(\mathbf{13})]_n$ consists of alternating single and double loops (Fig. 5.7d), with this motif being a consequence of the 6-connecting node presented by ligand **13**. The use of the term 'node' in a 1D-chain is 'subjective',[1] since the chain can be described unambiguously in terms of a combination of metal linkers and ligand linkers. Topologically, the 1D-chains in Scheme 5.4 are all equivalent, but they are structurally distinct in terms of the organisation of the chemical building blocks, with, for example, Scheme 5.4d and 5.4e having enclosed space within the 1D-chain.

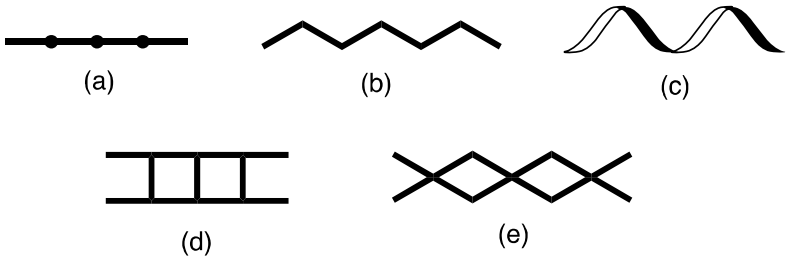

Scheme 5.4 Examples of structure types found in 1D-coordination polymers: (a) linear chain, (b) zigzag chain, (c) helical chain, (d) ladder, (e) series of loops with 4-connecting nodes. Scheme reproduced from the open access reference.[96]

The versatility of terpyridine as a building block for 1D-CPs is worthy of comment. Starting from a 2,2':6',2"-tpy ligand, $\{M(tpy)_2\}^{n+}$ units can be functionalized in the 4'-position to provide a linear building block. An example is $[Ru(pytpy)_2]^{2+}$ (pytpy = 4'-(4-pyridyl)-2,2':6',2"-terpyridine), the $[PF_6]^-$ salt of which reacts with $AgNO_3$ in aqueous MeCN solution to give $[\{Ru(pytpy)_2Ag(NCMe)(NO_3)\}_n][NO_3]_{2n}\cdot H_2O\cdot MeCN$ containing the 1D-chain (Fig. 5.9a).[229] The linearity (Scheme 5.4a and Fig. 5.9a) of the chain is a consequence of the directionalities of the outer pyridine donors in the $[Ru(pytpy)_2]^{2+}$ unit coupled with the N–Ag–N angle of 150.4(1)°. In contrast, ongoing from pytpy to 4-pyridinecarbaldehyde (2,2':6',2"-terpyridin-4'-yl)hydrazone (**L14**, Fig. 5.9b), a significant degree of curvature is introduced into the $[Ru(\mathbf{L14})_2]^{2+}$ unit compared to $[Ru(pytpy)_2]^{2+}$. This renders the $[Ru(\mathbf{L14})_2]^{2+}$ domain responsive to the formation of 1D-chains comprising a string of loops as seen in $[\{Fe(NCS)_2(Ru(\mathbf{L14})_2)_2\}_n]^{4n+}$ (Fig. 5.9b).[230]

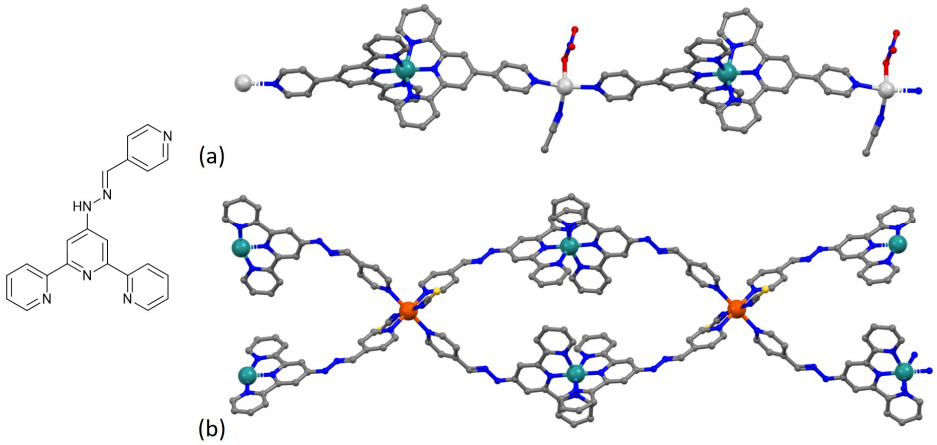

Figure 5.9 (a) Part of the linear 1D-chain in $[\{Ru(pytpy)_2Ag(NCMe)(NO_3)\}_n][NO_3]_{2n}\cdot n H_2O\cdot n MeCN$ (CSD refcode WICSIL). (b) Structure of ligand **L14** and part of the chain comprising interconnected loops in $[\{Fe(NCS)_2(Ru(\mathbf{L14})_2)_2\}_n][Fe_2(NCS)_6(OEt)_2(EtOH)_2]_n[NCS]_{2n}\cdot 4n EtOH\cdot n H_2O$ (CSD refcode TOPLIU).

Zigzag chains (Scheme 5.4b) directed by metal paddle-wheel domains such as $\{Zn_2(\mu\text{-}O_2CMe)_4\}$ and $\{Cu_2(\mu\text{-}O_2CMe)_4\}$ are well illustrated for a wide range of 4'-substituted 4,2':6',4''-tpy ligands (e.g. Fig. 5.10a)[231] and the conformational flexibility of the 3,2':6',3''-tpy domain leads to structural variants on the zigzag backbone[232]. Multiply-stranded chains[83] which retain the zigzag profile arise when multinuclear metal units can bind to more than two ligands, e.g. $[Cd_2(OAc)_4(4'\text{-}(4\text{-}PhC_6H_4)\text{-}4,2':6',4''\text{-}tpy)]_n$ in which each $\{Cd_2(OAc)_4\}$ (a non-paddle wheel motif) binds to four N donors (Fig. 5.10b)[233], and $[Cu_4(\mu_3\text{-}OH)_2(OAc)_6(4'\text{-}(4\text{-}MeOC_6H_4)\text{-}3,2':6',3''\text{-}tpy)_2]_n$ (Fig. 5.10c)[234]. In contrast, the rotational freedom of the ferrocenyl core in the tetratopic ligand 1,1'-bis(4,2':6',4''-terpyridin-4'-yl)ferrocene allows the assembly of a double-stranded chain in which the ligand 'folds over' to produce the two strands (Fig. 5.10c)[235]. Helical chains are also common. Many are based upon tetrahedral $\{Zn_2X_2N_2\}$ domains, and are exemplified by $[ZnCl_2(4,2':6',4''\text{-}tpy)]_n$ which was the first coordination polymer reported which was directed by a 4,2':6',4''-tpy ligand[236]. Ladders (Scheme 5.4d) in which the uprights and rungs of the ladder are both defined by ligand linkers are less common, and one example is $[Cd_2(4'\text{-}(4\text{-}MeOC_6H_4)\text{-}4,2':6',4''\text{-}tpy)_3(NO_3)_4]_n$ (Fig. 5.10e).[237]

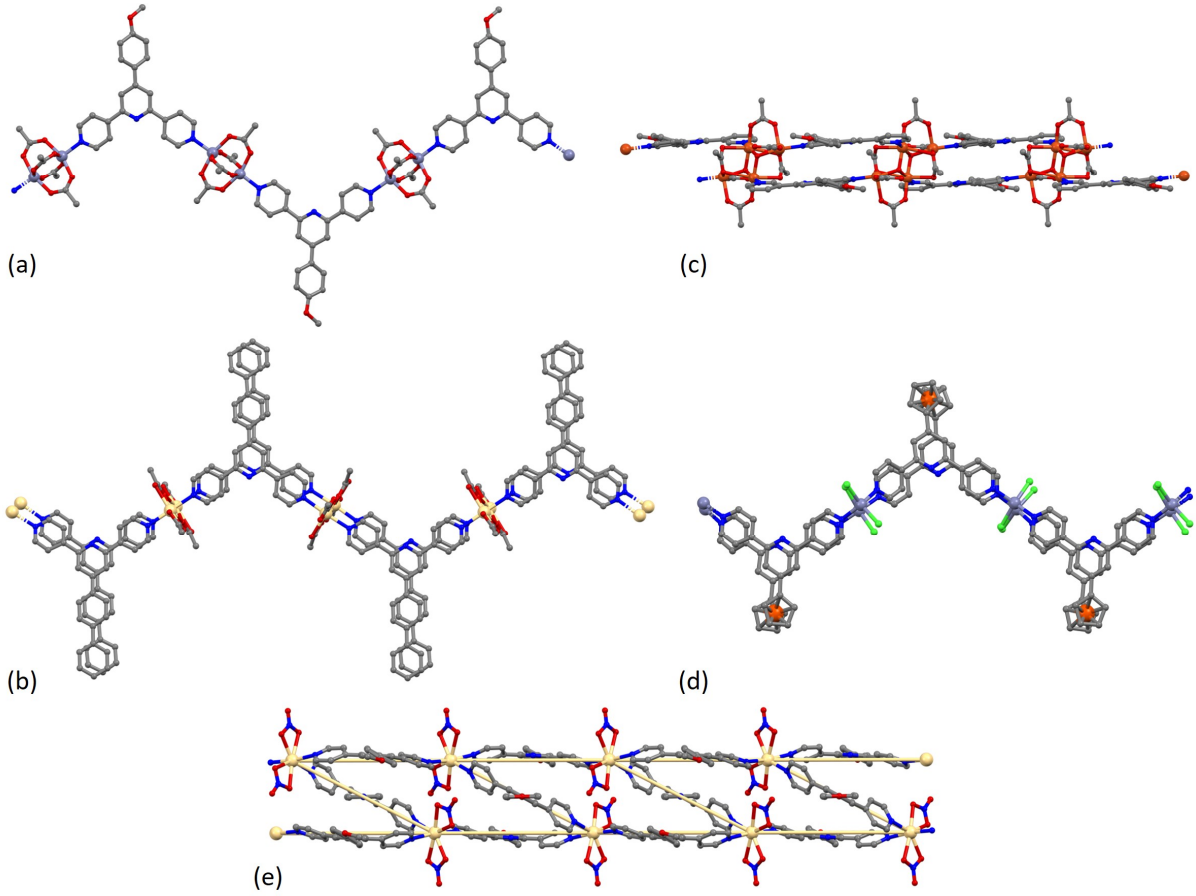

Figure 5.10 (a) Part of the zigzag chain in $[Zn_2(OAc)_4(4'\text{-}(4\text{-}MeOC_6H_4)\text{-}4,2':6',4''\text{-}tpy)]_n$ (CSD refcode SOXSEF). Parts of the double stranded zigzag chains in (b) $[Cd_2(OAc)_4(4'\text{-}(4\text{-}PhC_6H_4)\text{-}4,2':6',4''\text{-}tpy)]_n$ (refcode RIGJEY), (c) $[Cu_4(\mu_3\text{-}OH)_2(OAc)_6(4'\text{-}(4\text{-}MeOC_6H_4)\text{-}3,2':6',3''\text{-}tpy)_2]_n$ (refcode KUCHIC), and (d) $[Zn_2Cl_2(1,1'\text{-}bis(4,2':6',4''\text{-}terpyridin\text{-}4'\text{-}yl)ferrocene)]_n$ (refcode UMUYUY). (e) Part of the ladder assembly in $[Cd_2(4'\text{-}(4\text{-}MeOC_6H_4)\text{-}4,2':6',4''\text{-}tpy)_3(NO_3)_4]_n$ (refcode BUDZIL); the Cd....Cd vectors which define the ladder are highlighted.

This short survey is not comprehensive, but illustrates the range of 1D-coordination polymers that can be assembled using ligands with 2,2':6',2"-, 3,2':6',3"- and 4,2':6',4"-tpy metal-binding domains. To the best of our knowledge, the looped-structure of the chain in the solvates of $[Cu_3(hfacac)_6(\mathbf{13})]_n$ presented in this chapter is unique among terpyridine-based complexes.

5.7 Assembly of (6,3)-networks

Preliminary data revealed the assembly of the solvated $[Cu_3(hfacac)_6(\mathbf{14})]_n$ in each solvent combination EtOH/$CHCl_3$, *n*-BuOH/$CHCl_3$ and $(C_2H_4O)_2$/$CHCl_3$. All three compounds are 2D-coordination polymers with comparable repeating units, but due to the incompleteness of the structures, no details on angles and distances are given. Therefore, only the essential characteristics of the assemblies are discussed. In each case, the repeating unit contains one tris(4,2':6',4''-tpy) ligand **14** and three Cu(II) centres. The repeat unit of the EtOH/$CHCl_3$ solvated structure is illustrated in Fig. 5.11 without the disordered and incomplete CF_3 groups.

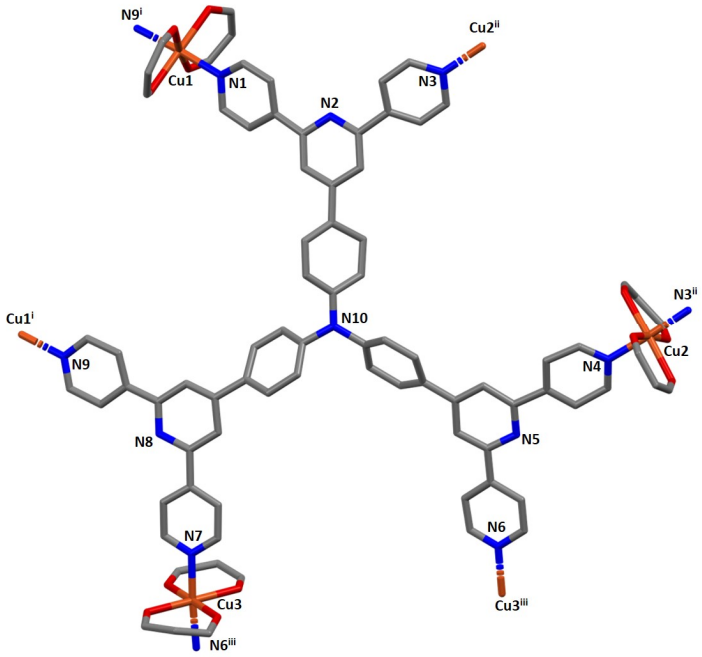

Figure 5.11 The repeat unit in the coordination network of solvated $[Cu_3(hfacac)_6(\mathbf{14})]_n$ with symmetry-generated atoms. For clarity, H atoms, CF_3 groups and solvent molecules are omitted. Symmetry codes: i = 2–*x*, –*y*, 1–*z*; ii = –*x*, 1–*y*, 2–*z*; iii = 1–*x*, 2–*y*, 1–*z*.

The Cu(II) centres are octahedrally sited, with a *trans*-arrangement of the two pyridine donors of two different ligands. The metal centres, therefore, act as linkers. The three arene spacers in **14** have a propeller shaped geometry which is characteristic for triarylamine derivatives.[238-240] The twist minimises repulsive H...H interactions. Consequently, ligand **14** is chiral and is found in the 2D network as a racemic mixture, Λ and Δ. The coordinated molecule has some flexibility, as the amine core does not lie on the plane generated by N2, N5 and N8 (Fig. 5.12). However, the tertiary amine is not the reason for the curvature since the three C–N–C angles subtended at N10 are close to 120°. It follows that the coordinated **14** possesses an umbrella shape (Fig. 5.12).

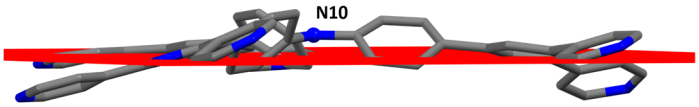

Figure 5.12 The nitrogen N10 out of the plane originated from N2, N5 and N8. Atom labels are shown in Fig. 5.11. For clarity, H atoms, {Cu(hfacac)$_2$} linkers and solvent molecules are omitted.

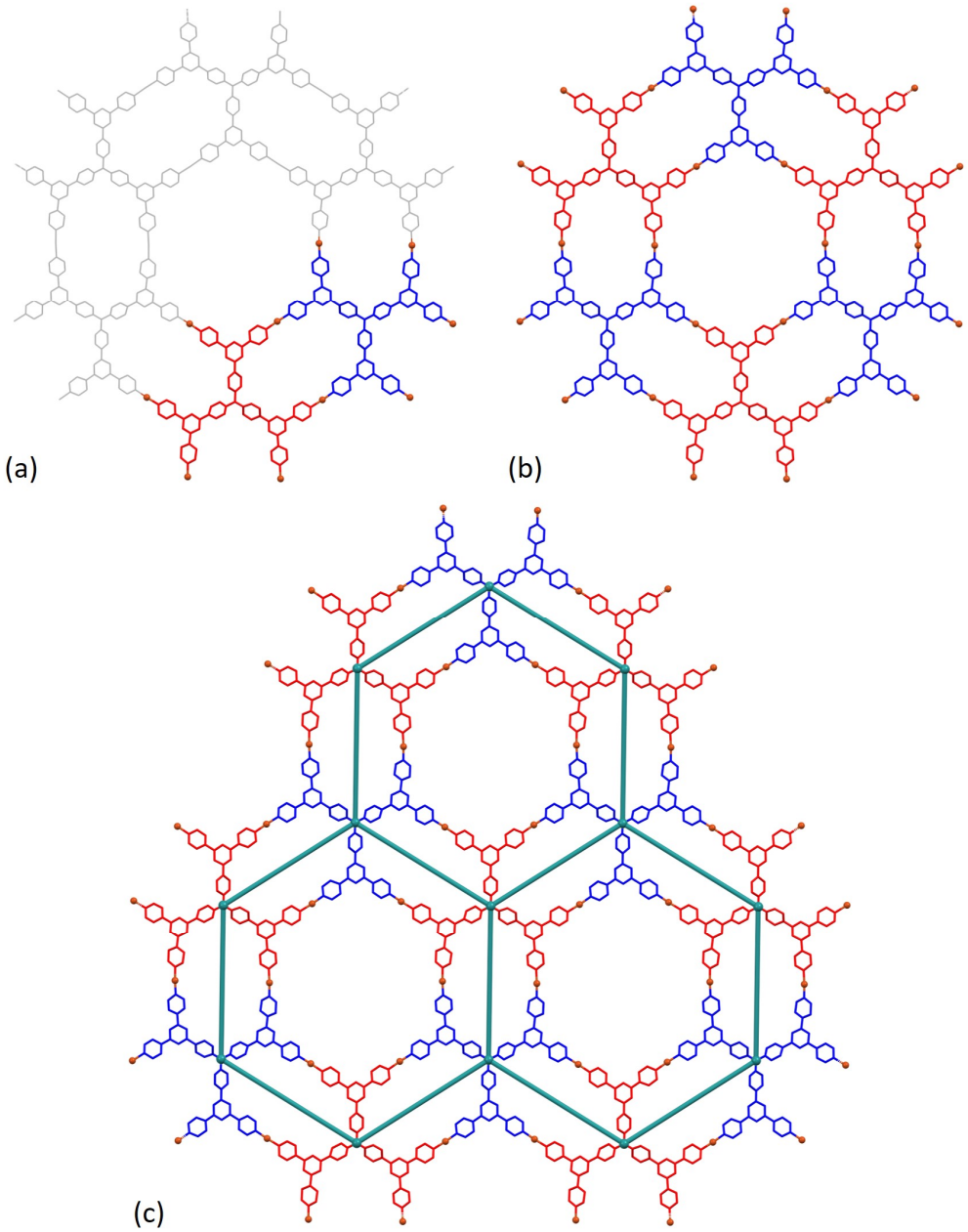

Figure 5.13 (a) Motif consisting of two ligands **14** (red and blue) and two Cu(II) linkers. (b) The hexagon ring in the 2D-polymer with six terpyridine units and equal number of copper centres. (c) Part of [Cu$_3$(hfacac)$_6$(**14**)]$_n$ highlighting the (6,3)-net determined by the tertiary amines (green nodes). Tris(terpyridine) building blocks are alternating coloured in blue and red. For clarity, H atoms, coordinated [hfacac]$^-$ ligands and solvent are omitted.

Each tris(4,2':6',4"-terpyridine) ligand binds through the outer pyridine rings with six different [Cu(hfacac)$_2$] linkers (Fig. 5.11). Pairs of Cu(II) centres bridge two ligands **14** (Fig. 5.13a) generating a small centrosymmetric metallomacrocycle in which the four pyridine donors arise from four different terpyridine domains. As a result, each tris(terpyridine) **14** interacts across the six Cu centres with three other ligands. The second and big centrosymmetric metallomacrocycle is composed of six different terpyridine units from six distinct ligands and as many metal linkers generating a hexagonal hole (Fig. 5.13b). The combination of hexagons and elongated smaller macrocycles forms the 2D-polymer (Fig. 5.13c). From a topological point of view, the tertiary amine is the 3-connecting node and the unique shortest circuit is six-membered (Fig. 5.13c). So the net symbol is (6,3). It should come as no surprise that local chemical geometry is different from node connectivity. A network is a topological description and is not concerned with the geometrical layout of the chemical building blocks. Due to the umbrella shaped conformation of ligand **14**, the individual layers follow a corrugated arrangement, where the nodes are alternatively placed on two parallel planes (Fig. 14a). In consequence, the six-membered shortest circuits adopt the chair conformation rather than being planar (Fig. 14b). Although **14** is chiral, the triarylamine cores alternate their chirality Λ and Δ on the two planes respectively, making the network achiral.

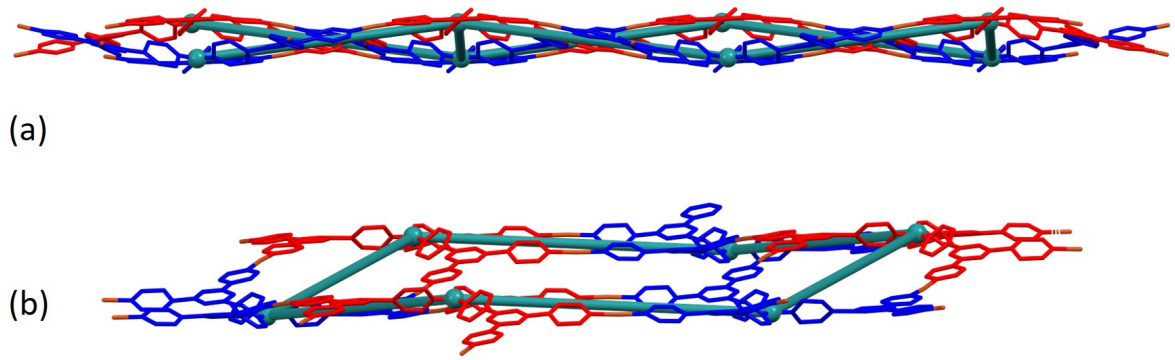

Figure 5.14 (a) (6,3) Net observed through the two parallel planes generated by the tertiary amines nodes (green). (b) The six-membered shortest circuit in chair conformation. For clarity, H atoms, coordinated [hfacac]$^-$ ligands and solvent are omitted.

5.8 Bulk sample analysis

After four single-crystals of [Cu$_3$(hfacac)$_6$(**13**)]$_n$·2.8*n*MeC$_6$H$_5$·0.4*n*CHCl$_3$ had been selected for single-crystal X-ray structure determination, the bulk material was analysed by PXRD. The crystals lose solvent rapidly on exposure to air and were, therefore, analysed wet and without washing them. Despite careful handling of the crystals, loss of solvent could not be avoided, and as a consequence, the PXRD spectrum was of poor quality. Confirmation that the single-crystal selected was representative of the main phase of the bulk sample came from a comparison of the experimental PXRD pattern (shown in red in Fig. 5.15) with the pattern predicted from the single-crystal structure (black traces in Fig. 5.15). Minor phases observed in the PXRD spectrum of the bulk material could not be assigned and most likely appear as a consequence of solvent loss during sample preparation and measurement. The differences in intensities (blue traces in Fig. 5.15) can be justified in terms of differences in the preferred orientations of the crystallites in the bulk powder samples.

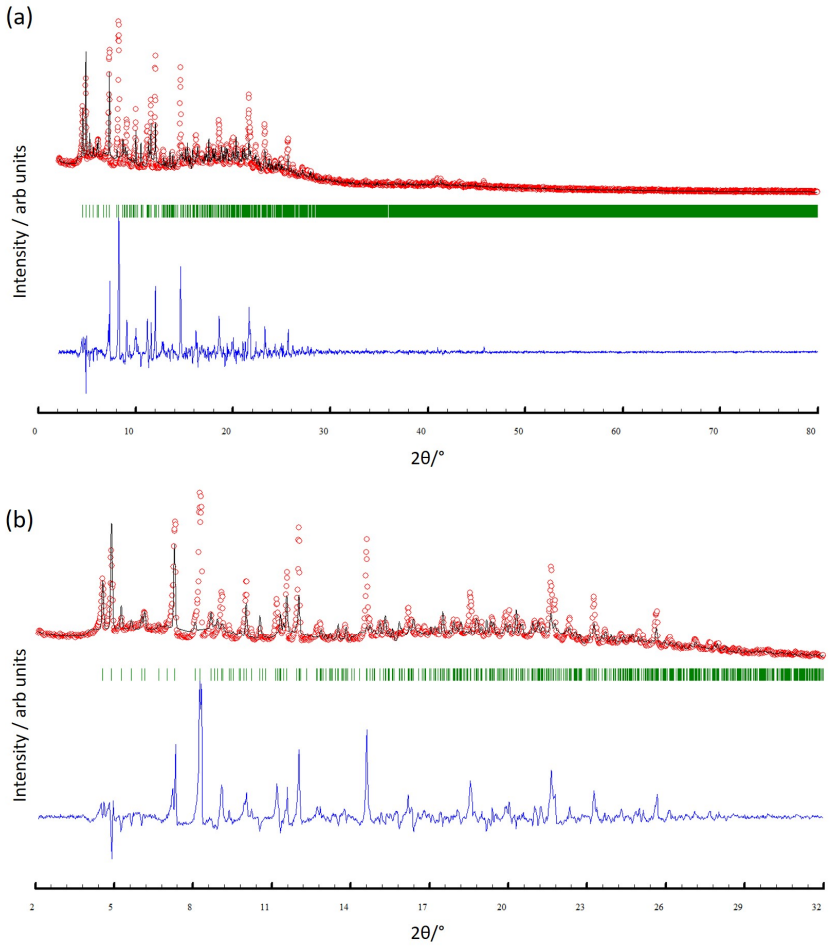

Figure 5.15 (a) X-ray diffraction (CuKα1 radiation) pattern (red circles) of the bulk crystalline material of $[Cu_3(hfacac)_6(\mathbf{13})]_n \cdot 2.8n MeC_6H_5 \cdot 0.4n CHCl_3$, fitting the predicted pattern from the single-crystal structure. The black lines are the best fit from Rietveld refinements, and green lines display the Bragg peak positions. The blue plot gives the difference between calculated and experimental points (see text). (b) Expansion in the 2-32° range. Figures reproduced from the open access reference.[96]

5.9 Conclusions

Six tris(terpyridine) ligands **9**-**14** were prepared and characterised, three with 4,2':6',4''-tpy units and three with 3,2':6',3''-tpy metal-binding domains. The crystal structure of **9** was determined. It possesses a propeller-shaped structure and efficient face-to-face π-stacking interactions predominate in the packing. The reaction of **13** with $[Cu(hfacac)_2] \cdot H_2O$ under ambient crystal growth conditions by layering using a combination of $CHCl_3$ and toluene unexpectedly led to the assembly of the 1D-coordination polymer $[Cu_3(hfacac)_6(\mathbf{13})]_n \cdot 2.8n MeC_6H_5 \cdot 0.4n CHCl_3$. This possesses an unusual 1D-chain consisting of a series of alternating single and double loops in which the $\{Cu(hfacac)_2(N_1)(N_2)\}$ units display a *cis*-arrangement of N atoms. In coordinated ligand **13**, two of the crystallographically independent 3,2':6',3''-tpy domains adopt conformation **C** (Scheme 5.3), while the third exhibits conformation **B**. PXRD confirms that the single-crystal structure is representative of the bulk material. A preliminary structural analysis has also shown that a switch from toluene to 1,2-dichlorobenzene has no effect on the assembly of the network.

Preliminary structural data for single-crystals grown from the reactions between **14** and $[Cu(hfacac)_2] \cdot H_2O$ revealed the formation of three solvated 2D-assemblies $[Cu_3(hfacac)_6(\mathbf{14})]_n$. Despite being

obtained from three different solvent combinations (EtOH/$CHCl_3$, *n*-BuOH/$CHCl_3$ and $(C_2H_4O)_2$/$CHCl_3$), the compounds are essentially isostructural and show a corrugated arrangement. The flattened structure can be described as a chamfered hexagonal grid. It consists of hexagons and elongated smaller macrocycles, arranged so that each hexagon is surrounded only by elongated macrocycles and each elongated macrocycle borders two hexagons and four elongated macrocycles. Topologically, the assemblies are (6,3) nets in which the tertiary amine present in **14** is the node.

6 General conclusion and outlook

In this thesis, tetratopic bis(3,2':6',3''-tpy) and bis(4,2':6',4''-tpy), hexatopic tris(3,2':6',3''-tpy) and tris(4,2':6',4''-tpy) ligands were synthesised and their ability to form multidimensional assemblies with different metal salts was investigated. Not all of the ligands presented here have led to the successful structural characterisations of coordination polymers. Difficulties arose especially when these ligands showed poor solubility in typical organic solvents. The use of compounds with solubilising substituents, from the short methyl group to longer alkyloxy or phenylalkoxy chains, has solved this problem to a great extent.

Reactions of the multitopic ligands with numerous metal salts were investigated, and $[Cu(hfacac)_2]\cdot H_2O$ has been by far the most successful, making it possible to obtain single-crystals structures even with the tris(terpyridine) ligands. Premature precipitation of the tris(terpyridine) ligand in the crystallisation setup was often observed when the solvent for the metal salt was an anti-solvent for the ligand; the crystal growth experiments were always done by layering. The versatile solubility of $[Cu(hfacac)_2]\cdot H_2O$ in a wide variety of organic solvents allowed the use of solvents compatible with large, multitopic ligands leading to successful single-crystal growth. The less soluble $[Zn(hfacac)_2]\cdot 2H_2O$ gave no X-ray quality single-crystals when reacted with the hexatopic ligands and only one compound with a tetratopic ligand led to X-ray quality crystals and successful structure determination. $[M(hfacac)_2]$ (M = Cu, Zn) units act as 2-connecting building blocks. This limits their role to that of a linker and 3D assemblies from these metal salts are unlikely to be obtained. The combination of both 4-connecting ligands and metal salts offers the potential to achieve 3D architectures. Cobalt(II) thiocyanate proved to be a valuable metal salt and several series of 3D coordination assemblies were obtained, although its application is limited due to its solubility in only a few solvents.

The structures of the coordination polymers are difficult to predict and serendipity always plays a part in self-assembly. However, some trends in the formation of coordination polymers using ligands with multiple terpyridine domains have been noticed in the course of this thesis.

The combination of bis(3,2':6',3''-tpy) ligands (4-connecting nodes) with $[M(hfacac)_2]$ (M = Cu, Zn) (linkers) led to a series of two-dimensional (4,4) networks. The nature of the investigated substituents attached to the phenylene spacer in the bis(3,2':6',3''-tpy) ligands, the crystallisation solvent, as well as the *cis*- or *trans*-configuration of ligands at the metal centre were found not to influence the underlying topology of the resulting network.

By using bis(3,2':6',3''-tpy) ligands and $Co(SCN)_2$, which both act as 4-connecting nodes, permitted a step into the realm of 3D architectures. Once again, the various substituents on the central phenylene ring were found to play no important role in the assembly process, while the solvents used for crystal growth by layering had a decisive influence. A *cds* topology was encountered when MeOH and chlorobenzene were employed as crystallisation solvents, while trinodal self-penetrating networks were observed when chlorobenzene was replaced by chloroform. Whether or not the chlorobenzene templates the assembly remains unclear. This trend was confirmed in the recent findings of Simona Capomolla,[190, 191] a former Master's candidate in the Constable-Housecroft research group. The only exception to this trend comes from the work of Maximilian Klein, a former PhD candidate in the same group. This is a *pts* network which assembled from a combination of $Co(NCS)_2$ and a bis(3,2':6',3''-tpy)

ligand with the more sterically demanding *n*-octyloxy chains; this *pts* net was also obtained with $CHCl_3$ and MeOH.[92, 187] However, the bulk material from which the single-crystal was chosen was not analysed by PXRD and no statements can be made about its representativeness. As an outlook, further attempts should be made to reproduce the *pts* network and to investigate at which point the steric hindrance of the substituents causes a break in the structural pattern.

The move from tetratopic to hexatopic tpy ligands opens up the possibility of combining six-connecting units with metal centres of choice. Once again, the use of $[Cu(hfacac)_2]$ as a building block, acting as a linker, proved its worth. The absence of analogous structures of coordination polymers containing tris(terpyridine) ligands in the literature does not allow us to establish a trend as for the crystal structures obtained with the bis(3,2':6',3''-terpyridine) ligands described above. However, this does not preclude observations from being made. Reaction between $[Cu(hfacac)_2]\cdot H_2O$ and tris(3,2':6',3''-terpyridine) or tris(4,2':6',4''-terpyridine) ligands gave rise to a 1-dimensional coordination polymer and a 2-dimensional network, respectively. Different crystallisation solvents led to isostructural networks for each. Once again, it appears that the solvent plays a minor role when it comes to 1D and 2D terpyridine-based assemblies. The correlation between greater vectorial flexibility of the ligand and less control over the final assembly was confirmed. The reaction between a tris(4,2':6',4''-terpyridine) ligand and $[Cu(hfacac)_2]\cdot H_2O$ provided a relatively predictable hexagonal grid. On the other hand, the combination of a conformationally flexible 6-connecting tris(3,2':6',3''-terpyridine) ligand with a metal linker led unexpectedly to a 1D chain. The tris(3,2':6',3''-tpy) and tris(4,2':6',4''-tpy) compounds were chosen to demonstrate the possibility of extending terpyridine ligands beyond the usual 2-4 connections. Furthermore, coordination polymers containing tris(terpyridine) ligands have been studied for 20 years, but studies were only based on the 2,2':6',2''-isomer and without ever knowing the detailed structure.[206-217] The latter materials have very interesting properties, e.g. electrochromism and humidity-responsive ionic conduction, [210, 212-216] and therefore structural investigations are urgently needed to better understand the structure-property relationships. These initial results are the start of a systematic approach towards this class of ligands, in which nature of the central spacer and of the solubilizing chain will have to be modified incrementally.

7 Experimental part

7.1 Materials and methods

7.1.1 Chemicals

3-Acetylpyridine, 4-acetylpyridine, 1,3,5-tribromobenzene and benzene-1,3,5-tricarbaldehyde were purchased from Acros Organics, and $[Cu(hfacac)_2]\cdot H_2O$ from abcr GmbH. $[Zn(hfacac)_2]\cdot 2H_2O$, $Co(NCS)_2$, $[Pd(PPh_3)_4]$, 1-bromo-2-ethylbutane, tris(4-formylphenyl)amine and 2,5-dibromobenzene-1,4-diol were bought from Sigma-Aldrich, and bis(pinacolato)diboron and $[Pd(dppf)Cl_2]$ from Fluorochem. (2-Bromoethyl)benzene and 1-bromo-3-phenylpropane were purchased from Alfa Aesar and Fluka, respectively. All chemicals were used as received.

1,3,5-Tribromo-2,4,6-trimethylbenzene,[241] 4,4'-oxydibenzaldehyde[145] and bis(4-bromophenyl)sulfide[150] were prepared as previously described in literature. 4'-(4-Bromophenyl)-3,2':6',3''-terpyridine and 4'-(4-bromophenyl)-4,2':6',4''-terpyridine were prepared according to the one-pot methods of Hanan[93] as reported by Zhang[227] but using KOH in place of NaOH.

7.1.2 General methods and analysis

Analytical thin-layer chromatography was conducted with pre-coated silica gel 60 F_{254} or with aluminium oxide 60 F_{254}, neutral, aluminium sheets and visualized using ultraviolet light (254 and 366 nm). Neutral aluminium oxide 60 F_{254} (20 x 20 cm; 1.5 mm) sheets were used for the preparative layer chromatography (PLC). Flash column chromatography was performed on a Biotage Selekt system with self-packed silica gel columns (SiliaFlash® P60, 40–63 µm, 230 400 mesh from SiliCycle Inc.) or using Biotage Sfär Silica HC D columns (50g, 20 µm) and monitoring and collecting at 254 and 366 nm.

^1H and $^{13}C\{^1H\}$ NMR spectra were recorded on a Bruker Avance III-500 spectrometer at 298 K. The ^1H and ^{13}C NMR chemical shifts were referenced with respect to the residual solvent peak (δ 2.50 for DMSO-d_5 and δ 39.5 for DMSO-d_6; δ 7.26 for $CHCl_3$ and δ 77.2 for $CDCl_3$; δ 8.03 for $(CD_3)_2NC(O)H$ and δ 163.2 for DMF-d_7). MALDI-TOF mass spectra were recorded on a Shimadzu MALDI 8020 using α-cyano-4-hydroxycinnamic acid (CHCA) or 2,5-dihydroxybenzoic acid (DHB) as the matrix, in some cases without using matrix. Electrospray ionization (ESI) mass spectra were performed using a Shimadzu LCMS-2020 instrument. Samples were introduced as 200–800 µM solutions in MeOH, in some cases with NaCl added. Elemental analyses and high-resolution electrospray (HR-ESI) mass spectra were measured by the analysis service of the University of Basel using a Vario MICRO Cube device or Bruker maXis 4G QTOF instrument. PerkinElmer UATR Two and Shimadzu UV-2600 instruments were used to record FT-infrared (IR) and UV-Vis absorption spectra respectively. Melting points were determined using a Stuart melting point SMP 30 device.

Reactions and procedures under microwave conditions were carried out in a Biotage Initiator 8 reactor. Microwave vials were from Biotage and were selected depending on the required solvent volume. For centrifugation an Eppendorf Centrifuge 5415 R was used with 2, 10 and 50 mL samples.

7.2 Synthesis of the ligands

Some syntheses listed below were carried out several times to obtain sufficient material for the crystallisation experiments and the largest scale in each case is given here. Yields stated are typical for repeated preparations.

7.2.1 Synthesis of the angular bis(terpyridine) ligands

4,4'-Sulfanediyldibenzaldehyde

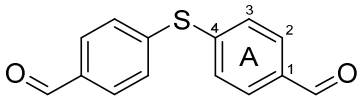

n-BuLi in *n*-hexane (1.6 M, 13.8 mL, 5.88 mmol) was added slowly at -78 °C under an N_2 atmosphere over a period of 15 min to a suspension of bis(4-bromophenyl)sulfide (3.04 g, 8.84 mmol) in dry THF (20 mL). After 2 h, dry DMF (1.71 mL, 22.1 mmol) was added. The resulting white suspension was then stirred for a further 30 min under an N_2 atmosphere and was then allowed to warm up from -78 °C to room temperature. The suspension was neutralized with 3 M HCl (15 mL) and extracted with Et_2O (3 x 20 mL). The organic layers were dried over $MgSO_4$ and the solvents were removed under vacuum. The crude product was washed in refluxing petroleum ether, collected by filtration and then dried *in vacuo*. 4,4'-Sulfanediyldibenzaldehyde was isolated as an off-white solid (1.96 g, 8.09 mmol, 91.5%). ^{1}H NMR (500 MHz, $CDCl_3$): δ/ppm 10.00 (s, 2H, H^{CHO}), 7.84 (d, *J* = 8.4 Hz, 4H, H^{A2}), 7.50 (d, *J* = 8.3 Hz, 4H, H^{A3}). MALDI-TOF-MS (matrix: CHCA) *m/z* 242.29 $[M]^+$ (calc. 242.04).

Bis(4-(3,2':6',3''-terpyridin-4'-yl)phenyl)ether (1)

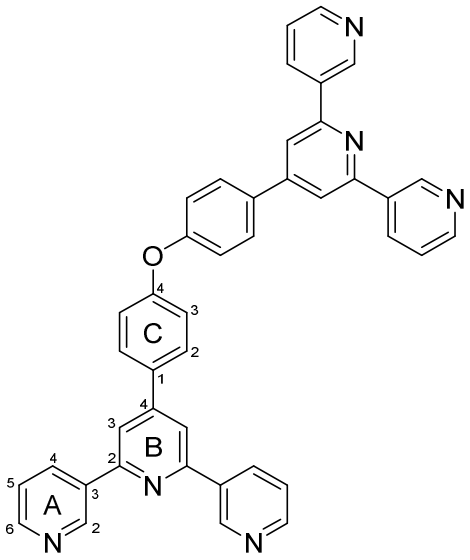

4,4'-Oxydibenzaldehyde (1.00 g, 4.42 mmol) was dissolved in EtOH (35 mL), and 3-acetylpyridine (2.68 g, 2.43 mL, 22.1 mmol) was added to the solution followed by crushed KOH (1.24 g, 22.1 mmol) in one portion. Aqueous NH_3 solution (32%, 32.1 mL) was added slowly and the reaction mixture was stirred at room temperature for 5 days. The yellowish solid that formed was collected by filtration, washed

with water (2 x 20 mL) and EtOH (2 x 10 mL). The crude product was dissolved in the minimum volume of hot $CHCl_3$. EtOH was added to the solution until precipitation just started and the solution then cooled to +5 °C. After 1 day, the white precipitate that formed was collected by filtration, washed with EtOH and Et_2O and dried *in vacuo* overnight. The product was isolated as a white powder **1** (800 mg, 1.26 mmol, 28.6%). M.p. = 291.2-297.7 °C. ^{1}H NMR (500 MHz, $CDCl_3$): δ/ppm 9.39 (d, *J* = 1.7 Hz, 4H, H^{A2}), 8.72 (dd, *J* = 4.9, 1.6 Hz, 4H, H^{A6}), 8.53 (dt, *J* = 8.1, 2.0 Hz, 4H, H^{A4}), 7.96 (s, 4H, H^{B3}), 7.80 (d, *J* = 8.7 Hz, 4H, H^{C2}), 7.48 (dd, *J* = 7.9, 4.8 Hz, 4H, H^{A5}), 7.27 (d, *J* = 8.7 Hz, 4H, H^{C3}). $^{13}C\{^1H\}$ NMR (126 MHz, $CDCl_3$): δ/ppm 158.2 (C^{C4}), 155.7 (C^{B2}), 150.2 (C^{B4}), 148.6 (C^{A2}), 140.5 (C^{A6}), 134.8 (C^{A3}), 134.7 (C^{A4}), 133.8 (C^{C1}), 129.0 (C^{C2}), 123.8 (C^{A5}), 119.9 (C^{C3}), 117.6 (C^{B3}). UV-Vis (CH_2Cl_2, 2.6 × 10^{-5} mol dm^{-3}) λ/nm 266 (ε/dm^3 mol^{-1} cm^{-1} 58,710). MALDI-TOF-MS (No matrix) *m/z* 633.05 $[M+H]^+$ (calc. 633.24). HR-ESI MS *m/z* 633.2390 $[M+H]^+$ (calc. 633.2397), 317.1235 $[M+2H]^{2+}$ (calc. 317.1235). Satisfactory elemental analysis could not be obtained.

Bis(4-(3,2':6',3''-terpyridin-4'-yl)phenyl)sulfide (2)

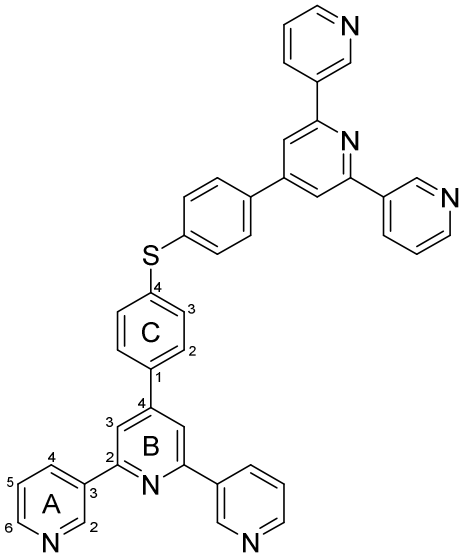

4,4'-Sulfanediyldibenzaldehyde (485 mg, 2.00 mmol) was dissolved in EtOH (60 mL), and 3-acetylpyridine (1.09 g, 0.991 mL, 9.00 mmol) was added to the solution followed by crushed KOH (505 mg, 9.00 mmol) in one portion. Aqueous NH_3 solution (32%, 6.7 mL) was added slowly and the reaction mixture was stirred at room temperature for 3 days. The off-white solid that formed was collected by filtration, washed with water (2 x 20 mL), EtOH (2 x 10 mL) and Et_2O (2 x 20 mL), and then dried *in vacuo* (ca. 72 h). The product was isolated as an off-white powder **2** (290 mg, 0.447 mmol, 22.3%). M.p. = 289.8-291.5 °C. ^{1}H NMR (500 MHz, $CDCl_3$): δ/ppm 9.38 (dd, *J* = 2.3, 0.9 Hz, 4H, H^{A2}), 8.72 (dd, *J* = 4.8, 1.7 Hz, 4H, H^{A6}), 8.52 (ddd, *J* = 7.9, 2.3, 1.7 Hz, 4H, H^{A4}), 7.95 (s, 4H, H^{B3}), 7.75 (d, *J* = 8.4 Hz, 4H, H^{C2}), 7.59 (d, *J* = 8.5 Hz, 4H, H^{C3}), 7.47 (ddd, *J* = 7.9, 4.8, 0.9 Hz, 4H, H^{A5}). $^{13}C\{^1H\}$ NMR (126 MHz, $CDCl_3$): δ/ppm 155.8 (C^{B2}), 150.5 (C^{A6}), 150.1 (C^{B4}), 148.6 (C^{A2}), 137.4 (C^{C1+C4}), 134.7 (C^{A3+A4}), 131.9 (C^{C3}), 128.2 (C^{C2}), 123.8 (C^{A5}), 117.6 (C^{B3}). UV-Vis (DMF, 2.1 × 10^{-5} mol dm^{-3}) λ/nm 316 (ε/dm^3 mol^{-1} cm^{-1} 31,490). MALDI-TOF-MS (matrix: CHCA) *m/z* 649.62 $[M+H]^+$ (calc. 649.22). HR-ESI MS *m/z* 649.2174 $[M+H]^+$ (calc. 649.2169). Satisfactory elemental analysis could not be obtained.

Bis(4-(4,2':6',4''-terpyridin-4'-yl)phenyl)ether (3)

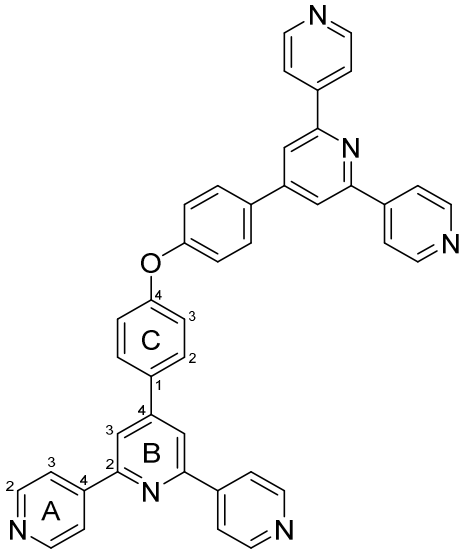

4,4'-Oxydibenzaldehyde (452 mg, 2.00 mmol) was dissolved in EtOH (50 mL), and 4-acetylpyridine (1.09 g, 1.00 mL, 9.00 mmol) was added to the solution followed by crushed KOH (505 mg, 9.00 mmol) in one portion. Aqueous NH_3 solution (32%, 6.7 mL) was added slowly and the reaction mixture was stirred at room temperature for 5 days. The off-white solid that formed was collected by filtration, washed with water (2 x 20 mL), EtOH (2 x 10 mL) and Et_2O (2 x 20 mL), and then dried *in vacuo* (ca. 24 h). The product was isolated as an off-white powder **3** (634 mg, 1.00 mmol, 50.0%). Decomposition > 177 °C. ^{1}H NMR (500 MHz, $CDCl_3$): δ/ppm 8.81 (d, *J* = 6.2 Hz, 8H, H^{A2}), 8.10 (d, *J* = 6.2 Hz, 8H, H^{A3}), 8.05 (s, 4H, H^{B3}), 7.80 (d, *J* = 8.7 Hz, 4H, H^{C2}), 7.28 (d, *J* = 8.7 Hz, 4H, H^{C3}). ^{13}C{^{1}H} NMR (126 MHz, $CDCl_3$): δ/ppm 158.3 (C^{C4}), 155.5 (C^{B2}), 150.6 (C^{A2}), 150.5 (C^{B4}), 146.2 (C^{A4}), 133.6 (C^{C1}), 129.1 (C^{C2}), 121.4 (C^{A3}), 119.9 (C^{C3}), 118.9 (C^{B3}). UV-Vis ($CHCl_3$, 2.2×10^{-5} mol dm^{-3}) λ/nm 270 (ε/dm^3 mol^{-1} cm^{-1} 50,420). MALDI-TOF-MS (matrix: CHCA) *m/z* 633.24 $[M+H]^+$ (calc. 633.24). HR-ESI MS *m/z* 633.2387 $[M+H]^+$ (calc. 633.2397), 317.1232 $[M+2H]^{2+}$ (calc. 317.1235). Satisfactory elemental analysis could not be obtained.

Bis(4-(4,2':6',4''-terpyridin-4'-yl)phenyl)sulfide (4)

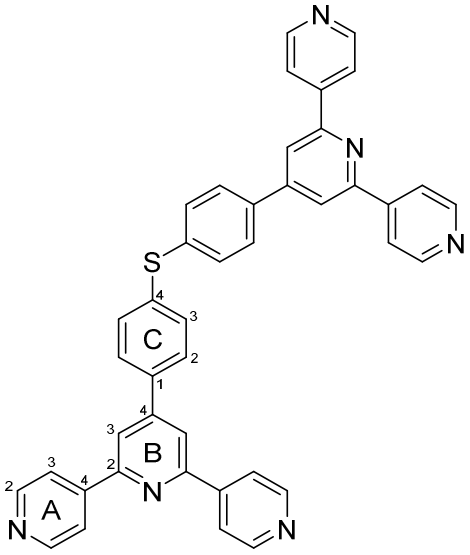

4,4'-Sulfanediyldibenzaldehyde (485 mg, 2.00 mmol) was dissolved in EtOH (60 mL), and 4-acetylpyridine (1.09 g, 1.00 mL, 9.00 mmol) was added to the solution followed by crushed KOH (505 mg, 9.00 mmol) in one portion. Aqueous NH_3 solution (32%, 6.7 mL) was added slowly and the reaction mixture was stirred at room temperature for 1 day. The yellow solid that formed was collected by filtration, washed with water (2 x 20 mL) and EtOH (2 x 10 mL). The crude product was dissolved in the minimum volume of hot DMF and the solution was allowed to cool to room temperature. After 1 day, the yellow precipitated that formed was collected by filtration, washed with CH_2Cl_2 and dried *in vacuo* (ca. 72 h). and the product isolated as a yellow powder **4** (446 mg, 0.687 mmol, 34.4%). M.p. = 239.5-240.5 °C. ^{1}H NMR (500 MHz, DMF-d_7): δ/ppm 8.84 (d, J = 6.2 Hz, 8H, H^{A2}), 8.66 (s, 4H, H^{B3}), 8.45 (d, J = 6.1 Hz, 8H, H^{A3}), 8.31 (d, J = 8.5 Hz, 4H, H^{C2}), 7.69 (d, J = 8.4 Hz, 4H, H^{C3}). ^{13}C{^{1}H} NMR (126 MHz, DMF-d_7): δ/ppm 156.2 (C^{B2}), 151.7 (C^{A2}), 150.7 (C^{B4}), 146.8 (C^{A4}), 137.9 (C^{C4}), 137.6 (C^{C1}), 132.6 (C^{C3}), 129.9 (C^{C2}), 122.4 (C^{A3}), 120.0 (C^{B3}). UV-Vis (DMF, 2.1 × 10^{-5} mol dm^{-3}) λ/nm 312 (ε/dm^3 mol^{-1} cm^{-1} 41,050). MALDI-TOF-MS (matrix: CHCA) *m/z* 649.56 $[M+H]^+$ (calc. 649.22). HR-ESI MS *m/z* 649.2164 $[M+H]^+$ (calc. 649.2169). Satisfactory elemental analysis could not be obtained.

7.2.2 Synthesis of 1,4-bis(phenylalkoxy)-2,5-bis(3,2':6',3''terpyridin-4'-yl)benzene ligands

1,4-Dibromo-2,5-bis(2-phenylethoxy)benzene (5a)

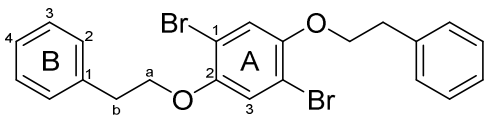

Dry DMF (40 mL) was added to a mixture of anhydrous K_2CO_3 (3.61 g, 26.1 mmol), 2,5-dibromobenzene-1,4-diol (2.00 g, 7.47 mmol) and (2-bromoethyl)benzene (3.66 mL, 26.1 mmol). The solution was stirred and heated to 100 °C under a nitrogen atmosphere for 22 h. The mixture was then cooled to room temperature, poured onto ice water (200 mL) and stirred for 20 min. The resulting suspension was extracted with $CHCl_3$ (3 × 100 mL), dried with $MgSO_4$ and concentrated *in vacuo*. The red-brown solid was recrystallised from a mixture of hot MeOH and $CHCl_3$ (cooled down to room

temperature). The filtrate was reduced to half its original volume, and then cooled to 5 °C to yield a second crop of crystalline product. Off-white crystals were isolated by filtration, washed with MeOH and then dried *in vacuo* for 2 days (2.55 g, 5.36 mmol, 71.7%). M.p. = 126.5-127.0 °C. ^{1}H NMR (500 MHz, DMSO-d_6): δ/ppm 7.34 (overlapping m+s, 6H, H^{B2+A3}), 7.30 (t, *J* = 7.6 Hz, 4H, H^{B3}), 7.21 (t, *J* = 7.2, 2H, H^{B4}), 4.21 (t, *J* = 6.7 Hz, 4H, H^{a}), 3.02 (t, *J* = 6.7 Hz, 4H, H^{b}). ^{13}C{^{1}H} NMR (500 MHz, DMSO-d_6): δ/ppm 149.3 (C^{A2}), 138.1 (C^{B1}), 129.1 (C^{B2}), 128.2 (C^{B3}), 126.3 (C^{B4}), 118.1 (C^{A3}), 110.4 (C^{A1}), 70.2 (C^{a}), 34.9 (C^{b}). UV-Vis (MeCN, 2.0 × 10^{-5} mol dm^{-3}) λ/nm 210 (ε/dm^3 mol^{-1} cm^{-1} 48,300), 232 sh (14,300), 300 (5,760). HR-ESI MS *m/z* 498.9699 [M+Na]$^+$ (calc. 498.9702). Found C 55.09, H 4.01; required for $C_{22}H_{20}Br_2O_2$: C 55.49, H 4.23.

1,4-Dibromo-2,5-bis(3-phenylpropoxy)benzene (6a)

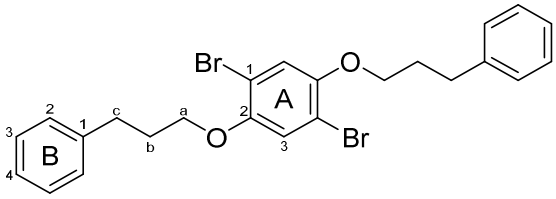

Dry DMF (40 mL) was added to a mixture of anhydrous K_2CO_3 (3.61 g, 26.1 mmol), 2,5-dibromobenzene-1,4-diol (2.00 g, 7.47 mmol) and (3-bromopropyl)benzene (3.97 mL, 26.1 mmol). The yellow-brown suspension was stirred and heated to 100 °C under a nitrogen atmosphere for 22 h. The pale yellow mixture was cooled to room temperature, poured onto ice water (200 mL) and stirred for 20 min. The resulting suspension was extracted with CH_2Cl_2 (3 × 100 mL), dried with $MgSO_4$ and concentrated *in vacuo*. The ochre solid was recrystallised from a mixture of hot MeOH and $CHCl_3$ which was cooled down to room temperature. Colourless crystals were isolated by filtration, washed with MeOH, and then dried *in vacuo* overnight (3.29 g, 6.52 mmol, 87.3%). M.p. = 86.4-87.8 °C. ^{1}H NMR (500 MHz, DMSO-d_6): δ/ppm 7.34 (s, 2H, H^{A3}), 7.29 (t, *J* = 7.4 Hz, 4H, H^{B3}), 7.22 (d, *J* = 6.7 Hz, 4H, H^{B2}), 7.18 (t, *J* = 7.2 Hz, 2H, H^{B4}), 4.00 (t, *J* = 6.2 Hz, 4H, H^{a}), 2.77 (t, *J* = 7.6 Hz, 4H, H^{c}), 1.99 (m, 4H, H^{b}). ^{13}C{^{1}H} NMR (500 MHz, DMSO-d_6): δ/ppm 149.4 (C^{A2}), 141.2 (C^{B1}), 128.4 (C^{B2}/C^{B3}), 128.3 (C^{B2}/C^{B3}), 125.9 (C^{B4}), 118.3 (C^{A3}), 110.6 (C^{A1}), 68.7 (C^{a}), 31.3 (C^{c}), 30.3 (C^{b}). UV-Vis (MeCN, 2.0 × 10^{-5} mol dm^{-3}) λ/nm 210 (ε/dm^3 mol^{-1} cm^{-1} 52,000), 232 sh (13,700), 302 (5,510). HR-ESI MS *m/z* 527.0017 [M+Na]$^+$ (calc. 527.0015). Found C 57.27, H 4.68; required for $C_{24}H_{24}Br_2O_2$: C 57.17, H 4.80.

2,5-Bis(2-phenylethoxy)terephthalaldehyde (5b)

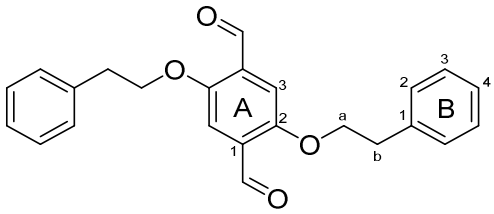

n-BuLi in *n*-hexane (1.6 M, 3.68 mL, 5.88 mmol) was added slowly at 0 °C under N_2 atmosphere over a period of 15 min to a suspension of 1,4-dibromo-2,5-bis(2-phenylethoxy)benzene (800 mg, 1.68 mmol) in dry Et_2O (50 mL). After 4.5 h, dry DMF (0.46 mL, 5.9 mmol) was added. The resulting suspension was then stirred for a further 22 h under an N_2 atmosphere while warming up from 0 °C to room temperature. The light yellow suspension was neutralized with saturated aqueous NH_4Cl and extracted

with $CHCl_3$ (3 x 75 mL). The organic layers were dried over $MgSO_4$ and concentrated *in vacuo*. The crude product was purified by column chromatography using EtOAc in cyclohexane (2-5% gradient) as eluent. Compound **5b** was isolated as a yellow microcrystalline solid (373 mg, 0.996 mmol, 59.3%). M.p. = 168.8-169.2 °C. ^{1}H NMR (500 MHz, DMSO-d_6): δ/ppm 10.25 (s, 2H, H^{CHO}), 7.40 (s, 2H, H^{A3}), 7.34-7.28 (m, 8H, H^{B2+B3}), 7.22 (m, 2H, H^{B4}), 4.36 (t, *J* = 6.5 Hz, 4H, H^a), 3.08 (t, *J* = 6.5 Hz, 4H, H^b). $^{13}C\{^1H\}$ NMR (126 MHz, DMSO-d_6): δ/ppm 188.9 (C^{CHO}), 154.5 (C^{A2}), 138.3 (C^{B1}), 129.0 (C^{A1+B2}), 128.3 (C^{B3}), 126.3 (C^{B4}), 112.2 (C^{A3}), 69.7 (C^a), 34.8 (C^b). UV-Vis ($CHCl_3$, 3.0×10^{-5} mol dm^{-3}) λ/nm 274 (ε/dm^3 mol^{-1} cm^{-1} 15,640), 283 sh (12,940), 398 (6,060). MALDI-TOF-MS (matrix: DHB) *m/z* 374.67 $[M]^+$ (calc. 374.15). Found C 76.01, H 6.06; required for $C_{24}H_{22}O_4$: C 76.99, H 5.92.

2,5-Bis(3-phenylpropoxy)terephthalaldehyde (6b)

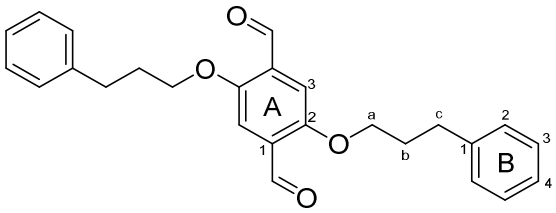

n-BuLi in *n*-hexane (1.6 M, 7.43 mL, 11.9 mmol) was added slowly at 0 °C under N_2 atmosphere over a period of 15 min to a suspension of 1,4-dibromo-2,5-bis(3-phenylpropoxy)benzene (1.50 g, 2.97 mmol). After 2.5 h, dry DMF (0.92 mL, 12 mmol) was added. The resulting solution was then stirred for a further 22 h under an N_2 atmosphere while warming up from 0 °C to room temperature. The light yellow suspension was neutralized with saturated aqueous NH_4Cl and extracted with $CHCl_3$ (3 x 75 mL). The organic layers were dried over $MgSO_4$ and concentrated *in vacuo*. The crude material was purified by column chromatography using 5% EtOAc in cyclohexane as eluent. The solid product was recrystallised from hot EtOAc (cooled to –20 °C). Yellow crystals were isolated by filtration, washed with cold EtOAc and cyclohexane, and dried *in vacuo* for 2 h to afford **6b** (445 mg, 1.11 mmol, 37.2%). M.p. = 112.0-112.8 °C. ^{1}H NMR (500 MHz, DMSO-d_6): δ/ppm 10.34 (s, 2H, H^{CHO}), 7.38 (s, 2H, H^{A3}), 7.30-7.22 (m, 8H, H^{B2+B3}), 7.18 (m, 2H, H^{B4}), 4.14 (t, *J* = 6.2 Hz, 4H, H^a), 2.78 (dd, *J* = 8.5, 6.7 Hz, 4H, H^c), 2.12-2.04 (m, 4H, H^b). $^{13}C\{^1H\}$ NMR (126 MHz, DMSO-d_6): δ/ppm 189.1 (C^{CHO}), 154.5 (C^{A2}), 141.4 (C^{B1}), 128.9 (C^{A1}), 128.3 (C^{B2+B3}), 125.83 (C^{B4}), 111.9 (C^{A3}), 68.3 (C^a), 31.6 (C^c), 30.2 (C^b). UV-Vis ($CHCl_3$, 3.0×10^{-5} mol dm^{-3}) λ/nm 276 (ε/dm^3 mol^{-1} cm^{-1} 16,060), 283 sh (13,280), 401 (6,300). MALDI-TOF-MS (matrix: CHCA) *m/z* 402.67 $[M]^+$ (calc. 402.18). Found C 77.41, H 6.55; required for $C_{26}H_{26}O_4$: C 77.59, H 6.51.

1,4-Bis(2-phenylethoxy)-2,5-bis(3,2':6',3''-terpyridin-4'-yl)benzene (5)

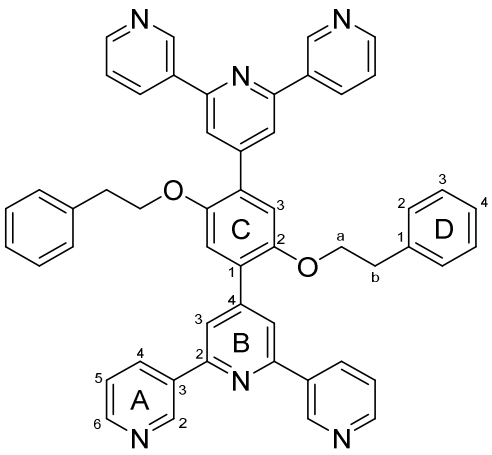

2,5-Bis(2-phenylethoxy)terephthalaldehyde (286 mg, 0.764 mmol) was dissolved in EtOH (20 mL), and 3-acetylpyridine (463 mg, 0.421 mL, 3.82 mmol) was added to the solution followed by crushed KOH (214 mg, 3.82 mmol) in one portion. Aqueous NH_3 solution (32%, 4.78 mL) was added slowly and the reaction mixture was stirred at room temperature for 6 days. The brownish solid that formed was collected by filtration, washed with water (2 x 20 mL), EtOH (2 x 10 mL) and Et_2O (2 x 20 mL), and then dried *in vacuo* overnight (ca. 16 h). The product was isolated as a white powder **5** (206 mg, 0.264 mmol, 34.5%). M.p. = 248.8-249.7 °C. ^{1}H NMR (500 MHz, DMSO-d_6): δ/ppm 9.43 (dd, *J* = 2.3, 0.9 Hz, 4H, H^{A2}), 8.71 (dd, *J* = 4.7, 1.6 Hz, 4H, H^{A6}), 8.58 (ddd, *J* = 8.0, 2.3, 1.7 Hz, 4H, H^{A4}), 8.19 (s, 4H, H^{B3}), 7.60 (ddd, *J* = 8.0, 4.8, 0.9 Hz, 4H, H^{A5}), 7.48 (s, 2H, H^{C3}), 7.16 – 7.11 (m, 4H, H^{D2}), 7.09 – 7.03 (m, 6H, H^{D3+D4}), 4.41 (t, *J* = 6.4 Hz, 4H, H^{a}), 2.99 (t, *J* = 6.4 Hz, 4H, H^{b}). ^{13}C{^{1}H} NMR (126 MHz, DMSO-d_6): δ/ppm 153.9 (C^{B2}), 150.1 (C^{A6}), 149.9 (C^{C2}), 148.2 (C^{A2}), 147.7 (C^{C1}), 138.4 (C^{D1}), 134.4 (C^{A4}), 134.1 (C^{A3}), 128.7 (C^{D2}), 128.4 (C^{B4}), 128.1 (C^{D3}), 126.1 (C^{D4}), 123.9 (C^{A5}), 120.5 (C^{B3}), 115.6 (C^{C3}), 69.6 (C^{a}), 35.0 (C^{b}). UV-Vis ($CHCl_3$, 2.0 × 10^{-5} mol dm^{-3}) λ/nm 280 sh (ε/dm^3 mol^{-1} cm^{-1} 49,380), 315 (23,880). MALDI-TOF-MS (matrix: CHCA) *m/z* 781.24 $[M+H]^+$ (calc. 781.33). HR-ESI MS *m/z* 781.3277 $[M+H]^+$ (calc. 781.3286), 391.1680 $[M+2H]^{2+}$ (calc. 391.1679). Satisfactory elemental analysis could not be obtained.

1,4-Bis(3-phenylpropoxy)-2,5-bis(3,2':6',3''-terpyridin-4'-yl)benzene (6)

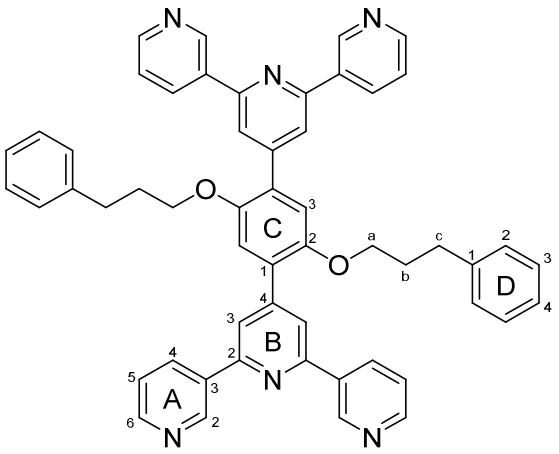

2,5-Bis(3-phenylpropoxy)terephthalaldehyde (300 mg, 0.745 mmol) was dissolved in EtOH (15 mL), 3-acetylpyridine (451 mg, 0.410 mL, 3.73 mmol) was added to the solution followed by crushed KOH (209 mg, 3.73 mmol) in one portion. Aqueous NH_3 solution (32%, 4.66 mL) was added slowly and the reaction mixture was stirred at room temperature for 5 days. The brownish solid that formed was collected by filtration, washed with water (2 x 20 mL), EtOH (2 x 10 mL) and Et_2O (2 x 20 mL), and then dried *in vacuo* (ca. 24 h). The product was isolated as an off-white powder **6** (215 mg, 0.266 mmol, 35.7%). M.p. = 203.4-204.6 °C. ^{1}H NMR (500 MHz, DMSO-d_6): δ/ppm 9.49 (dd, *J* = 2.3, 0.9 Hz, 4H, H^{A2}), 8.70 (dd, *J* = 4.7, 1.7 Hz, 4H, H^{A6}), 8.67 (ddd, *J* = 8.0, 2.3, 1.7 Hz, 4H, H^{A4}), 8.34 (s, 4H, H^{B3}), 7.58 (ddd, *J* = 8.0, 4.8, 0.9 Hz, 4H, H^{A5}), 7.52 (s, 2H, H^{C3}), 7.13 – 7.05 (m, 6H, H^{D3+D4}), 6.91 (m, 4H, H^{D2}), 4.20 (t, *J* = 5.9 Hz, 4H, H^a), 2.61 (m, 4H, H^c), 1.96 (m, 4H, H^b). ^{13}C{^{1}H} NMR (126 MHz, DMSO-d_6): δ/ppm 154.0 (C^{B2}), 150.1 (C^{A6+C2}), 148.1 (C^{A2}), 147.7 (C^{C1}), 141.2 (C^{D1}), 134.4 (C^{A4}), 134.1 (C^{A3}), 128.6 (C^{B4}), 128.2 (C^{D3}), 128.0 (C^{D2}), 125.7 (C^{D4}), 123.9 (C^{A5}), 120.6 (C^{B3}), 115.7 (C^{C3}), 68.3 (C^a), 31.8 (C^c), 30.8 (C^b). UV-Vis ($CHCl_3$, 2.1 × 10^{-5} mol dm^{-3}) λ/nm 280 sh (ε/dm^3 mol^{-1} cm^{-1} 40,850), 316 (19,120). MALDI-TOF-MS (matrix: CHCA) *m/z* 809.31 $[M+H]^+$ (calc. 809.36). HR-ESI MS *m/z* 809.3596 $[M+H]^+$ (calc. 809.3599), 405.1841 $[M+2H]^{2+}$ (calc. 405.1836), 270.4589 $[M+3H]^{3+}$ (calc. 270.4581). Found C 79.52, H 5.49, N 9.98; required for $C_{54}H_{44}N_6O_2$: C 80.17, H 5.48, N 10.39.

7.2.3 Synthesis of 1,4-bis(alkyloxy)-2,5-bis(3,2':6',3''terpyridin-4'-yl)benzene ligands

1,4-Dibromo-2,5-bis(2-ethylbutoxy)benzene (7a)

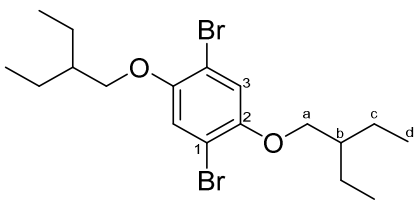

Dry DMF (30 mL) was added to a mixture of anhydrous K_2CO_3 (2.19 g, 15.8 mmol), 2,5-dibromobenzene-1,4-diol (1.50 g, 5.60 mmol) and 1-bromo-2-ethylbutane (2.31 g, 14.0 mmol). The solution was heated (with stirring) to 100 °C under N_2 for 18 h. The mixture was cooled to room

temperature, poured onto ice/water (100 mL) and stirred for 20 min. The resulting suspension was extracted with CH_2Cl_2 (3 × 75 mL) and then the volume was reduced and dried *in vacuo* for 15 h at 45 °C to yield 1,4-dibromo-2,5-bis(2-ethylbutoxy)benzene as a dark brown oil (2.33 g, 5.34 mmol, 95.4%). ^{1}H NMR (500 MHz, $CDCl_3$): δ/ppm 7.08 (s, 2H, H^3), 3.84 (d, *J* = 5.6 Hz, 4H, H^a), 1.77 – 1.63 (m, 2H, H^b), 1.58–1.43 (m, 8H, H^c), 0.94 (t, *J* = 7.5 Hz, 12H, H^d). ^{13}C{^{1}H} NMR (126 MHz, $CDCl_3$): δ/ppm 150.3 (C^2), 118.4 (C^3), 111.2 (C^1), 72.3 (C^a), 41.1 (C^b), 23.5 (C^c), 11.3 (C^d). MALDI-TOF-MS *m/z* 436.04 $[M+H]^+$ (calc. 436.04).

2,5-Bis(2-ethylbutoxy)benzene-1,4-dicarbaldehyde (7b)

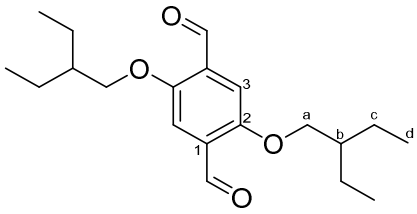

1,4-Dibromo-2,5-bis(2-ethylbutoxy)benzene (1.50 g, 3.44 mmol) was dissolved in dry Et_2O (100 mL) and a solution of *n*-BuLi in *n*-hexane (1.6 M, 6.45 mL, 10.3 mmol) was added slowly at 0 °C under an N_2 atmosphere over a period of 15 min. After 2 h, dry DMF (0.798 mL, 10.3 mmol) was added to the white suspension. The mixture was stirred for 1 day under N_2 while warming from 0 °C to room temperature. The reaction mixture was neutralized with saturated aqueous NH_4Cl solution and extracted with CH_2Cl_2 (150 mL). The organic layers were dried over $MgSO_4$ and concentrated *in vacuo*. The product was obtained as a yellow oil (1.15 g, 3.44 mmol, 100%). ^{1}H NMR (500 MHz, $CDCl_3$): δ/ppm 10.52 (s, 2H, H^{CHO}), 7.44 (s, 2H, H^3), 3.99 (d, *J* = 5.6 Hz, 4H, H^a), 1.77 – 1.68 (m, 2H, H^b), 1.54 – 1.45 (m, 8H, H^c), 0.94 (t, *J* = 7.5 Hz, 12H, H^d). ^{13}C{^{1}H} NMR (126 MHz, $CDCl_3$): δ/ppm 189.5 (C^{CHO}), 155.6 (C^2), 129.5 (C^1), 111.7 (C^3), 71.3 (C^a), 41.1 (C^b), 23.6 (C^c), 11.30 (C^d). MALDI-TOF-MS *m/z* 336.17 $[M+2H]^+$ (calc. 336.23); ESI-MS (MeOH, NaCl) 421.21 $[M+2MeOH+Na]^+$ (calc. 421.26), 389.20 $[M+MeOH+Na]^+$ (base peak, calc. 389.23).

2,5-Bis(3-methylbutoxy)benzene-1,4-dicarbaldehyde (8b)

2,5-Bis(3-methylbutoxy)benzene-1,4-dicarbaldehyde has previously been reported.[192, 193] It was prepared in the same manner as 2,5-bis(2-ethylbutoxy)benzene-1,4-dicarbaldehyde and the ^{1}H and ^{13}C{^{1}H) NMR data were in accord with published data.[192, 193]

1,4-bis(2-ethylbutoxy)-2,5-bis(3,2':6',3''-terpyridin-4'-yl)benzene (7)

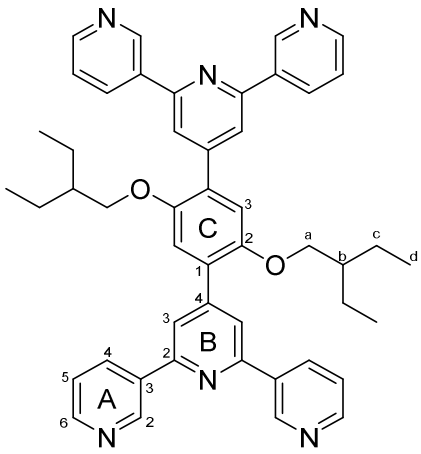

2,5-Bis(2-ethylbutoxy)benzene-1,4-dicarbaldehyde (579 mg, 1.70 mmol) was dissolved in EtOH (50 mL). 3-Acetylpyridine (927 mg, 0.842 mL, 7.65 mmol) was added followed by crushed KOH (429 mg, 7.65 mmol) in one portion. Aqueous NH_3 solution (30%, 14.3 mL) was slowly added and the reaction mixture was stirred at room temperature for 3 days. The solid that formed was collected by decantation, washed with water (3 × 10 mL) and ethanol (3 × 10 mL) and then dried *in vacuo* overnight. The product was isolated as a light-yellow powder (317 mg, 0.428mmol, 25.2%). M.p. = 209–212 °C. ^{1}H NMR (500 MHz, $CDCl_3$): δ/ppm 9.39 (dd, *J* = 2.3, 0.9 Hz, 4H, H^{A2}), 8.72 (dd, *J* = 4.7, 1.7 Hz, 4H, H^{A6}), 8.54 (m, 4H, H^{A4}), 8.02 (s, 4H, H^{B3}), 7.48 (m, 4H, H^{A5}), 7.17 (s, 2H, H^{C3}), 3.95 (d, *J* = 5.5 Hz, 4H, H^{a}), 1.65–1.58 (m, 2H, H^{b}), 1.42–1.32 (m, 8H, H^{c}), 0.82 (t, *J* = 7.5 Hz, 12H, H^{d}). $^{13}C\{^1H\}$ NMR (500 MHz, $CDCl_3$): δ/ppm 154.8 (C^{B2}), 150.8 (C^{C2}), 150.4 (C^{A6}), 148.5 (C^{A2}), 148.2 (C^{C1}), 134.8 (C^{A3}), 134.6 (C^{A4}), 129.5 (C^{B4}), 123.8 (C^{A5}), 120.4 (C^{B3}), 115.2 (C^{C3}), 71.7 (C^{a}), 41.3 (C^{b}), 23.6 (C^{c}), 11.3 (C^{d}). UV-Vis ($CHCl_3$, 1.2×10^{-5} mol dm^{-3}) λ/nm 244 (ε/dm^3 mol^{-1} cm^{-1} 52,000) 278 sh (42,300), 318 (18,100), 354 (9,800). MALDI-TOF-MS *m/z* 741.34 $[M+H]^+$ (calc. 741.39). Found C 77.25, H 6.56, N 11.03; required for $C_{48}H_{48}N_6O_2$ C 77.81, H 6.53, N 11.34.

1,4-bis(3-methylbutoxy)-2,5-bis(3,2':6',3''-terpyridin-4'-yl)benzene (8)

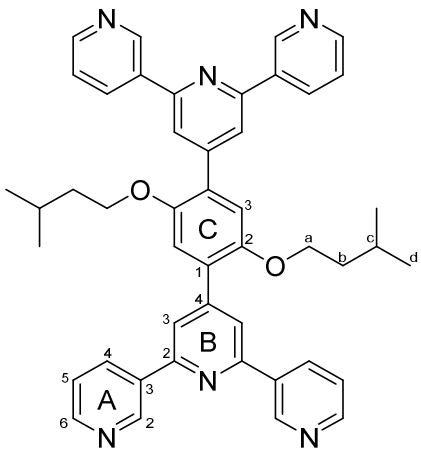

2,5-Bis(3-methylbutoxy) benzene-1,4-dicarbaldehyde (509 mg, 1.66 mmol) was dissolved in EtOH (30 mL) and then 3-acetylpyridine (905 mg, 0.823 mL, 7.47 mmol) was added. Crushed KOH (419 mg, 7.47 mmol) was then added in one portion. Aqueous NH_3 solution (30%, 12.8 mL) was slowly added

and the reaction mixture was stirred at room temperature for 1 day. The solid that formed was collected by filtration, washed with water (3 × 10 mL) and ethanol (3 × 10 mL) and then dried *in vacuo* for 3 days. The product was isolated as a slightly yellowish powder (207 mg, 0.290 mmol, 17.5%). M.p. = 220–221 °C. ^{1}H NMR (500 MHz, $CDCl_3$): δ/ppm 9.38 (dd, J = 2.3, 0.9 Hz, 4H, H^{A2}), 8.72 (dd, J = 4.7, 1.7 Hz, 4H, H^{A6}), 8.53 (dt, *J* = 8.0, 2.0 Hz, 4H, H^{A4}), 8.03 (s, 4H, H^{B3}), 7.48 (ddd, J = 8.0, 4.8, 0.9 Hz, 4H, H^{A5}), 7.17 (s, 2H, H^{C3}), 4.09 (t, *J* = 6.4 Hz, 4H, H^{a}), 1.79–1.71 (m, 2H, H^{c}), 1.66 (m, 4H, H^{b}), 0.86 (d, *J* = 6.6 Hz, 12H, H^{d}). ^{13}C{^{1}H} NMR (500 MHz, $CDCl_3$): δ/ppm 154. (C^{B2}), 150.71 (C^{C2}), 150.4 (C^{A6}), 148.5 (C^{A2}), 148.1 (C^{C1}), 134.9 (C^{A3}), 134.6 (C^{A4}), 129.4 (C^{B4}), 123.8 (C^{A5}), 120.4 (C^{B3}), 115.3 (C^{C3}), 68.1 (C^{a}), 38.2 (C^{b}), 25.2 (C^{c}), 22.6 (C^{d}). UV-Vis ($CHCl_3$, 1.0×10^{-5} mol dm^{-3}) λ/nm 244 (ε / dm^3 mol^{-1} cm^{-1} 44,600) 279 sh (36,200), 318 (16,500), 354 (9,800). MALDI-TOF-MS *m/z* 713.41 $[M+H]^+$ (calc. 713.36). HR-ESI MS *m/z* 713.3587 $[M+H]^+$ (calc. 713.3599), 357.1836 $[M+2H]^{2+}$ (calc. 357.1836). Satisfactory elemental analysis could not be obtained.

7.2.4 Synthesis of star tris(terpyridine) ligands

1,3,5-Tris(4,2':6',4''-terpyridin-4'-yl)benzene (9)

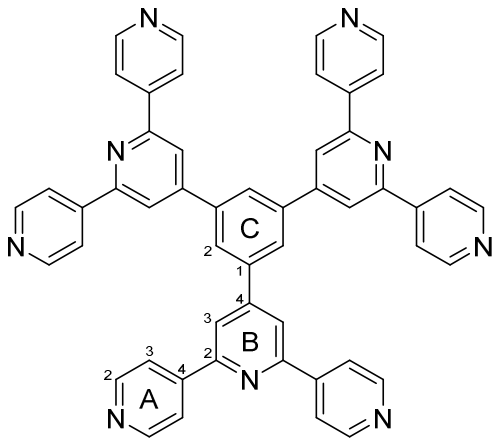

Benzene-1,3,5-tricarbaldehyde (300 mg, 1.81 mmol) was dissolved in 25 mL EtOH, then 4-acetylpyridine (1.51 mL, 13.6 mmol) was added to the solution followed by crushed KOH (762 mg, 13.6 mmol) added in one portion. Aqueous NH_3 solution (32%, 17 mL) was slowly added and the reaction mixture stirred at room temperature for 3 days. The solid that formed was collected by centrifugation, washed with water (3 x 50 mL), ethanol (2 x 50 mL) and diethyl ether (2 x 50 mL), and then dried *in vacuo* overnight. The product was recrystallised from 40 mL hot DMF (cooled down to 5 °C). Pale yellow crystals were isolated by filtration, washed with ethanol and then dried *in vacuo* for 24 hours. **9**·1.5DMF (341 mg, 0.390 mmol, 21.5%). M.p. > 390 °C. ^{1}H NMR (500 MHz, DMSO-d_6): δ/ppm 8.81 (m, 12H, H^{A2}), 8.80 (s, 3H, H^{C2}), 8.77 (s, 6H, H^{B3}), 8.41 (d, *J* = 6.16 Hz, 12H, H^{A3}). ^{13}C{^{1}H} NMR (126 MHz, DMSO-d_6): δ/ppm 154.5 (C^{B2}), 150.4 (C^{A2}), 150.1 (C^{B4}), 145.4 (C^{A4}), 139.3 (C^{C1}), 128.1 (C^{C2}), 121.4 (C^{A3}), 120.0 (C^{B3}). UV-Vis (DMF, 1.0×10^{-5} mol dm^{-3}) λ/nm 306 (ε/dm^3 mol^{-1} cm^{-1} 30,600). MALDI-TOF-MS *m/z* 772.03 $[M+H]^+$ (calc. 772.29). Found C 75.92, H 4.85, N 16.56; required for $C_{51}H_{33}N_9$·1.5DMF: C 75.62, H 4.97, N 16.68.

1,3,5-Tris(3,2':6',3''-terpyridin-4'-yl)benzene (10)

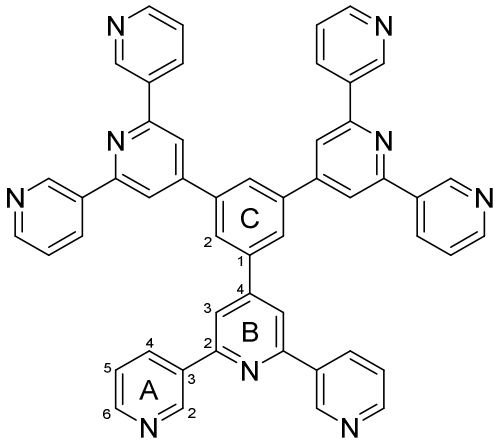

Benzene-1,3,5-tricarbaldehyde (300 mg, 1.81 mmol) was dissolved in 25 mL EtOH, then 3-acetylpyridine (1.49 mL, 13.6 mmol) was added to the solution followed crushed KOH (762 mg, 13.6 mmol) added in one portion. Aqueous NH_3 solution (32%, 17 mL) was slowly added and the reaction mixture stirred at room temperature for 3 days. The solid that formed was collected by centrifugation, washed with water (3 x 50 mL), ethanol (3 x 30 mL) and then dried *in vacuo*. The product was dissolved in the minimum amount of $CHCl_3$, then 100 mL Et_2O were added and the mixture was cooled down to -20 °C. After one day a colourless precipitate was isolated by cold filtration, washed with 5 mL Et_2O and then dried *in vacuo* for 24 hours (172 mg, 0.223 mmol, 12.3%). M.p. > 390 °C. ^{1}H NMR (500 MHz, DMSO-d_6): δ/ppm 9.61 (dd, *J* = 2.3, 0.9 H, 6H, H^{A2}), 8.79 (s, 3H, H^{C2}), 8.77 (ddd, *J* = 8.0, 2.4, 1.7 H, 6H, H^{A4}), 8.72 (dd, J = 4.7, 1.7 Hz, 6H, H^{A6}), 8.68 (s, 6H, H^{B3}), 7.62 (ddd, *J* = 8.0, 4.7, 0.9 Hz, 6H, H^{A5}). $^{13}C\{^1H\}$ NMR (126 MHz, DMSO-d_6): δ/ppm 154.8 (C^{B2}), 150.2 (C^{A6}), 149.6 (C^{B4}), 148.5 (C^{A2}), 139.4 (C^{C1}), 134.6 (C^{A4}), 134.0 (C^{A3}), 127.8 (C^{C2}), 123.8 (C^{A5}), 118.5 (C^{B3}). UV-Vis (DMF, 1.0 × 10^{-5} mol dm^{-3}) λ/nm 312 (ε/dm^3 mol^{-1} cm^{-1} 25,700). MALDI-TOF-MS *m/z* 772.33 $[M+H]^+$ (calc. 772.29). Found C 79.02, H 4.31, N 16.58; required for $C_{51}H_{33}N_9$: C 79.36, H 4.31, N 16.33.

4'-(4-(4,4,5,5-Tetramethyl-1,3,2-dioxaborolan-2-yl)phenyl)-4,2':6',4''-terpyridine (11a)

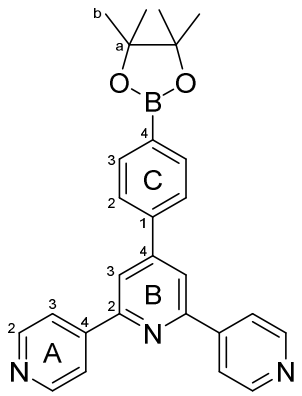

A 20 mL microwave vial was charged with $[Pd(dppf)Cl_2]$ (69.6 mg, 85.2 µmol), KOAc (836 mg, 8.52 mmol) and bis(pinacolato)diboron (B_2pin_2, 762 mg, 2.97 mmol) and flushed with nitrogen. Degassed DMF (14 mL) and 4'-(4-bromophenyl)-4,2':6',4''-terpyridine (1099 mg, 2.83 mmol) were then added. The mixture was stirred and heated in the microwave at 120 °C for 5.5 h under nitrogen.

Toluene (100 mL) was added to the product and the toluene-DMF mixture washed with water (3 x 100 mL). The toluene layer was dried over $MgSO_4$ and filtered. The solvent was removed from the filtrate by rotary evaporation to give a pale yellow solid. The residue was dissolved in the minimum amount of hot $CHCl_3$/hexane (1:1) and then precipitated at –20 °C to give a colourless solid. The product was isolated by filtration, washed with EtOH and hexane and then dried *in vacuo*. The filtrate was dried and the yellow residue purified by column chromatography (eluent: 30 % acetone - 70 % cyclohexane) to yield a second crop of product (661 mg, 1.52 mmol, 53.7 %). M.p. = 229.8-231.5 °C. ^{1}H NMR (500 MHz, $CDCl_3$): δ/ppm 8.80 (d, *J* = 6.1 Hz, 4H, H^{A2}), 8.09 (d, *J* = 6.2 Hz, 4H, H^{A3}), 8.06 (s, 2H, H^{B3}), 8.00 (d, *J* = 8.1 Hz, 2H, H^{C3}), 7.75 (d, *J* = 8.2 Hz, 2H, H^{C2}), 1.39 (s, 12 H, H^{b}). $^{13}C\{^1H\}$ NMR (126 MHz, $CDCl_3$): δ/ppm 155.5 (C^{B2}), 151.2 (C^{B4}), 150.7 (C^{A2}), 146.2 (C^{A4}), 140.6 (C^{C1}), 135.9 (C^{C3}), 130.5 (C^{C4}), 126.6 (C^{C2}), 121.4 (C^{A3}), 119.2 (C^{B3}), 84.3 (C^{a}), 25.1 (C^{b}). UV-Vis ($CHCl_3$, 2.6 × 10^{-5} mol dm^{-3}) λ/nm 264 (ε/dm^3 mol^{-1} cm^{-1} 45,466). MALDI-TOF-MS *m/z* 436.19 $[M+H]^+$ (calc. 436.22). Found C 73.68, H 6.08, N 9.83; required for $C_{27}H_{26}N_3O_2B$: C 74.49, H 6.02, N 9.65.

4'-(4-(4,4,5,5-Tetramethyl-1,3,2-dioxaborolan-2-yl)phenyl)-3,2':6',3''-terpyridine (12a)

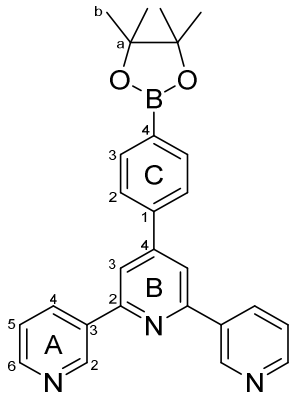

A 20 mL microwave vial was charged with $[Pd(dppf)Cl_2]$ (69.8 mg, 85.5 µmol), KOAc (839 mg, 8.55 mmol) and B_2pin_2 (765 mg, 2.98 mmol) and flushed with nitrogen. Degassed DMF (14 mL) and 4'-(4-bromophenyl)-3,2':6',3''-terpyridine (1103 mg, 2.98 mmol') were then added. The mixture was stirred and heated in the microwave at 120 °C for 5.5 h under nitrogen. $CHCl_3$ (100 mL) was added to the product and the $CHCl_3$-DMF mixture washed with water (3 x 100 mL). The $CHCl_3$ layer was dried over $MgSO_4$ and filtered. The solvent was removed by rotary evaporation to give a brown residue. Purification by column chromatography (eluent: 80 % EtOAc - 20 % cyclohexane) gave the desired product (516 g, 1.19 mmol, 41.7 %) as a colourless solid. M.p. = 187.0-187.2 °C. ^{1}H NMR (500 MHz, $CDCl_3$): δ/ppm 9.39 (dd, *J* = 2.3, 0.9 Hz, 2H, H^{A2}), 8.71 (dd, *J* = 4.8, 1.6 Hz, 2H, H^{A6}), 8.51 (ddd, *J* = 7.9, 2.3, 1.7 Hz, 2H, H^{A4}), 7.99 (d, *J* = 8.2 Hz, 2H, H^{C3}), 7.97 (s, 2H, H^{B3}), 7.76 (d, *J* = 8.1 Hz, 2H, H^{C2}), 7.47 (ddd, *J* = 7.9, 4.8, 0.9 Hz, 2H, H^{A5}), 1.39 (s, 12 H, H^{b}). $^{13}C\{^1H\}$ NMR (126 MHz, $CDCl_3$): δ/ppm 155.6 (C^{B2}), 150.9 (C^{B4}), 150.4 (C^{A6}), 148.7 (C^{A2}), 140.9 (C^{C1}), 135.8 (C^{C3}), 134.8 (C^{A3}), 134.7 (C^{A4}), 130.2 (C^{C4}), 126.6 (C^{C2}), 123.8 (C^{A5}), 118.0 (C^{B3}), 84.3 (C^{a}), 25.1 (C^{b}). UV-Vis ($CHCl_3$, 2.6 × 10^{-5} mol dm^{-3}) λ/nm 263 (ε/dm^3 mol^{-1} cm^{-1} 41,712). MALDI-TOF-MS *m/z* 436.16 $[M+H]^+$ (calc. 436.22). Found C 74.08, H 5.88, N 9.52; required for $C_{27}H_{26}N_3O_2B$: C 74.49, H 6.02, N 9.65.

1,3,5-Tris[4-(4'-4,2':6',4''-terpyridinyl)phenyl]benzene (11)

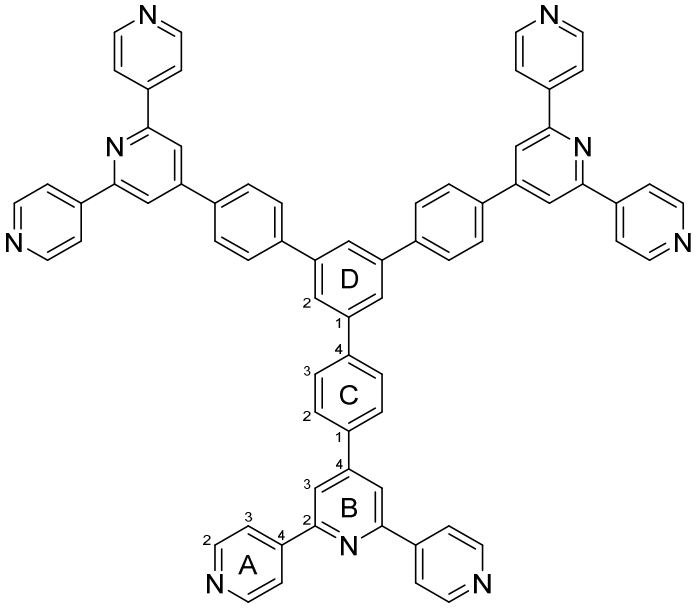

In a Schlenk tube, a mixture of 4'-(4-(4,4,5,5-tetramethyl-1,3,2-dioxaborolan-2-yl)phenyl)-4,2':6',4''-terpyridine (634 mg, 1.46 mmol), 1,3,5-tribromobenzene (115 mg, 0.364 mmol), $Pd(PPh_3)_4$ (42 mg 0.036 mmol), 0.2 M aqueous Na_2CO_3 (10.9 mL, 2.18 mmol) and degassed THF (53 mL) was refluxed for 12 h under nitrogen. The off-white precipitate was isolated by filtration, washed with H_2O, THF and Et_2O. The white solid was dried under vacuum at 80 °C to constant weight (137 mg, 0.137 mmol, 37.6 %). M.p. > 390 °C. ^{1}H NMR (500 MHz, DMSO-d_6 + TFA-*d*): δ/ppm 9.15 (d, *J* = 6.1 Hz, 12H, H^{A2}), 9.11 (d, *J* = 6.2 Hz, 12H, H^{A3}), 8.98 (s, 6H, H^{B3}), 8.35 (d, *J* = 7.9 Hz, 6H, H^{C2}), 8.17 (m, 9H, H^{C3+D2}). ^{13}C{^{1}H} NMR (126 MHz, DMSO-d_6 + TFA-*d*): δ/ppm 154.3 (C^{A4}), 152.6 (C^{B2}), 151.8 (C^{B4}), 143.1 (C^{A2}), 142.7 (C^{C4}), 141.9 (C^{D1}), 136.1 (C^{C1}), 129.1 (C^{C2}), 128.8 (C^{C3}), 126.1 (C^{D2}), 125.2 (C^{A3}), 123.3 (C^{B3}). UV-Vis (Benzonitrile, 8.6×10^{-6} mol dm^{-3}) λ/nm 307 (ε/dm^3 mol^{-1} cm^{-1} 88,183). MALDI-TOF-MS *m/z* 1000.30 $[M+H]^+$ (calc. 1000.39). HR-ESI MS *m/z* 1000.3860 $[M+H]^+$ (calc. 1000.3871).

1,3,5-Tris[4-(4'-3,2':6',3''-terpyridinyl)phenyl]benzene (12)

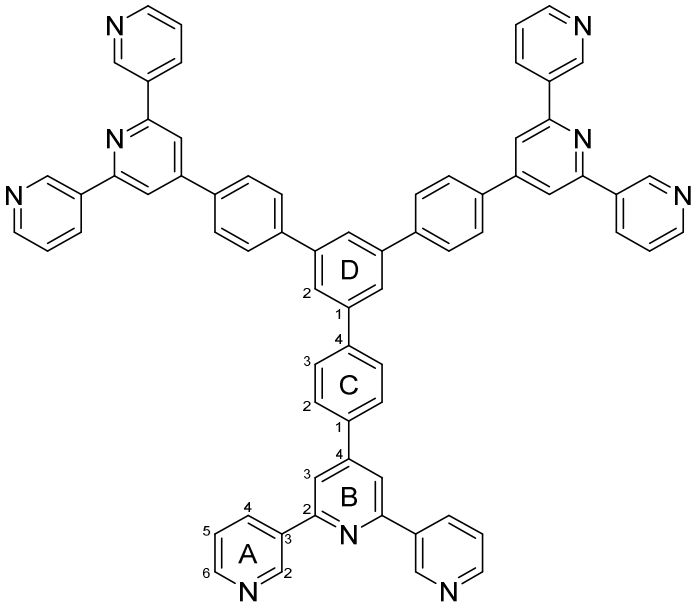

In a Schlenk tube, a mixture of 4'-(4-(4,4,5,5-tetramethyl-1,3,2-dioxaborolan-2-yl)phenyl)-3,2':6',3''-terpyridine (675 mg, 1.55 mmol), 1,3,5-tribromobenzene (122 mg, 0.388 mmol), $Pd(PPh_3)_4$ (45 mg 0.039 mmol), 0.2 M aqueous Na_2CO_3 (11.6 mL, 2.33 mmol) and degassed THF (56 mL) was refluxed for 12 h under nitrogen. The off-white precipitate was isolated by filtration, washed with H_2O, THF and Et_2O. The off-white solid was dried under vacuum at 80 °C to constant weight (313 mg, 0.313 mmol, 80.7 %). M.p. = over 390 °C. ^{1}H NMR (500 MHz, DMF-d_7): δ/ppm 9.68 (dd, *J* = 2.4, 0.9 Hz, 6H, H^{A2}), 8.86 (ddd, *J* = 8.1, 2.4, 1.7 Hz, 6H, H^{A4}), 8.77 (dd, *J* = 4.7, 1.6 Hz, 6H, H^{A6}), 8.62 (s, 6H, H^{B3}), 8.43 (d, *J* = 8.5 Hz, 6H, H^{C2}), 8.34 (s, 3H, H^{D2}), 8.31 (d, *J* = 8.5 Hz, 6H, H^{C3}), 7.66 (ddd, *J* = 7.9, 4.7, 0.9 Hz, 6H, H^{A5}). $^{13}C\{^1H\}$ NMR (126 MHz, DMF-d_7): δ/ppm 155.6 (C^{B2}), 150.7 (C^{A6}), 150.3 (C^{B4}), 149.0 (C^{A2}), 141.9 (C^{C4+D1}), 137.4 (C^{C1}), 134.8 (C^{A3+A4}), 128.5 (C^{C2}), 128.5 (C^{C3}), 125.5 (C^{D2}), 124.1 (C^{A5}), 117.9 (C^{B3}). UV-Vis (DMF, 8.0×10^{-6} mol dm^{-3}) λ/nm 305 (ε/dm^3 mol^{-1} cm^{-1} 108,675). MALDI-TOF-MS *m/z* 1000.41 $[M+H]^+$ (calc. 1000.39). HR-ESI MS *m/z* 1000.3859 $[M+H]^+$ (calc. 1000.3871).

1,3,5-Trimethyl-2,4,6-tris[4-(4'-3,2':6',3''-terpyridinyl)phenyl]benzene (13)

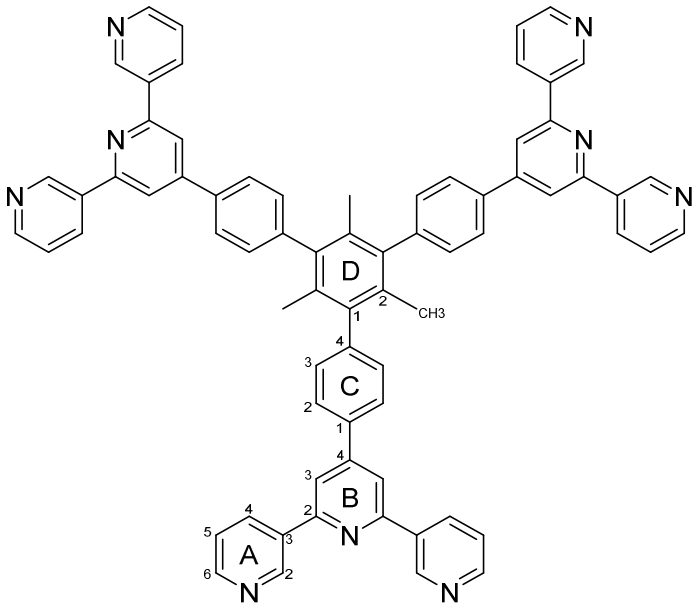

In a Schlenk tube, a mixture of 4'-(4-(4,4,5,5-tetramethyl-1,3,2-dioxaborolan-2-yl)phenyl)-3,2':6',3''-terpyridine (200 mg, 0.459 mmol), 1,3,5-tribromo-2,4,6-trimethylbenzene (36.4 mg, 0.102 mmol), Na_2CO_3 (162 mg, 1.53 mmol), and a solvent mixture of water (8 mL) and toluene (8 mL) were added. The system was freeze-pump-thawed (3 times), back filled with nitrogen; and then [Pd(dppf)Cl_2] (14.9 mg, 0.0204 mmol) was added. The resultant suspension was refluxed for 1 hour under nitrogen. The aqueous layer was extracted with $CHCl_3$ (3 x 20 mL). The combined organic phase was dried ($MgSO_4$) and concentrated *in vacuo* to give a brown residue. An initial purification was performed by a single PLC (neutral Alox, eluent: $CHCl_3$); then the mixture was divided into 4 portions and each was separately purified by PLC under the same conditions. A colourless solid was isolated (34.9 mg, 0.033 mmol, 32.8 %). M.p. > 390 °C. ^{1}H NMR (500 MHz, DMF-d_7): δ/ppm 9.66 (dd, *J* = 2.3, 0.9 Hz, 6H, H^{A2}), 8.84 (ddd, *J* = 8.0, 2.3, 1.6 Hz, 6H, H^{A4}), 8.75 (dd, *J* = 4.7, 1.7 Hz, 6H, H^{A6}), 8.61 (s, 6H, H^{B3}), 8.41 (d, *J* = 8.5 Hz, 6H, H^{C2}), 7.64 (ddd, *J* = 8.0, 4.7, 0.9 Hz, 6H, H^{A5}), 7.57 (d, *J* = 8.5 Hz, 6H, H^{C3}), 1.93 (s, 9H, H^{CH3}). ^{13}C{^{1}H} NMR (126 MHz, DMF-d_7): δ/ppm 155.6 (C^{B2}), 150.7 (C^{A6}), 150.4 (C^{B4}), 148.9 (C^{A2}), 143.6 (C^{C4}), 139.8 (C^{D1}), 136.3 (C^{C1}), 134.8 (C^{A3+A4}), 132.9 (C^{D2}), 130.6 (C^{C3}), 128.3 (C^{C2}), 124.1 (C^{A5}), 117.8 (C^{B3}), 19.6 (C^{CH3}). UV-Vis ($CHCl_3$, 8.0×10^{-6} mol dm^{-3}) λ/nm 272 (ε/dm^3 mol^{-1} cm^{-1} 121,400). MALDI-TOF-MS *m/z* 1042.48 $[M+H]^+$ (calc. 1042.43). HR-ESI MS *m/z* 1042.4313 $[M+H]^+$ (calc. 1042.4334), 521.7207 $[M+2H]^{2+}$ (calc. 521.7206).

Tris(4-(4,2':6',4''-terpyridin-4'-yl)phenyl)amine (14)

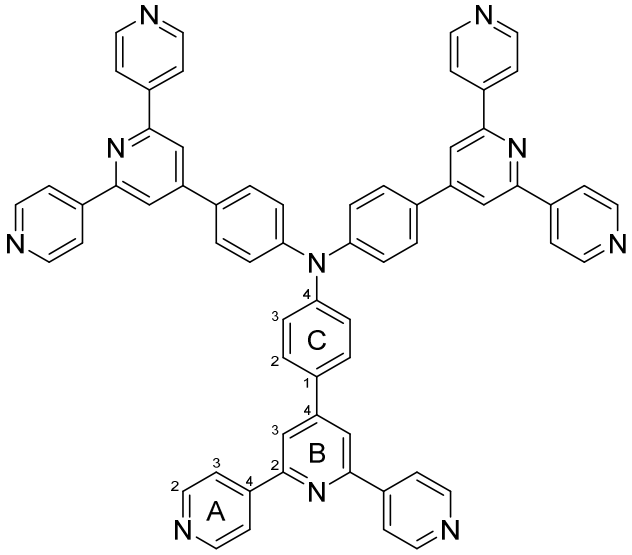

Tris(4-formylphenyl)amine (400 mg, 1.18 mmol) was dissolved in 40 mL THF, then 4-acetylpyridine (1.05 mL, 9.44 mmol) was added to the solution followed by crushed KOH (993 mg, 17.7 mmol) added in one portion. NH_3 solution (32%, 60 mL) was slowly added and the reaction mixture was stirred at room temperature for 15 days. A yellow precipitate was isolated by filtration, washed with EtOH (3 x 50 mL) and Et_2O (2 x 50 mL), and then dried *in vacuo* overnight (371 mg, 0.396 mmol, 33.5%). Decomposition > 185 °C. ^{1}H NMR (500 MHz, DMSO-d_6): δ/ppm 8.79 (d, *J* = 6.1 Hz, 12H, H^{A2}), 8.51 (s, 6H, H^{B3}), 8.35 (d, *J* = 6.2 Hz, 12H, H^{A3}), 8.18 (d, *J* = 8.8 Hz, 6H, H^{C2}), 7.36 (d, *J* = 8.8 Hz, 6H, H^{C3}). ^{1}H NMR (500 MHz, $CDCl_3$): δ/ppm 8.82 (d, *J* = 6.2 Hz, 12H, H^{A2}), 8.10 (d, *J* = 6.2 Hz, 12H, H^{A3}), 8.06 (s, 6H, H^{B3}), 7.76 (d, *J* = 8.6 Hz, 6H, H^{C2}), 7.41 (d, *J* = 8.6 Hz, 6H, H^{C3}). ^{13}C{^{1}H} NMR (126 MHz, $CDCl_3$): δ/ppm 155.6 (C^{B2}), 150.7 (C^{A2}), 150.3 (C^{B4}), 148.3 (C^{C4}), 146.2 (C^{A4}), 133.2 (C^{C1}), 128.6 (C^{C2}), 125.1 (C^{C3}), 121.4 (C^{A3}), 118.6 (C^{B3}). UV-Vis ($CHCl_3$, 8.0 × 10^{-6} mol dm^{-3}) λ/nm 295 sh (ε/dm^3 mol^{-1} cm^{-1} 26,270), 377 (34,440). MALDI-TOF-MS *m/z* 939.31 $[M+H]^+$ (calc. 939.37). HR-ESI MS *m/z* 939.3662 $[M+H]^+$ (calc. 939.3667). Satisfactory elemental analysis could not be obtained.

7.3 Crystal growth: coordination polymers

7.3.1 (4,4)-nets with [M(hfacac)$_2$] (M = Cu, Zn)

$[Cu_2(hfacac)_4(5)]_n \cdot 3.6n(1,2\text{-}Cl_2C_6H_4) \cdot 2nCHCl_3$

A 1,2-dichlorobenzene (8 mL) solution of $[Cu(hfacac)_2]\cdot H_2O$ (12 mg, 0.024 mmol) was layered over a $CHCl_3$ solution (5 mL) of **5** (7.8 mg, 0.010 mmol) in a crystallisation tube (i.d. = 13.6 mm, vol. = 24 mL) sealed with a septum. Light green plate-like crystals visible to the eye were first obtained after 17 days, and a single-crystal was selected for X-ray diffraction. The remaining crystals were analysed by powder X-ray diffraction (PXRD) and FT-IR spectroscopy.

$[Zn_2(hfacac)_4(5)]_n \cdot n MeC_6H_5 \cdot 1.8n CHCl_3$

A toluene (8 mL) solution of $[Zn(hfacac)_2]\cdot 2H_2O$ (13 mg, 0.025 mmol) was layered over a $CHCl_3$ solution (5 mL) of **5** (7.8 mg, 0.010 mmol) in a crystallisation tube (i.d. = 13.6 mm, vol. = 24 mL) sealed with a septum. Colourless block-like crystals visible to the eye were first obtained after 1 month, and a single-crystal was selected for X-ray diffraction. The remaining crystals were analysed by PXRD. FT-IR spectroscopic data could not be obtained.

$[Cu_2(hfacac)_4(6)]_n \cdot n MeC_6H_5 \cdot 2n H_2O$

A toluene (8 mL) solution of $[Cu(hfacac)_2]\cdot H_2O$ (12 mg, 0.024 mmol) was layered over a $CHCl_3$ solution (5 mL) of **6** (8.1 mg, 0.010 mmol) in a crystallisation tube (i.d. = 13.6 mm, vol. = 24 mL) sealed with a septum. Light green block-like crystals visible to the eye were first obtained after 1 month, and a single-crystal was selected for X-ray diffraction. The remaining crystals were analysed by PXRD and FT-IR spectroscopy.

$[Cu_2(hfacac)_4(6)]_n \cdot 2.8n C_6H_5Cl$

A chlorobenzene (8 mL) solution of $[Cu(hfacac)_2]\cdot H_2O$ (12 mg, 0.024 mmol) was layered over a $CHCl_3$ solution (5 mL) of **6** (8.1 mg, 0.010 mmol) in a crystallisation tube (i.d. = 13.6 mm, vol. = 24 mL) sealed with a septum. Light green block-like crystals visible to the eye were first obtained after 1 month, and a single-crystal was selected for X-ray diffraction. The remaining crystals were analysed by PXRD and FT-IR spectroscopy.

$[Cu_2(hfacac)_4(6)]_n \cdot 2n(1,2\text{-}Cl_2C_6H_4) \cdot 0.4n CHCl_3 \cdot 0.5n H_2O$

A 1,2-dichlorobenzene (8 mL) solution of $[Cu(hfacac)_2]\cdot H_2O$ (12 mg, 0.024 mmol) was layered over a $CHCl_3$ solution (5 mL) of **6** (8.1 mg, 0.010 mmol) in a crystallisation tube (i.d. = 13.6 mm, vol. = 24 mL) sealed with a septum. Light green plate-like crystals visible to the eye were first obtained after 1 month, and a single-crystal was selected for X-ray diffraction. The remaining crystals were analysed by PXRD and FT-IR spectroscopy.

7.3.2 3D-nets with $Co(NCS)_2$ 4-connecting nodes

$[Co(NCS)_2(7)]_n \cdot n MeOH \cdot 3n CHCl_3$

A MeOH (8 mL) solution of $Co(NCS)_2$ (1.8 mg, 0.010 mmol) was layered over a $CHCl_3$ (5 mL) solution of ligand **7** (7.41 mg; 0.01 mmol) in a crystallisation tube (inner dimeter = 13.6 mm, volume = 24 mL). This was left to stand at room temperature. Orange block-like crystals visible to the eye were first obtained after 15 days and a single-crystal was selected for X-ray diffraction after another 4 days. A portion of the remaining crystals was mounted wet in a sample holder (to avoid loss of solvent from the crystals) and analysed by powder X-ray diffraction.

$[Co(NCS)_2(8)]_n$·0.8*n*MeOH·1.8*n*$CHCl_3$

A MeOH (8 mL) solution of $Co(NCS)_2$ (1.8 mg, 0.010 mmol) was layered over a $CHCl_3$ (5 mL) solution of ligand **8** (6.33 mg, 0.01 mmol) in a crystallisation tube (inner dimeter = 13.6 mm, volume = 24 mL) which was left to stand at room temperature. Orange block-like crystals visible to the eye were first obtained after 7 days and an X-ray quality crystal was selected after 2 months. A portion of the remaining crystals was mounted wet in a sample holder (to avoid loss of solvent from the crystals) and analysed by PXRD.

$[Co(NCS)_2(5)]_n$·2.5*n*C_6H_5Cl

A MeOH (8 mL) solution of $Co(NCS)_2$ (1.8 mg, 0.010 mmol) was layered over a chlorobenzene solution (5 mL) of **5** (7.8 mg, 0.010 mmol) in a crystallisation tube (i.d. = 13.6 mm, vol. = 24 mL) sealed with a septum. Pink block-like crystals visible to the eye were first obtained after 17 days, and a single-crystal was selected for X-ray diffraction. The remaining crystals were analysed by PXRD and FT-IR spectroscopy.

$Co(NCS)_2$ and ligand 5 in MeOH and $CHCl_3$

A MeOH (8 mL) solution of $Co(NCS)_2$ (1.8 mg, 0.010 mmol) was layered over a $CHCl_3$ solution (5 mL) of **5** (7.8 mg, 0.010 mmol) in a crystallisation tube (i.d. = 13.6 mm, vol. = 24 mL) sealed with a septum. Pink block-like crystals visible to the eye were first obtained after 23 days, and a single-crystal was selected for X-ray diffraction.

7.3.3 Coordination polymers with tris(terpyridine) ligands

$[Cu_3(hfacac)_6(13)]_n$·2.8*n*MeC_6H_5·0.4*n*$CHCl_3$

A toluene (7 mL) solution of $[Cu(hfacac)_2]\cdot H_2O$ (7.6 mg, 16 µmol) was layered over a $CHCl_3$ solution (6 mL) of **13** (5.2 mg, 5.0 µmol) in a crystallisation tube (i.d. = 13.6 mm, vol. = 24 mL) initially sealed with a septum; after 10 days a syringe-needle was introduced into the septum opening the tube to the air. The tube was left to stand at room temperature (ca. 22 °C) for 10 days. A fine light green suspension was obtained and removed by filtration. The filtrate was left to evaporate in the air in a test tube with a septum pierced with a syringe-needle. Light green block-like crystals visible to the eye were first obtained after three months, and four single-crystals were selected for X-ray diffraction after another month. All the remaining crystals were mounted wet in a sample holder (to avoid loss of solvent from the crystals) and analysed by powder X-ray diffraction).
In an another attempt, compound **13** (5.2 mg, 5.0 µmol) was dissolved in $CHCl_3$ (6 mL), and then a solution of $[Cu(hfacac)_2]\cdot H_2O$ (15.3 mg, 31.0 µmol) in toluene (6 mL) was added. A formation of a pale green precipitate was immediately observed. After filtration, the solution was left to evaporate in the air in a test tube with a septum pierced with a syringe-needle. Light green block-like crystals were obtained after 3 months, and cell checks revealed that these were $[Cu_3(hfacac)_6(\mathbf{13})]_n$·2.8*n*$MeC_6H_5$·0.4*n*$CHCl_3$ (cell parameters, a = 20.784(6) Å, b = 21.270(3) Å, c = 34.158(9) Å, β = 103.57(2)°).
An additional reaction was carried out to prepare a sample for E.A. and FT-IR spectroscopy. Compound **13** (10.4 mg, 10.0 µmol) was dissolved in $CHCl_3$ (6 mL), and then a solution of $[Cu(hfacac)_2]\cdot H_2O$

(15.3 mg, 0.031 mmol) in toluene (6 mL) was added. A formation of a pale green precipitate was immediately observed. The solid that formed was collected by centrifugation, washed with $CHCl_3$ and toluene, and then dried *in vacuo*. The product was isolated as a pale green powder. Yield for $[Cu_3(hfacac)_6(\mathbf{13})]_n \cdot 0.5n MeC_6H_5$ (25.0 mg, 10.0 µmol, 99.2 %). Found C 50.77, H 2.64, N 5.34; required for $C_{105.5}H_{61}Cu_3F_{36}N_9O_{12}$: C 50.26, H 2.44, N 5.00. PXRD showed that the resultant product was amorphous.

$[Cu(hfacac)_2]\cdot H_2O$ and ligand 13 in 1,2-dichlorobenzene and $CHCl_3$

A 1,2-dichlorobenzene (6 mL) solution of $[Cu(hfacac)_2]\cdot H_2O$ (7.6 mg, 16 µmol) was layered over a $CHCl_3$ solution (6 mL) of **13** (5.2 mg, 5.0 µmol) and anthracene (13.4 mg, 75.0 µmol) in a crystallisation tube (i.d. = 13.6 mm, vol. = 24 mL) initially sealed with a septum. After 3 months a fine light green suspension had formed and was removed by filtration. The filtrate was left to evaporate in the air in a test tube with a septum pierced with a syringe-needle. Light green block-like crystals visible to the eye were first obtained after 1 year, and a single-crystal was selected for X-ray diffraction after another month.

$[Cu(hfacac)_2]\cdot H_2O$ and ligand 14 in EtOH and $CHCl_3$

A EtOH (7 mL) solution of $[Cu(hfacac)_2]\cdot H_2O$ (6.69 mg, 14.0 µmol) was layered over a $CHCl_3$ solution (6 mL) of **14** (3.76 mg, 4.00 µmol) in a crystallisation tube (i.d. = 13.6 mm, vol. = 24 mL) sealed with a septum. Light green block-like crystals visible to the eye were first obtained after 3 weeks, and a single-crystal was selected for X-ray diffraction.

$[Cu(hfacac)_2]\cdot H_2O$ and ligand 14 in *n*-BuOH and $CHCl_3$

A *n*-BuOH (7 mL) solution of $[Cu(hfacac)_2]\cdot H_2O$ (6.69 mg, 14.0 µmol) was layered over a $CHCl_3$ solution (6 mL) of **14** (3.76 mg, 4.00 µmol) in a crystallisation tube (i.d. = 13.6 mm, vol. = 24 mL) sealed with a septum. Light green block-like crystals visible to the eye were first obtained after 1 month, and a single-crystal was selected for X-ray diffraction.

$[Cu(hfacac)_2]\cdot H_2O$ and ligand 14 in 1,4-dioxane and $CHCl_3$

A 1,4-dioxane (7 mL) solution of $[Cu(hfacac)_2]\cdot H_2O$ (6.69 mg, 14.0 µmol) was layered over a $CHCl_3$ solution (6 mL) of **14** (3.76 mg, 4.00 µmol) in a crystallisation tube (i.d. = 13.6 mm, vol. = 24 mL) sealed with a septum. Light green plate-like crystals visible to the eye were first obtained after 1 month, and a single-crystal was selected for X-ray diffraction after another 4 months.

7.4 Crystallography

7.4.1 Single-crystal X-Ray diffraction

Single-crystal data for **5a** (polymorph I), and **6a**, **5b**, $[Cu_2(hfacac)_4(\mathbf{5})]_n \cdot 3.6n(1,2\text{-}Cl_2C_6H_4) \cdot 2nCHCl_3$, $[Co(NCS)_2(\mathbf{8})]_n \cdot 0.8n MeOH \cdot 1.8nCHCl_3$, $[Co(NCS)_2(\mathbf{5})]_n \cdot 2.5nC_6H_5Cl$ and **9**·1.75DMF were collected on a STOE StadiVari diffractometer equipped with a Metaljet D2 source (GaKα radiation) and a Pilatus300K detector. Crystallographic data for **5a** (polymorph II), **6b** and $[Co(NCS)_2(\mathbf{7})]_n \cdot n MeOH \cdot 3nCHCl_3$ were collected using a Bruker APEX-II CCD diffractometer with CuKα radiation. Single-crystal data of $[Zn_2(hfacac)_4(\mathbf{5})]_n \cdot nMeC_6H_5 \cdot 1.8nCHCl_3$ was collected with CuKα radiation on an Agilent SuperNova, Dual-source, with an Atlas detector. For $[Cu_2(hfacac)_4(\mathbf{6})]_n \cdot nMeC_6H_5 \cdot 2nH_2O$, $[Cu_2(hfacac)_4(\mathbf{6})]_n \cdot 2.8nC_6H_5Cl$ and $[Cu_2(hfacac)_4(\mathbf{6})]_n \cdot 2n(1,2\text{-}Cl_2C_6H_4) \cdot 0.4nCHCl_3 \cdot 0.5nH_2O$, data collection was performed on a Rigaku-Oxford Diffraction XtaLAB Synergy-S dual source diffractometer equipped with a Cu and Mo PhotonJet microfocus X-ray sources and a Dectris Pilatus3 R 200K HPC detector. All these structures were solved using ShelXT v. 2018/2[242] and Olex2[243], and the model was refined with ShelXL v. 2018/3.[244] For $[Cu_3(hfacac)_6(\mathbf{13})]_n \cdot 2.8nMeC_6H_5 \cdot 0.4nCHCl_3$, a X06DA-PXIII beamline at the Swiss Light Source (Paul Scherrer Institute, 5232 Villigen, Switzerland) with synchrotron radiation (0.72083 Å) and a PILATUS 2M-F detector were used. In this case, data reduction, solution, and refinement used the programs XDS,[245] Olex2,[243] and ShelXL 2018/3.[244] All H atoms were included at geometrically calculated positions. C(H) and C(H,H) groups were refined using a riding model with U_{iso} = 1.2 of the parent atom, while in the case of the group C(H,H,H) U_{iso} is 1.5. Structure analysis used CSD Mercury 2021.3.0.[180]

In $[Cu_2(hfacac)_4(\mathbf{5})]_n \cdot 3.6n(1,2\text{-}Cl_2C_6H_4) \cdot 2nCHCl_3$, a CF_3 group of the polymer and 1,2-dichlorobenzene solvent molecules were disordered and were refined with geometrical constraints and constraints on their thermal parameters. One CF_3 of one the $[hfacac]^-$ ligand in $[Zn_2(hfacac)_4(\mathbf{5})]_n \cdot nMeC_6H_5 \cdot 1.8nCHCl_3$ was disordered over 2 orientations. The central phenylene spacer with its 3-phenylethoxy substituent in $[Zn_2(hfacac)_4(\mathbf{5})]_n \cdot nMeC_6H_5 \cdot 1.8nCHCl_3$ was disordered in a 1:1 ratio. In the absence of the phenyl moiety, once a toluene and once a chloroform molecule were present instead. The toluene molecule was further rotationally disordered; the position of the disordered methyl group could only be identified for half of the half occupied toluene molecule. Geometrical constraints and restraints on their thermal parameters were used to model them. In $[Cu_2(hfacac)_4(\mathbf{6})]_n \cdot nMeC_6H_5 \cdot 2nH_2O$ and $[Cu_2(hfacac)_4(\mathbf{6})]_n \cdot 2.8nC_6H_5Cl$, both solvent and one $[hfacac]^-$ ligand were disordered requiring geometrical restraints and restraints on their thermal parameters in the modelling process. All the $[hfacac]^-$ ligands in $[Cu_2(hfacac)_4(\mathbf{6})]_n \cdot 2n(1,2\text{-}Cl_2C_6H_4) \cdot 0.4nCHCl_3 \cdot 0.5nH_2O$ were disordered over two positions with 1:1 ratio. Geometrical constraints for the aromatic ring and restraints for the thermal parameters had to be used to treat the solvent molecules.

In $[Co(NCS)_2(\mathbf{7})]_n \cdot n MeOH \cdot 3nCHCl_3$, one $CHCl_3$ molecule was located and refined, and the Olex2 implementation of SQUEEZE[246] was used to treat the rest of the solvent region. A solvent mask was calculated and 1044.0 electrons were found in a volume of 3742.0 $Å^3$ in one void. This is consistent with the presence of $2CHCl_3$ and $1CH_3OH$ per formula unit which account for 1072.0 electrons. The formulae and dependent numbers were adapted to account for this. Due to their thermal motion, the aliphatic chains had to be heavily restrained with SIMU, SADI and DFIX restraints and were refined isotropically. In $[Co(NCS)_2(\mathbf{8})]_n \cdot 0.8n MeOH \cdot 1.8nCHCl_3$, the aliphatic chains display orientational and vibrational disorder and were modelled with the use of SADI and DFIX restraints, one chain over two

sites of partial occupancies 0.60/0.40 and the other chain with equal occupancy sites; some atoms were refined isotropically. Disorder in one thiocyanate ligand was modelled with two sites for the S atom of partial occupancies 0.75/0.25. All the solvent molecules present in this structure were modelled with partial occupancies. In $[Co(NCS)_2(\mathbf{5})]_n \cdot 2.5n C_6H_5Cl$ the sulfur atom of the $[NCS]^-$ unit and the phenylethyl substituent suffered from disorder. Geometrical constraints for the aromatic rings and constraints for their thermal parameters had to be used to treat the disordered chlorobenzene molecules and phenylethyl substituent in the modelling process.

In $[Cu_3(hfacac)_6(\mathbf{13})]_n \cdot 2.8n MeC_6H_5 \cdot 0.4n CHCl_3$ some CF_3 groups of the polymer and solvent molecules were disordered and were refined isotropically with geometrical restraints. A certain amount of the solvent was removed using the solvent mask procedure, and this was added to the formulae and appropriated numbers. A mask was also used to treat the solvent region in **9**; 1.75 DMF molecules were found and added to the formulae and numbers.

In the structural discussions, only the major (or one of the equal) occupancy sites are considered in each disordered entity. Some structures show relative high R_1/R_2 values, which is not unexpected, given the disorder present in some metal complexes and co-solvate molecules.

7.4.2 Powder X-Ray diffraction

PXRD data were collected at room temperature in transmission mode using a Stoe Stadi P diffractometer, equipped with CuKα1 radiation (Ge(111) monochromator) and a DECTRIS MYTHEN 1K detector. Whole-pattern decomposition (profile matching) analysis of the diffraction patterns was done using either overlay in Excel or the package FULLPROF SUITE (v. September 2020)[247, 248] using a previously determined instrument resolution function based on a NIST640d standard. The structural models were derived from the single-crystal X-ray diffraction data. When FULLPROF SUITE was used, refined parameters in Rietveld were scale factor, zero shift, lattice parameters, metal and halogen atomic positions, background points, and peaks shapes as a Thompson Cox Hastings pseudo-Voigt function. Preferred orientations as a March–Dollase multi-axial phenomenological model were incorporated into the analysis.

7.4.3 Crystallographic data

Precursor and ligand structures

5a (polymorph I): $C_{22}H_{20}Br_2O_2$ M_r = 476.20, colourless block, triclinic, space group *P*–1, a = 8.2806(13), b = 10.6327(16), c = 22.885(4) Å, α = 91.027(14), β = 91.663(14), γ = 89.806(13)°, V = 2013.7(6) Å^3, D_c = 1.571 g cm^{-3}, T = 200 K, Z = 4, μ(GaKα) = 3.586 mm^{-1}. Total 33981 reflections, 8265 unique (R_{int} = 0.0216). Refinement of 7408 reflections (470 parameters) with $I > 2\sigma(I)$ converged at final R_1 = 0.0380 (R_1 all data = 0.0406), wR_2 = 0.1047 ($wR2$ all data = 0.1076), F(000) = 952, gof = 1.084. CCDC 2061062.

5a (polymorph II): $C_{22}H_{20}Br_2O_2$ M_r = 476.20, colourless block, orthorhombic, space group *Pbca*, a = 10.5176(7), b = 8.2178(5), c = 22.7853(14) Å, V = 1969.4(2) Å^3, D_c = 1.606 g cm^{-3}, T = 200 K, Z = 4, μ(CuKα) = 5.321 mm^{-1}. Total 11852 reflections, 1812 unique (R_{int} = 0.0389). Refinement of 1798 reflections (118 parameters) with $I > 2\sigma(I)$ converged at final R_1 = 0.0346 (R_1 all data = 0.0348), wR_2 = 0.0882 ($wR2$ all data = 0.0883), F(000) = 952, gof = 1.131. CCDC 2068243.

6a: $C_{24}H_{24}Br_2O_2$, M_r = 504.25, colourless plate, triclinic, space group *P*–1, *a* = 9.9626(4), *b* = 10.2503(4), *c* = 17.6464(7) Å, α = 82.754(3), β = 77.201(3), γ = 67.946(3)°, *V* = 1626.85(12)Å^3, D_c = 1.544 g cm^{-3}, *T* = 150 K, *Z* = 3, μ(GaKα) = 3.218 mm^{-1}. Total 18658 reflections, 6466 unique (R_{int} = 0.0418). Refinement of 6040 reflections (397 parameters) with $I > 2\sigma(I)$ converged at final R_1 = 0.0564 (R_1 all data = 0.0587), wR_2 = 0.1521 ($wR2$ all data = 0.1554), F(000) = 762, gof = 1.035. CCDC 2061063.

5b: $C_{24}H_{22}O_4$, M_r = 374.41, yellow block, monoclinic, $P2_1/n$, *a* = 12.4540(7), *b* = 5.4805(2), *c* = 14.1111(7) Å, β = 104.263(4)°, *V* = 933.45(8) Å^3, D_c = 1.332 g cm^{-3}, *T* = 150 K, *Z* = 2, μ(CuKα) = 0.462 mm^{-1}. Total 5213 reflections, 1854 unique (R_{int} = 0.0802). Refinement of 1614 reflections (127 parameters) with $I > 2\sigma(I)$ converged at final R_1 = 0.1118 (R_1 all data = 0.1152), wR_2 = 0.2784 (wR_2 all data = 0.2849), F(000) = 396, gof = 1.258. CCDC 2162893.

6b: $C_{26}H_{26}O_4$, M_r = 402.47, yellow plate, orthorhombic, *Pbca*, *a* = 9.0988(6), *b* = 8.7410(6), *c* = 27.1654(17) Å, *V* = 2160.5(2) Å^3, D_c = 1.237 g cm^{-3}, *T* = 150 K, *Z* = 4, μ(CuKα) = 0.661 mm^{-1}. Total 14033 reflections, 1995 unique (R_{int} = 0.0334). Refinement of 1817 reflections (136 parameters) with $I > 2\sigma(I)$ converged at final R_1 = 0.0354 (R_1 all data = 0.0386), wR_2 = 0.0950 (wR_2 all data = 0.0984), F(000) = 856, gof = 1.015. CCDC 2162895.

9·1.75DMF: $C_{51}H_{33}N_9{\cdot}C_{5.25}H_{12.25}N_{1.75}O_{1.75}$, M_r = 899.78, yellow block, orthorhombic, *Pbca*, *a* = 20.3991(5), *b* = 15.4857(3), *c* = 30.0422(5) Å, *V* = 9490.2(3) Å^3, *T* = 150 K, *Z* = 8, μ(GaKα) = 0.405. Total 59250 reflections, 9577 unique (R_{int} = 0.0486). Refinement of 5670 reflections (541 parameters) with $I > 2\sigma(I)$ converged at final R_1 = 0.0515 (R_1 all data = 0.0746), wR_2 = 0.1520 (wR_2 all data = 0.1612), F(000) = 3776, gof = 1.177. CCDC 2096132.

Coordination polymers

$[Cu_2(hfacac)_4(\mathbf{5})]_n{\cdot}3.6n(1,2\text{-}Cl_2C_6H_4){\cdot}2n CHCl_3$: $C_{95.6}H_{60.4}Cl_{13.2}Cu_2F_{24}N_6O_{10}$, M_r = 2504.12, green plate, monoclinic, $P2_1/n$, *a* = 11.9740(4), *b* = 24.5642(6), *c* = 19.0265(6) Å, β = 94.874(3)°, *V* = 5576.1(3) Å^3, D_c = 1.491 g cm^{-3}, *T* = 130 K, *Z* = 2, μ(GaKα) = 4.547 mm^{-1}. Total 62274 reflections, 11193 unique (R_{int} = 0.1234). Refinement of 8115 reflections (635 parameters) with $I > 2\sigma(I)$ converged at final R_1 = 0.1224 (R_1 all data = 0.1547), wR_2 = 0.3685 (wR_2 all data = 0.4112), F(000) = 2509, gof = 1.027. CCDC 2162894.

$[Zn_2(hfacac)_4(\mathbf{5})]_n{\cdot}n MeC_6H_5{\cdot}1.8n CHCl_3$: $C_{80.80}H_{53.80}Cl_{5.40}F_{24}N_6O_{10}Zn_2$, M_r = 2046.87, colourless block, monoclinic, $P2_1/n$, *a* = 14.31144(10), *b* = 14.96748(10), *c* = 22.80527(13) Å, β = 93.1070(6)°, *V* = 4877.85(5) Å^3, D_c = 1.394 g cm^{-3}, *T* = 160 K, *Z* = 2, μ(CuKα) = 2.854 mm^{-1}. Total 81497 reflections, 10223 unique (R_{int} = 0.0282). Refinement of 9342 reflections (724 parameters) with $I > 2\sigma(I)$ converged at final R_1 = 0.0797 (R_1 all data = 0.0839), wR_2 = 0.2452 (wR_2 all data = 0.2527), F(000) = 2047, gof = 1.042. CCDC 2162898.

$[Cu_2(hfacac)_4(\mathbf{6})]_n{\cdot}n MeC_6H_5{\cdot}2n H_2O$: $C_{81}H_{56}Cu_2F_{24}N_6O_{12}$, M_r = 1888.39, green block, triclinic, *P*–1, *a* = 8.9300(2), *b* = 15.7218(3), *c* = 16.4219(3) Å, α = 100.0302(15), β = 93.7146(16), γ = 96.8981(18)°, *V* = 2245.22(8) Å^3, D_c = 1.397 g cm^{-3}, *T* = 160 K, *Z* = 1, μ(CuKα) = 1.554 mm^{-1}. Total 29179 reflections, 9228 unique (R_{int} = 0.0311). Refinement of 8012 reflections (731 parameters) with $I > 2\sigma(I)$ converged at

final R_1 = 0.0758 (R_1 all data = 0.0830), wR_2 = 0.2299 (wR_2 all data = 0.2463), F(000) = 954, gof = 1.070. CCDC 2162896.

$[Cu_2(hfacac)_4(\mathbf{6})]_n \cdot 2.8n C_6H_5Cl$: $C_{90.8}H_{61}Cl_{2.8}Cu_2F_{24}N_6O_{10}$, M_r = 2078.39, green block, triclinic, *P*–1, a = 8.9544(2), b = 15.7417(4), c = 16.3905(4) Å, α = 100.053(2), β = 94.071(2), γ = 97.071(2)°, V = 2247.46(10) Å^3, D_c = 1.536 g cm^{-3}, T = 160 K, Z = 1, μ(CuKα) = 2.342 mm^{-1}. Total 33912 reflections, 8919 unique (R_{int} = 0.0466). Refinement of 7542 reflections (714 parameters) with $I > 2\sigma(I)$ converged at final R_1 = 0.0932 (R_1 all data = 0.1035), wR_2 = 0.2661 (wR_2 all data = 0.2839), F(000) = 1049, gof = 1.040. CCDC 2162897.

$[Cu_2(hfacac)_4(\mathbf{6})]_n \cdot 2n(1,2\text{-}Cl_2C_6H_4) \cdot 0.4n CHCl_3 \cdot 0.5n H_2O$: $C_{86.40}H_{56.40}Cl_{5.20}Cu_2F_{24}N_6O_{10.50}$, M_r = 2113.99, green plate, triclinic, *P*–1, a = 9.0105(3), b = 15.1823(4), c = 19.9645(3) Å, α = 109.391(2), β = 92.202(2), γ = 100.595(2)°, V = 2517.67(12) Å^3, D_c = 1.394 g cm^{-3}, T = 160 K, Z = 1, μ(CuKα) = 2.676 mm^{-1}. Total 39796 reflections, 9979 unique (R_{int} = 0.0629). Refinement of 6887 reflections (882 parameters) with $I > 2\sigma(I)$ converged at final R_1 = 0.0984 (R_1 all data = 0.1225), wR_2 = 0.2869 (wR_2 all data = 0.3162), F(000) = 1063, gof = 1.209. CCDC 2162899.

$[Co(NCS)_2(\mathbf{7})]_n \cdot n MeOH \cdot 3n CHCl_3$: $C_{54}H_{54}Cl_9CoN_8O_3S_2$, M_r = 1305.15, orange block, monoclinic, space group *C*2/*c*, a = 37.514(3), b = 17.4813(11), c = 26.6265(17) Å, β = 133.660(3)°, V = 12632.4(15) Å^3, D_c = 1.373 g cm^{-3}, T = 130 K, Z = 8, μ(CuKα) = 6.630 mm^{-1}. Total 69524 reflections, 9110 unique (R_{int} = 0.02879). Refinement of 5412 reflections (552 parameters) with $I > 2\sigma(I)$ converged at final R_1 = 0.1118 (R_1 all data = 0.1470), wR_2 = 0.3236 (wR_2 all data = 0.3606), gof = 1.228, CCDC 1954948.

$[Co(NCS)_2(\mathbf{8})]_n \cdot 0.8n MeOH \cdot 1.8n CHCl_3$: $C_{50.6}H_{49}Cl_{5.4}CoN_8O_{2.8}S_2$, M_r = 1128.46, orange plate, monoclinic, space group *C*2/*c*, a = 37.7611(9), b = 17.3396(3), c = 27.5031(6) Å, β = 135.1980(10)°, V = 12689.5(5) Å^3, D_c = 1.181 g cm^{-3}, T = 130 K, Z = 8, μ(GaKα) = 3.447 mm^{-1}. Total 91813 reflections, 12996 unique (R_{int} = 0.1323). Refinement of 8243 reflections (655 parameters) with $I > 2\sigma(I)$ converged at final R_1 = 0.1424 (R_1 all data = 0.1884), wR_2 = 0.4180 (wR_2 all data = 0.5084), gof = 0.918, CCDC 1954949.

$[Co(NCS)_2(\mathbf{5})]_n \cdot 2.5n C_6H_5Cl$: $C_{69}H_{52.5}Cl_{2.5}CoN_8O_2S_2$, M_r = 1237.36, pink block, monoclinic, space group $P2_1/n$, a = 15.0141(2), b = 14.5575(3), c = 16.8220(2) Å, β = 115.0370(10)°, V = 3331.26(9) Å^3, D_c = 1.234 g cm^{-3}, T = 130 K, Z = 2, μ(GaKα) = 2.662 mm^{-1}, 43829 reflections measured, 6694 unique (R_{int} = 0.0607). Refinement of 5387 reflections (369 parameters) with $I > 2\sigma(I)$ converged at final R_1 = 0.0980 (R_1 all data = 0.1139), wR_2 = 0.2424 (wR_2 all data = 0.2521), gof = 1.040. CCDC 2204765.

$[Cu_3(hfacac)_6(\mathbf{13})]_n \cdot 2.8n MeC_6H_5 \cdot 0.4n CHCl_3$: $C_{122}H_{80.1}Cl_{1.2}Cu_3F_{36}N_9O_{12}$, M_r = 2781.21, green block, monoclinic, $P2_1/n$, a = 19.889(4), b = 21.178(4), c = 34.375(7) Å, β = 104.32(3)°, V = 14029(5) Å^3, T = 100 K, Z = 4, μ(synchrotron) = 0.595. Total 531703 reflections, 29721 unique (R_{int} = 0.0862). Refinement of 20415 reflections (1623 parameters) with $I > 2\sigma(I)$ converged at final R_1 = 0.1912 (R_1 all data = 0.2092), wR_2 = 0.4998 (wR_2 all data = 0.5408), F(000) = 5610, gof = 1.177. CCDC 2096133.

8 References

1. S. R. Batten, S. M. Neville and D. R. Turner, *Coordination Polymers: Design, Analysis and Application*, RSC Publishing, Cambridge, 2009.
2. J. E. Berger, *Kerrn aller Fridrichs=Städtschen Begebenheiten*, Manuskript, Berlin, ca.1730 (Berlin, Staatsbibliothek zu Berlin—Preußischer Kulturbesitz, Handschriftenabteilung, Ms. Boruss. quart. 124).
3. K. A. Hofmann and F. Küspert, *Z. Anorg. Chem.*, 1897, **15**, 204-207.
4. H. M. Powell and J. H. Rayner, *Nature*, 1949, **163**, 566-567.
5. J. H. Rayner and H. M. Powell, *J. Chem. Soc.*, 1952, 319-328.
6. H. J. Buser, D. Schwarzenbach, W. Petter and A. Ludi, *Inorg. Chem.*, 1977, **16**, 2704-2710.
7. O. M. Yaghi, M. J. Kalmutzki and C. S. Diercks, *Introduction to Reticular Chemistry: Metal-Organic Frameworks and Covalent Organic Frameworks*, Wiley, Weinheim, 2019.
8. H. G. Buttner, G. J. Kearley, C. J. Howard and F. Fillaux, *Acta Crystallogr., Sect. B: Struct. Sci.*, 1994, **B50**, 431-435.
9. B. F. Hoskins and R. Robson, *J. Am. Chem. Soc.*, 1989, **111**, 5962-5964.
10. B. F. Hoskins and R. Robson, *J. Am. Chem. Soc.*, 1990, **112**, 1546-1554.
11. R. W. Gable, B. F. Hoskins and R. Robson, *J. Chem. Soc., Chem. Commun.*, 1990, 762-763.
12. B. F. Abrahams, B. F. Hoskins and R. Robson, *J. Chem. Soc., Chem. Commun.*, 1990, 60-61.
13. B. F. Abrahams, B. F. Hoskins and R. Robson, *J. Am. Chem. Soc.*, 1991, **113**, 3606-3607.
14. B. F. Abrahams, B. F. Hoskins, J. Liu and R. Robson, *J. Am. Chem. Soc.*, 1991, **113**, 3045-3051.
15. S. R. Batten, B. F. Hoskins and R. Robson, *J. Chem. Soc., Chem. Commun.*, 1991, 445-447.
16. B. F. Abrahams, M. J. Hardie, B. F. Hoskins, R. Robson and G. A. Williams, *J. Am. Chem. Soc.*, 1992, **114**, 10641-10643.
17. B. F. Abrahams, B. F. Hoskins, D. M. Michail and R. Robson, *Nature*, 1994, **369**, 727-729.
18. B. F. Abrahams, M. J. Hardie, B. F. Hoskins, R. Robson and E. E. Sutherland, *J. Chem. Soc., Chem. Commun.*, 1994, 1049-1050.
19. B. F. Hoskins, R. Robson and N. V. Y. Scarlett, *J. Chem. Soc., Chem. Commun.*, 1994, 2025-2026.
20. B. F. Hoskins, R. Robson and N. V. Y. Scarlett, *Angew. Chem. Int. Ed.*, 1995, **34**, 1203-1204.
21. S. R. Batten, B. F. Hoskins and R. Robson, *J. Am. Chem. Soc.*, 1995, **117**, 5385-5386.
22. S. R. Batten, B. F. Hoskins and R. Robson, *Angew. Chem. Int. Ed.*, 1995, **34**, 820-822.
23. R. Robson, B. F. Abrahams, S. R. Batten, R. W. Gable, B. F. Hoskins and J. Liu, in *Supramolecular Architecture*, American Chemical Society, 1992, vol. 499, ch. 19, pp. 256-273.
24. S. R. Batten and R. Robson, *Angew. Chem. Int. Ed.*, 1998, **37**, 1460-1494.
25. R. Robson, *J. Chem. Soc., Dalton Trans.*, 2000, 3735-3744.
26. A. F. Wells, *Three-dimensional Nets and Polyhedra*, Wiley, New York, 1977.
27. A. F. Wells, *Further Studies of Three-dimensional Nets*, American Crystallographic Association, Knoxville, TN, 1979.
28. A. F. Wells, *Structural Inorganic Chemistry*, Oxford University Press, Oxford, 5th edn., 1984.
29. S. R. Batten, N. R. Champness, X.-M. Chen, J. Garcia-Martinez, S. Kitagawa, L. Öhrström, M. O'Keeffe, M. Paik Suh and J. Reedijk, *Pure Appl. Chem.*, 2013, **85**, 1715-1724.
30. Y.-M. Zhang, D.-Y. Hou, G. Xin and T.-C. Li, *Acta Crystallogr., Sect. E: Struct. Rep. Online*, 2010, **E66**, m287.
31. S. R. Batten and K. S. Murray, *Aust. J. Chem.*, 2001, **54**, 605-609.
32. S. R. Batten, *J. Solid State Chem.*, 2005, **178**, 2475-2479.
33. C. Janiak, L. Uehlin, H.-P. Wu, P. Klüfers, H. Piotrowski and T. G. Scharmann, *J. Chem. Soc., Dalton Trans.*, 1999, 3121-3131.
34. C. Janiak, *Dalton Trans.*, 2003, 2781-2804.
35. J.-P. Zhang, Y.-Y. Lin, X.-C. Huang and X.-M. Chen, *Chem. Commun.*, 2005, 1258-1260.
36. S. S. Capomolla, G. Manfroni, A. Prescimone, E. C. Constable and C. E. Housecroft, *Polyhedron*, 2022, **224**, 116005.

37. S. R. Batten, A. R. Harris, P. Jensen, K. S. Murray and A. Ziebell, *J. Chem. Soc., Dalton Trans.*, 2000, 3829-3836.
38. S. A. Barnett, A. J. Blake, N. R. Champness and C. Wilson, *Dalton Trans.*, 2005, 3852-3861.
39. M. Hanack, A. Hirsch and H. Lehmann, *Angew. Chem. Int. Ed.*, 1990, **29**, 1467-1468.
40. L. J. Twyman and A. S. H. King, *Chem. Commun.*, 2002, 910-911.
41. H. Hou, Y. Wei, Y. Song, Y. Zhu, L. Li and Y. Fan, *J. Mater. Chem.*, 2002, **12**, 838-843.
42. H. Hou, X. Meng, Y. Song, Y. Fan, Y. Zhu, H. Lu, C. Du and W. Shao, *Inorg. Chem.*, 2002, **41**, 4068-4075.
43. E. Barea, J. A. R. Navarro, J. M. Salas, N. Masciocchi, S. Galli and A. Sironi, *Inorg. Chem.*, 2004, **43**, 473-481.
44. S. R. Batten, in *Comprehensive Coordination Chemistry III*, eds. E. C. Constable, G. Parkin and L. Que Jr, Elsevier, Oxford, 2021, vol. 2, pp. 368-388.
45. J. D. Evans, B. Garai, H. Reinsch, W. Li, S. Dissegna, V. Bon, I. Senkovska, R. A. Fischer, S. Kaskel, C. Janiak, N. Stock and D. Volkmer, *Coord. Chem. Rev.*, 2019, **380**, 378-418.
46. S. R. Halper, L. Do, J. R. Stork and S. M. Cohen, *J. Am. Chem. Soc.*, 2006, **128**, 15255-15268.
47. M. Du, C.-P. Li and X.-J. Zhao, *Cryst. Growth Des.*, 2006, **6**, 335-341.
48. H. Li, M. Eddaoudi, M. O'Keeffe and O. M. Yaghi, *Nature*, 1999, **402**, 276-279.
49. K. N. Lazarou, V. Psycharis, A. Terzis and C. P. Raptopoulou, *Polyhedron*, 2011, **30**, 963-970.
50. G. Manfroni, A. Prescimone, S. R. Batten, Y. M. Klein, D. J. Gawryluk, E. C. Constable and C. E. Housecroft, *Crystals*, 2019, **9**, 529.
51. C. P. Raptopoulou, *Journal*, 2021, **14**.
52. X.-M. Chen and M.-L. Tong, *Acc. Chem. Res.*, 2007, **40**, 162-170.
53. F. Millange, R. El Osta, M. E. Medina and R. I. Walton, *CrystEngComm*, 2011, **13**, 103-108.
54. E. Biemmi, S. Christian, N. Stock and T. Bein, *Microporous Mesoporous Mater.*, 2009, **117**, 111-117.
55. A. Martinez Joaristi, J. Juan-Alcañiz, P. Serra-Crespo, F. Kapteijn and J. Gascon, *Cryst. Growth Des.*, 2012, **12**, 3489-3498.
56. Y.-R. Lee, J. Kim and W.-S. Ahn, *Korean J. Chem. Eng.*, 2013, **30**, 1667-1680.
57. M. O'Keeffe, M. A. Peskov, S. J. Ramsden and O. M. Yaghi, *Acc. Chem. Res.*, 2008, **41**, 1782-1789.
58. O. M. Yaghi, M. O'Keeffe, N. W. Ockwig, H. K. Chae, M. Eddaoudi and J. Kim, *Nature*, 2003, **423**, 705-714.
59. C. E. Housecroft and E. C. Constable, *Chem. Commun.*, 2020, **56**, 10786-10794.
60. C. Bonneau, M. O'Keeffe, D. M. Proserpio, V. A. Blatov, S. R. Batten, S. A. Bourne, M. S. Lah, J.-G. Eon, S. T. Hyde, S. B. Wiggin and L. Öhrström, *Cryst. Growth Des.*, 2018, **18**, 3411-3418.
61. P. Jensen, S. R. Batten, G. D. Fallon, B. Moubaraki, K. S. Murray and D. J. Price, *Chem. Commun.*, 1999, 177-178.
62. W. M. Meier, D. H. Olson and C. Baerlocher, *Atlas of zeolite framework types*, Elsevier, Amsterdam, 5th edn., 2001.
63. RCSR, http://rcsr.anu.edu.au, Accessed 8 November, 2022.
64. J. L. C. Rowsell, A. R. Millward, K. S. Park and O. M. Yaghi, *J. Am. Chem. Soc.*, 2004, **126**, 5666-5667.
65. V. Subramaniyam, P. V. Ravi and M. Pichumani, *J. Mol. Struct.*, 2022, **1251**, 131931.
66. C. A. Hunter, *Angew. Chem. Int. Ed.*, 1995, **34**, 1079-1081.
67. H.-J. Chen, L.-Q. Chen, L.-R. Lin, L.-S. Long and L.-S. Zheng, *Inorg. Chem.*, 2021, **60**, 6986-6990.
68. M. Andruh, J.-P. Costes, C. Diaz and S. Gao, *Inorg. Chem.*, 2009, **48**, 3342-3359.
69. C. Janiak, T. G. Scharmann, W. Günther, F. Girgsdies, H. Hemling, W. Hinrichs and D. Lentz, *Chem. Eur. J.*, 1995, **1**, 637-644.
70. M. Eddaoudi, D. B. Moler, H. Li, B. Chen, T. M. Reineke, M. O'Keeffe and O. M. Yaghi, *Acc. Chem. Res.*, 2001, **34**, 319-330.
71. T. P. Vaid, S. P. Kelley and R. D. Rogers, *IUCrJ*, 2017, **4**, 380-392.
72. A. Y. Robin and K. M. Fromm, *Coord. Chem. Rev.*, 2006, **250**, 2127-2157.
73. C. Janiak and J. K. Vieth, *New J. Chem.*, 2010, **34**, 2366-2388.

74. X. Yin, A. Alsuwaidi and X. Zhang, *Microporous Mesoporous Mater.*, 2022, **330**, 111633.
75. M. Eddaoudi, J. Kim, M. O'Keeffe and O. M. Yaghi, *J. Am. Chem. Soc.*, 2002, **124**, 376-377.
76. M. Eddaoudi, J. Kim, N. Rosi, D. Vodak, J. Wachter, M. O'Keeffe and O. M. Yaghi, *Science*, 2002, **295**, 469-472.
77. C. J. Höller, M. Mai, C. Feldmann and K. Müller-Buschbaum, *Dalton Trans.*, 2010, **39**, 461-468.
78. A. Q. Wu, G.-H. Guo, C. Yang, F.-K. Zheng, X. Liu, G.-C. Guo, J.-S. Huang, Z.-C. Dong and Y. Takano, *Eur. J. Inorg. Chem.*, 2005, **2005**, 1947-1954.
79. M. Du, C.-P. Li, C.-S. Liu and S.-M. Fang, *Coord. Chem. Rev.*, 2013, **257**, 1282-1305.
80. S. M. Elahi, M. Raizada, P. K. Sahu and S. Konar, *Chem. Eur. J.*, 2021, **27**, 5858-5870.
81. E. C. Constable and C. E. Housecroft, *Coord. Chem. Rev.*, 2017, **350**, 84-104.
82. E. C. Constable, *Coord. Chem. Rev.*, 2008, **252**, 842-855.
83. C. E. Housecroft, *Dalton Trans.*, 2014, **43**, 6594-6604.
84. C. E. Housecroft, *CrystEngComm*, 2015, **17**, 7461-7468.
85. C. E. Housecroft and E. C. Constable, *Chimia*, 2019, **73**, 462-467.
86. C. E. Housecroft and E. C. Constable, *Molecules*, 2021, **26**, 3110.
87. B. Liu, L. Hou, W.-P. Wu, A.-N. Dou and Y.-Y. Wang, *Dalton Trans.*, 2015, **44**, 4423-4427.
88. Y. Wu, J. Wu, Z. Luo, J. Wang, Y. Li, Y. Han and J. Liu, *RSC Adv.*, 2017, **7**, 10415-10423.
89. F. Yuan, C.-M. Yuan, H.-M. Hu, T.-T. Wang and C.-S. Zhou, *J. Solid State Chem.*, 2018, **258**, 588-601.
90. C. E. Housecroft and E. C. Constable, *J. Inorg. Organomet. Polym. Mater.*, 2018, **28**, 414-427.
91. J. Yoshida, S.-i. Nishikiori and H. Yuge, *J. Coord. Chem.*, 2013, **66**, 2191-2200.
92. Y. M. Klein, E. C. Constable, C. E. Housecroft and A. Prescimone, *CrystEngComm*, 2015, **17**, 2070-2073.
93. J. Wang and G. S. Hanan, *Synlett*, 2005, 1251-1254.
94. F. Kröhnke, *Synthesis*, 1976, **1**, 1-24.
95. D. Rocco, C. E. Housecroft and E. C. Constable, *Molecules*, 2019, **24**, 1799.
96. G. Manfroni, A. Prescimone, E. C. Constable and C. E. Housecroft, *CrystEngComm*, 2022, **24**, 491-503.
97. E. Loukopoulos and G. E. Kostakis, *J. Coord. Chem.*, 2018, **71**, 371-410.
98. J. Chen, K. Shen and Y. Li, *ChemSusChem*, 2017, **10**, 3165-3187.
99. S. Mukherjee, A. Kumar and M. J. Zaworotko, in *Metal-Organic Frameworks (MOFs) for Environmental Applications*, ed. S. K. Ghosh, Elsevier, Amsterdam, 2019, pp. 5-61.
100. K. Sumida, D. L. Rogow, J. A. Mason, T. M. McDonald, E. D. Bloch, Z. R. Herm, T.-H. Bae and J. R. Long, *Chem. Rev.*, 2012, **112**, 724-781.
101. J. Duan, W. Jin and S. Kitagawa, *Coord. Chem. Rev.*, 2017, **332**, 48-74.
102. Y. Peng and W. Yang, *Adv. Mater. Interfaces*, 2020, **7**, 1901514.
103. R.-B. Lin, S. Xiang, H. Xing, W. Zhou and B. Chen, *Coord. Chem. Rev.*, 2019, **378**, 87-103.
104. Y. Zhang, X. Cheng, X. Jiang, J. J. Urban, C. H. Lau, S. Liu and L. Shao, *Mater. Today*, 2020, **36**, 40-47.
105. Y. Ye, L. Gong, S. Xiang, Z. Zhang and B. Chen, *Adv. Mater.*, 2020, **32**, 1907090.
106. J. Deng, F. Wu, P. Yu and L. Mao, *Appl. Mater. Today*, 2018, **11**, 338-351.
107. J.-Q. Liu, Z.-D. Luo, Y. Pan, A. K. Singh, M. Trivedi and A. Kumar, *Coord. Chem. Rev.*, 2020, **406**, 213145.
108. D. O'Nolan and M. J. Zaworotko, in *Hot Topics in Crystal Engineering*, ed. K. Rissanen, Elsevier, 2021, ch. 2, pp. 17-60.
109. M. G. Nijkamp, J. E. M. J. Raaymakers, A. J. van Dillen and K. P. de Jong, *Appl Phys. A*, 2001, **72**, 619-623.
110. A. R. Millward and O. M. Yaghi, *J. Am. Chem. Soc.*, 2005, **127**, 17998-17999.
111. K. Koh, A. G. Wong-Foy and A. J. Matzger, *J. Am. Chem. Soc.*, 2009, **131**, 4184-4185.
112. H. Furukawa, N. Ko, Y. B. Go, N. Aratani, S. B. Choi, E. Choi, A. Ö. Yazaydin, R. Q. Snurr, M. O'Keeffe, J. Kim and O. M. Yaghi, *Science*, 2010, **329**, 424-428.
113. N. L. Rosi, J. Eckert, M. Eddaoudi, D. T. Vodak, J. Kim, M. O'Keeffe and O. M. Yaghi, *Science*, 2003, **300**, 1127-1129.

114. P. D. C. Dietzel, B. Panella, M. Hirscher, R. Blom and H. Fjellvåg, *Chem. Commun.*, 2006, 959-961.
115. E. D. Bloch, W. L. Queen, R. Krishna, J. M. Zadrozny, C. M. Brown and J. R. Long, *Science*, 2012, **335**, 1606-1610.
116. T. Pham, K. A. Forrest, R. Banerjee, G. Orcajo, J. Eckert and B. Space, *J. Phys. Chem. C*, 2015, **119**, 1078-1090.
117. T. M. McDonald, W. R. Lee, J. A. Mason, B. M. Wiers, C. S. Hong and J. R. Long, *J. Am. Chem. Soc.*, 2012, **134**, 7056-7065.
118. Z. Qiao, N. Wang, J. Jiang and J. Zhou, *Chem. Commun.*, 2016, **52**, 974-977.
119. Y. Inokuma, T. Arai and M. Fujita, *Nat. Chem.*, 2010, **2**, 780-783.
120. M. Hoshino, A. Khutia, H. Xing, Y. Inokuma and M. Fujita, *IUCrJ*, 2016, **3**, 139-151.
121. Y. Matsuda, T. Mitsuhashi, S. Lee, M. Hoshino, T. Mori, M. Okada, H. Zhang, F. Hayashi, M. Fujita and I. Abe, *Angew. Chem. Int. Ed.*, 2016, **55**, 5785-5788.
122. M. Fujita, Y. J. Kwon, S. Washizu and K. Ogura, *J. Am. Chem. Soc.*, 1994, **116**, 1151-1152.
123. D. N. Dybtsev and K. P. Bryliakov, *Coord. Chem. Rev.*, 2021, **437**, 213845.
124. M. Kurmoo, *Chem. Soc. Rev.*, 2009, **38**, 1353-1379.
125. M. D. Allendorf, C. A. Bauer, R. K. Bhakta and R. J. T. Houk, *Chem. Soc. Rev.*, 2009, **38**, 1330-1352.
126. G. Wang, M. Chen, J. Wang, Z. Jiang, D. Liu, D. Lou, H. Zhao, K. Li, S. Li, T. Wu, Z. Jiang, X. Sun and P. Wang, *J. Am. Chem. Soc.*, 2020, **142**, 7690-7698.
127. Z. Zhang, Y. Li, B. Song, Y. Zhang, X. Jiang, M. Wang, R. Tumbleson, C. Liu, P. Wang, X.-Q. Hao, T. Rojas, A. T. Ngo, J. L. Sessler, G. R. Newkome, S. W. Hla and X. Li, *Nat. Chem.*, 2020, **12**, 468-474.
128. D. Liu, M. Chen, Y. Li, Y. Shen, J. Huang, X. Yang, Z. Jiang, X. Li, G. R. Newkome and P. Wang, *Angew. Chem. Int. Ed.*, 2018, **57**, 14116-14120.
129. X. Lu, X. Li, Y. Cao, A. Schultz, J.-L. Wang, C. N. Moorefield, C. Wesdemiotis, S. Z. D. Cheng and G. R. Newkome, *Angew. Chem. Int. Ed.*, 2013, **52**, 7728-7731.
130. G. R. Newkome, P. Wang, C. N. Moorefield, T. J. Cho, P. P. Mohapatra, S. Li, S.-H. Hwang, O. Lukoyanova, L. Echegoyen, J. A. Palagallo, V. Iancu and S.-W. Hla, *Science*, 2006, **312**, 1782-1785.
131. M. Wang, C. Wang, X.-Q. Hao, J. Liu, X. Li, C. Xu, A. Lopez, L. Sun, M.-P. Song, H.-B. Yang and X. Li, *J. Am. Chem. Soc.*, 2014, **136**, 6664-6671.
132. T. Wu, J. Yuan, B. Song, Y.-S. Chen, M. Chen, X. Xue, Q. Liu, J. Wang, Y.-T. Chan and P. Wang, *Chem. Commun.*, 2017, **53**, 6732-6735.
133. S.-Y. Wang, J.-H. Fu, Y.-P. Liang, Y.-J. He, Y.-S. Chen and Y.-T. Chan, *J. Am. Chem. Soc.*, 2016, **138**, 3651-3654.
134. Z. Jiang, Y. Li, M. Wang, D. Liu, J. Yuan, M. Chen, J. Wang, G. R. Newkome, W. Sun, X. Li and P. Wang, *Angew. Chem. Int. Ed.*, 2017, **56**, 11450-11455.
135. Z. Jiang, Y. Li, M. Wang, B. Song, K. Wang, M. Sun, D. Liu, X. Li, J. Yuan, M. Chen, Y. Guo, X. Yang, T. Zhang, C. N. Moorefield, G. R. Newkome, B. Xu, X. Li and P. Wang, *Nat. Commun.*, 2017, **8**, 15476.
136. Z. Zhang, H. Wang, X. Wang, Y. Li, B. Song, O. Bolarinwa, R. A. Reese, T. Zhang, X.-Q. Wang, J. Cai, B. Xu, M. Wang, C. Liu, H.-B. Yang and X. Li, *J. Am. Chem. Soc.*, 2017, **139**, 8174-8185.
137. S. Chakraborty and G. R. Newkome, *Chem. Soc. Rev.*, 2018, **47**, 3991-4016.
138. G. R. Newkome, T. J. Cho, C. N. Moorefield, R. Cush, P. S. Russo, L. A. Godínez, M. J. Saunders and P. Mohapatra, *Chem. Eur. J.*, 2002, **8**, 2946-2954.
139. S.-H. Hwang, C. N. Moorefield, F. R. Fronczek, O. Lukoyanova, L. Echegoyen and G. R. Newkome, *Chem. Commun.*, 2005, 713-715.
140. Y.-T. Chan, X. Li, C. N. Moorefield, C. Wesdemiotis and G. R. Newkome, *Chem. Eur. J.*, 2011, **17**, 7750-7754.
141. Y.-T. Chan, C. N. Moorefield, M. Soler and G. R. Newkome, *Chem. Eur. J.*, 2010, **16**, 1768-1771.
142. Y.-P. Liang, Y.-J. He, Y.-H. Lee and Y.-T. Chan, *Dalton Trans.*, 2015, **44**, 5139-5145.

143. C. E. Housecroft and E. C. Constable, in *Comprehensive Coordination Chemistry III*, eds. E. C. Constable, G. Parkin and L. Que Jr, Elsevier, Oxford, 2021, vol. 7, pp. 121-173.
144. C. F. Lim and J. M. Tanski, *J. Chem. Crystallogr.*, 2007, **37**, 587-595.
145. O. Dann, J. Ruff, H.-P. Wolff and H. Grießmeier, *Liebigs Ann. Chem.*, 1984, **1984**, 409-425.
146. A. Parikh, H. Parikh and K. Parikh, in *Named Reactions in Organic Synthesis*, Foundation Books, New Delhi, 2006, pp. 79-81.
147. J. Chen, Y. Zhang, L. Liu, T. Yuan and F. Yi, *Phosphorus Sulfur Silicon Relat. Elem.*, 2012, **187**, 1284-1290.
148. A. R. Hajipour, R. Pourkaveh and H. Karimi, *Appl. Organomet. Chem.*, 2014, **28**, 879-883.
149. A. R. Hajipour and S. Jajarmi, *Appl. Organomet. Chem.*, 2016, **30**, 566-570.
150. J. Ye, Z. Chen, M.-K. Fung, C. Zheng, X. Ou, X. Zhang, Y. Yuan and C.-S. Lee, *Chem. Mater.*, 2013, **25**, 2630-2637.
151. J.-T. Yu, H. Guo, Y. Yi, H. Fei and Y. Jiang, *Adv. Synth. Catal.*, 2014, **356**, 749-752.
152. N. Taniguchi, *Synlett*, 2005, 1687-1690.
153. P. Yang, M.-S. Wang, J.-J. Shen, M.-X. Li, Z.-X. Wang, M. Shao and X. He, *Dalton Trans.*, 2014, **43**, 1460-1470.
154. C. Liu, Y.-B. Ding, X.-H. Shi, D. Zhang, M.-H. Hu, Y.-G. Yin and D. Li, *Cryst. Growth Des.*, 2009, **9**, 1275-1277.
155. L. Zhang, C.-J. Li, J.-E. He, Y.-Y. Chen, S.-R. Zheng, J. Fan and W.-G. Zhang, *J. Solid State Chem.*, 2016, **233**, 444-454.
156. T. Song, L. Zhang, P. Zhang, J. Zeng, T. Wang, A. Ali and H. Zeng, *J. Mater. Chem. A*, 2017, **5**, 6013-6018.
157. N. Li, Q.-E. Zhu, H.-M. Hu, H.-L. Guo, J. Xie, F. Wang, F.-X. Dong, M.-L. Yang and G.-L. Xue, *Polyhedron*, 2013, **49**, 207-215.
158. J. Zhang, B. Xu, F. Luo, G. Tang and C. Zhang, *Polyhedron*, 2019, **169**, 51-57.
159. N. Chen, M.-X. Li, P. Yang, X. He, M. Shao and S.-R. Zhu, *Cryst. Growth Des.*, 2013, **13**, 2650-2660.
160. Y. Cheng, M.-L. Yang, H.-M. Hu, B. Xu, X. Wang and G. Xue, *J. Solid State Chem.*, 2016, **239**, 121-130.
161. T.-T. Wang, J.-L. Zhang, H.-M. Hu, Y. Cheng, L.-L. Xue, X. Wang and B.-Z. Wang, *Polyhedron*, 2018, **151**, 43-50.
162. L.-N. Zheng, Y. Cheng, H.-M. Hu, C. Bai, X. Wang and G. Xue, *J. Solid State Chem.*, 2019, **272**, 210-220.
163. L. Lu, J. Wang, W.-P. Wu, A. Ma, J.-Q. Liu, R. Yadav and A. Kumar, *J. Lumin.*, 2017, **186**, 40-47.
164. S. A. Sotnik, R. A. Polunin, M. A. Kiskin, A. M. Kirillov, V. N. Dorofeeva, K. S. Gavrilenko, I. L. Eremenko, V. M. Novotortsev and S. V. Kolotilov, *Inorg. Chem.*, 2015, **54**, 5169-5181.
165. L. Li, Y. Z. Zhang, C. Yang, E. Liu, J. A. Golen and G. Zhang, *Polyhedron*, 2016, **105**, 115-122.
166. D. Toledo, A. Vega, N. Pizarro, R. Baggio, O. Peña, T. Roisnel, J.-Y. Pivan and Y. Moreno, *J. Solid State Chem.*, 2017, **253**, 78-88.
167. T.-H. Zhang, C. Bai, H.-M. Hu, J.-L. Zhang, X.-Y. Li, X. Wang and B.-Z. Wang, *J. Solid State Chem.*, 2021, **298**, 122148.
168. N. Li, H.-L. Guo, H.-M. Hu, J. Song, B. Xu, M.-L. Yang, F.-X. Dong and G.-L. Xue, *J. Solid State Chem.*, 2013, **198**, 416-423.
169. G. Manfroni, S. S. Capomolla, A. Prescimone, E. C. Constable and C. E. Housecroft, *Inorganics*, 2021, **9**, 54.
170. Y. M. Klein, A. Prescimone, M. B. Pitak, S. J.Coles, E. C. Constable and C. E. Housecroft, *CrystEngComm*, 2016, **18**, 4704-4707.
171. Y. M. Klein, A. Prescimone, M. Neuburger, E. C. Constable and C. E. Housecroft, *CrystEngComm*, 2017, **19**, 2894-2902.
172. C. L. Moy, R. Kaliappan and A. J. McNeil, *J. Org. Chem.*, 2011, **76**, 8501-8507.
173. E. R. T. Tiekink, *CrystEngComm*, 2021, **23**, 904-928.
174. D. Schollmeyer, O. V. Shishkin, T. Rühl and M. O. Vysotsky, *CrystEngComm*, 2008, **10**, 715-723.

175. O. V. Shishkin, *Chem. Phys. Lett.*, 2008, **458**, 96-100.
176. G. Manfroni, A. Prescimone, E. C. Constable and C. E. Housecroft, *Crystals*, 2021, **11**, 325.
177. T. Steiner, *Angew. Chem. Int. Ed.*, 2002, **41**, 48-76.
178. A. Bondi, *J. Phys. Chem.*, 1964, **68**, 441-451.
179. T. S. Spilfogel, H. M. Titi and T. Friščić, *Cryst. Growth Des.*, 2021, **21**, 1810-1832.
180. C. F. Macrae, I. Sovago, S. J. Cottrell, P. T. A. Galek, P. McCabe, E. Pidcock, M. Platings, G. P. Shields, J. S. Stevens, M. Towler and P. A. Wood, *J. Appl. Crystallogr.*, 2020, **53**, 226-235.
181. W. W. Ellis, M. Schmitz, A. A. Arif and P. J. Stang, *Inorg. Chem.*, 2000, **39**, 2547-2557.
182. N. Portolés-Gil, S. Gómez-Coca, O. Vallcorba, G. Marbán, N. Aliaga-Alcalde, A. López-Periago, J. A. Ayllón and C. Domingo, *RSC Adv.*, 2020, **10**, 45090-45104.
183. G. Novitchi, S. Jiang, S. Shova, F. Rida, I. Hlavička, M. Orlita, W. Wernsdorfer, R. Hamze, C. Martins, N. Suaud, N. Guihéry, A.-L. Barra and C. Train, *Inorg. Chem.*, 2017, **56**, 14809-14822.
184. E. C. Constable, C. E. Housecroft, S. Vujovic and J. A. Zampese, *CrystEngComm*, 2014, **16**, 3494-3497.
185. S. Vujovic, E. C. Constable, C. E. Housecroft, C. D. Morris, M. Neuburger and A. Prescimone, *Polyhedron*, 2015, **92**, 77-83.
186. Y. M. Klein, A. Prescimone, M. Karpacheva, E. C. Constable and C. E. Housecroft, *Polymers*, 2018, **10**, 1369.
187. Y. M. Klein, E. C. Constable, C. E. Housecroft and A. Prescimone, *CrystEngComm*, 2022, **24**, 5170-5170.
188. Y. M. Klein, A. Prescimone, E. C. Constable and C. E. Housecroft, *Materials*, 2017, **10**, 728.
189. D.-S. Li, Y.-P. Wu, J. Zhao, J. Zhang and J. Y. Lu, *Coord. Chem. Rev.*, 2014, **261**, 1-27.
190. S. S. Capomolla, G. Manfroni, A. Prescimone, E. C. Constable and C. E. Housecroft, *Molecules*, 2022, **27**, 4995.
191. S. S. Capomolla, G. Manfroni, A. Prescimone, E. C. Constable and C. E. Housecroft, *Helv. Chim. Acta*, 2022, e202200131.
192. J.-Y. Jin, Z.-Z. Jin, Y. Xia, Z.-Y. Zhou, X. Wu, D.-X. Zhu and Z.-M. Su, *Polymer*, 2007, **48**, 4028-4033.
193. P. Shao, Z. Li, J. Luo, H. Wang and J. Qin, *Synth. Commun.*, 2005, **35**, 49-53.
194. O. Delgado-Friedrichs and M. O'Keeffe, *Acta Crystallogr., Sect. A: Found. Crystallogr.*, 2003, **A59**, 351-360.
195. E. C. Constable and A. M. W. C. Thompson, *J. Chem. Soc., Chem. Commun.*, 1992, 617-619.
196. A. Wild, A. Winter, F. Schlütter and U. S. Schubert, *Chem. Soc. Rev.*, 2011, **40**, 1459-1511.
197. J.-L. Wang, X. Li, C. D. Shreiner, X. Lu, C. N. Moorefield, S. R. Tummalapalli, D. A. Medvetz, M. J. Panzner, F. R. Fronczek, C. Wesdemiotis and G. R. Newkome, *New J. Chem.*, 2012, **36**, 484-491.
198. T.-Z. Xie, S.-Y. Liao, K. Guo, X. Lu, X. Dong, M. Huang, C. N. Moorefield, S. Z. D. Cheng, X. Liu, C. Wesdemiotis and G. R. Newkome, *J. Am. Chem. Soc.*, 2014, **136**, 8165-8168.
199. M. Chen, D. Liu, J. Huang, Y. Li, M. Wang, K. Li, J. Wang, Z. Jiang, X. Li and P. Wang, *Inorg. Chem.*, 2019, **58**, 11146-11154.
200. S. Chakraborty, K. J. Endres, R. Bera, L. Wojtas, C. N. Moorefield, M. J. Saunders, N. Das, C. Wesdemiotis and G. R. Newkome, *Dalton Trans.*, 2018, **47**, 14189-14194.
201. E. C. Constable, C. E. Housecroft and I. Poleschak, *Inorg. Chem. Commun.*, 1999, **2**, 565-568.
202. E. C. Constable, O. Eich and C. E. Housecroft, *Inorg. Chem. Commun.*, 1999, **2**, 431-433.
203. E. C. Constable and P. Harverson, *Polyhedron*, 1999, **18**, 3093-3106.
204. E. C. Constable, O. Eich, C. E. Housecroft and D. C. Rees, *Inorg. Chim. Acta*, 2000, **300-302**, 158-168.
205. E. C. Constable, O. Eich, D. Fenske, C. E. Housecroft and L. A. Johnston, *Chem. Eur. J.*, 2000, **6**, 4364-4370.
206. T. K. Sievers, A. Vergin, H. Möhwald and D. G. Kurth, *Langmuir*, 2007, **23**, 12179-12184.
207. T. Bauer, A. D. Schlüter and J. Sakamoto, *Synlett*, 2010, 877-880.
208. H. Maeda, R. Sakamoto and H. Nishihara, *Coord. Chem. Rev.*, 2017, **346**, 139-149.

209. Y. Kuai, T. Yang, F. Yuan, Y. Dong, Q. Song, C. Zhang and W.-Y. Wong, *Dyes Pigm.*, 2021, **194**, 109623.
210. S. Roy and C. Chakraborty, *ACS Appl. Mater. Interfaces*, 2020, **12**, 35181-35192.
211. C.-W. Hu, T. Sato, J. Zhang, S. Moriyama and M. Higuchi, *ACS Appl. Mater. Interfaces*, 2014, **6**, 9118-9125.
212. R. K. Pandey, M. D. Hossain, T. Sato, U. Rana, S. Moriyama and M. Higuchi, *RSC Adv.*, 2015, **5**, 49224-49230.
213. Y. Kuai, W. Li, Y. Dong, W.-Y. Wong, S. Yan, Y. Dai and C. Zhang, *Dalton Trans.*, 2019, **48**, 15121-15126.
214. S. Roy and C. Chakraborty, *Chem. Commun.*, 2021, **57**, 7565-7568.
215. Y. Liu, R. Sakamoto, C.-L. Ho, H. Nishihara and W.-Y. Wong, *J. Mater. Chem. C*, 2019, **7**, 9159-9166.
216. K. Takada, R. Sakamoto, S.-T. Yi, S. Katagiri, T. Kambe and H. Nishihara, *J. Am. Chem. Soc.*, 2015, **137**, 4681-4689.
217. T. Tsukamoto, K. Takada, R. Sakamoto, R. Matsuoka, R. Toyoda, H. Maeda, T. Yagi, M. Nishikawa, N. Shinjo, S. Amano, T. Iokawa, N. Ishibashi, T. Oi, K. Kanayama, R. Kinugawa, Y. Koda, T. Komura, S. Nakajima, R. Fukuyama, N. Fuse, M. Mizui, M. Miyasaki, Y. Yamashita, K. Yamada, W. Zhang, R. Han, W. Liu, T. Tsubomura and H. Nishihara, *J. Am. Chem. Soc.*, 2017, **139**, 5359-5366.
218. C. R. Groom, I. J. Bruno, M. P. Lightfoot and S. C. Ward, *Acta Crystallogr., Sect. B: Struct. Sci., Cryst. Eng. Mater.*, 2016, **B72**, 171-179.
219. I. J. Bruno, J. C. Cole, P. R. Edgington, M. Kessler, C. F. Macrae, P. McCabe, J. Pearson and R. Taylor, *Acta Crystallogr., Sect. B: Struct. Sci.*, 2002, **B58**, 389-397.
220. O. S. Taniya, D. S. Kopchuk, A. F. Khasanov, I. S. Kovalev, S. Santra, G. V. Zyryanov, A. Majee, V. N. Charushin and O. N. Chupakhin, *Coord. Chem. Rev.*, 2021, **442**, 213980.
221. M. Cavazzini, S. Quici, C. Scalera, F. Puntoriero, G. La Ganga and S. Campagna, *Inorg. Chem.*, 2009, **48**, 8578-8592.
222. H. L. Nguyen, C. Gropp, Y. Ma, C. Zhu and O. M. Yaghi, *J. Am. Chem. Soc.*, 2020, **142**, 20335-20339.
223. J. N. Moorthy and P. Natarajan, *Chem. Eur. J.*, 2010, **16**, 7796-7802.
224. H. Yamagishi, H. Sato, A. Hori, Y. Sato, R. Matsuda, K. Kato and T. Aida, *Science*, 2018, **361**, 1242-1246.
225. T. Liu, B. Wang, R. He, H. Arman, K. S. Schanze, S. Xiang, D. Li and B. Chen, *Can. J. Chem.*, 2020, **98**, 352-357.
226. M. F. N. N. Carvalho, M. T. A. Fernanda, M. G. Adelino and J. L. P. Armando, *J. Organomet. Chem.*, 2003, **679**, 143-147.
227. C.-L. Liu, C.-J. Zheng, X.-K. Liu, Z. Chen, J.-P. Yang, F. Li, X.-M. Ou and X.-H. Zhang, *J. Mater. Chem. C*, 2015, **3**, 1068-1076.
228. C. Janiak, *J. Chem. Soc., Dalton Trans.*, 2000, 3885-3896.
229. J. E. Beves, E. C. Constable, C. E. Housecroft, C. J. Kepert and D. J. Price, *CrystEngComm*, 2007, **9**, 456-459.
230. J. E. Beves, E. C. Constable, C. E. Housecroft, C. J. Kepert, M. Neuburger, D. J. Price, S. Schaffner and J. A. Zampese, *Dalton Trans.*, 2008, 6742-6751.
231. Y. M. Klein, E. C. Constable, C. E. Housecroft, J. A. Zampese and A. Crochet, *CrystEngComm*, 2014, **16**, 9915-9929.
232. D. Rocco, S. Novak, A. Prescimone, E. C. Constable and C. E. Housecroft, *Chemistry*, 2021, **3**, 182-198.
233. E. C. Constable, C. E. Housecroft, M. Neuburger, J. Schönle, S. Vujovic and J. A. Zampese, *Polyhedron*, 2013, **60**, 120-129.
234. D. Rocco, G. Manfroni, A. Prescimone, Y. M. Klein, D. J. Gawryluk, E. C. Constable and C. E. Housecroft, *Polymers*, 2020, **12**, 318.
235. Y. M. Klein, A. Prescimone, E. C. Constable and C. E. Housecroft, *Inorg. Chem. Comm.*, 2016, **70**, 118-120.

236. M. Barquín, J. Cancela, M. J. González Garmendia, J. Quintanilla and U. Amador, *Polyhedron*, 1998, **17**, 2373-2378.
237. Y. M. Klein, E. C. Constable, C. E. Housecroft and A. Prescimone, *Inorg. Chem. Commun.*, 2014, **49**, 41-43.
238. E. Moulin, J. J. I. V. Armao and N. Giuseppone, *Acc. Chem. Res.*, 2019, **52**, 975-983.
239. A. N. Sobolev, V. K. Belsky, I. P. Romm, N. Y. Chernikova and E. N. Guryanova, *Acta Crystallogr., Sect. C: Cryst. Struct. Commun.*, 1985, **C41**, 967-971.
240. L. Zou, S. Guo, H. Lv, F. Chen, L. Wei, Y. Gong, Y. Liu and C. Wei, *Dyes Pigm.*, 2022, **198**, 109958.
241. J. E. Anthony, S. I. Khan and Y. Rubin, *Tetrahedron Lett.*, 1997, **38**, 3499-3502.
242. G. Sheldrick, *Acta Crystallogr., Sect. A: Found. Adv.*, 2015, **A71**, 3-8.
243. O. V. Dolomanov, L. J. Bourhis, R. J. Gildea, J. A. K. Howard and H. Puschmann, *J. Appl. Crystallogr.*, 2009, **42**, 339-341.
244. G. Sheldrick, *Acta Crystallogr., Sect. C: Struct. Chem.*, 2015, **C71**, 3-8.
245. W. Kabsch, *Acta Crystallogr., Sect. D: Biol. Crystallogr.*, 2010, **D66**, 125-132.
246. A. Spek, *Acta Crystallogr., Sect. C: Struct. Chem.*, 2015, **C71**, 9-18.
247. J. Rodríguez-Carvajal, *Physica B Condens. Matter*, 1993, **192**, 55-69.
248. T. Roisnel and J. Rodríguez-Carvajal, in *In Materials Science Forum. Proceedings of the European Powder Diffraction Conf. (EPDIC 7)*, Barcelona, Spain, 2001, pp. 118-123.

9 Appendix

9.1 NMR spectra of angular bis(terpyridine) ligands

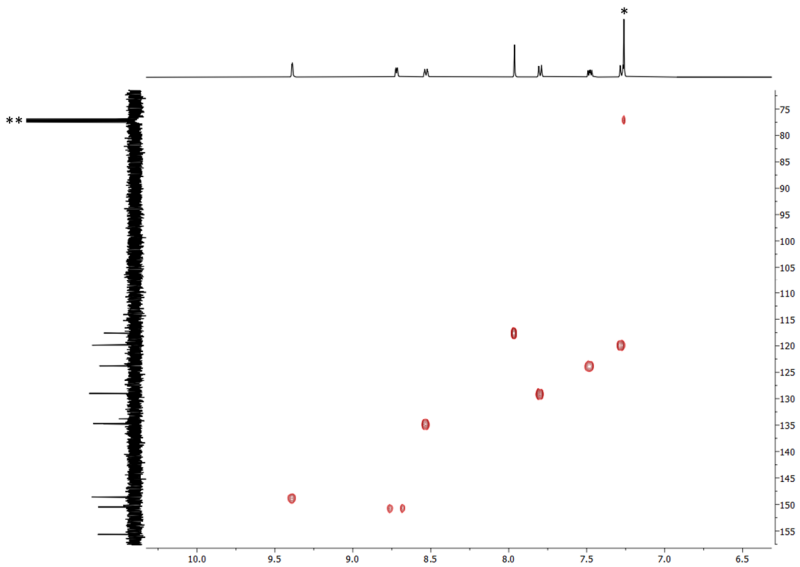

Figure S1 HMQC spectrum (^{1}H 500 MHz, ^{13}C{^{1}H} 126 MHz, $CDCl_3$, 298 K) of **1**. * = $CHCl_3$, ** = $CDCl_3$

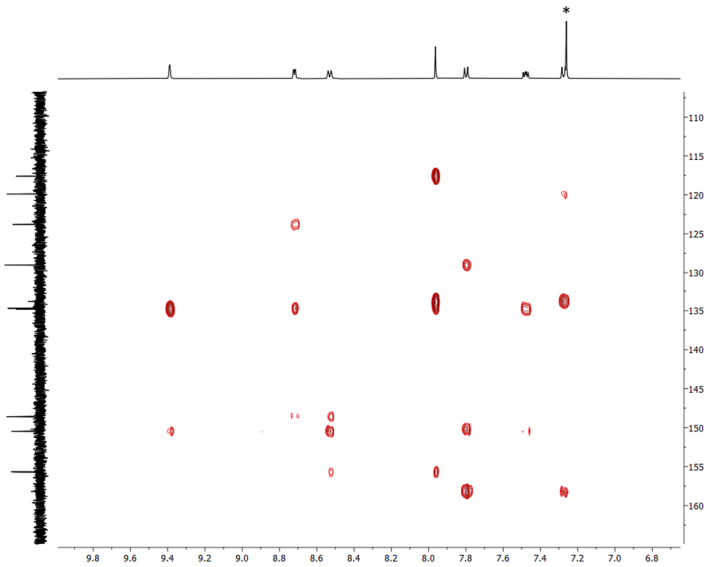

Figure S2 HMBC spectrum (^{1}H 500 MHz, ^{13}C{^{1}H} 126 MHz, $CDCl_3$, 298 K) of **1**. * = $CHCl_3$

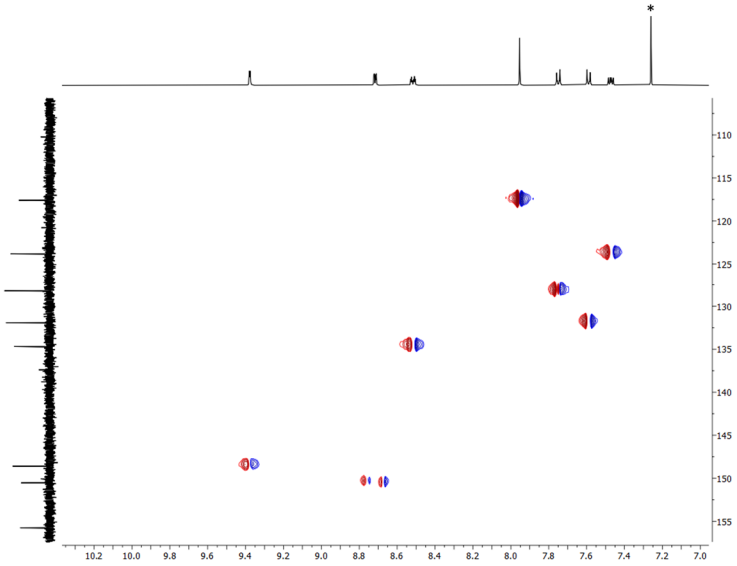

Figure S3 HMQC spectrum (^{1}H 500 MHz, ^{13}C{^{1}H} 126 MHz, $CDCl_3$, 298 K) of **2**. * = $CHCl_3$

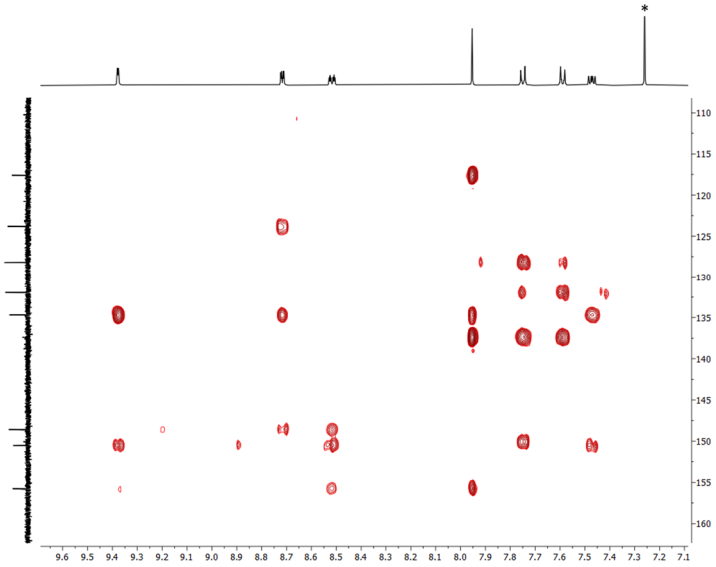

Figure S4 HMBC spectrum (^{1}H 500 MHz, ^{13}C{^{1}H} 126 MHz, $CDCl_3$, 298 K) of **2**. * = $CHCl_3$

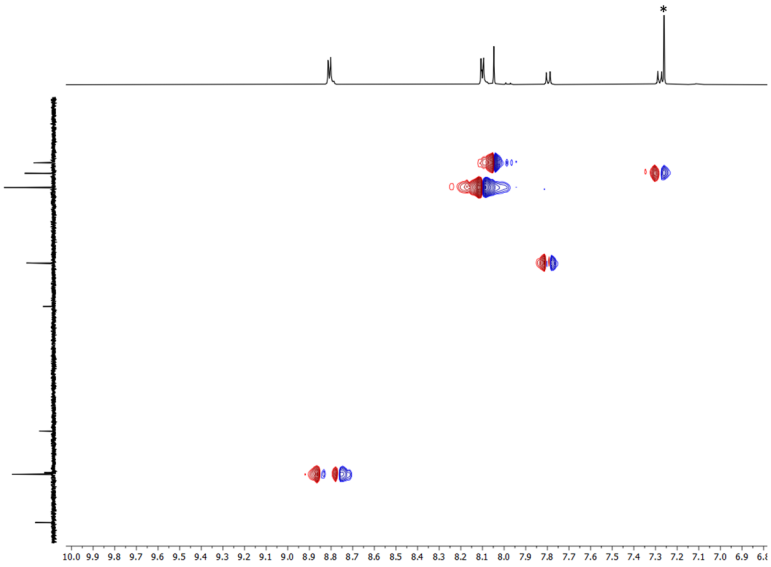

Figure S5 HMQC spectrum (^{1}H 500 MHz, ^{13}C{^{1}H} 126 MHz, $CDCl_3$, 298 K) of **3**. * = $CHCl_3$

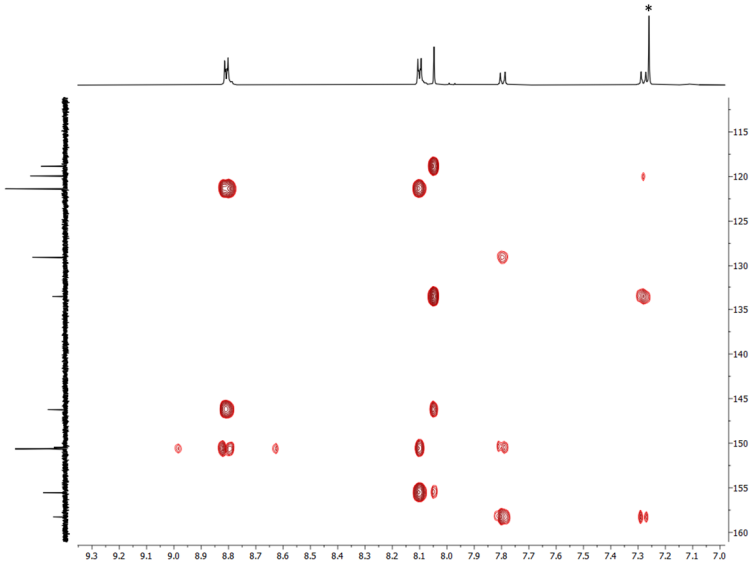

Figure S6 HMBC spectrum (^{1}H 500 MHz, ^{13}C{^{1}H} 126 MHz, $CDCl_3$, 298 K) of **3**. * = $CHCl_3$

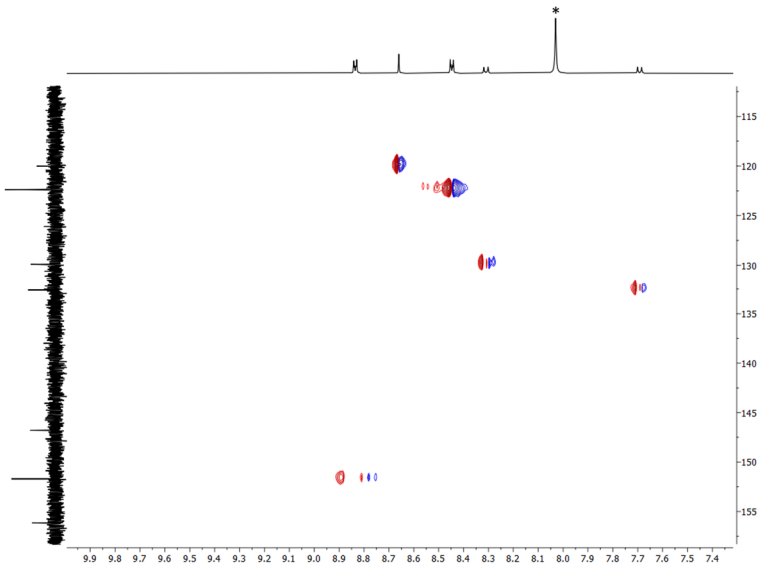

Figure S7 HMQC spectrum (^{1}H 500 MHz, ^{13}C{^{1}H} 126 MHz, DMF-d_7, 298 K) of **4**. * = DMF-d_6

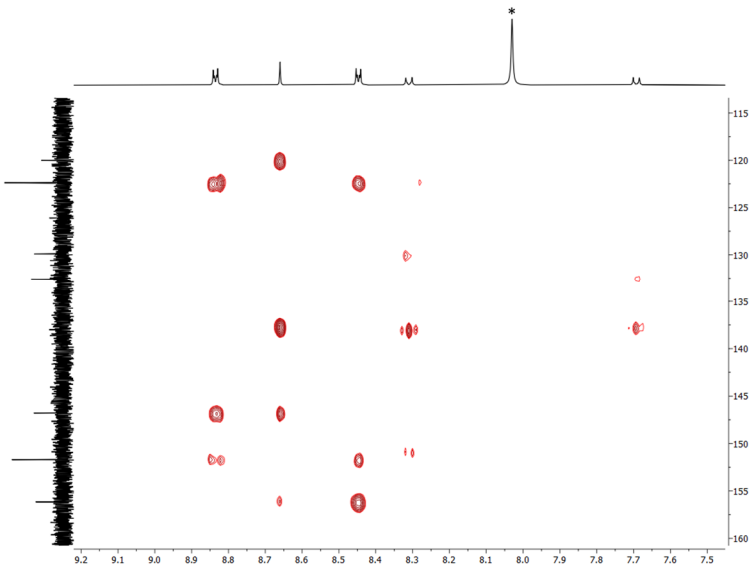

Figure S8 HMBC spectrum (^{1}H 500 MHz, ^{13}C{^{1}H} 126 MHz, DMF-d_7, 298 K) of **4**. * = DMF-d_6

9.2 NMR spectra of 1,4-bis(phenylalkoxy)-2,5-bis(3,2':6',3''terpyridin-4'-yl)benzene ligands

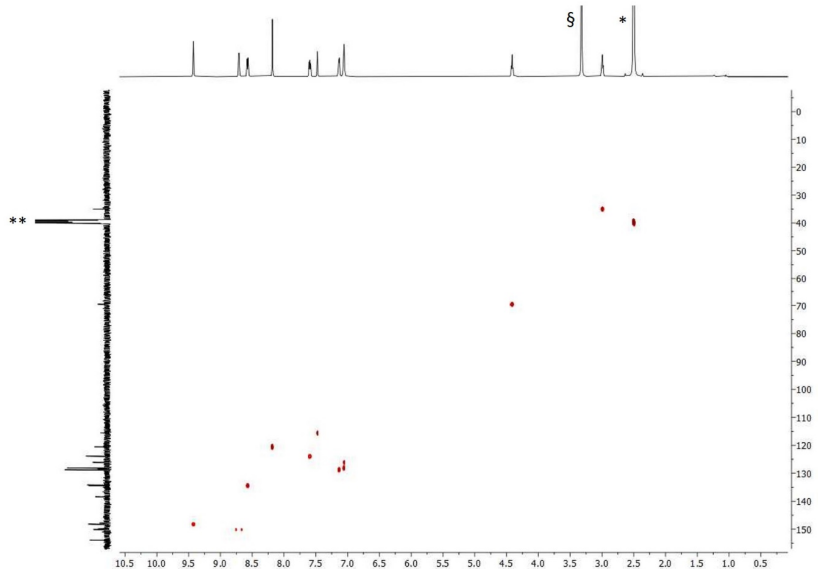

Figure S9 HMQC spectrum (^{1}H 500 MHz, ^{13}C{^{1}H} 126 MHz, DMSO-d_6, 298 K) of **5**. * = DMSO-d_5, ** = DMSO-d_6, § = H_2O

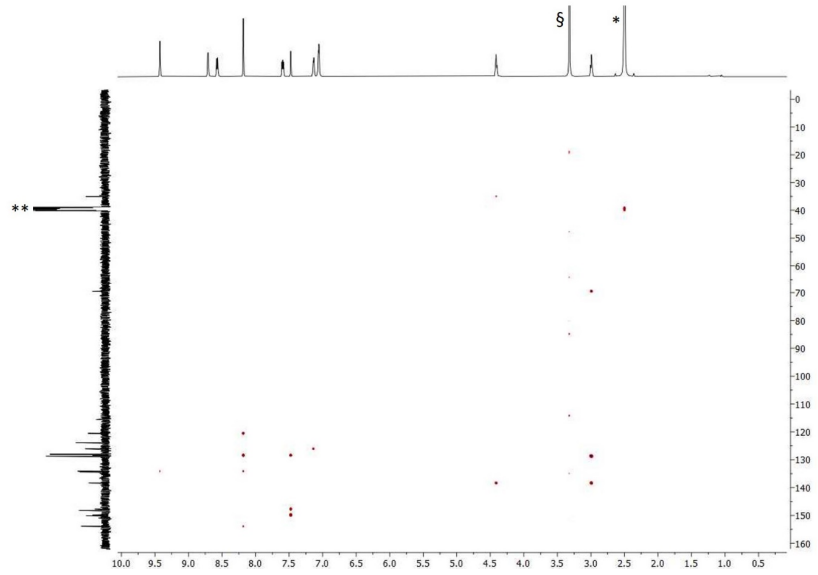

Figure S10 HMBC spectrum (^{1}H 500 MHz, ^{13}C{^{1}H} 126 MHz, DMSO-d_6, 298 K) of **5**. * = DMSO-d_5, ** = DMSO-d_6, § = H_2O

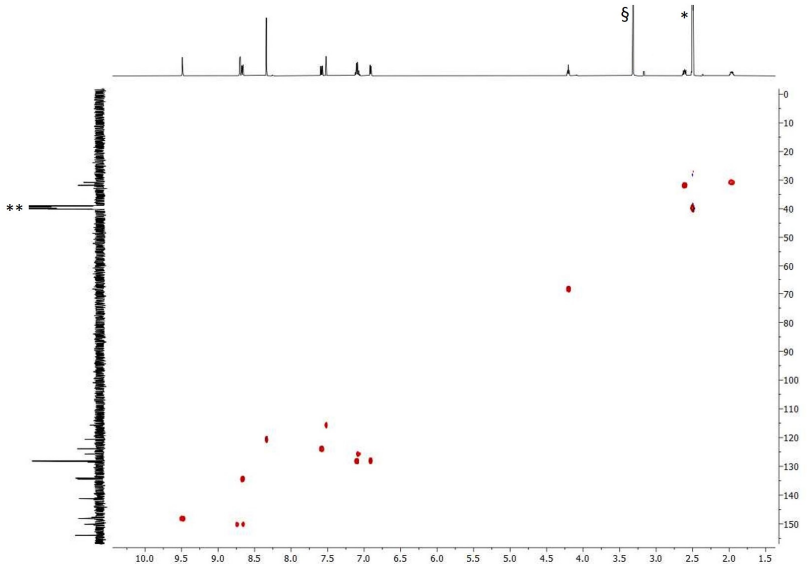

Figure S11 HMQC spectrum (^{1}H 500 MHz, ^{13}C{^{1}H} 126 MHz, DMSO-d_6, 298 K) of **6**. * = DMSO-d_5, ** = DMSO-d_6, § = H_2O

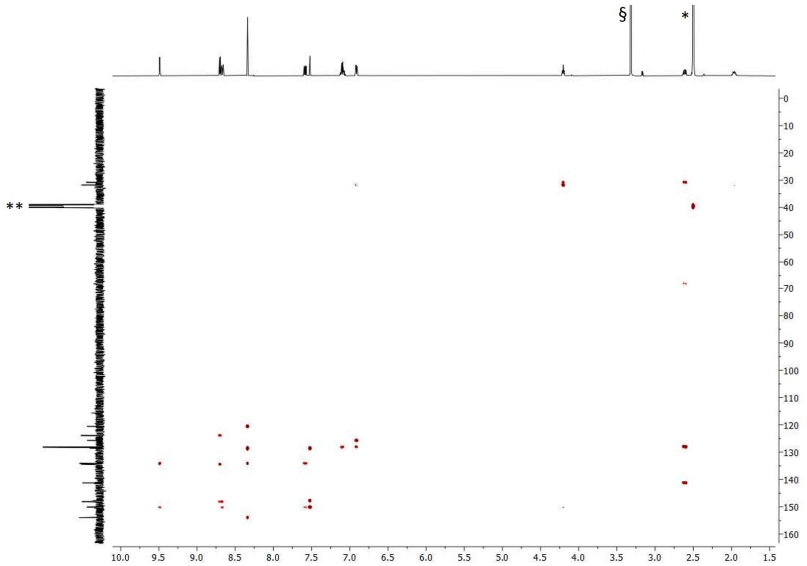

Figure S12 HMBC spectrum (^{1}H 500 MHz, ^{13}C{^{1}H} 126 MHz, DMSO-d_6, 298 K) of **6**. * = DMSO-d_5, ** = DMSO-d_6, § = H_2O

9.3 NMR spectra of 1,4-bis(alkyloxy)-2,5-bis(3,2':6',3''terpyridin-4'-yl)benzene ligands

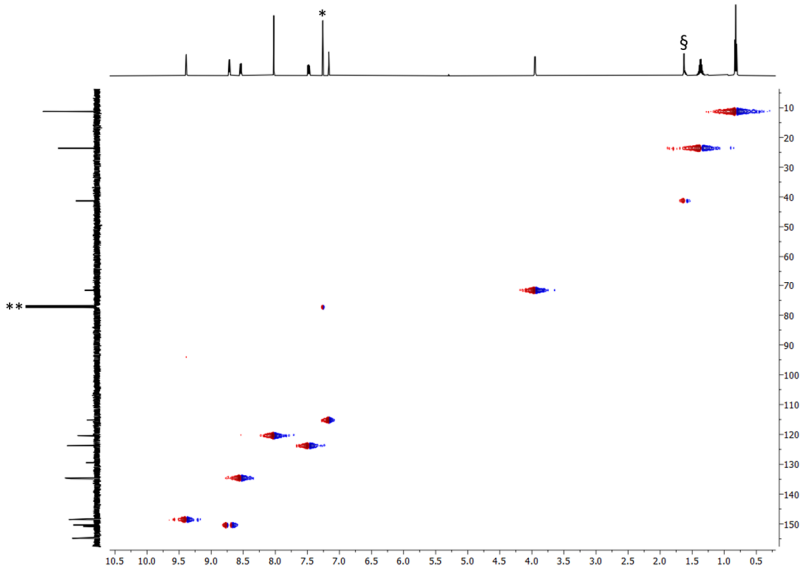

Figure S13 HMQC spectrum (^{1}H 500 MHz, ^{13}C{^{1}H} 126 MHz, $CDCl_3$, 298 K) of **7**. * = $CHCl_3$, ** = $CDCl_3$, § = H_2O

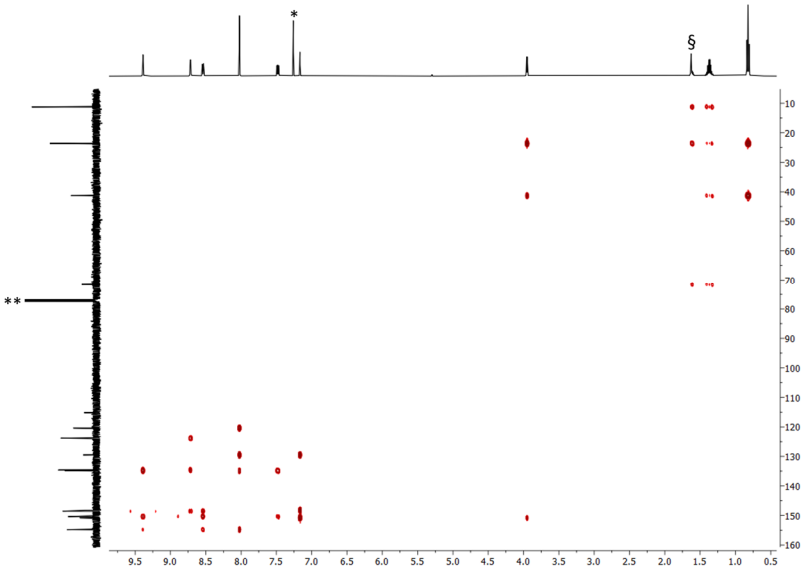

Figure S14 HMBC spectrum (^{1}H 500 MHz, ^{13}C{^{1}H} 126 MHz, $CDCl_3$, 298 K) of **7**. * = $CHCl_3$, ** = $CDCl_3$, § = H_2O

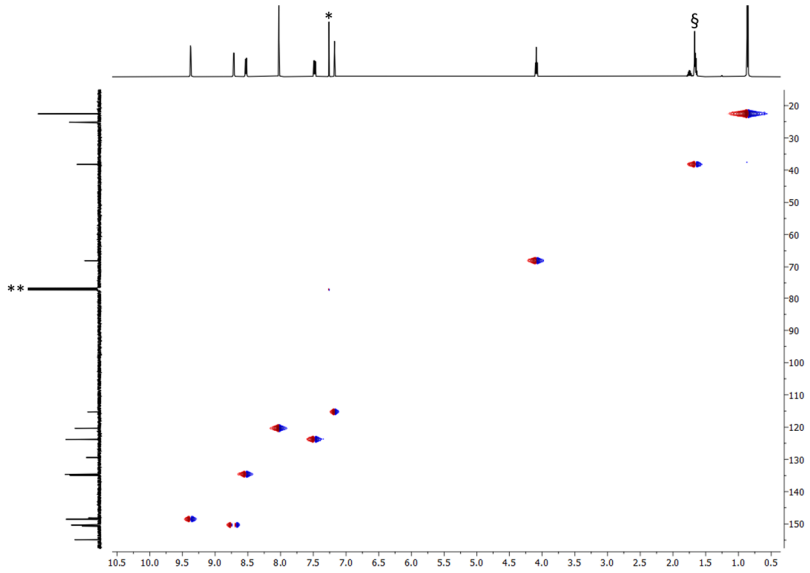

Figure S15 HMQC spectrum (^{1}H 500 MHz, ^{13}C{^{1}H} 126 MHz, $CDCl_3$, 298 K) of **8**. * = $CHCl_3$, ** = $CDCl_3$, § = H_2O

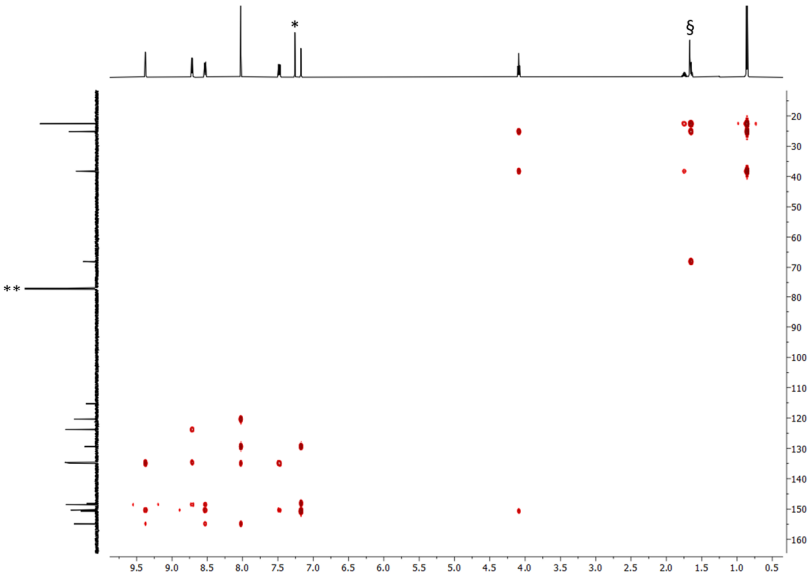

Figure S16 HMBC spectrum (^{1}H 500 MHz, ^{13}C{^{1}H} 126 MHz, $CDCl_3$, 298 K) of **8**. * = $CHCl_3$, ** = $CDCl_3$, § = H_2O

9.4 NMR spectra of star tris(terpyridine) ligands

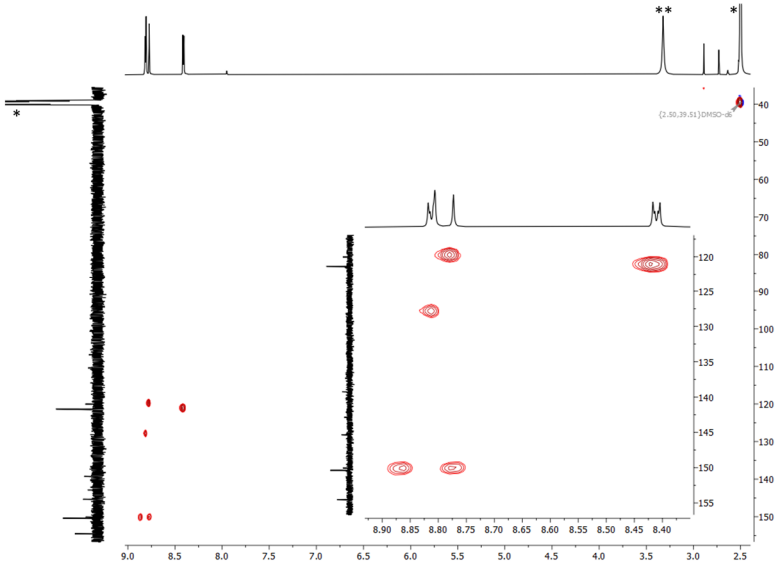

Figure S17 HMQC spectrum (^{1}H 500 MHz, ^{13}C{^{1}H} 126 MHz, DMSO-d_6, 298 K) of compound **9**. * = DMSO-d_6, ** = H_2O

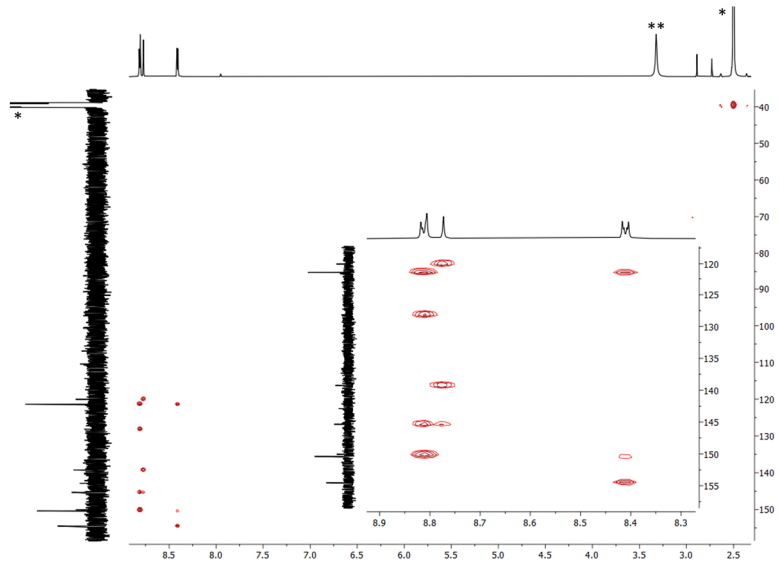

Figure S18 HMBC spectrum (^{1}H 500 MHz, ^{13}C{^{1}H} 126 MHz, DMSO-d_6, 298 K) of compound **9**. * = DMSO-d_6, ** = H_2O

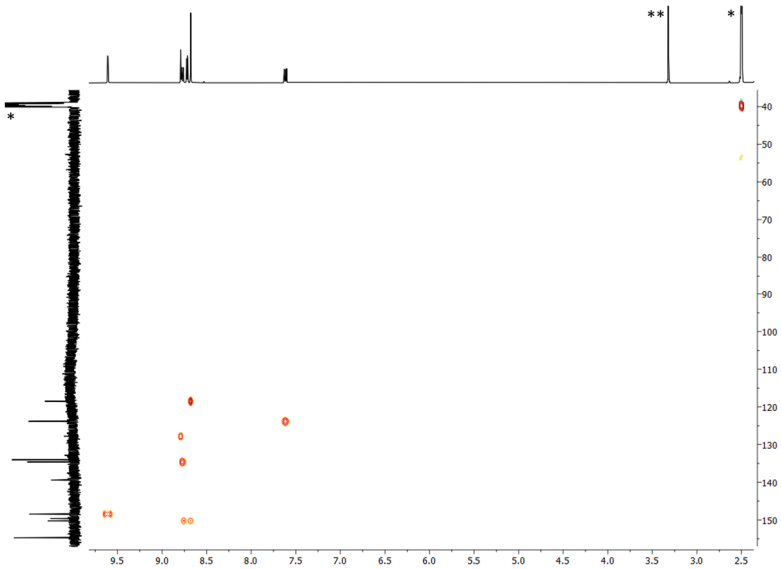

Figure S19 HMQC spectrum (^{1}H 500 MHz, ^{13}C{^{1}H} 126 MHz, DMSO-d_6, 298 K) of compound **10**. * = DMSO-d_6, ** = H_2O

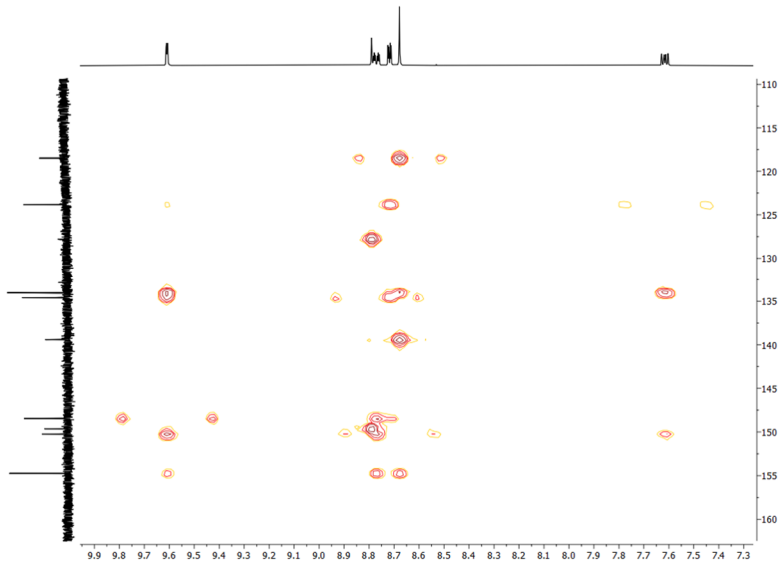

Figure S20 HMBC spectrum (^{1}H 500 MHz, ^{13}C{^{1}H} 126 MHz, DMSO-d_6, 298 K) of compound **10**.

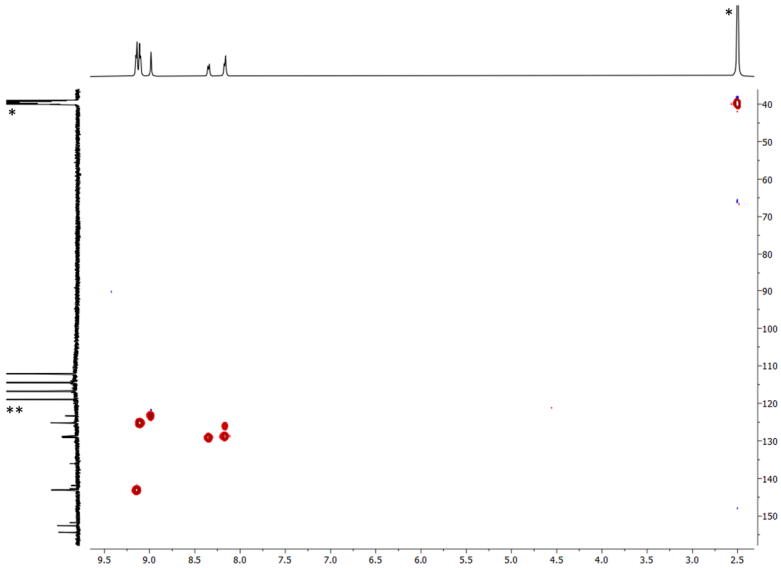

Figure S21 HMQC spectrum (^{1}H 500 MHz, ^{13}C{^{1}H} 126 MHz, DMSO-d_6 + TFA-*d*, 298 K) of **11**. * = DMSO-d_6, ** = CF_3COOD

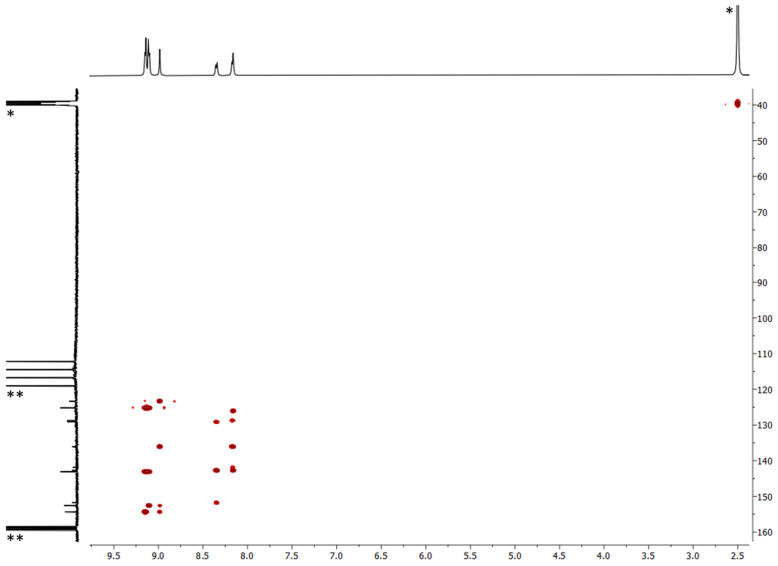

Figure S22 HMBC spectrum (^{1}H 500 MHz, ^{13}C{^{1}H} 126 MHz, DMSO-d_6 + TFA-d, 298 K) of **11**. * = DMSO-d_6, ** = CF_3COOD

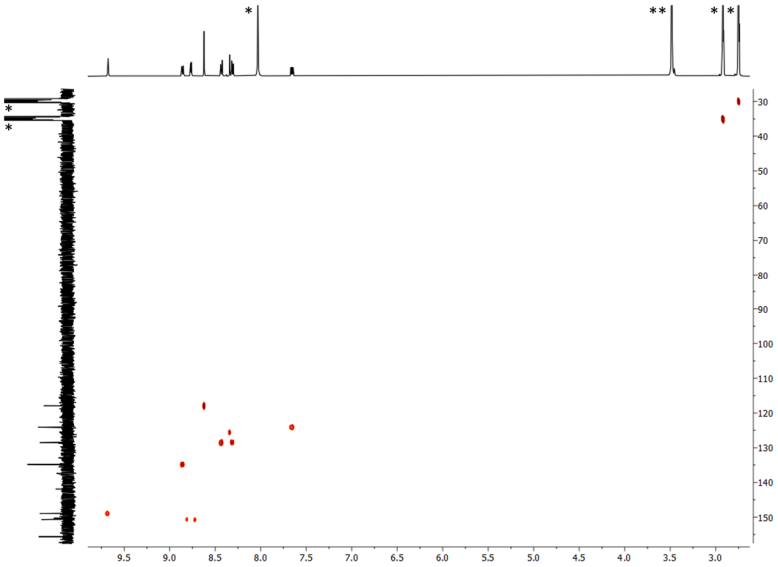

Figure S23 HMQC spectrum (^{1}H 500 MHz, ^{13}C{^{1}H} 126 MHz, DMF-d_7, 298 K) of **12**. * = DMF-d_7, ** = H_2O

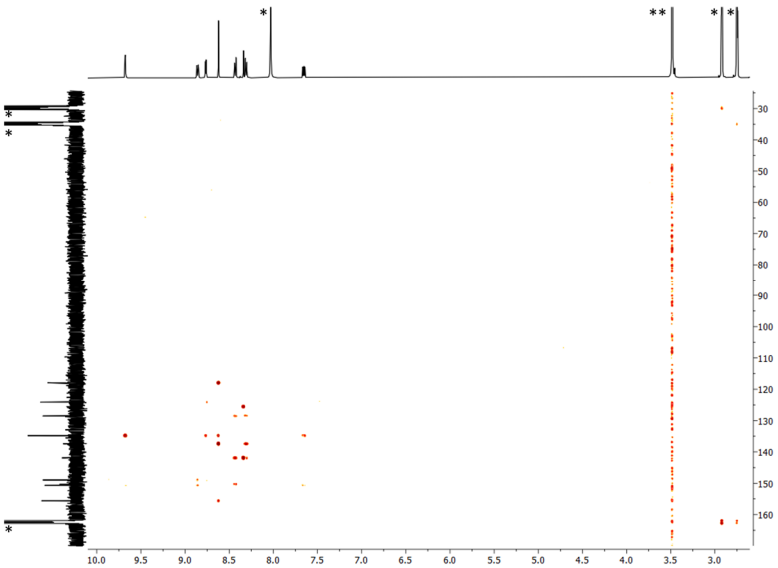

Figure S24 HMBC spectrum (^{1}H 500 MHz, ^{13}C{^{1}H} 126 MHz, DMF-d_7, 298 K) of **12**. * = DMF-d_7, ** = H_2O

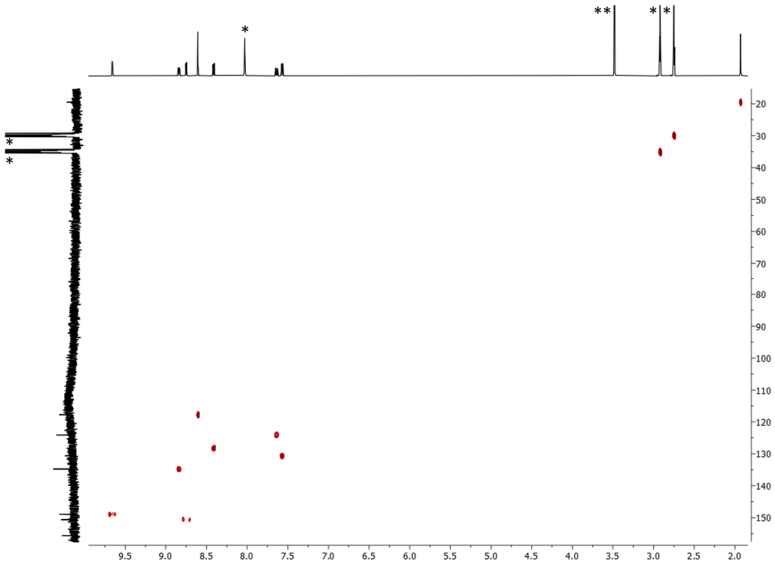

Figure S25 HMQC spectrum (^{1}H 500 MHz, ^{13}C{^{1}H} 126 MHz, DMF-d_7, 298 K) of **13**. * = DMF-d_7, ** = H_2O

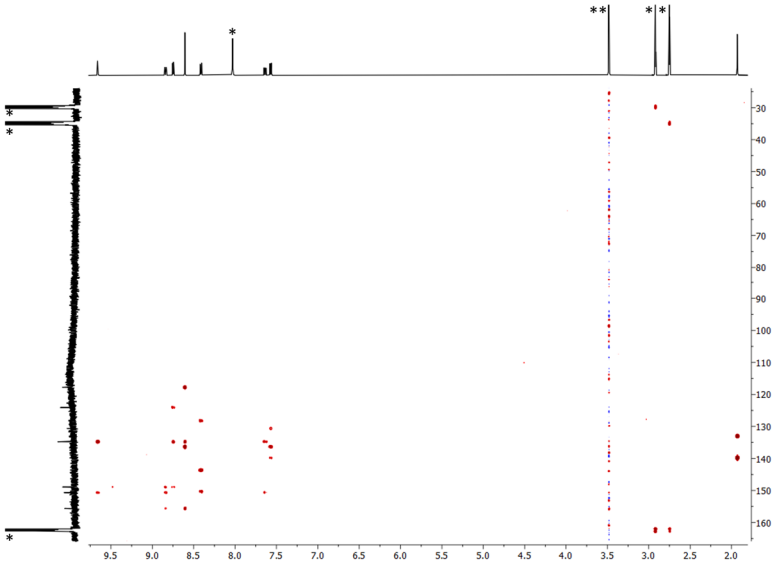

Figure S26 HMBC spectrum (^{1}H 500 MHz, ^{13}C{^{1}H} 126 MHz, DMF-d_7, 298 K) of **13**. * = DMF-d_7, ** = H_2O

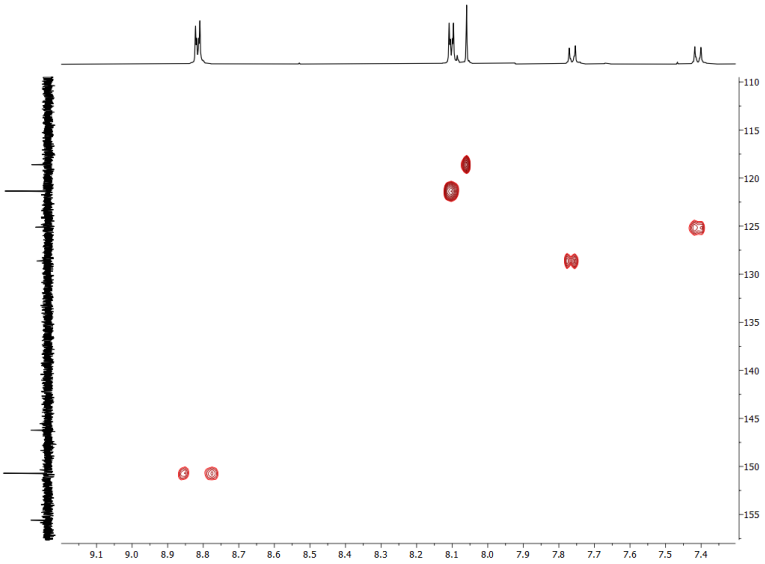

Figure S27 HMQC spectrum (^{1}H 500 MHz, ^{13}C{^{1}H} 126 MHz, $CDCl_3$, 298 K) of **14**.

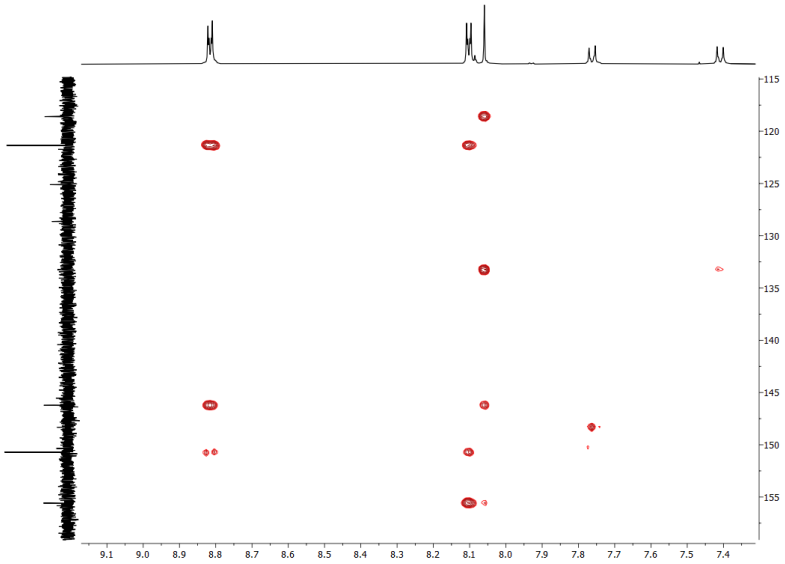

Figure S28 HMBC spectrum (^{1}H 500 MHz, ^{13}C{^{1}H} 126 MHz, $CDCl_3$, 298 K) of **14**.

9.5 Other spectroscopic data

Complete spectroscopic data of the ligands and their precursors, including original ^{1}H and ^{13}C{^{1}H} NMR spectra, UV-Vis absorption spectra, FT-IR spectra, MALDI-TOF and HR-ESI mass spectra can be found in the links below:

https://zenodo.org/record/6006054
https://zenodo.org/record/7227912
https://zenodo.org/record/6005879
https://zenodo.org/record/6032986